UNIVERSITY OF READING

Department of Meteorology

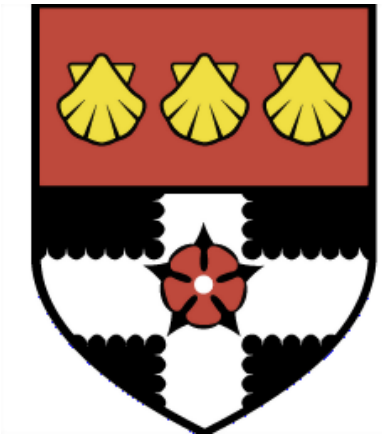

What determines the location and intensity of the Intertropical Convergence Zone?

Joshua Talib

A thesis submitted for the degree of Doctor of Philosophy

5th April 2019

Declaration

I confirm that this is my own work and the use of all material from other sources has been properly and fully acknowledged.

Joshua Talib

Dedication

To Nanny Jean and Grandad Talib.

For all your faith, prayer, and support.

Abstract

The Intertropical Convergence Zone (ITCZ) is a discontinuous, zonal precipitation band that plays a crucial role in the global hydrological cycle. Across a hierarchy of models, including prescribed sea surface temperature (SST) aquaplanet simulations, a substantial inter-model variability in ITCZ characteristics exists and the ITCZ is sensitive to the representation of convection. To understand the mechanisms driving ITCZ characteristics the sensitivity of the ITCZ to convective mixing is investigated. In prescribed-SST aquaplanet simulations stronger convective mixing favours a single ITCZ, associated with increased boundary-layer moist static energy (MSE) required for deep convection. However, varying insolation and prescribed SSTs demonstrates that boundary conditions affect this sensitivity.

Further analysis focuses on two key processes in the sensitivity of the ITCZ to convective mixing: cloud-radiation effects (CRE; atmospheric heating due to cloud-radiation interactions) and atmosphere-ocean coupling. The role of CRE is explored using simulations with CRE removed or prescribed as a diurnally-varying, zonal-mean climatology. Removing CRE promotes a double ITCZ, associated with upper-tropospheric cooling, whilst prescribing CRE reduces the sensitivity by approximately 50%. The remaining sensitivity when prescribing CRE is associated with surface latent heat fluxes. The effect of coupling is investigated using an idealised modelling framework in which the atmosphere is coupled to a two-layer ocean with an Ekman-driven ocean energy transport (OET). Coupling substantially reduces the sensitivity of the ITCZ location associated with meridional SST gradient changes. Decreasing convective mixing increases the meridional SST gradient which promotes a single ITCZ and offsets the effect of a reduced boundary-layer MSE required for deep convection. Prescribed OET simulations reveal that OET plays a minimal role in the reduced sensitivity. The important role of interactive SSTs indicates that prescribing SST may overemphasise the sensitivity of the ITCZ to a parameterisation or atmospheric forcing. Future modelling development efforts need to consider surface-atmosphere interactions.

Acknowledgements

This thesis represents three and half years of hard work, dedication, learning, and enjoyment. All of which could not be achieved without the support of my family, friends, and colleagues. I am extremely grateful to you all.

I would like to acknowledge my three supervisors, Steve Woolnough, Nick Klingaman, and Chris Holloway. This PhD has been huge learning curve and I cannot think of three better supervisors to have received guidance from. Commencing this PhD was a huge leap for me and it with the support of my supervisors that I gained the confidence and ability to address challenging questions in climate science. I look forward to working and collaborating with them in the future.

Thank you to Rowan Sutton, Michaela Hegglin, and Mat Collins for their feedback during monitoring committees and the viva examination. The feedback I received substantially improved this thesis and encouraged broader thinking regarding the science questions addressed. I would also like to acknowledge the SCENARIO NERC Doctoral Training Partnership and the Department of Meteorology for supporting this project.

Thank you to friends and colleagues both inside and outside of the Department of Meteorology who made my time at the University of Reading such an enjoyable experience. I cannot name you all here but a particular thanks to Jacob Maddison, Alice Barratt, Abby Brown, and Joseph Diwakar. Whether it was a prolonged discussion during a fifteen mile run, a lengthy phone conversation, or continued enthusiasm to keep going, I cannot thank you enough and I am so privileged to have your friendship.

Finally, the biggest gratitude to my family. Mum, Dad, thank you for the continued love, encouragement, and support to follow my ambitions. I cannot believe what I have achieved and could not have done it without you. During this PhD I lost two incredible grandparents, Mohamed Talib and Jean

Gallagher. This PhD is dedicated to them both, as without their inherited wisdom I would not have successfully achieved this doctorate. We lost Nan five days before my viva examination, but I know with full confidence that she is celebrating in heaven. Make sure you give my thanks to Jesus Nan!

Contents

Chapter 1

Introduction

The Intertropical Convergence Zone (ITCZ) is one of the most important components of the climate system. Livelihoods of over three billion people depend on the seasonal cycle of tropical precipitation which is predominately associated with the seasonal ITCZ migration. The ITCZ is associated with a tropical belt of deep convective clouds (Waliser and Gautier, 1993), a maximum in time-mean precipitation (Schneider et al., 2014), and a maximum in lower-tropospheric convergence (Berry and Reeder, 2014). The ascent associated with the ITCZ combined with sub-tropical subsidence and low-level flow towards the ITCZ, forms the meridional overturning circulation known as the "Hadley cell". Contemporary climate models exhibit substantial large-scale tropical rainfall biases associated with mean circulation errors (Lin, 2007). Aquaplanet simulations with prescribed sea surface temperatures (SSTs) show a substantial inter-model variability of the ITCZ amongst atmospheric models (Blackburn et al., 2013). To support the development of climate models and reduce tropical precipitation biases, this thesis aims to understand the mechanisms responsible for ITCZ characteristics in aquaplanet simulations.

In the tropics, rain tends to be concentrated in compact bands or belts (Waliser and Gautier, 1993; Bony et al., 2015). The ITCZ is a discontinuous zonal precipitation belt with some of heaviest precipitation observed on Earth (Fig. 1.1). Globally, the ITCZ has a zonal-mean, time-mean position of approximately 6°N and migrates between approximately 10°S in boreal winter and 10°N in boreal summer (Waliser and Gautier, 1993; Bischoff and Schneider, 2014). The seasonal cycle of the ITCZ location plays a key role in the major monsoon systems (Bordoni and Schneider, 2008; Bony et al., 2015). Across Africa and Asia, agricultural and forestry industries account for approximately 11% of gross domestic product (GDP) (FAO, 2018); industries that heavily rely on freshwater supplies associated with the ITCZ. Understanding the behaviour of the ITCZ to improve climate simulations

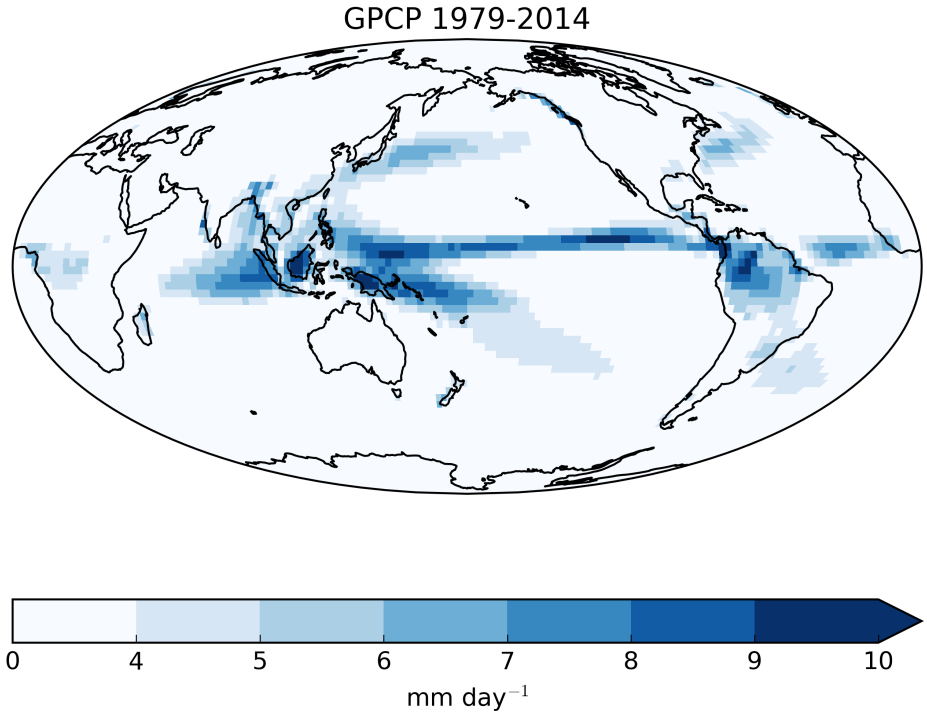

Figure 1.1: *Time-mean precipitation (mm day^{-1}) from Global Precipitation Climatology Project (GPCP) for 1979 to 2014.*

of tropical precipitation plays a crucial role in enhancing agricultural practises, protecting endangered wildlife species, minimising loss from flooding, preventing water-sourced conflicts, and harnessing hydroelectric power. For example, approximately 10% of India's electricity is generated from hydroelectric sources (CEA, 2018). To improve predictions of hydroelectric power capability in India and other tropical countries, a greater understanding of tropical rain belts is required to improve climate simulations (Basu, 2005).

In this chapter a brief overview of the dynamics of the ITCZ is presented (section 1.1) followed by a discussion of the simulated ITCZ across a hierarchy of models (section 1.2). After this sections 1.3 and 1.4 present the objectives and outline of this thesis respectively.

1.1 ITCZ dynamics

ITCZ characteristics vary across daily-to-weekly timescales and over synoptic length-scales due to a number of reasons including: interactions with synoptic disturbances such as tropical cyclones (Berry and Reeder, 2014); intra-seasonal variability of the tropical atmosphere (Wang and Magnusdottir, 2006); and surface-atmosphere interactions (Lindzen and Hou, 1988; Mobis and Stevens, 2012; Wei

and Bordoni, 2018). Seasonally, the ITCZ migrates towards the warmer hemisphere (Donohoe et al., 2013) following the latitude of maximum insolation (Waliser and Gautier, 1993; Wei and Bordoni, 2018). Paeloclimate records indicate the ITCZ shifting towards the warmer hemisphere on millenial scales (Peterson et al., 2000; Haug et al., 2001). For example during the Holocene, orbital forced changes in insolation warmed the Southern Hemisphere (SH) more than the Northern Hemisphere (NH), associated with a southward ITCZ shift (Haug et al., 2001). The seasonal cycle of the ITCZ also varies regionally. For example over the Pacific Ocean, the ITCZ remains in the NH all year round, migrating between approximately 2°N and 9°N latitude (Fig. 1.2a; Schneider et al., 2014), whilst in ocean basins with large adjacent tropical land masses, ITCZ shifts are much more dramatic (Fig. 1.2b). Amplified meridional ITCZ shifts over land are associated with the major monsoon systems and thermal property differences between the land and ocean.

Whilst the ITCZ is regarded as the ascending branch of the Hadley circulation (Fig. 1.3b), changes in ITCZ characteristics are associated with circulations on a variety of scales. Mesoscale circulations influence the poleward migration of major monsoon systems (Birch et al., 2014), and planetary scale circulations connect the ITCZ to extratropical forcing (Kang et al., 2008). Recently developed energetic frameworks (section 2.2; Kang et al., 2008; Bischoff and Schneider, 2014) have been used to understand ITCZ characteristics (Frierson and Hwang, 2012; Donohoe et al., 2013; Bischoff and Schneider, 2016). Moist static energy (MSE) is a key component of these frameworks and is the sum of the thermal, latent and gravitational potential energy of an air parcel. MSE (h, J kg^{-1}) is defined as:

$$h = C_p T + gZ + L_v q \tag{1.1}$$

where C_p is the specific heat capacity (J kg^{-1} K^{-1}); g is Earth's gravitational constant (m s^{-2}); L_v is the latent heat of vaporisation (J kg^{-1}); and T (K), Z (m) and q (kg kg^{-1}) are the temperature, geopotential height, and specific humidity of the air parcel respectively. In the lower tropical ($\leq$30° latitude) troposphere MSE is dominated by latent energy and the temperature component of dry static energy (Fig. 1.3a). Specific humidity and temperature decrease with height, whilst geopotential increases. In the tropics a mid-tropospheric MSE minimum is observed alongside greater MSE in the upper-troposphere compared to the lower-troposphere (Fig. 1.3a). The vertical MSE gradient in the tropics is typically associated with the Hadley circulation transporting energy poleward away from the ITCZ; the direction of MSE transport is inferred from the direction of the upper-branch of the Hadley circulation. The ITCZ location is commonly diagnosed where the column-integrated MSE transport equals zero (i.e. Kang et al., 2008; Donohoe et al., 2013; Schneider et al., 2014; Bischoff and Schneider, 2016); the divergence of the column-integrated MSE transport equals the atmospheric

energy input (AEI) at equilibrium (section 2.2; Neelin and Held, 1987). This thesis, along with other studies (e.g. Kang et al., 2008; Donohoe et al., 2013; Bischoff and Schneider, 2014), uses an AEI framework to understand the mechanisms controlling ITCZ characteristics.

1.2 Modelling the ITCZ

Modelling tropical rainfall is one of the greatest challenges faced in climate science. Despite ongoing improvements, climate models still exhibit large-scale tropical rainfall biases. For example, general circulation models (GCMs) typically predict too little South Asian monsoon precipitation (Sperber et al., 2013; Bush et al., 2015). Projections in tropical rainfall and circulation remain uncertain in sign and magnitude (Knutti and Sedláček, 2013; Chadwick et al., 2013). The response of tropical rainfall to anthropogenic climate change depends on complex interactions and feedbacks between the large-scale flow, convection, and clouds (Voigt and Shaw, 2015; Voigt et al., 2016). For example, the radiative effect of clouds influences the intensity and structure of the Hadley circulation (section 2.4; Harrop and Hartmann, 2016; Popp and Silvers, 2017), hence, uncertainty in projected changes in clouds leads to uncertainty in projected circulation changes. The gap in understanding interactions between the large-scale flow, clouds, and convection has motivated the World Climate Research Program to launch a Grand Challenge on "clouds, circulation and climate sensitivity" (Bony et al., 2015).

Even when averaging simulated precipitation temporally and zonally, most coupled GCMs overestimate tropical precipitation (Fig. 1.4; Lin, 2007; De Szoeke and Xie, 2008). In the real world a single NH precipitation maximum is observed (Figs. 1.1 and 1.4), whilst in the majority of Coupled Model Intercomparison Project Phase 5 (CMIP5) models, two peaks in tropical precipitation are simulated: one in the NH and another in the SH (Fig. 1.4). This bias is commonly known as the "double ITCZ bias", a double ITCZ referring to two tropical precipitation maxima, and is associated with too much precipitation in the South Pacific Convergence Zone (SPCZ) and a rainfall band in each hemisphere across the Central and East Pacific (Lin, 2007; Hwang and Frierson, 2013; Oueslati and Bellon, 2015). As the double ITCZ bias remains in prescribed-SST atmosphere-only simulations and the bias in a coupled GCM can be predicted from the hemispheric asymmetry in net-downward surface energy flux in the corresponding atmosphere-only configuration, it is argued that atmospheric models are the dominant cause of the double ITCZ bias (Mobis and Stevens, 2012; Xiang et al., 2017).

Aquaplanet simulations provide an idealised modelling environment in which some complex boundary conditions in tropical circulation, such as land-sea contrasts and orography, are removed (Neale and Hoskins, 2001). In an aquaplanet the full dynamics and parameterisations of a climate

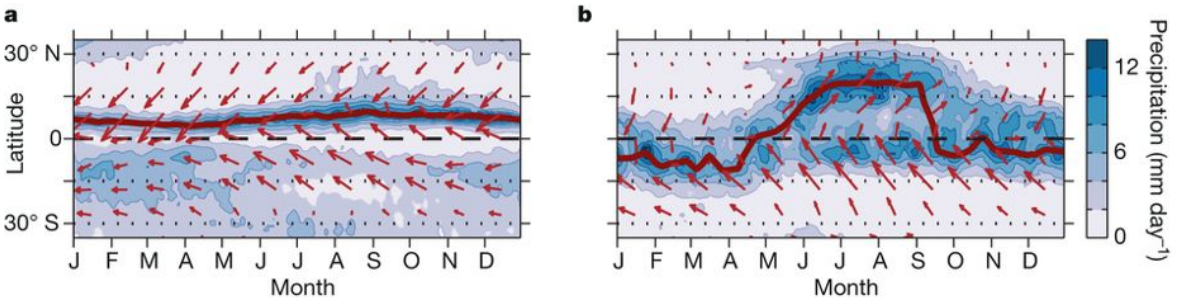

Figure 1.2: *Seasonal cycle of zonal-mean precipitation (filled, mm day^{-1}) and 10 m winds (red arrows, m s^{-1}) over the (a) Pacific (160°E to 100°W) and (b) South Asian monsoon (65°E to 95°E) regions. Red lines denote latitude of maximum precipitation. Daily precipitation and winds are taken from Tropical Rainfall Measuring Mission (TRMM) Multisatellite Precipitation Analysis and ECMWF Interim reanalysis respectively, for 1998 to 2012. To smooth the data temporally and spatially a rolling-mean of 11 days and 1° latitude is applied. The longest wind vector (in (b) at 18°S in September) corresponds to a wind speed of 9.1 m s^{-1}. Left and right arrow directions indicate westward and eastward wind components, respectively. Reproduced from Schneider et al. (2014).*

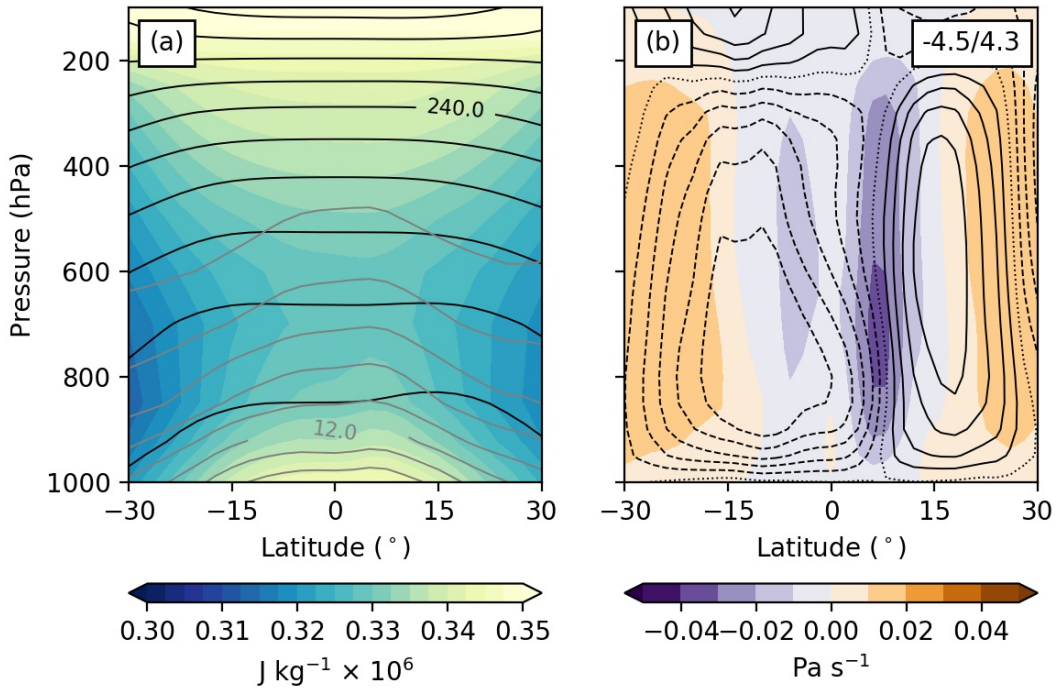

Figure 1.3: *NCEP (National Centers for Environmental Prediction) reanalysis 1979 to 2014 (Kalnay et al., 1996), zonal-mean, time-mean meridional cross sections of: (a) MSE (J kg^{-1} K^{-1}, filled), temperature (K, black contour lines) and specific humidity (g kg^{-1}, grey contour lines); (b) mass meridional streamfunction (kg s^{-1}, line contours) and vertical velocity (Pa s^{-1}, filled). In (a) intervals of 10K and 2 g kg^{-1} are used for temperature and specific humidity respectively. In (b) intervals of 1 × 10^{10} are used with dashed and dotted lines representing negative and zero values respectively. In (b) the maximum time-mean, zonal-mean magnitude of the mass meridional streamfunction in the SH and NH is printed in the top right-hand corner.*

model are retained, hence, aquaplanets bridge the gap between idealised dynamical core experiments with simplified representations of physical processes and climate simulations with continents and topography. An aquaplanet modelling configuration can be used to test hypotheses and to understand

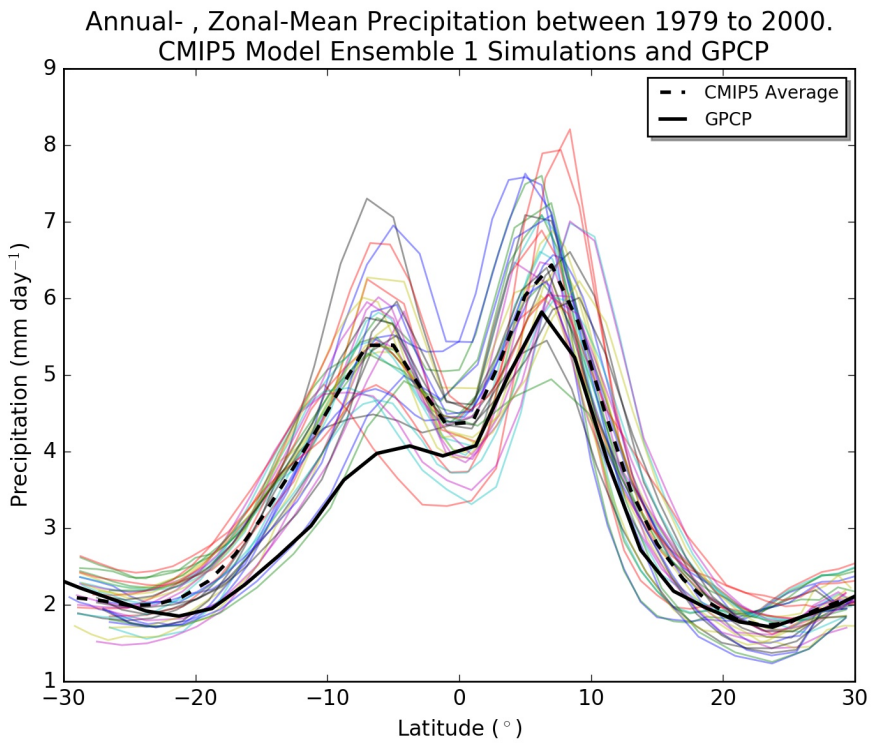

Figure 1.4: *Zonal-mean, time-mean tropical precipitation (mm day^{-1}) between 1979 and 2000 in GPCP (black solid line) and CMIP5 simulations (coloured lines). The CMIP5 average is denoted by the dashed black line.*

the interactions between atmospheric dynamics and parameterisations without the complexities introduced by land. Initial aquaplanet simulations represented the ocean surface with a set of idealised prescribed SSTs (Hess et al., 1993; Numaguti, 1995; Neale and Hoskins, 2001; Mobis and Stevens, 2012). Even in this configuration, a substantial inter-model variability of tropical precipitation is simulated; some GCMs simulate a single ITCZ and others a double ITCZ (Blackburn et al., 2013). The use of a zonally-uniform prescribed SST aquaplanet configuration has been to understand the sensitivity of the ITCZ to changes in model physics, dynamics and boundary conditions. Examples include changing model resolution (Williamson, 2008; Landu et al., 2014), changing the representation of convection (section 2.5), altering SSTs (section 2.3), changing the Coriolis force (Kirtman and Schneider, 2000; Chao and Chen, 2004), changing the representation of cloud radiation interactions (section 2.4), and changing insolation characteristics (section 2.3). More recent studies that employ aquaplanet simulations couple the atmosphere to a slab ocean with a prescribed ocean energy transport (OET) (e.g. Voigt et al., 2016; Wei and Bordoni, 2018). Doing so permits interactive SSTs and is energetically consistent. However, aquaplanet configurations of GCMs coupled to a slab ocean produce a broad range of tropical precipitation mean states (Voigt et al., 2016).

1.3 Objectives of this thesis

Through investigating the sensitivity of the simulated ITCZ to convective mixing in aquaplanets, this thesis aims to understand the mechanisms controlling ITCZ characteristics and support the development of climate models. GCM experiments show that tropical circulation is sensitive to convective parameterisation across a hierarchy of models (section 2.5; Mobis and Stevens, 2012; Song and Zhang, 2018). In particular, the technique used to parameterise convective mixing, the interaction between a convective parcel and the local environment, plays a substantial role in this sensitivity (section 2.5; Mobis and Stevens, 2012; Oueslati and Bellon, 2013). Whilst studies have explored the sensitivity of the ITCZ to convective mixing in coupled and atmosphere-only simulations with topography and land (Terray, 1998; Oueslati and Bellon, 2013; Bush et al., 2015), the mechanisms responsible for this sensitivity remain to be understood. Through deciphering the mechanisms responsible for the sensitivity of the ITCZ to convective mixing in aquaplanets, this study provides a greater insight of the processes responsible for the sensitivity in more complex GCMs. Previous studies also show that cloud-radiation interactions play a role in determining tropical circulation characteristics (section 2.4; Slingo and Slingo, 1988; Harrop and Hartmann, 2016). However, the role of cloud-radiation interactions in the sensitivity of the ITCZ to the representation of convection is yet to be explored. Hence, the first two objectives of this thesis are:

1. To understand the mechanisms responsible for the sensitivity of the ITCZ to convective mixing.
2. To isolate the role of cloud-radiation interactions in the sensitivity of the ITCZ to convective mixing.

Changing the idealised boundary conditions, such as the prescribed SSTs or insolation, influences ITCZ characteristics (section 2.3; Mobis and Stevens, 2012; Wei and Bordoni, 2018). The sensitivity of the ITCZ to an atmospheric forcing or parameterisation can vary temporally and spatially in atmosphere-only GCM experiments with topography and land (e.g. Oueslati and Bellon, 2013; Bush et al., 2015). Aquaplanet studies also show a sensitivity of the mean-state to SSTs and insolation (Hess et al., 1993; Wei and Bordoni, 2018). For example, changing from equinoctial to solstitial boundary conditions broadens and shifts the ITCZ poleward (Blackburn et al., 2013; Merlis et al., 2013). Due to the substantial sensitivity of the mean-state to the boundary conditions, the third objective is:

3. To determine the importance of the prescribed atmosphere boundary conditions for the sensitivity of the ITCZ to convective mixing.

To address the aforementioned objectives, atmosphere-only prescribed-SST aquaplanet simulations are employed (section 3.2). Whilst a prescribed-SST aquaplanet configuration is regularly used to

investigate climate dynamics (e.g. Hess et al., 1993; Neale and Hoskins, 2001; Mobis and Stevens, 2012), the use of fixed SSTs may overemphasise certain atmospheric processes that are less relevant in more realistic coupled model setups. For example, previous research shows that coupling the atmosphere to an ocean model with an interactive OET substantially reduces the sensitivity of the ITCZ to hemispherically asymmetric atmospheric forcing (section 2.6; Green and Marshall, 2017; Kang et al., 2018). The effect of coupling on the sensitivity of the ITCZ to the representation of convection remains to be determined. In light of this, the final objective of this thesis is:

4. To quantify the effect of atmosphere-ocean coupling on the sensitivity of the ITCZ to convective mixing.

To achieve this objective an idealised modelling framework is developed: the atmosphere is coupled to a two-layer ocean model with an interactive Ekman-driven OET (section 6.2.1). As previous studies show that OET plays a role in determining ITCZ characteristics (Green and Marshall, 2017; Kang et al., 2018), prescribed-OET simulations are also employed to understand the effect of interactive OET on the sensitivity of the ITCZ to convective mixing.

1.4 Outline of this thesis

Chapter 2 expands on this chapter by providing an overview of scientific background concerning the mechanisms that control Hadley circulation and ITCZ characteristics (sections 2.1 and 2.2, respectively). This is followed by a discussion of previous studies that have investigated the sensitivity of the ITCZ to the representation of convection (section 2.5) and boundary conditions (section 2.3). Sections 2.4 and 2.6 then discuss the role of cloud-radiation interactions and the impact of atmosphere-ocean coupling, respectively, in determining tropical circulation characteristics. Sections 2.1 to 2.6 motivate the objectives of this thesis (section 1.3), and section 2.7 concludes chapter 2 by highlighting the key points from previous research.

Chapter 3 describes the modelling environment used for experiments employed in this thesis. The Met Office Unified Model (MetUM) Global Atmosphere 6.0 (GA6.0) is introduced along with a brief description of performed sensitivity experiments. In this thesis two aquaplanet configurations are used: (1) an atmosphere-only configuration with zonally-symmetric prescribed SSTs (section 3.2) and (2) an idealised coupled configuration with the atmosphere coupled to a two-layer ocean model (section 3.3). Atmosphere-only, prescribed-SST simulations are employed to address objectives 1 to 3 in section 1.3. The design of the atmosphere-ocean coupled model permits an interactive OET; the fourth thesis objective (section 1.3) is addressed using this model configuration.

To improve understanding of the mechanisms that control ITCZ characteristics and address the first thesis objective (section 1.3), chapter 4 investigates the sensitivity of the ITCZ to convective mixing in prescribed-SST aquaplanet simulations. Section 4.3 discusses the sensitivity of the ITCZ to convective mixing, whilst section 4.4 isolates the role of cloud-radiation interactions in the sensitivity, addressing the second thesis objective (section 1.3), by employing simulations with prescribed cloud-radiation interactions. Work from chapter 4 including the mechanisms responsible for the sensitivity of the ITCZ to convective mixing and the role of cloud-radiation interactions has been published in the Journal of Climate (Talib et al., 2018). Enhancing work from chapter 4 and addressing the third thesis objective (section 1.3), chapter 5 explores the effect of the boundary conditions on the sensitivity of the ITCZ to convective mixing. The sensitivity of the ITCZ to convective mixing is investigated when using solstitial boundary conditions and compared with equinoctial simulations employed in chapter 4.

Coupling the atmosphere to an ocean with an interactive OET reduces the sensitivity of the ITCZ to hemispherically asymmetric forcing and atmospheric parameterisation (section 2.6; Oueslati and Bellon, 2013; Green and Marshall, 2017). To understand the effect of atmosphere-ocean coupling on the sensitivity of the ITCZ to convective mixing and address the fourth thesis objective (section 1.3), a two-layer ocean model is developed (sections 3.3, 6.2.1 and 6.2.2) and coupled to MetUM GA6.0. Section 6.3 describes the mean-state simulated using the coupled model and section 6.4 discusses the sensitivity of the ITCZ to convective mixing in coupled simulations. Coupling substantially changes the sensitivity of the ITCZ to convective mixing; to further understand the mechanisms responsible, prescribed-SST and prescribed-OET simulations are employed in section 6.5.

In chapter 7 a summary of key findings is presented. This includes summarising the progress made in achieving the thesis objectives (section 7.1), discussing the implications of the work presented (section 7.2), and summarising the limitations of this study and the avenues for future work (section 7.3).

Chapter 2

Scientific Background

The ITCZ plays an important role in the tropical hydrological cycle (chapter 1) and the Earth's energy and momentum budgets (section 2.2). This, as well as contemporary coupled and atmosphere-only GCMs poorly simulating the ITCZ (section 1.2), has motivated a plethora of studies to enhance understanding of the driving mechanisms of the tropical circulation. Whilst GCM experiments can be used to validate hypotheses, their complexity makes it challenging to understand the mechanisms controlling the tropical circulation. In light of this, several theoretical frameworks have been proposed to understand tropical circulation characteristics (sections 2.1 and 2.2; Held and Hou, 1980; Bischoff and Schneider, 2014). Modelling and observational studies show that sea surface temperatures (SSTs), insolation (Donohoe et al., 2013; Wei and Bordoni, 2018), and cloud-radiation interactions (Slingo and Slingo, 1988; Bony et al., 2015; Harrop and Hartmann, 2016) are key components of the climate system that control ITCZ characteristics (sections 2.3 and 2.4). In light of the substantial inter-model variability of ITCZ characteristics across a hierarchy of models (section 1.2; Lin, 2007; Blackburn et al., 2013; Voigt et al., 2016), GCM experiments have been performed to investigate the sensitivity of the simulated ITCZ to parameterisations and atmospheric forcing. The ITCZ is sensitive to the convective parameterisation (section 2.5; Terray, 1998; Song and Zhang, 2018) and the ability for the ocean to respond to atmospheric changes (section 2.6; Green and Marshall, 2017; Hawcroft et al., 2017).

To develop understanding of the mechanisms that control ITCZ characteristics, this thesis explores the sensitivity of the ITCZ to convective mixing. In this chapter a review of scientific literature motivating the objectives of this thesis (section 1.3) and supporting subsequent analysis (chapters 4 to 6) is presented. Sections 2.1 and 2.2 discuss theoretical frameworks that have been developed to understand Hadley circulation and ITCZ characteristics. Section 2.3 presents research showing a

sensitivity of the ITCZ to insolation and SSTs, whilst section 2.4 illustrates the role of cloud-radiation interactions in driving the mean tropical circulation. Sections 2.5 and 2.6 discuss the sensitivity of the tropical climate to the representation of convection and atmosphere-ocean interactions respectively. Section 2.7 closes the chapter with a summary of presented research.

2.1 Mechanisms controlling the Hadley circulation

To comprehend the processes that determine ITCZ characteristics requires an understanding of the mechanisms that drive the Hadley circulation. The simplest idealisation of the Hadley cell is a circulation that transports heat from the equator to the pole (Hadley, 1735) and removes tropical inertial instability (Plumb and Hou, 1992; Emanuel, 1995). However, a Hadley circulation is still observed in aquaplanet simulations with a perpetual, globally-uniform SST and solar forcing (Kirtman and Schneider, 2000) and angular momentum conservation prohibits the Hadley cell extending to the poles (Ferrel, 1856). To illustrate the influence of angular momentum, specific angular momentum (M_A, kg m^2 s^{-1}) is defined:

$$M_A = (\Omega a cos(\phi) + u) a cos(\phi) \tag{2.1}$$

where Ω denotes the planetary rotation rate (rad s^{-1}); a denotes the Earth's radius (m); u and ϕ denote the air parcel's zonal wind velocity (m s^{-1}) and latitude (degrees). Assuming at the equator the flow is weak and u equals zero, associated with equatorial ascent, then $M_A = \Omega a^2$. An angular-momentum conserving circulation would exhibit winds of (Vallis, 2017):

$$u = \Omega a \frac{sin^2(\phi)}{cos(\phi)} \tag{2.2}$$

Given the Earth's rotation rate, (2.2) implies zonal wind speeds of 32.2 m s^{-1} at 15° latitude, 134 m s^{-1} at 30° latitude, and 697 m s^{-1} at 60° latitude; angular momentum conservation predicts unrealistically large wind speeds at high latitudes. In a low Rossby number scenario ($Ro = \frac{u}{fL}$), surface winds and the mean meridional circulation are tightly related due to dominant terms in the near-surface zonal momentum equation (Held, 2018):

$$\frac{\partial(\rho u)}{\partial t} \approx \rho f v - \frac{\partial p}{\partial x} - \frac{\partial \mathcal{F}_x}{\partial z} \tag{2.3}$$

where $\mathcal{F}_x$ denotes the zonal surface stress (N m^{-2}); ρ denotes density (kg m^{-3}); f denotes the Coriolis parameter (rad s^{-1}); p denotes pressure (Pa); and v denotes the meridional wind (m s^{-1}). Taking a zonal-mean, time-mean and assuming that surface stresses only occur in the boundary layer gives,

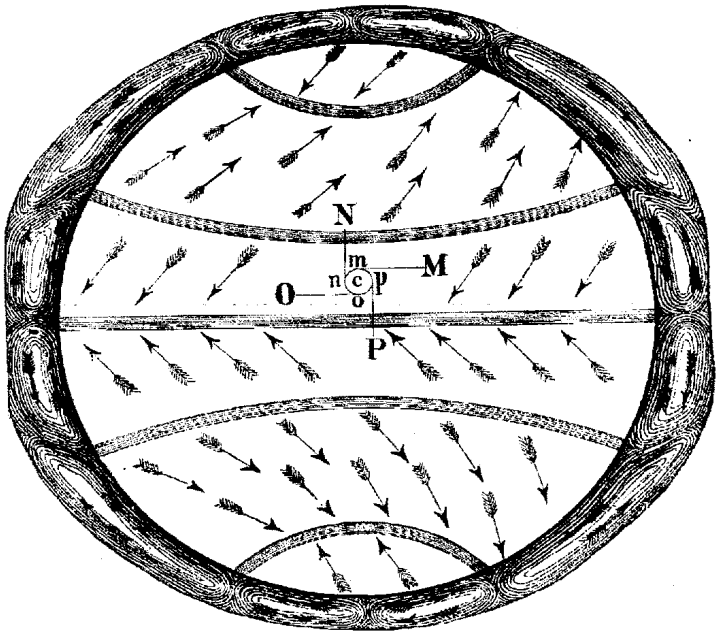

Figure 2.1: *A schematic of the general atmospheric circulation reproduced from Ferrel (1856). Arrows denote low-level wind and contours around the perimeter show the overturning circulations.*

$$f \int_0^{BL} [\overline{\rho v}] = -[\overline{\mathcal{F}_s}] \tag{2.4}$$

where BL denotes the top of the boundary layer; [ ] and — denote the zonal-mean and time-mean respectively. As long as the stress exerted by the surface onto the atmosphere is directed opposite to the mean surface wind, (2.4) shows that surface westerlies and easterlies correspond to a poleward and equatorward boundary-layer mass transport respectively. Even though f is small in the tropics, the length scale of the Hadley cell is large enough for a low Rossby number approximation. Hence, (2.4) associates surface tropical easterlies with an equatorward boundary-layer mass transport. Combining this knowledge with the association in (2.2) that as an air parcel moves to higher latitudes its zonal velocity must increase to ensure angular momentum conservation (2.2), studies associate the Hadley circulation edge to the location where the zonal wind changes from east to west (Ferrel, 1856; Del Genio and Suozzo, 1987; Walker and Schneider, 2006). GCM experiments show a sensitivity of the Hadley circulation to the planetary rotation rate (Del Genio and Suozzo, 1987; Walker and Schneider, 2006). Decreasing Ω increases the latitude at which the zonal wind changes from eastward to westward, thereby increasing the Hadley cell width and equator-to-pole heat flux, and decreasing the meridional temperature gradient. However, it is unlikely that angular momentum is the only factor influencing the Hadley circulation width. Angular momentum conservation diagnoses an unrealistic subtropical jet (Held, 2018) and takes no consideration of the energy imbalance between the tropics and sub-tropics.

Held and Hou (1980) develop an axisymmetric two-layer model that predicts Hadley circulation characteristics through combining angular momentum and energy conservation with thermal wind balance. Three assumptions are taken during model development:

1. The circulation is steady.
2. The upper branch of the Hadley circulation conserves angular momentum and friction weakens the equatorward flow in the lower branch.
3. The circulation is in thermal wind balance.

The meridionally varying top of the atmosphere (TOA) energy flux is associated with a latitudinal temperature contrast that drives the mean circulation. Held and Hou (1980) parameterise radiation as a relaxation towards a radiative-equilibrium potential temperature (θ_E, K) profile:

$$\frac{D\theta}{Dt} = \frac{\theta_E - \theta}{\tau} \tag{2.5}$$

where θ denotes the potential temperature (K); τ denotes the relaxation timescale (s); and subscript E denotes the radiative-equilibrium profile. θ_E is defined as $\theta_{E0} - \Delta\theta_E(sin^2(\phi))$ where θ_{E0} is the equatorial radiative-equilibrium potential temperature and $\Delta\theta_E$ is the equator-to-pole difference in radiative-equilibrium potential temperature. The flow in the upper-layer conserves M_A (2.1); the zonal wind is determined by (2.2). The upper-layer wind is also in thermal wind balance with the latitudinal temperature contrast in the bottom layer, hence:

$$f\frac{\partial u}{\partial z} = f\frac{u}{H_{HC}} = -\frac{g}{\theta_0}\frac{\partial \theta}{\partial y} \tag{2.6}$$

where $\frac{\partial u}{\partial z}$ is simplified to $\frac{u}{H_{HC}}$, and H_{HC} denotes the Hadley circulation height (m). Assuming small-angle approximation ($\sin\theta \approx \theta$), inserting (2.2) into (2.6) and integrating meridionally gives (Held and Hou, 1980):

$$\theta = \theta_0 - \frac{\Omega^2\theta_{E0}}{2ga^2H_{HC}}y^4 \tag{2.7}$$

where θ_0 is the equatorial potential temperature yet to be determined. Held and Hou (1980) then introduce two constraints: (1) the circulation is energetically closed and no energy is transported from the Hadley cell to higher latitudes; and (2) temperature is continuous poleward of the Hadley circulation associated with the atmosphere being in radiative equilibrium and the suppression of baroclinic instabilities. Using these two constraints, Held and Hou (1980) formulate a solution for θ_0 and conclude the following for the latitude of the Hadley circulation edge (ϕ_H, $^\circ$):

$$\phi_H = \left(\frac{5\Delta\theta_E g H_{HC}}{3\Omega^2\theta_{E0}}\right)^{\frac{1}{2}} \tag{2.8}$$

Using values on Earth, (2.8) predicts ϕ_H at approximately 27° latitude. (2.8) shows that the Hadley circulation width is proportional to the square root of the meridional radiative-equilibrium potential temperature gradient, and increasing Ω narrows the Hadley circulation width, in agreement with previously discussed GCM experiments (Del Genio and Suozzo, 1987; Walker and Schneider, 2006).

Associating the theoretical framework by Held and Hou (1980) to ITCZ characteristics, Vallis (2017) consider (2.5) at the equator and assume a balance between adiabatic cooling and radiative heating to determine the Hadley circulation strength:

$$w\frac{\partial\theta}{\partial z} \approx \frac{\theta_{E0} - \theta}{\tau} \tag{2.9}$$

where w is the vertical wind (m s^{-1}). If radiative forcing is the dominant cause of static instability, then the strength of the Hadley circulation can be determined by:

$$w \approx \frac{H_{HC}}{\theta_0\Delta_v}\frac{\theta_{E0} - \theta}{\tau} \tag{2.10}$$

where Δ_v is the temperature difference between the two layers. (2.10) reveals that ascent associated with the ITCZ depends on the Hadley circulation height, the vertical temperature gradient, and the equator-to-pole temperature gradient. For example, a greater meridional temperature gradient is associated with an intensified ITCZ.

Although Held and Hou (1980) provide insight into the controlling mechanisms of the Hadley circulation, there are several issues. First, (2.10) under predicts the strength of the Hadley circulation, which has been associated with the lack of turbulent eddies (Walker and Schneider, 2006), second, it is unrealistic to assume the Hadley circulation is energetically closed, and third, Held and Hou (1980) disregard the effect of moisture. To overcome these struggles several studies suggest a consideration of turbulent eddies (Eady, 1950; Held, 2001; Walker and Schneider, 2006). Turbulent eddies change the upper-level zonal wind at mid- to high-latitudes ($\geq 30°$ latitude) breaking the angular-momentum constraint (2.2). A change in zonal wind changes the meridional temperature gradient (2.6) and the Hadley circulation characteristics (2.8, 2.10). For example, decreased zonal wind is associated with a decreased meridional gradient in surface temperature (2.6) and a narrower, weaker Hadley circulation (2.8, 2.10). To understand the mechanisms driving the Hadley circulation a consideration of the energy and momentum budgets is required alongside processes poleward of the Hadley circulation.

2.2 Mechanisms controlling the ITCZ

A plethora of studies propose different mechanisms that control the ITCZ location; the majority argue that the ITCZ location is controlled by a balance between local surface evaporation and moisture convergence (Charney, 1971; Holton et al., 1971; Liu et al., 2010; Mobis and Stevens, 2012). Surface evaporation and tropospheric radiative cooling destabilise the tropical atmosphere and lead to convection which then causes tropospheric warming and low-level mass convergence (Charney, 1971). In the case of organised convection, the initial instability generates a feedback in which convection leads to stronger low-level mass convergence and convection intensification. Holton et al. (1971) expand on this idea by arguing that the zonal discontinuity of the ITCZ on daily timescales is associated with westward propagating wave disturbances controlling surface convergence and the location of deep convection. Liu et al. (2010) distinguish between the important mechanisms responsible for a single and double ITCZ; a single, equatorial ITCZ is maintained by moisture convergence whilst a double ITCZ is maintained by local surface evaporation. In a double ITCZ scenario, strong off-equatorial winds increase off-equatorial surface evaporation and convection (Liu et al., 2010); the double ITCZ is maintained through a wind-evaporation feedback. However, whilst it is generally agreed that the ITCZ location depends on moisture convergence and latent heating, discerning causality remains a challenge due to the strong positive feedback between the two factors.

To overcome the challenge of causality in the feedback loop between latent heating and moisture convergence, Neelin and Held (1987) use the vertically-integrated energy transport to eliminate zeroth-order balances in vertically-integrated temperature and moisture equations (Held, 2018). The energy transport associated with the mean circulation is equal to the difference in MSE transport between the upper and lower branches of the Hadley circulation (Fig. 2.2). The mass transports in the two branches must vertically conserve mass, hence, the MSE transport by the mean circulation is predominately controlled by the MSE difference in the two branches. This MSE difference is commonly referred to as “gross moist stability”. Gross moist stability is a fundamental metric that has been used to understand tropical circulation characteristics (Kang et al., 2009; Popp and Silvers, 2017; Wei and Bordoni, 2018). For example, Kang et al. (2009) use gross moist stability to predict the tropical circulation response to a hemispherically asymmetric extratropical thermal forcing.

Gross moist stability is just one example of using MSE to diagnose ITCZ characteristics. Several studies propose that the ITCZ is collocated where the zonal-mean meridional MSE flux equals zero

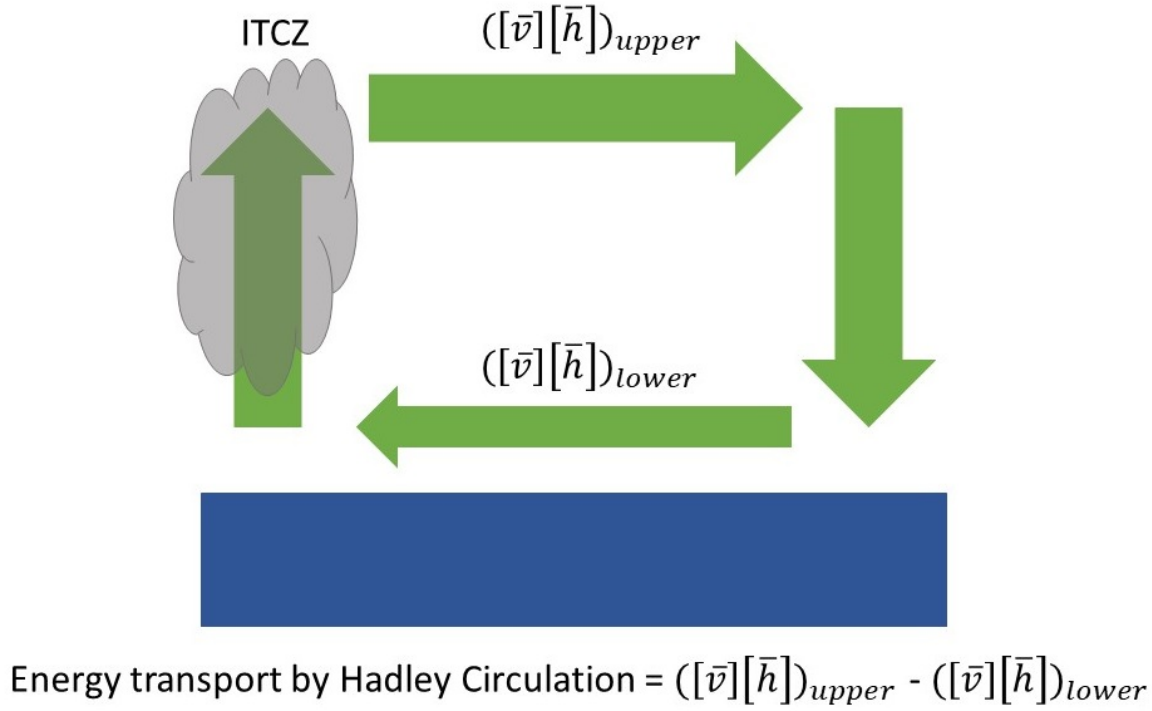

Figure 2.2: *A schematic showing the energy transports associated with the Hadley circulation. v and h denote meridional wind (m s^{-1}) and moist static energy (J kg^{-1}) respectively, whilst [ ] and ¯ denote zonal-mean and time-mean respectively.*

(Broccoli et al., 2006; Kang et al., 2008; Donohoe et al., 2013), whilst Bischoff and Schneider (2014) relate the ITCZ location to the atmospheric energy input (AEI), which equals the meridional divergence of MSE flux at equilibrium. AEI is the energy input into the atmosphere when considering surface and top of the atmosphere (TOA) energy budgets (later shown in equations 2.14 and 2.16). Mobis and Stevens (2012) propose that the ITCZ location is determined by the boundary-layer MSE as it plays a key role in convection intensity. If off-equatorial boundary-layer MSE is high enough, off-equatorial deep convection is initiated, decreasing equatorward winds and moisture flux at lower latitudes and favouring a double ITCZ (Liu et al., 2010; Mobis and Stevens, 2012). However, the required boundary-layer MSE needed for deep convection depends on free-tropospheric dry static energy (DSE; MSE without the contributions from latent energy) and atmospheric instability (Mobis and Stevens, 2012; Landu et al., 2014). Reduced free-tropospheric DSE increases atmospheric instability and encourages off-equatorial deep convection and a double ITCZ (Harrop and Hartmann, 2016).

Several studies illustrate a sensitivity of the ITCZ location to extratropical forcing (Chiang et al., 2003; Chiang and Bitz, 2005; Zhang and Delworth, 2005; Broccoli et al., 2006; Yoshimori and Broccoli, 2008). Chiang and Bitz (2005) find a substantial sensitivity of the ITCZ to NH sea ice coverage in slab-ocean simulations with a prescribed ocean energy transport (OET), whilst Zhang and Delworth (2005) and Broccoli et al. (2006) show the ITCZ is sensitive to freshwater

input into the North Atlantic Ocean due to a weaker thermally-driven ocean circulation that leads to hemispherically asymmetric temperature changes. Paleoclimate studies also associate ITCZ shifts with variations in extratropical climate (e.g. Wang et al., 2004). Whilst studies highlighted a sensitivity of the ITCZ to extra-tropical processes, a quantifiable relationship between the tropical circulation and extra-tropical processes was yet to be presented.

Kang et al. (2008) proposed that the ITCZ location is associated with the cross-equatorial atmospheric energy transport (AET) which is controlled by the inter-hemispheric AEI asymmetry. A northward ITCZ displacement from the equator is anti-correlated with a northward cross-equatorial AET, providing that the strength of the mass meridional overturning circulation increases with meridional distance from the ascending branch (Donohoe et al., 2013). Slab-ocean coupled simulations, employed to investigate the mean-state response to different radiative forcings, illustrate that cross-equatorial AET is controlled by the inter-hemispheric AEI difference and can be influenced by a various forcings including radiation (Kang et al., 2008, 2009; Yoshimori and Broccoli, 2009). Since Kang et al. (2008), the AEI framework has been used to understand sub-seasonal variability of the ITCZ location (Donohoe et al., 2013) and projected tropical circulation changes due to anthropogenic forcing (Frierson and Hwang, 2012). For example, Donohoe et al. (2013) find a strong correlation (R^2 value of approximately 0.99) between the ITCZ location and the monthly-averaged cross-equatorial AET between the years of 1981 to 2010 (Fig. 2.3a). Sub-seasonal variability of the ITCZ location is also strongly correlated (R^2 value of approximately 0.94) to the inter-hemispheric difference in mean tropical SST, however the difference in tropical SST lags the cross-equatorial AET and ITCZ location by approximately one month due to a lagged response between SST and the surface energy flux.

On the other hand, observational studies of ITCZ variability indicate that the ITCZ location is sensitive to the tropical SST gradient (Chiang et al., 2002, 2003; Koutavas and Lynch-Stieglitz, 2003; Rincón-Martínez et al., 2010). For example over the Pacific Ocean, substantial zonal and temporal differences in ITCZ characteristics are associated with SST differences. In the West Pacific during boreal winter, the ITCZ is broad and centered in the SH, whilst in the East Pacific, a weak narrow NH ITCZ is observed. Changes in the ITCZ location have also been associated with the El Niño-Southern Oscillation (ENSO, Bain et al., 2011; Berry and Reeder, 2014). During a strong positive ENSO event the ITCZ shifts southward (Bain et al., 2011). The sensitivity of the ITCZ to ENSO and tropical SST gradients cannot be easily explained by changes in the cross-equatorial AET as both are associated with hemispherically symmetric AEI changes. In light of this, Bischoff and Schneider (2014) develop an AEI framework to associate the ITCZ location to the equatorial AEI (AEI_0).

Bischoff and Schneider (2014) develop a quantitative, diagnostic framework that not only relates the ITCZ location to the cross-equatorial AET but also considers the equatorial AEI. The framework is developed from the zonal-mean atmospheric MSE budget (Neelin and Held, 1987):

$$[\overline{AEI}] = \partial_t[\overline{h_e}] + \partial_y[\widehat{\overline{vh}}] \tag{2.11}$$

where AEI is the AEI (W m^{-2}); vh is the meridional MSE flux (W m^{-1}), (v is meridional wind [m s^{-1}]; h is MSE [J kg^{-1}]); h_e is the moist enthalpy (J kg^{-1}); $[\quad]$, $\overline{\quad}$ and $\widehat{\quad}$ denote a zonal-mean, a time-mean and a mass-weighted vertical integral respectively; ∂_y is the meridional derivative; and ∂_t is the time derivative. Local Cartesian coordinates are printed with $y = a\phi^r$, where a is Earth's radius (m) and ϕ^r is latitude in radians, but all calculations are performed in spherical coordinates. The location where $[\widehat{\overline{vh}}]$ changes sign, and therefore is approximately zero, is commonly referred to as the "energy flux equator". Bischoff and Schneider (2014) assume that $[\widehat{\overline{vh}}]$ in the tropics is dominated by the zonal-mean circulation, such that, the energy flux equator and ITCZ are collocated. Through a first-order Taylor expansion of the equatorial $[\widehat{\overline{vh}}]$, Bischoff and Schneider (2014) show that the ITCZ location/energy flux equator (δ) depends on the equatorial MSE flux ($[\widehat{\overline{vh}}]_0$) and equatorial AEI ($[\overline{AEI}]_0$):

$$[\widehat{\overline{vh}}]_\delta = [\widehat{\overline{vh}}]_0 + a\partial_y[\widehat{\overline{vh}}]_0\delta \tag{2.12}$$

where subscripts 0 and δ denote the value at the equator and ITCZ respectively. Solving for δ and assuming $[\widehat{\overline{vh}}]_\delta \approx 0$:

$$\delta \approx -\frac{1}{a}\frac{[\widehat{\overline{vh}}]_0}{[\overline{AEI}]_0} \tag{2.13}$$

with AEI defined as:

$$[\overline{AEI}] = [\overline{S}] - [\overline{L}] - [\overline{O}] \tag{2.14}$$

where S is the net incoming shortwave radiative flux at the top of the atmosphere (TOA), L is the outgoing TOA longwave radiative flux, and O is the net-downward surface flux. However, (2.13) assumes the MSE flux associated with the mean circulation is increasing monotonically with latitude. When $[\overline{AEI}]_0$ is negative, $[\widehat{\overline{vh}}]$ is no longer increasing monotonically as an equatorward energy transport is required at low latitudes for equilibrium. In this scenario two energy flux equators are diagnosed. Bischoff and Schneider (2016) retain higher-order terms in the Taylor expansion to derive

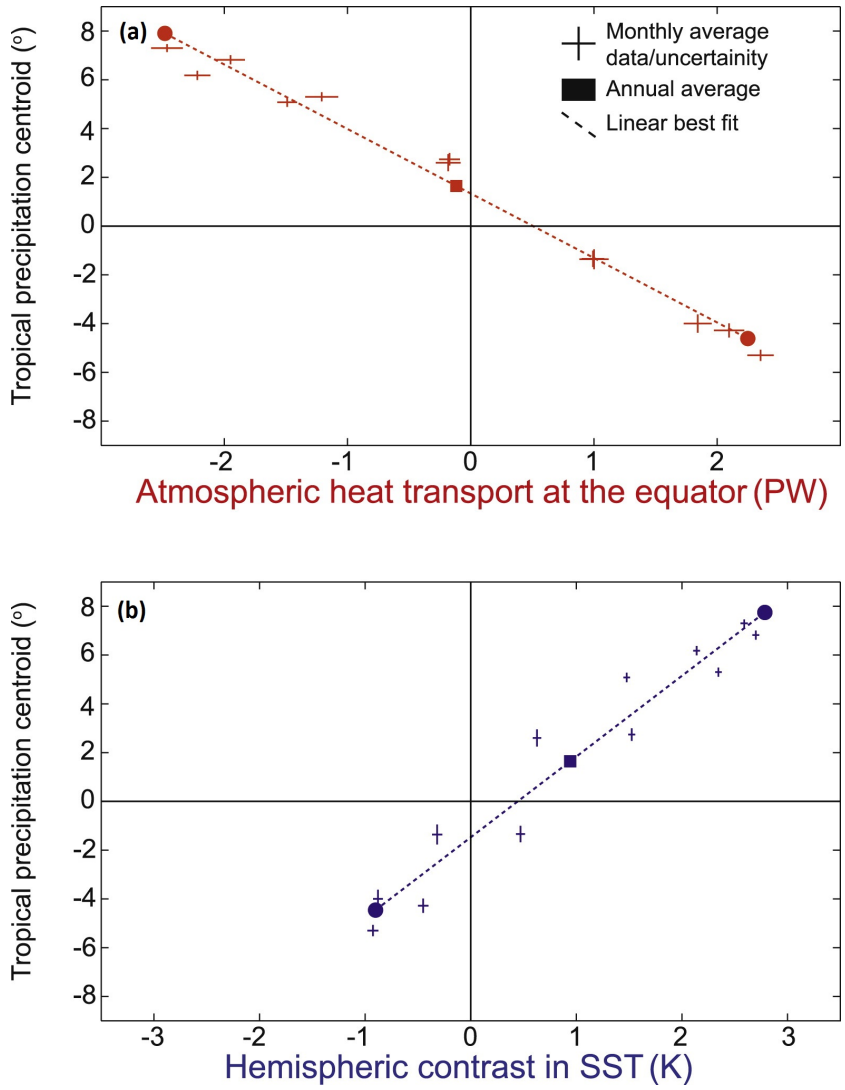

Figure 2.3: *Scatterplot of seasonal cycle of the tropical precipitation centroid (°) against (a) cross-equatorial AET (PW) and (b) interhemispheric tropical SST difference (K). Data is taken from 1981 to 2010. Each cross is centred on a monthly average; the length of the cross on each axis represents the 95% confidence interval assessed from the interannual variability. The filled box is the annual average and the dashed line is the linear best fit to monthly averages. Adapted from Donohoe et al. (2013); panel labels have been added.*

a framework for negative $[\overline{AEI}]_0$:

$$\delta \approx \pm\frac{1}{a}\left\{-\frac{6([\overline{AEI}])_0}{\partial_{yy}([\overline{AEI}])_0}\right\}^{\frac{1}{2}} + \frac{[\widehat{\overline{vh}}]_0}{2a([\overline{AEI}])_0} \tag{2.15}$$

Note (2.15) is from a corrigendum for the original paper.

Bischoff and Schneider (2014) explore the relationship derived in (2.13) using an idealised slab-ocean GCM with a prescribed OET. They investigate the effects of changing $[\overline{AEI}]_0$ and $[\widehat{\overline{vh}}]_0$ through changing the prescribed OET and atmospheric longwave absorption. Changing these components changes the tropical surface temperature and global-mean atmospheric temperature respectively. Increased $[\overline{AEI}]_0$ decreases the latitude of the ITCZ whilst increased $[\widehat{\overline{vh}}]_0$ increases the latitude of the ITCZ. Bischoff and Schneider (2016), using a slab-ocean GCM, change the tropical and

extra-tropical components of the prescribed OET. Increasing poleward OET in the tropics decreases $[\overline{AEI}]_0$. For double ITCZ scenarios, and if $[\widehat{\overline{vh}}]_0$ is negligible, decreasing $[\overline{AEI}]_0$ shifts the energy flux equators poleward. The diagnosed energy flux equators from (2.13) and (2.15) are collocated with the ITCZ in GCM simulations preformed by Bischoff and Schneider (2014) and Bischoff and Schneider (2016), highlighting an association between AEI and the ITCZ. The diagnostic framework has also been implemented to understand ITCZ variations in the real world; (2.13) captures the seasonal cycle of the zonal-mean ITCZ in reanalyses (Adam et al., 2016a).

However, Bischoff and Schneider (2014) define AEI from the perspective of slab-ocean simulations in which OET is prescribed (2.14). Prescribing OET fixes the net-downward surface energy flux (O) and only the TOA energy budget ($S - L$) is permitted to vary. As a result the response of surface energy budget components are limited and the role of surface-flux feedbacks in driving ITCZ characteristics is reduced. In this thesis prescribed-SST atmosphere-only simulations and slab-ocean simulations with an interactive OET are employed (chapter 3), hence changes in O may occur. As the surface energy budget can vary for the majority of simulations in this thesis, AEI is rewritten as:

$$[\overline{AEI}] = [\overline{SW}] + [\overline{LW}] + [\overline{H}] \tag{2.16}$$

where SW and LW denote the net atmospheric heating from shortwave and longwave radiation respectively, and H denotes the atmospheric heating from surface sensible and latent heat fluxes. From an AEI perspective, Mobis and Stevens (2012) severely constrain H in a subset of experiments by prescribing the surface winds when computing the surface fluxes. This reduces the sensitivity of the ITCZ to the convective parameterisation (section 2.5).

2.3 Sensitivity of tropical precipitation to insolation and sea surface temperature

SSTs and insolation are two key factors influencing the AEI; insolation affects the net-downward TOA SW radiative flux whilst SSTs play a key role in determining the surface radiative and turbulent fluxes, hence the AEI framework (Kang et al., 2009; Bischoff and Schneider, 2014) indicates a sensitivity of the ITCZ to these factors. Both observational (Oort and Rasmussen, 1970; Waliser and Graham, 1993; Halpern and Hung, 2001) and modelling (Hess et al., 1993; Wei and Bordoni, 2018) studies show a sensitivity of the ITCZ to SSTs. For example, the seasonal cycle of the zonal-mean ITCZ location is associated with changes in the location and intensity of the SST maximum (Waliser and Gautier, 1993; Wei and Bordoni, 2018). SSTs have also been associated with minimal equatorial convection over the central and eastern Pacific and Atlantic Oceans (Waliser and Graham, 1993).

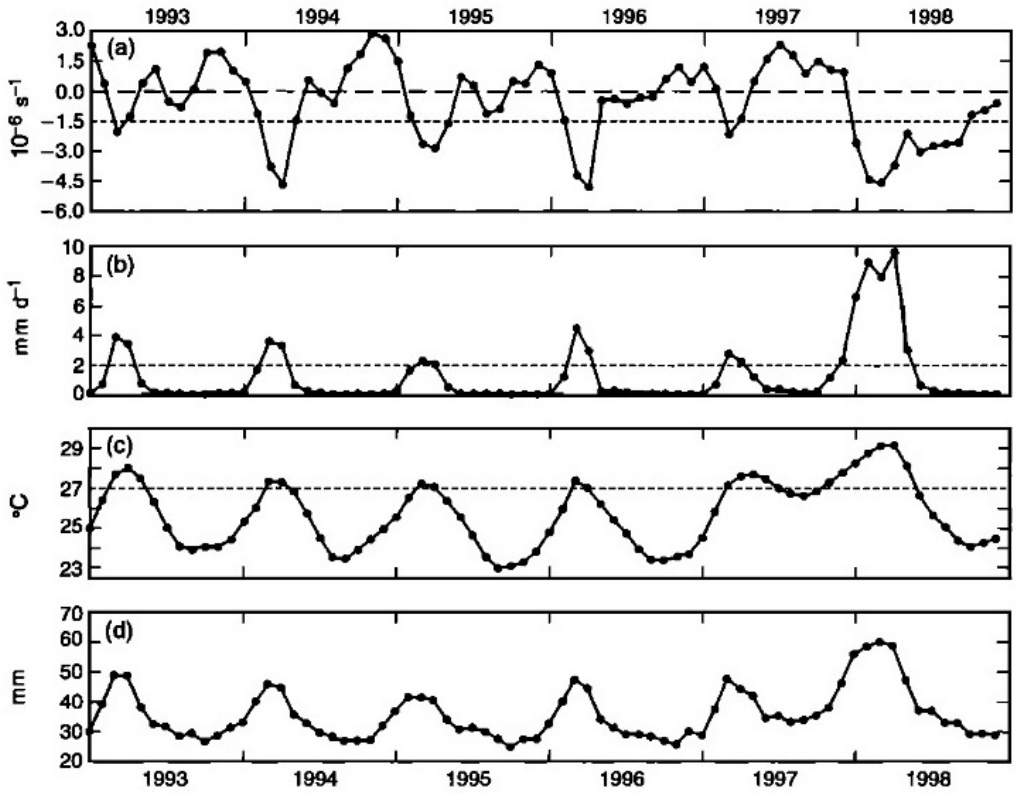

Figure 2.4: *Monthly-mean, regional-mean (a) surface wind divergence (s^{-1}), (b) precipitation (mm day^{-1}), (c) SST ($^{\circ}C$), and (d) column-integrated water vapour (mm) over the southeast Pacific Ocean (8°-2°S, 130°-90°W) during January 1993 to December 1998. In (a) dashed and dotted lines are used to denote zero divergence and a convergence threshold of 1.5 $\times$ 10^{-6} s^{-1} respectively. Dotted lines in (b) and (c) denote a rainfall threshold of 2 mm day^{-1} and where SST equals 27°C respectively. Reproduced from Halpern and Hung (2001).*

Equatorial upwelling, driven by the meridional Ekman-driven circulation (Schneider, 2018), reduces equatorial SSTs and increases the tendency of a double ITCZ (Waliser and Gautier, 1993). The increased tendency of the double ITCZ is associated with a reduced AEI_0 (section 2.2). Halpern and Hung (2001) illustrate an association between observed SSTs and precipitation over the southeast Pacific Ocean (8°-2°S, 130°-90°W) during 1993 to 1998. Annual maxima in precipitation and column-integrated water vapour are associated with the annual maximum SST and the annual minimum in mass divergence (Fig. 2.4). Increased precipitation across the region during the 1997/1998 El Niño event was associated with warmer than average SSTs during the months of peak precipitation (March and April) and the preceding six months.

Tropical precipitation biases in coupled GCMs have been associated with SST biases (Mechoso et al., 1995; Dai, 2006; De Szoeke and Xie, 2008; Oueslati and Bellon, 2015). Dai (2006) associate the double-ITCZ bias in coupled GCMs to a westward extension of the cold tongue over the tropical Pacific. De Szoeke and Xie (2008) show that in several CMIP3 simulations, biases in the seasonal cycle of the ITCZ location over the East Pacific are associated with SST biases. Bellucci et al. (2010) argue that the magnitude of the double-ITCZ bias in each coupled GCM simulation used for the

Intergovernmental Panel on Climate Change (IPCC) Fourth Assessment Report (AR4) is associated with the critical SST required for deep convection and the average SST in the southeast Pacific Ocean. A double ITCZ is favoured if the critical SST is colder than the average SST over the region.

There are two arguments that have been proposed to explain the sensitivity of the ITCZ to SSTs. First, Neelin and Held (1987) propose that SSTs play the dominant role in determining boundary-layer MSE and location of convection through surface fluxes. The ITCZ is typically observed close to the boundary-layer MSE maximum (Mobis and Stevens, 2012; Popp and Silvers, 2017) and therefore the factors that affect boundary-layer MSE also affect the ITCZ. Second, Lindzen and Nigam (1987) and Sobel (2007) propose that SST gradients drive the atmospheric circulation and moisture convergence, thus influencing ITCZ characteristics. Lindzen and Nigam (1987), through developing a one-layer model to represent the tropical boundary-layer, illustrate that convergence driven by observed surface temperatures is similar to the real world. However, the association between SSTs and the ITCZ cannot fully explain simulated precipitation in GCM experiments (Kirtman and Schneider, 2000; Bretherton et al., 2005; Mobis and Stevens, 2012). Prescribed-SST simulations show a sensitivity of the ITCZ to the representation of convection (section 2.5; Numaguti, 1995; Mobis and Stevens, 2012; Williamson et al., 2013) and convective aggregation occurs when using uniform SSTs (Kirtman and Schneider, 2000; Bretherton et al., 2005). Arguing that ITCZ characteristics are predominantly controlled by SSTs also disregards the argument that moisture convergence is partly driven by free-tropospheric convective heating (Charney and Eliassen, 1964; Charney, 1971; Bellon and Sobel, 2010; Liu et al., 2010) and that the ITCZ itself can affect the tropical circulation through cloud radiative effects (section 2.4).

Tropical SSTs depend on insolation, hence the Hadley circulation and ITCZ are sensitive to insolation across a hierarchy of models. Merlis et al. (2013) and Wei and Bordoni (2018) illustrate a sensitivity of the ITCZ to insolation in a coupled aquaplanet modelling configuration. When coupling an aquaplanet configuration of the Geophysical Fluid Dynamics Laboratory (GFDL) Atmosphere Model version 2 (AM2) to a slab-ocean, two hemispherically symmetric Hadley circulations are simulated given perpetual equinoctial insolation (Merlis et al., 2013). Given perpetual solstitial insolation, the Hadley circulation changes to a strong, thermally direct cross-equatorial cell in the winter hemisphere, accompanied by a cell in the summer hemisphere, associated with an off-equatorial ITCZ (Merlis et al., 2013; Wei and Bordoni, 2018). The change in tropical circulation structure is associated with SST changes (Merlis et al., 2013; Wei and Bordoni, 2018) and compliments conclusions reached by Lindzen and Hou (1988), who applied an asymmetric SST profile to the theoretical model developed by Held and Hou (1980); an off-equatorial SST maximum results in a strengthened cross-equatorial winter hemisphere cell and a precipitation peak in the summer

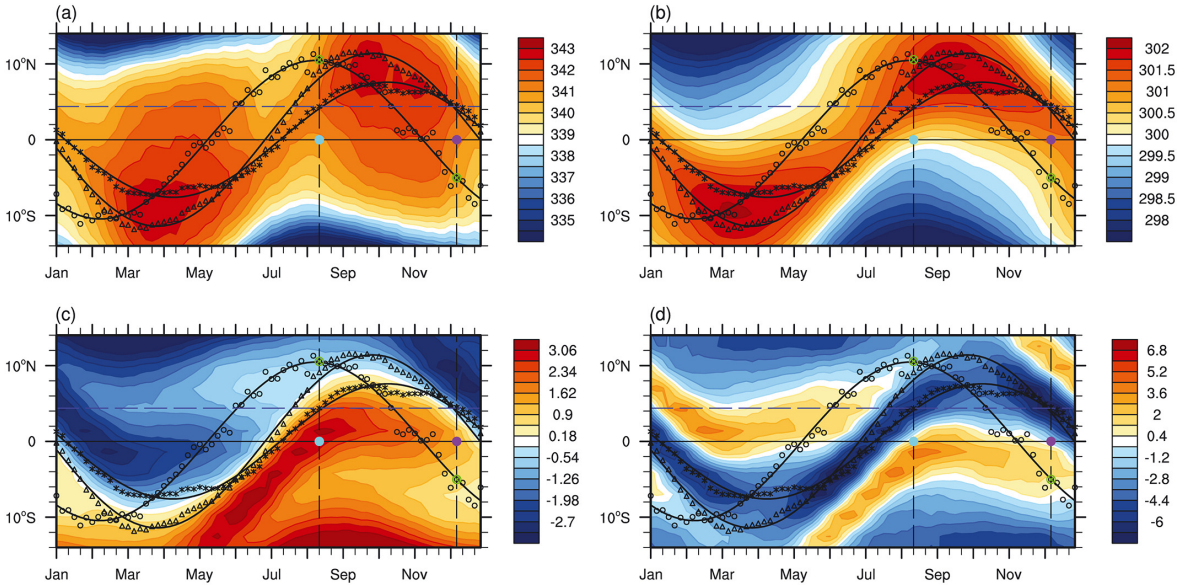

Figure 2.5: *Filled contours illustrate seasonal evolution of the zonal-mean (a) MSE (10^3 J kg^{-1}), (b) temperature (K), (c) meridional gradient of temperature (10^{-6}K m^{-1}), and (d) the meridional divergence of the temperature gradient (10^{-12} K m^{-2}) at the lowest model level from a 15-year AM2 aquaplanet simulation coupled to a slab-ocean with a seasonally-varying insolation. Open circles, open triangles and asterisks denote the pentad-average zonal-mean energy flux equator, location where the mass meridional streamfunction equals zero, and the location of the precipitation centroid (Frierson and Hwang, 2012) respectively. Solid thick black lines show their annual harmonics. Vertical black dashed lines indicate pentads 11 to 15 August and 6 to 10 December, respectively, which have the same ITCZ location, shown by the horizontal blue dashed line, but different energy flux equators, denoted by the crossed green circles. Cyan and purple dots denote the equator at the 11 to 15 August and the 6 to 10 December, respectively. The disparity between the ITCZ location and the energy flux equator during the 11 to 15 August and 6 to 10 December is discussed further in Wei and Bordoni (2018). Reproduced from Wei and Bordoni (2018).*

hemisphere Lindzen and Hou (1988). Wei and Bordoni (2018) illustrate an association between surface temperature and the ITCZ location through investigating the sensitivity of the ITCZ to the seasonal cycle of insolation in 15-year AM2 aquaplanet simulations coupled to a 20m slab-ocean. Surface temperatures play a role in the annual cycle of MSE across the deep tropics and influence the location of deep convection (Fig. 2.5; Neelin and Held, 1987; Wei and Bordoni, 2018); the ITCZ is collocated to the minimum of the divergence of the SST gradient (Fig. 2.5d). The constraint of surface thermodynamics on the ITCZ is associated with a phase lag between the seasonal cycle of the ITCZ location and the energy flux equator (comparing open circles and astericks in Fig 2.5). This phase lag illustrates a weakness in understanding the ITCZ from an AEI perspective (section 2.2; Kang et al., 2008; Donohoe et al., 2013; Bischoff and Schneider, 2014, 2016) and is discussed further in section 5.5.

In agreement with simulations coupled to a slab-ocean, prescribed-SST aquaplanet experiments show a sensitivity of the ITCZ to SSTs (Hess et al., 1993; Numaguti, 1995; Mobis and Stevens, 2012; Williamson et al., 2013). Decreasing the meridional SST gradient shifts the ITCZ poleward and favours a double ITCZ (Fig. 2.6; Hess et al., 1993; Mobis and Stevens, 2012). However, the

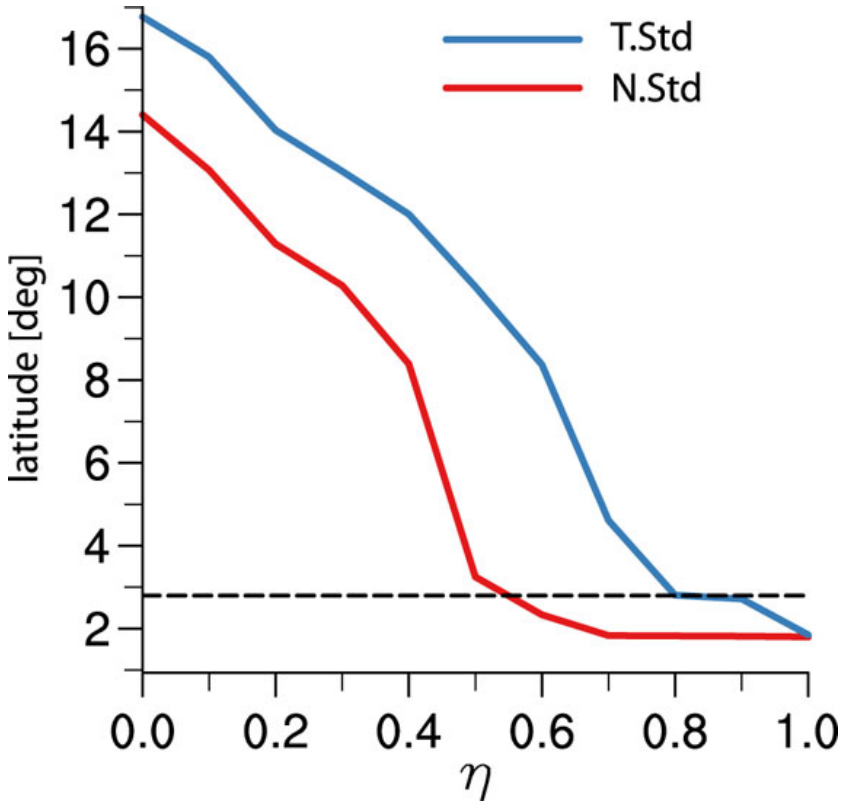

Figure 2.6: *Position of the ITCZ (°) in an aquaplanet configuration of the ECHAM6 GCM as a function of η given the Tiedtke (blue line) and Nordeng (red line) convective parameterisations. η describes the SST gradient; when η equals 0.5 the Qobs SST profile (equation 3.3) is prescribed. Decreasing η decreases the SST gradient, and increasing η increases the SST gradient. The horizontal dashed line marks the latitude where the double ITCZ merges into a single ITCZ. Reproduced from Mobis and Stevens (2012).*

sensitivity of the ITCZ to the SST gradient depends on the convective parameterisation (Fig. 2.6, section 2.5). Bellon and Sobel (2010) show a sensitivity of the ITCZ to the SST gradient when using a quasi-equilibrium tropical circulation model developed by Sobel and Neelin (2006). Decreasing the SST gradient increases the latitude at which the minimum boundary-layer MSE required for deep convection is achieved. The initiation of off-equatorial convection leads to free-tropospheric convective heating, which further amplifies off-equatorial convection (Charney, 1971; Bellon and Sobel, 2010), reduces the equatorward moisture flux and prohibits equatorial convection (Mobis and Stevens, 2012). Convective heating differences associated with different convective parameterisations results in a dependence of the sensitivity of the ITCZ to the SST gradient on the convective parameterisation (section 2.5).

As well as showing a sensitivity of the ITCZ to the SST gradient, studies also illustrate a sensitivity of the ITCZ to the location of the SST maximum (Hess et al., 1993; Numaguti, 1995; Williamson et al., 2013). Williamson et al. (2013) compare the ITCZ response when shifting Qobs (equation 3.3; Neale and Hoskins, 2001) northwards by 5° latitude in climate simulations by sixteen GCMs in an aquaplanet configuration. The ITCZ weakens, broadens, and shifts northwards in all models, associated with a strengthened cross-equatorial SH Hadley circulation. However, the ITCZ and

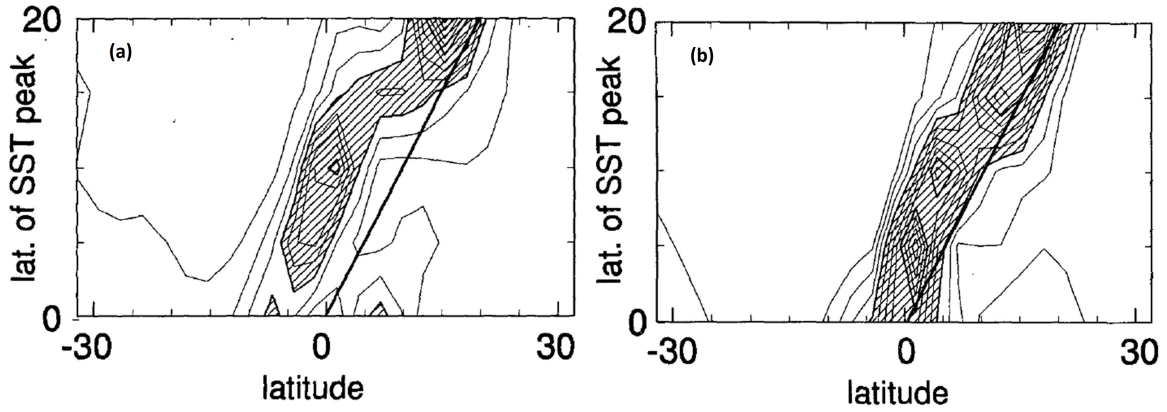

Figure 2.7: *(a) Zonal-mean, time-mean precipitation (W m^{-2}) as function of latitude of the prescribed SST maximum (°) from aquaplanet simulations using the Kuo (1974) convective parameterisation. Contour intervals of 50W m^{-2} (approximately 1.7 mm day^{-1}) with areas over 200 W m^{-2} (approximately 6.9 mm day^{-1}) shaded. (b) Same as (a) but for simulations with a fixed meridional wind speed in the computation of latent heat fluxes. Adapted from Numaguti (1995); combined figures 2 and 8 and added panel labels.*

SST maximum are not always collocated in the same hemisphere. For example, Numaguti (1995) perform a series of aquaplanet simulations using the Kuo (1974) convective parameterisation with SST maxima at 0°, 5°N, 10°N, 15°N, and 20°N. An NH ITCZ is found when the latitude of SST maximum is greater than 10°N, however, an SH and equatorial ITCZ are found given an SST maximum at 5°N and 10°N respectively (Fig. 2.7a). The SH ITCZ given an SST maximum at 5°N is associated with a negative AEI between 5°S and 5°N due to low surface winds and small latent heat fluxes (Numaguti, 1995). Negative AEI requires MSE convergence for equilibrium (Bischoff and Schneider, 2016), which in Numaguti (1995) is accomplished by the ITCZ being south of the equator. To illustrate the importance of latent heat flux on AEI and the ITCZ, Numaguti (1995) repeat simulations with the surface wind speed fixed in the computation of evaporation. Fixing the surface wind speed reduces the southward ITCZ shift given an SST maximum at 5°N (Fig. 2.7b), illustrating that surface-atmosphere interactions play an important role in determining the ITCZ location (Numaguti, 1995; Mobis and Stevens, 2012).

2.4 The role of cloud radiation interactions in determining tropical precipitation characteristics

Observing tropical clouds can reveal the dominating circulations. For example, deep cumulonimbus clouds highlight the Hadley and Walker circulations whilst low tropical clouds are a feature of subtropical anticyclones. However, not only are clouds markers for tropical circulation characteristics, but they also affect the circulation itself. Bony et al. (2015) summarise the interactions between the circulation and clouds into three categories: moisture phase changes; cloud-radiation interactions; and turbulent processes. Moisture phase changes, including condensation and evaporation, and

cloud-radiation interactions can lead to substantial temperature perturbations and affect circulation characteristics (Harrop and Hartmann, 2016; Kniffka et al., 2019). For example, free-tropospheric warming associated with deep convection can lead to intensified convection (Charney, 1971). Turbulent processes across a variety of scales can also affect the temperature distribution and large-scale atmospheric circulation (Birch et al., 2014). For example, cold pools associated with deep convection in the Sahara have been shown to initiate the formation of mesoscale circulations and change characteristics of the West African monsoon (Garcia-Carreras et al., 2013). This study focuses on the influence of cloud-radiation interactions in determining the tropical circulation mean-state.

Clouds not only affect radiative fluxes at the surface and TOA but also change radiative fluxes throughout the atmosphere. Most studies describe the "cloud radiative effect" (CRE) as the effect of clouds on the top of the atmosphere (TOA) energy budget, however in this study, CRE is defined as the AEI from cloudy-sky radiation. CRE is calculated using the difference between all-sky and clear-sky TOA and surface energy budgets:

$$\begin{aligned} CRE_{SW} &= (SW_{as}^{TOA} - SW_{as}^{SFC}) - (SW_{cls}^{TOA} - SW_{cls}^{SFC}) \\ CRE_{LW} &= (LW_{as}^{TOA} - LW_{as}^{SFC}) - (LW_{cls}^{TOA} - LW_{cls}^{SFC}) \\ CRE &= CRE_{SW} + CRE_{LW} \end{aligned} \tag{2.17}$$

where subscripts as and cls denote all-sky and clear-sky fluxes respectively; and superscripts TOA and SFC denote the net-downward TOA and surface flux respectively. CRE has a strong influence on tropical convection and Hadley circulation characteristics (Slingo and Slingo, 1988; Sherwood et al., 1994; Harrop and Hartmann, 2016). For example, CRE favours a single ITCZ in atmosphere-only experiments using various atmospheric models and model complexities (Li et al., 2015; Crueger and Stevens, 2015; Harrop and Hartmann, 2016; Popp and Silvers, 2017). The meridional gradient of CRE increases AEI across the tropics and decreases AEI across the extratropics (Allan, 2011), associated with an intensified Hadley circulation (Harrop and Hartmann, 2016; Popp and Silvers, 2017). As the ITCZ is typically found near the maximum boundary-layer MSE (Mobis and Stevens, 2012), Popp and Silvers (2017) propose that CRE increases MSE advection by the lower branches of the Hadley circulation and leads to an equatorward ITCZ contraction due to an equatorward shift of the boundary-layer MSE maxima. However, the mechanism proposed by Popp and Silvers (2017) is simply diagnostic. For example, a stronger mean circulation could increase low-level boundary-layer MSE in off-equatorial tropical latitudes, promoting off-equatorial deep convection and a double ITCZ. Popp and Silvers (2017) also disregard changes in mean atmospheric stability,

which have been shown to play a role in ITCZ characteristics (Numaguti, 1995; Oueslati and Bellon, 2013; Landu et al., 2014; Harrop and Hartmann, 2016). Harrop and Hartmann (2016) propose that longwave radiation absorption associated with deep convective clouds warms the free troposphere. The warmer free-troposphere increases atmospheric stability and the amount of MSE required for deep convection, promoting convection over warmer SSTs. Hence, in prescribed-SST aquaplanet simulations, convection occurs preferentially over warmer SSTs when including cloud-radiation interactions (Landu et al., 2014; Harrop and Hartmann, 2016; Popp and Silvers, 2017).

Whilst most recent studies conclude that the sensitivity of the ITCZ to CRE is controlled by free-tropospheric MSE (Oueslati and Bellon, 2013; Landu et al., 2014; Harrop and Hartmann, 2016), several studies highlight a sensitivity of tropical precipitation to low-level CRE (Fermepin and Bony, 2014; Dixit et al., 2018). For example, Fermepin and Bony (2014) find that low-level CRE increases tropical precipitation and intensifies the Hadley circulation in atmosphere-only simulations of IPSL-CM5A (Institute Pierre Simon Laplace Climate Model atmosphere-only version 5, Dufresne et al., 2013). Low-level CRE cools the sub-tropics (20° to 30°), increasing the AEI gradient across the tropics associated with an intensified Hadley circulation. Dixit et al. (2018) conclude that lower-tropospheric heating from upper-tropospheric deep tropical ($\pm 10^\circ$ latitude) clouds has the greatest effect on ITCZ characteristics. A shallow circulation in the lower troposphere is formed when removing cloud-radiation interactions throughout the entire troposphere or lower troposphere, leading to an anomalous import of MSE into the ITCZ region, increasing the required MSE export by deep convection and the ITCZ intensity. The larger sensitivity of the tropical circulation to low-level cloudy-sky heating compared to upper-level cloudy-sky heating in Dixit et al. (2018) is contradictory to the mechanism proposed by Harrop and Hartmann (2016). However, the vertical structure and intensity of CRE varies across models (Harrop and Hartmann, 2016), hence, the ITCZ response to removing CRE is model dependent.

Cloud-radiation interactions also play a substantial role in meridional ITCZ shifts (Voigt et al., 2014). Voigt et al. (2014) performed aquaplanet slab-ocean simulations using four atmospheric GCMs to investigate the role of CRE in the sensitivity of the ITCZ to hemispherically asymmetric albedo forcing. In the multi-model mean prescribing CRE reduced the ITCZ shift associated with hemispheric asymmetric albedo forcing. Fixing CRE and changing the albedo forcing from hemispherically symmetric to hemispherically asymmetric reduced the required cross-equatorial AET associated with a reduced ITCZ shift. However, a substantial inter-model spread in sign and magnitude was simulated. Variations in subtropical low clouds were mostly responsible for the inter-model spread. Studies also indicate that CRE is the dominant cause of inter-model spread in the response of tropical precipitation and circulation to surface warming (Voigt and Shaw, 2015; Oueslati et al., 2016). Voigt

and Shaw (2015) compared the precipitation response in aquaplanet configurations of MPI-ESM (Max Planck Institute for Meteorology Earth System Model, Stevens et al., 2013) and IPSL-CM5A to a 4K uniform surface warming from the Qobs profile (Neale and Hoskins, 2001). The models disagree on the response of tropical precipitation. In MPI-ESM the ITCZ narrows and intensifies by approximately 9 mm day^{-1}; in IPSL-CM5A, precipitation increases by approximately 1.5 mm day^{-1} across 15°S to 15°N. The disagreement amongst models is associated with the radiative response of tropical ice clouds (Voigt and Shaw, 2015). However, Fläschner et al. (2018) investigate the impact of CRE on the tropical circulation response to a 4K surface warming by analysing two sets of atmospheric GCMs in an aquaplanet configuration; one set with cloud-radiation interactions and the other without. The inter-model spread in the response of tropical circulation and precipitation is greater without CRE. Fläschner et al. (2018) conclude that the response of a shallow circulation that connects the subtropics and deep tropics plays a important role in changes of the inter-model spread when removing CRE.

The sensitivity of the tropical mean state to removing CRE is also associated with changes in tropical variability. Crueger and Stevens (2015) find a reduced MJO magnitude in four atmosphere-only GCM simulations when removing CRE. MJO initiation is favoured under low-level mean surface westerlies across the Indo-Pacific warm pool area (Zhang et al., 2006). Removing CRE favours a double ITCZ and weakens westerly winds over the Indo-Pacific region, reducing MJO amplitude (Crueger and Stevens, 2015). CRE has also been associated with intensified El Niño events and a weakening of the Walker circulation (Sherwood et al., 1994; Rädel et al., 2016). Rädel et al. (2016) performed two atmosphere-ocean coupled simulations using MPI-ESM, one with CRE and another without, and concluded that cloud-radiation interactions amplify the Bjerknes feedback mechanism (Bjerknes, 1969). During an El-Niño event positive SST anomalies in the central and eastern Pacific lead to a weakening of the Walker circulation, weakened easterlies in the west Pacific, and a reduced meridional thermocline tilt across the Pacific. Upper-tropospheric warming, associated with deep convection and positive SST anomalies, amplify the weakening of the Walker circulation and increase the magnitude of El-Niño events. However, Rädel et al. (2016) do not consider that weakened El-Niño events when removing CRE may be associated with mean tropical circulation changes. Removing CRE reduces equatorial convection (Li et al., 2015; Crueger and Stevens, 2015; Harrop and Hartmann, 2016; Popp and Silvers, 2017), hence, atmospheric warming associated with deep convection is less likely to weaken the Walker circulation and impact the magnitude of ENSO events.

2.5 Sensitivity of tropical precipitation to the representation of convection

As well as studies using GCMs to understand the driving mechanisms of the real world ITCZ, sensitivity experiments have been performed to understand the processes controlling the simulated ITCZ across a hierarchy of models. Understanding what controls the ITCZ in GCMs not only enhances knowledge of the processes controlling ITCZ characteristics but also supports model development. Fully-coupled GCM modelling studies show the ITCZ is sensitive to the convective parameterisation (Bacmeister et al., 2006; Zhang and Wang, 2006; Oueslati and Bellon, 2013; Bush et al., 2015; Song and Zhang, 2018). Song and Zhang (2018) demonstrate this sensitivity in two simulations of the National Center for Atmospheric Research Community Earth System Model version 1.2.1 (NCAR CESM 1.2.1) that take advantage of recent computational capabilities. Instead of representing one convective plume in a gridbox, a "spectral cloud model" that explicitly resolves all types of convective elements as a one-dimensional convective plume is implemented. Different convective elements are represented by changing a coefficient (C_E) between the lateral entrainment rate and buoyancy; a greater C_E value is associated with shallower convection. Both integrations were the same apart from alterations to the triggering and termination of convection and constraining the range of C_E used. In the original convection scheme the convective mass flux was determined by the amount of convective available potential energy (CAPE) calculated at the surface. In the updated scheme, CAPE is continuously calculated during parcel ascent and convection is terminated when CAPE is no longer diagnosed in the free-troposphere or when relative humidity is below 80% at the lifting condensation level. Song and Zhang (2018) also alter the spectral cloud model and predetermine the spectrum of cloud types. Through doing so, shallow convection and entrainment of dry, environmental air is increased. Altering the convective parameterisation has a substantial impact on the ITCZ; the double ITCZ bias is reduced, particularly over the East Pacific, and precipitation intensifies in convergence zones (Fig. 2.8). Work in this thesis, amongst others, aims to understand the mechanisms responsible for the sensitivity of the ITCZ to the convective parameterisation to understand the processes underlying tropical precipitation biases in GCMs (section 1.2).

A sensitivity of the ITCZ to the convective parameterisation is seen in prescribed-SST aquaplanet experiments (Hayashi and Sumi, 1986; Numaguti and Hayashi, 1991; Hess et al., 1993; Numaguti, 1995; Chao and Chen, 2004; Liu et al., 2010; Mobis and Stevens, 2012; Oueslati and Bellon, 2013), highlighting that to first order, the sensitivity is independent of land-surface effects. Aquaplanets provide a simplified framework to understand the effect of model parameterisation changes (section 1.2). Numaguti (1995) perform three aquaplanet simulations, each with a different convective parameterisation; the moist convective adjustment (MCA) scheme (Manabe et al., 1965), a modified Arakawa-Schubert scheme (Arakawa and Schubert, 1974) and the Kuo (1974) scheme. Each has

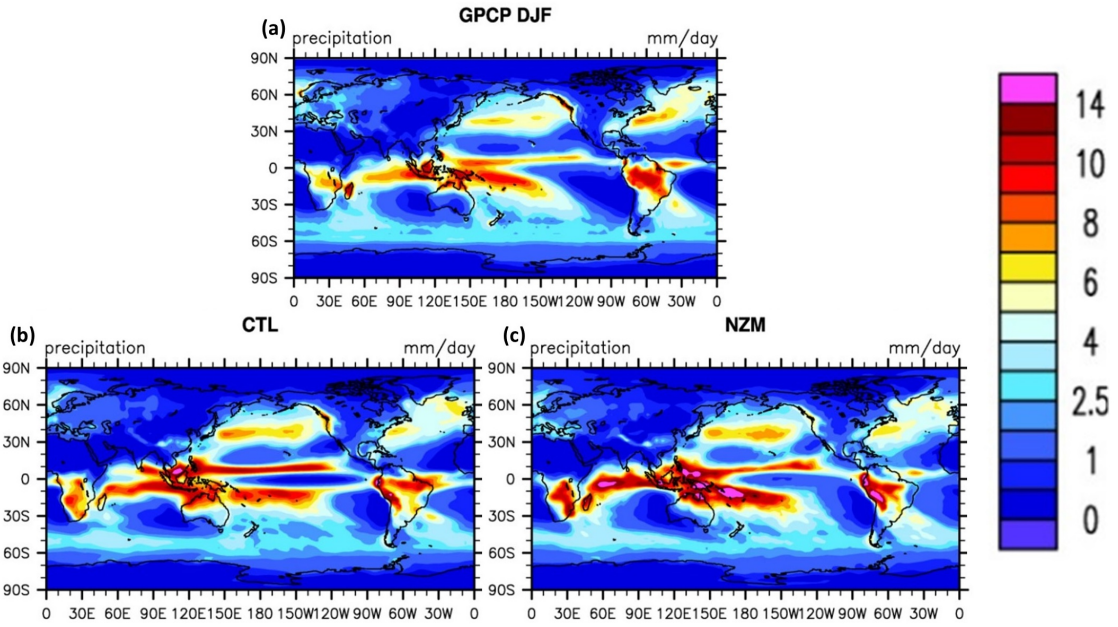

Figure 2.8: *December to February seasonal-mean precipitation (mm day^{-1}) in (a) GPCP between years 1979 to 2009, (b) and (c) 10-year integrations of the control and altered convective parameterisation in NCAR CESM1.2.1 respectively. The changes made to convective parameterisation are explained in section 2.5. Reproduced and adapted from Song and Zhang (2018); panel labels have been added.*

identical zonally uniform prescribed SSTs with an equatorial SST maximum. MCA produces a single ITCZ, whilst the Kuo and modified Arakawa-Schubert schemes produce a double ITCZ. The authors associate the sensitivity of the ITCZ structure to changes in the profile of convective heating. The Kuo and modified Arakawa-Schubert schemes simulate substantial convective heating throughout the free-troposphere, whilst convective heating for the MCA scheme, is restricted to the most unstable regions. The restriction of convective heating when using MCA prohibits deep convection poleward of the equatorial ITCZ. Changes in convective heating are associated with changes in the tropical circulation. Further studies also illustrate free-tropospheric characteristics play a key role in determining the ITCZ structure (Charney and Eliassen, 1964; Bellon and Sobel, 2010; Mobis and Stevens, 2012). However, the sensitivity of tropical precipitation to the convective parameterisation cannot be solely explained by processes in the free troposphere. Sumi (1992), who employed aquaplanet simulations using the Kuo (1974) and MCA schemes, show no sensitivity of the ITCZ to convective parameterisation. Sumi (1992) use a globally uniform prescribed SST, illustrating the importance of surface properties as studies that show a sensitivity of the ITCZ to convective parameterisation use meridionally-varying SSTs (Hess et al., 1993; Numaguti, 1995; Mobis and Stevens, 2012).

Tropical precipitation is not only sensitive to the choice of convective parameterisation, but also to individual processes in a convection scheme. A convective parcel interacts with its environment through “convective mixing”. Many studies conclude that the tropical mean state and variability is

sensitive to the representation of convective mixing (Bechtold et al., 2008; Oueslati and Bellon, 2013; Klingaman and Woolnough, 2014b; Bush et al., 2015). Convective mixing includes two processes: horizontal entrainment of typically drier, cooler air from the environment into the convective plume; and horizontal detrainment of typically warm, saturated air, associated with the convective plume, into the environment. The interaction in nature between a convective element and the environment is complex, but numerous convective parameterisation schemes, such as Tiedtke (1989) and Gregory and Rowntree (1990), treat convective mixing as a prescribed fractional mixing rate that depends primarily on height (de Rooy et al., 2013). An important component of parameterised convective mixing is the properties of entrained air, which are strongly related to height. The dominant height of entrained air is a disputed issue. Studies are divided on whether "lateral entrainment", cloud-air properties being continuously diluted during convective parcel ascent, or "organised entrainment", environmental air entrained at the cloud-top or cloud-base, plays the dominant role (de Rooy et al., 2013). Large-eddy simulations, those with resolutions between approximately 1 to 50m and that aim to resolve small-scale turbulent structures, show that lateral entrainment plays a greater role in shallow and deep convection compared to organised entrainment (Heus et al., 2008; de Rooy et al., 2013).

The complexity of parameterised convective mixing is variable across atmospheric models (de Rooy et al., 2013). In its simplest form entrainment (ϵ) can be formulated as:

$$\frac{1}{M}\frac{\partial M}{\partial z} = \epsilon \tag{2.18}$$

where M denotes the mass-flux (kg s^{-1}) and equals $\rho w_p a_p$ with w_p and a_p denoting the plume's velocity (m s^{-1}) and fractional area (m^2) respectively. However, large-eddy simulations illustrate a sensitivity of convective mixing to the cloud-layer depth (De Rooy and Siebesma, 2008) and environmental conditions (Derbyshire et al., 2004; Bechtold et al., 2008); both of which have not been regarded in (2.18). Several techniques have been proposed to account for environmental conditions in parameterised convective mixing. For example, Kain and Fritsch (1990) develop a buoyancy sorting regime and Bechtold et al. (2008) parameterise convective mixing so that it depends on relative humidity. However, both of these techniques fail to capture the variability in convective elements (de Rooy et al., 2013). More recent studies propose a stochastic approach to develop parameterised convective mixing (Sušelj et al., 2013); stochastic entrainment increases the variability of convective elements. The technique used to parameterise convective mixing in simulations employed in this thesis is discussed in section 3.1.

The influence of the environment on convection depends on the method used to parameterise con-

vective mixing. For example, increasing convective mixing increases the sensitivity of convection to environmental moisture (Klingaman and Woolnough, 2014b; Bush et al., 2015); increased convective mixing requires the environment to moisten or destabilise to maintain the same precipitation rate (Bush et al., 2015). Several studies show the ITCZ is sensitive to convective mixing across a hierarchy of models (Terray, 1998; Chikira, 2010; Mobis and Stevens, 2012; Oueslati and Bellon, 2013). Oueslati and Bellon (2013) investigate the sensitivity of the ITCZ to convective mixing in different configurations of the Centre National de Recherches Météorolqiques Coupled Global Climate Model version 5 (CNRM-CM5). Increased convective mixing reduces the systematic double ITCZ bias (section 1.2) in both atmosphere-only and coupled model configurations: the SH tropical rainfall band weakens and the precipitation bias associated with the SPCZ improves (Fig. 2.9). Increasing convective mixing also improves SH tropical precipitation in Terray (1998) and Chikira (2010). However, as shown in Song and Zhang (2018), enhanced entrainment overestimates precipitation in convergence zones (Fig. 2.9). Increased convective mixing suppresses convection in drier environments (Wang et al., 2007; Oueslati and Bellon, 2013; Klingaman and Woolnough, 2014b; Bush et al., 2015), increasing the moisture flux from subsidence zones into convergence regions (Terray, 1998; Oueslati and Bellon, 2013) and overestimating precipitation in convergence zones (Oueslati and Bellon, 2013).

The sensitivity of the ITCZ to convective mixing is also shown in prescribed-SST aquaplanet simulations: increasing convective mixing favours a single rather than double ITCZ (Mobis and Stevens, 2012; Oueslati and Bellon, 2013; Peatman et al., 2018). Oueslati and Bellon (2013) performed two prescribed-SST aquaplanet simulations using an idealised configuration of CNRM-CM5; control entrainment is doubled and halved. Doubling entrainment favours a single ITCZ. Through partitioning changes in the vertical pressure velocity probability distribution function into components of the dry static energy budget, Oueslati and Bellon (2013) conclude that changes in condensation, associated with deep convection, play the dominant role in large-scale circulation changes. Changes in latent heating, which depend on the convective parameterisation, lead to changes in low-level convergence, ascent and Hadley circulation characteristics (Numaguti, 1995; Oueslati and Bellon, 2013). Oueslati and Bellon (2013) also conclude that cloud-radiative feedbacks play a role in determining tropical circulation characteristics.

Whilst Numaguti (1995) and Oueslati and Bellon (2013) propose that changes in free-tropospheric convective heating play a substantial role in the sensitivity of the ITCZ to the representation of convection, Mobis and Stevens (2012) argue that changes in the boundary layer also play a substantial role in determining ITCZ characteristics. Mobis and Stevens (2012) perform two sets of simulations using an aquaplanet configuration of ECHAM6, the GCM developed by MPI. One set uses the Tiedtke (1989) convective parameterisation; and another set uses Nordeng (1994). In

Tiedtke (1989) the cloud base mass flux and organised entrainment are proportional to the moisture convergence. Organised detrainment occurs only at the cloud-top. Nordeng (1994) on the other hand, sets the cloud base mass flux using a quasi-equilibrium assumption for convective instability of the free-troposphere; integrated free-tropospheric buoyancy is relaxed to zero over a prescribed decay time, where buoyancy is related to the environmental lapse rate of DSE and the water vapour mixing ratio. Organised entrainment is based on the updraft buoyancy, whilst organised detrainment occurs above "the lowest possible organised detrainment level" (Mobis and Stevens, 2012). In general, Nordeng (1994) has greater convective mixing and the onset of convection is more stringent. Tiedtke (1989) produces a double ITCZ; Nordeng (1994) produces a single ITCZ. From observing that the ITCZ is located near the maximum boundary-layer MSE, Mobis and Stevens (2012) conclude that boundary-layer processes play a role in ITCZ characteristics. The MSE difference between the free troposphere and boundary layer determines the depth of convection; when the difference surpasses a threshold, dependent on the convective parameterisation, deep convection is initiated. Off-equatorial convection reduces equatorward low-level winds, decreasing equatorial evaporation, MSE and convection. Off-equatorial convection and reduced equatorward winds are also effective at lowering the maximum tropical boundary-layer MSE, leading to free-tropospheric cooling and an intensification of off-equatorial convection (Mobis and Stevens, 2012). The role of boundary-layer MSE is further emphasised by a minimal sensitivity of the ITCZ to the representation of convection in simulations where the surface wind speed is prescribed in the calculation of surface fluxes (Numaguti, 1995; Mobis and Stevens, 2012).

Along with a sensitivity of the tropical mean state to convective mixing, tropical variability and the climatic response to anthropogenic greenhouse gas release is also sensitive to convective mixing (Hirons et al., 2013; Klingaman and Woolnough, 2014b; Sherwood et al., 2014). Increasing convective mixing in an atmosphere-only configuration of the UK Met Office Hadley Centre Global Environment Model version 3 (HadGEM3) improves the strength, persistence and propagation of the MJO (Klingaman and Woolnough, 2014b). Increased convective mixing suppresses precipitation in drier environments and delays convection onset; greater low-level MSE is required to overcome decreased buoyancy associated with greater convective mixing. The delay of convection leads to greater accumulations of moisture and MSE anomalies and intensifies the active MJO (Hirons et al., 2013; Klingaman and Woolnough, 2014b). The same MJO response is observed when increasing the dependence of parameterised convection on environmental moisture by other methods (Bechtold et al., 2008; Hannah and Maloney, 2011; Benedict et al., 2013). The delayed onset of convection associated with increased convective mixing also improves the diurnal cycle of tropical precipitation; the onset of deep convection is delayed and the diurnal amplitude of precipitation over land is reduced (Wang et al., 2007; Hohenegger and Stevens, 2013). However, increasing

convective mixing also has negative impacts. For example, whilst Bush et al. (2015) find that increasing convective mixing in HadGEM3 GA2.0 reduces several Asian summer monsoon biases, in particular over the Western Equatorial Indian Ocean, overall the amplitude and spatial pattern of the South-East Asian monsoon is degraded. Klingaman and Woolnough (2014b) also find that increased convective mixing amplifies a cold bias in the tropical upper-troposphere due to a shallowing of deep convection. The sensitivity of the climate system to convective mixing also affects the uncertainty in anthropogenic climate change projections. Sherwood et al. (2014) show that approximately 50% of the spread in equilibrium climate sensitivity, the change in global mean temperature given a doubling of atmospheric carbon dioxide, amongst CMIP3 and CMIP5 models is associated with the difference in convective mixing between the lower and mid-troposphere. Greater convective mixing is simulated in the mid-troposphere compared to the lower-troposphere associated with low-level drying. As the atmosphere warms this difference in convective mixing increases, associated with a drier lower-troposphere, reduced low-level cloud cover, increased surface absorption of shortwave radiation, and surface warming. The rate at which the difference in convective mixing between the lower- and mid-troposphere increases is dependent on the rates simulated during preindustrial conditions, leading to a inter-model variability in equilibrium climate sensitivity.

2.6 The effect of coupling on the sensitivities of the ITCZ

Many studies have investigated the sensitivity of the ITCZ to a change in atmospheric forcing or parameterisation using prescribed-SST atmosphere-only simulations (e.g. Hess et al., 1993; Numaguti, 1995; Hoskins et al., 1999; Mobis and Stevens, 2012; Oueslati and Bellon, 2013). However, recent research has highlighted that not only are prescribed-SSTs energetically inconsistent, but they also disregard the effect of oceanic feedbacks. Oceanic processes play a key role in determining tropical atmosphere characteristics (e.g. Oueslati and Bellon, 2013; Green and Marshall, 2017; Schneider, 2018; Kang et al., 2018). Oueslati and Bellon (2013) show a reduced sensitivity of the ITCZ to convective mixing in an atmosphere-ocean coupled configuration of CNRM-CM5 compared to atmosphere-only experiments (Fig. 2.9). For example, boreal summer precipitation is more sensitive to convective mixing in an atmosphere-only configuration than in a coupled configuration (comparing Fig. 2.9c and f).

Idealised atmosphere-ocean coupled simulations show a sensitivity of the ITCZ to atmosphere-ocean interactions (Pike, 1971; Codron, 2012). Pike (1971) and Codron (2012) couple a two-layer numerical model of the tropical ocean, which resolves the Ekman-driven ocean circulation, to a zonally symmetric tropical atmosphere. The details of the Ekman-driven ocean circulation simulated

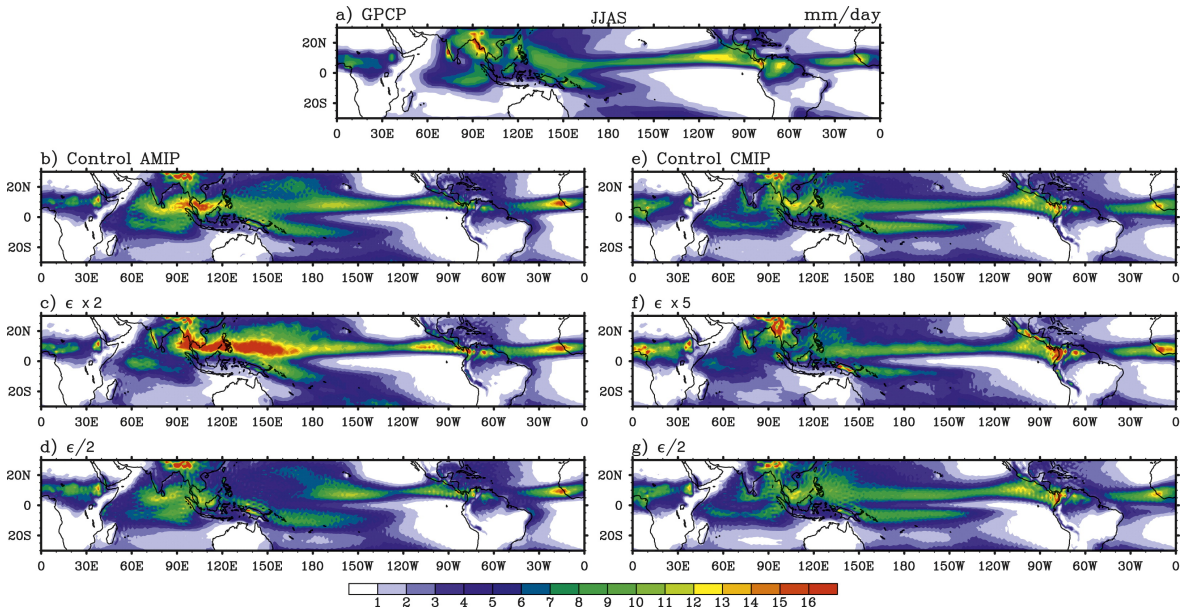

Figure 2.9: *The 1979 to 1999 seasonal-mean (June to September) precipitation (mm day^{-1}) from (a) GPCP, (b and d) atmosphere-only and (e and g) atmosphere-ocean coupled simulations of CNRM-CM5. Simulations employing default convective mixing are shown in (b) and (e), whilst (c) and (f) show the model output when convective mixing is multiplied by 2.0 and 5.0 respectively, and (d) and (g) when convective mixing is halved. Reproduced from Oueslati and Bellon (2013).*

is discussed in section 6.1. Pike (1971) and Codron (2012) both find that the surface mass divergence associated with the Ekman-driven circulation leads to equatorial upwelling, reduced equatorial SSTs, and a favouring of off-equatorial convection. The ITCZ is attracted towards the SST maximum due to increased boundary-layer MSE (Pike, 1971; Numaguti, 1995; Mobis and Stevens, 2012). As the ITCZ is typically located near the MSE maximum (Sobel and Neelin, 2006; Mobis and Stevens, 2012; Popp and Silvers, 2017), and the meridional Ekman-driven surface current has greater energy than the return flow in the deep layer (Codron, 2012; Schneider, 2018), the Ekman-driven ocean circulation transports energy from the ITCZ towards the sub-tropics. The energy transport associated with the Ekman-driven circulation has been associated with a reduced sensitivity of the ITCZ to hemispherically asymmetric atmospheric forcing (Kay et al., 2016; Tomas et al., 2016; Hawcroft et al., 2017; Green and Marshall, 2017). Green and Marshall (2017) impose a hemispherically asymmetric albedo profile in two configurations of a coupled atmosphere-ocean version of the MIT GCM. In one configuration the ocean is represented by a full dynamical ocean model; whilst in the other, the ocean is represented by a slab with prescribed OET computed from a simulation with a full dynamical ocean and hemispherically symmetric albedo. The hemispherically asymmetric albedo profile is associated with a northward ITCZ shift: the asymmetric profile increases and decreases surface albedo in SH and NH respectively, introducing an inter-hemispheric AEI asymmetry requiring a southward cross-equatorial AET associated with a NH ITCZ (section 2.2; Kang et al., 2008; Schneider et al., 2014). The meridional ITCZ shift associated with a hemispherically asymmetric albedo profile is four times smaller when the ocean is coupled to a full dynamical ocean compared to

a slab (Fig. 2.10a). In the simulation with the full dynamical ocean, the ocean circulation responds to the inter-hemispheric AEI difference, introducing a cross-equatorial oceanic energy flux and reducing the cross-equatorial AET and ITCZ shift (Fig. 2.10b).

Tomas et al. (2016) show the importance of atmosphere-ocean interactions on the sensitivity of the tropical atmosphere to hemispherically asymmetric forcing through investigating the sensitivity of the ITCZ to twenty-first century projected Arctic sea ice loss. They perform two sets of simulations using the Community Atmosphere Model version 4 (CAM4): first, a configuration where the atmosphere is coupled to a full dynamical ocean model, the Parallel Ocean Program version 2 (POP2); and second, a configuration where the atmosphere is coupled to a slab with a prescribed OET. Under each configuration two simulations are performed, the only difference being a change in the representation of sea ice conditions from those of the late twentieth century (1980-99) to those of the late twenty-first century (2080-99). The sea ice conditions are taken from a Community Climate System Model version 4 (CCSM4) simulation with historical and representation concentration pathway 8.5 (RCP8.5) radiative forcing. Values for the prescribed OET in the slab are taken from the fully coupled configuration with twentieth-century Arctic sea ice. The sensitivity of tropical precipitation to projected Arctic sea ice loss is much greater when coupling the atmosphere to a slab compared to coupling to a full dynamical ocean model (Fig. 2.11a,b). In the latter, hemispherically symmetric warming at high-latitudes and the equator is accompanied by an equatorially contracted and intensified ITCZ. Coupling to a slab on the other hand, leads to substantial asymmetric warming in high latitudes and a northward ITCZ shift (Fig. 2.11b). Coupling the atmosphere to a dynamical ocean enables both the AET and OET to respond to changes in forcing. Changing the sea-ice conditions reduces northward OET in the model configuration with a full dynamical ocean associated with a decreased change in AET and ITCZ location. Tomas et al. (2016) and Green and Marshall (2017) reveal that the sensitivity of the ITCZ to hemispherically asymmetric atmospheric forcing seen in GCM experiments with a slab ocean (Kang et al., 2008; Frierson and Hwang, 2012; Voigt et al., 2014) may be substantially damped when coupling the atmosphere to a dynamical ocean.

The effect of atmosphere-ocean coupling on the sensitivity of the ITCZ to hemispherically asymmetric forcing has changed perspectives on the mechanisms responsible for the double-ITCZ bias (section 1.2; Lin, 2007). Hwang and Frierson (2013) propose that the double-ITCZ bias in coupled GCMs is associated with too much surface absorption of solar radiation over the Southern Ocean; which is predominantly due to insufficient cloud optical depth around extratropical cyclones (Kay et al., 2016; Hawcroft et al., 2017). Reducing solar radiation surface absorption over the Southern Ocean was hypothesised to cool the SH, decrease northward cross-equatorial AET, and shift the

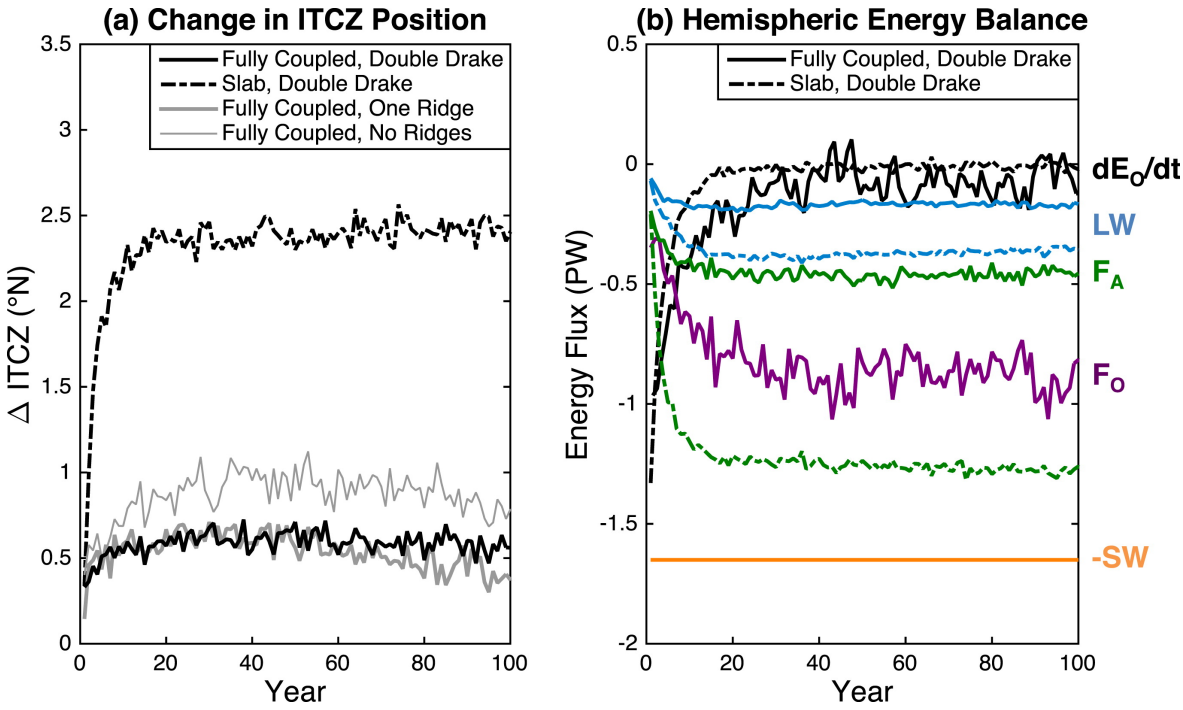

Figure 2.10: *Evolution of (a) ITCZ location and (b) cross-equatorial energy transport associated with shortwave radiation (orange), longwave radiation (blue), atmospheric energy flux (green) and oceanic energy flux (purple) when introducing a hemispherically asymmetric albedo profile. Solid and dashed lines denote solid and passive simulations respectively. Changes to the ocean basin geometry were also performed, discussed further in Green and Marshall (2017), and the response of the ITCZ in these simulations is denoted in (a) by grey lines. Reproduced from Green and Marshall (2017).*

ITCZ northwards (Hwang and Frierson, 2013). Kay et al. (2016) performed a series of CAM version 5 (CAM5) simulations to investigate the effect of solar radiation surface absorption biases in coupled GCMs on tropical precipitation characteristics. Through decreasing the temperature at which shallow convection detrains ice rather than liquid, thereby increasing supercooled cloud liquid, Kay et al. (2016) increase cloud albedo over the Southern Ocean. Increasing cloud albedo reduces the total northward cross-equatorial energy transport, however in coupled simulations, the ocean is responsible for 80% of the reduced transport. As a result, AET and tropical precipitation hardly changes. Kay et al. (2016) also perform simulations where the ocean model is represented by a slab with a prescribed OET. Through comparing the atmospheric response to increased cloud albedo over the Southern Ocean in both configurations, Kay et al. (2016) show that the sensitivity of the ITCZ to hemispherically asymmetric albedo changes is substantially greater when prescribing OET. Hawcroft et al. (2017), who increase SH mean albedo through adjustments in stratospheric optical depth, ocean albedo and cloud droplet number in HadGEM2-ES (Collins et al., 2011), also conclude that coupling the atmosphere to a full dynamical ocean reduces the sensitivity of the ITCZ to hemispherically asymmetric albedo changes. Understanding the sensitivity of the tropical atmosphere to a hemispherically asymmetric atmospheric forcing requires an ocean model with a prognostic OET.

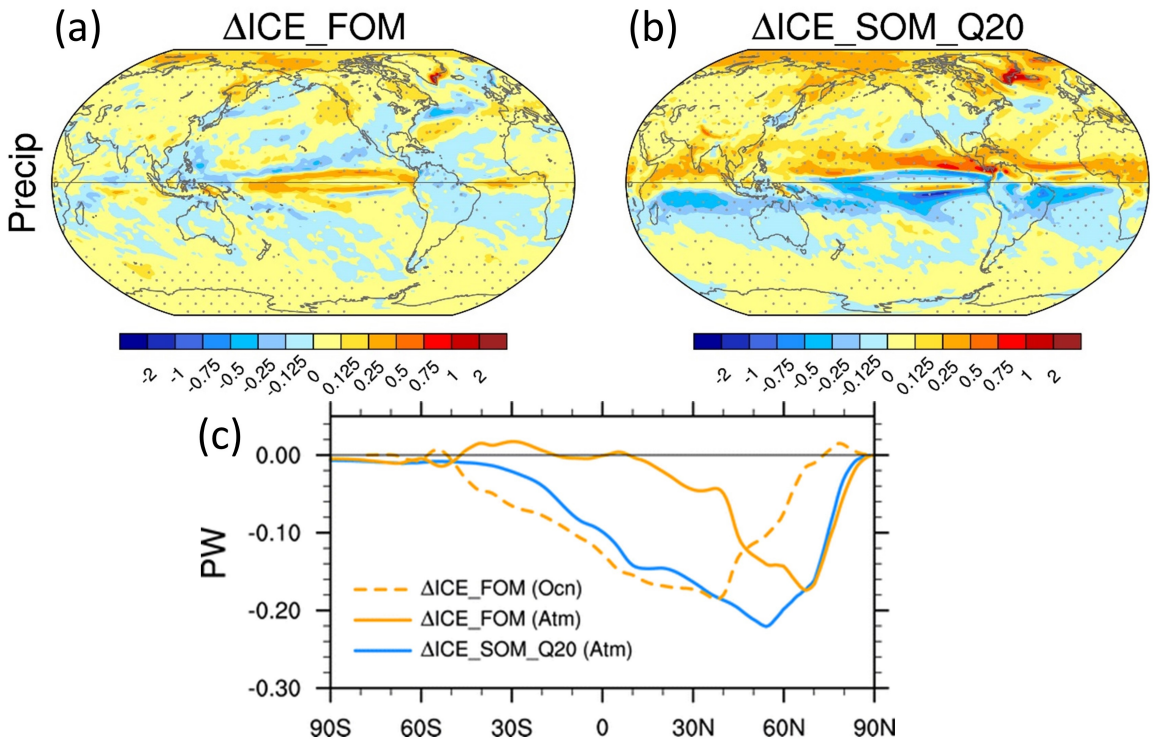

Figure 2.11: *Precipitation change (mm day^{-1}) when changing the representation of Arctic sea ice from twentieth to twenty-first century conditions in a model configuration when the CAM4 is coupled to (a) POP2 and (b) a slab-ocean with prescribed ocean heat transport. (c) The change in northward atmospheric (solid) and oceanic (dashed) energy transports when the atmosphere is coupled to a fully-dynamical ocean model (orange) and a slab-ocean (blue). Note, there is no change in the OET in the slab-ocean simulations as it is prescribed with the same values. Adapted from Tomas et al. (2016); combined two figures and inserted panel labels*

2.7 Summary

The ITCZ is a well-studied component of our climate system. Studies have proposed theoretical frameworks, utilised observational products, and performed GCM sensitivity experiments to better understand the processes determining ITCZ characteristics. Yet, whilst these studies provide an important insight into the mechanisms driving the ITCZ, state-of-the-art climate models still exhibit substantial biases in ITCZ characteristics (section 1.2). The ITCZ is sensitive to the representation of convection across a hierarchy of models (section 2.5). It has also been shown that cloud-radiation interactions play a substantial role in determining ITCZ characteristics (section 2.4). However, it remains to be answered whether cloud-radiation interactions play a role in the sensitivity of the ITCZ to the sub-gridscale representation of convection. In chapter 4 the role of CRE in the sensitivity of the ITCZ to convective mixing in prescribed-SST aquaplanet simulations is investigated. As studies show an association of ITCZ characteristics to AEI (section 2.2), investigating the sensitivity of AEI components to convective mixing is one of the techniques used to illustrate the importance of cloud-radiation interactions. A spatio-temporal variability in ITCZ characteristics, associated with insolation and SST changes, has also been shown in observations and GCMs (section 2.3). In light of this, work in chapter 5 explores whether changing the boundary conditions affects the

sensitivity of the ITCZ to convective mixing. Coupling the atmosphere to an ocean model with an interactive OET substantially reduces the sensitivity of the ITCZ to hemispherically asymmetric boundary conditions and the representation of convection (chapter 2.6). However, the mechanisms responsible for the reduced sensitivity of the ITCZ to the convective parameterisation are yet to be explained. The impact of atmosphere-ocean coupling on the sensitivity of the ITCZ to convective mixing is investigated in chapter 6 through employing a modelling framework with an interactive Ekman-driven OET.

Chapter 3

Methodology

This thesis contains a series of GCM experiments designed to investigate the sensitivity of the tropical atmosphere to the representation of convection and various boundary conditions. An aquaplanet configuration of the MetUM GA6.0 is employed for all simulations. This chapter gives an overview of the modelling techniques used. Section 3.1 introduces the atmospheric model and discusses its convective parameterisation scheme. Sections 3.2 and 3.3 discuss the model configuration for atmosphere-only and atmosphere-ocean coupled simulations respectively, as well as sensitivity experiments performed in each configuration.

3.1 Met Office Unified Model Global Atmosphere 6.0 configuration

Since July 2014, to the time of writing, Global Atmosphere 6.1 (GA6.1) has been operational at the U.K. Met Office for numerical weather prediction (NWP, Walters et al., 2017). All simulations in this thesis use GA6.0; a parallel version of GA6.1 with small differences in parameter settings. The only important difference that should be noted for this project between GA6.0 and GA6.1 is a change in the CAPE closure timescale, a parameter that determines the timescale to remove convective instability. The CAPE closure timescale is one hour in GA6.0 and thirty minutes in GA6.1. GA6.0 is the atmospheric model used in the Global Seasonal forecasting system version 5 (GloSea5) and has been utilised to develop the HadGEM3-GC2.0 (Hadley Centre Global Environment Model version 3 global coupled 2.0) climate model (Williams et al., 2018).

GA6.0 includes ENDGame (Even Newer Dynamics for General atmospheric modelling of the environment); a dynamical core that uses a semi-implicit, semi-Lagrangian framework to solve the non-hydrostatic, fully-compressible deep-atmosphere equations of motion (Wood et al., 2013).

Prognostic fields are discretised horizontally onto a regular latitude/longitude grid with Arakawa C-grid staggering (Arakawa and Lamb, 1977). Vertical discretisation employs Charney-Phillips staggering (Charney and Phillips, 1953) using terrain-following hybrid height coordinates; wind and density are calculated on the "ρ-grid" and all other variables, including temperature and geopotential, are calculated on the "θ-grid". Primary atmospheric prognostics include three-dimensional wind components, virtual dry potential temperature, Exner pressure and dry density (Walters et al., 2017). Moist prognostics, including water vapour concentration and cloud fields, are advected as free tracers.

All simulations use a twenty minute atmospheric timestep and an N96L85 (1.25° latitude $\times$ 1.875° longitude with 85 vertical levels) resolution. 50 model levels are below 18km and the top model level is fixed at 85km above the surface (Fig. 3.1). In MetUM GA6.0 physical parameterisations are categorised into "fast" (i.e. large-scale precipitation) and "slow" (i.e. atmospheric boundary-layer, convection) processes. The atmospheric timestep is split into an outer loop and an inner loop to improve numerical stability (Walters et al., 2017). The outer loop, iterated twice per timestep, calculates slow physical parameterisations and the semi-Lagrangian departure points. Within each outer loop, an inner loop is iterated twice and includes calculating the Coriolis term, non-linear terms, fast physical parameterisations, and pressure increments. The full radiation scheme is called hourly; on non-radiative timesteps corrections are made to the solar zenith angle following Manners et al. (2009).

Convective parameterisation represents the sub-gridscale transports of heat, moisture and momentum associated with cumulus clouds. In GA6.0 convection is classified into three types: shallow-, mid-, and deep-level convection. Each is represented by a mass-flux scheme based on Gregory and Rowntree (1990). The convective parameterisation scheme in GA6.0 consists of three stages: (1) the diagnosis of shallow or deep convection using boundary-layer diagnostics; (2) shallow or deep convection at diagnosed grid-points; (3) mid-level convection where instabilities are still present after shallow or deep convection. The diagnosis of shallow or deep convection is based on the undilute parcel ascent of unstable boundary-layer grid-points. Shallow convection is diagnosed if a parcel attains neutral buoyancy either below 2.5km or below the freezing level, or when the mean vertical velocity is less than 0.02 m s^{-1} at 1500m above the cloud-base. In all other cases deep convection is diagnosed if the ascent begins in the boundary-layer. Shallow convection uses a closure scheme based on Grant (2001); parameterised entrainment is based on cloud-resolving simulations (Grant and Brown, 1999). The mid-level convection scheme is similar to Gregory and Rowntree (1990) with an updated convective momentum transport scheme, (based on Gregory et al., 1997), and a CAPE closure. Mid-level convection is most often diagnosed overnight over land, when the boundary-layer is too stable for deep convection, or in mid-latitude storms (Walters et al., 2017). As this thesis focuses on understanding tropical precipitation using aquaplanet simulations, the effect of mid-level

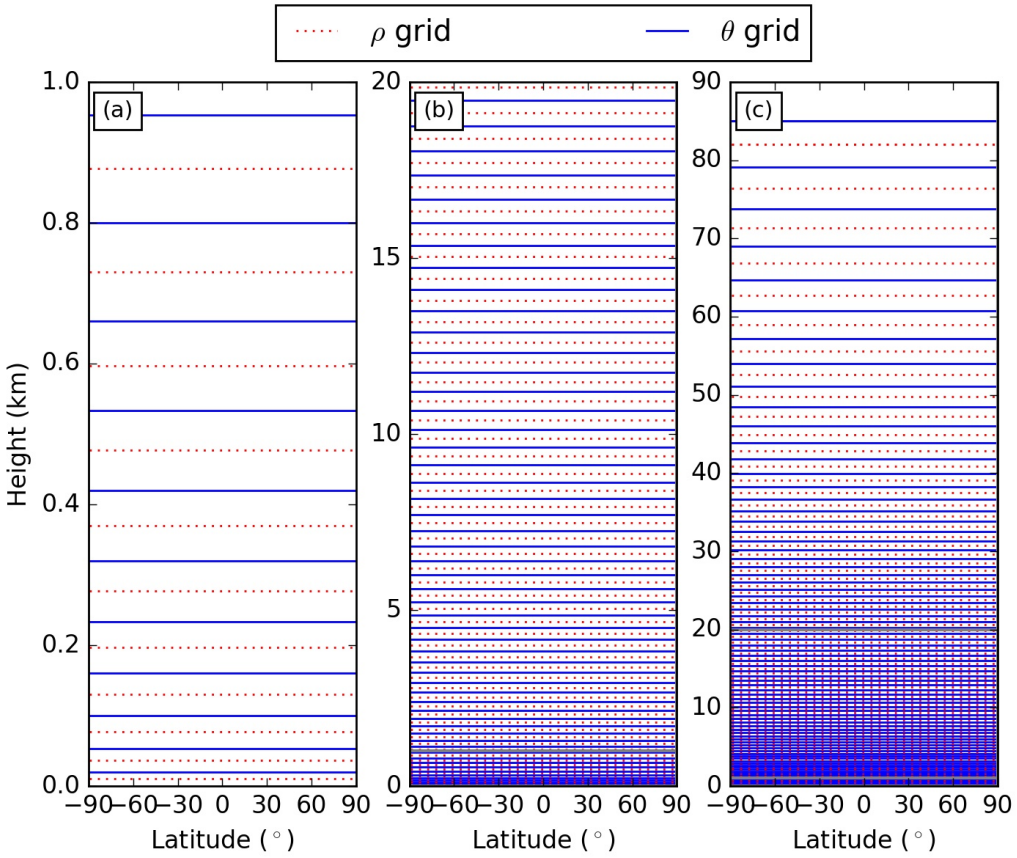

Figure 3.1: *Model heights (km) of ρ-grid (red dotted) and θ-grid (blue solid) in L85 vertical resolution. Levels are shown up to 1km, 20km and 90km in (a), (b) and (c) respectively. Vertical grey lines in (b) and (c) denote top of previous panels.*

convection on the simulated tropical circulation is expected to be minimal.

Parameterised deep convection is an altered form of the mass-flux scheme in Gregory and Rowntree (1990). Alterations include using a CAPE closure scheme based on Fritsch and Chappell (1980), a flux gradient approach for convective momentum transport, and a detrainment rate that depends on relative humidity (Derbyshire et al., 2011). In GCMs it is common to categorise convective mixing into two components: (1) lateral convective mixing, cloud-air properties being continuously diluted during ascent, and (2) organised convective mixing, the dilution of cloud-air properties at cloud-top or cloud-base. Organised convective mixing adapts to the convective plume buoyancy (Derbyshire et al., 2011). In GA6.0 the vertical profile of lateral entrainment (ϵ), the mass-flux from the environment into the convective plume, and detrainment (d_m), the mixing of air from the convective plume into the environment, in deep convection is calculated using:

$$\epsilon(z) = 4.5 f_{dp} \frac{p(z)\rho(z)g}{p_*^2} \tag{3.1}$$

$$d_m(z) = 3.0(1 - RH)\epsilon \tag{3.2}$$

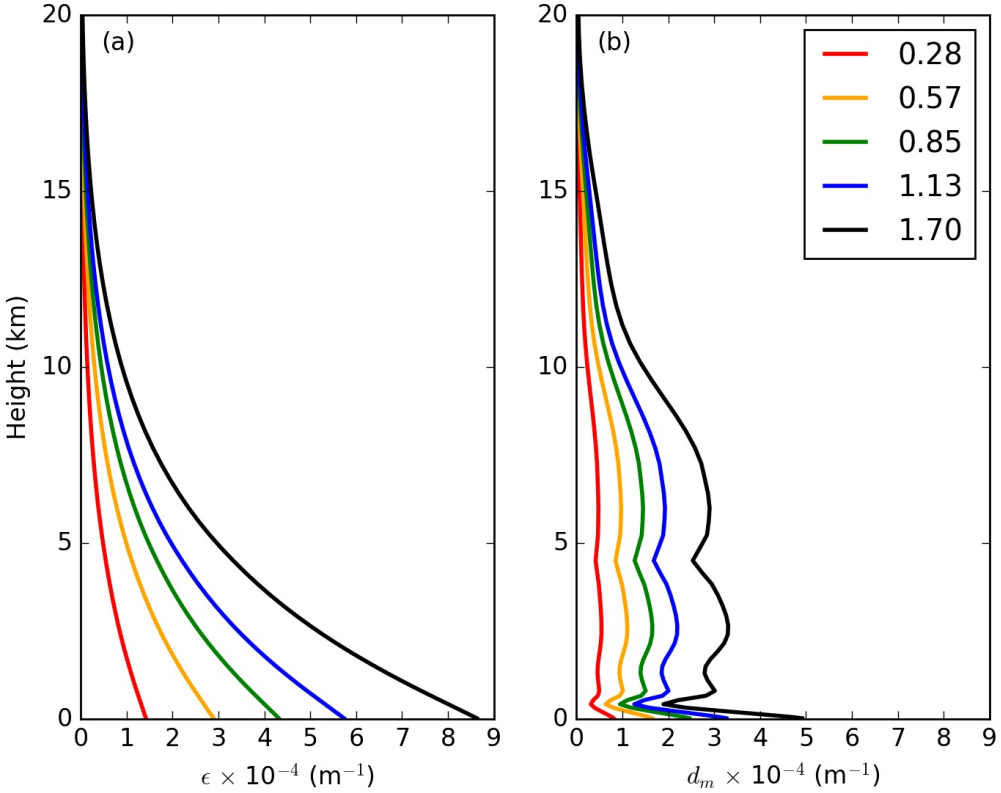

Figure 3.2: *Vertical profile of (a) ϵ and (b) d_m (m^{-1}) with f_{dp} equal to values used in simulations employed in chapter 4. Profiles of pressure, density and RH are kept constant using the meridional-mean, time-mean, zonal-mean values at latitudes with precipitation greater than 5 mm day^{-1} given f_{dp} equals 1.13.*

where ϵ and d_m are given as fractional mixing rates per unit length (m^{-1}); z is the model level height; p and p_* are pressure and surface pressure respectively (Pa); ρ is density (kg m^{-3}); g is gravitational acceleration (m s^{-2}); f_{dp} is a constant with a default value of 1.13 in GA6.0; RH is relative humidity. The use of relative humidity in (3.2) is often called "adaptive detrainment" (Martin et al., 2010; Derbyshire et al., 2011) and takes into account the influence of environmental moisture on convection (de Rooy et al., 2013). The convective upward mass flux and core updraught-area is sensitive to the environmental humidity in cloud-resolving simulations (Derbyshire et al., 2011); a greater environmental humidity is associated with an increased convective mass-flux.

In this study the representation of convection is modified by changing f_{dp} and hence altering ϵ and d_m. Figure 3.2 shows ϵ and d_m when changing f_{dp} to values used for simulations analysed in chapter 4 and given averages of pressure, density and RH at latitudes where precipitation is greater than 5 mm day^{-1} when f_{dp} equals 1.13. The profile of ϵ is associated with the vertical gradient of pressure and density, whilst d_m is associated with relative humidity changes. For example, the sharp reduction in d_m just above the surface is associated with increased relative humidity. Across the low- to mid-troposphere ($\leq$ 8km) d_m remains at approximately 3×10^{-4} m^{-1}; reduced ϵ is offset by

decreased relative humidity. Through changing f_{dp} the sensitivity of the ITCZ to convective mixing is investigated. In a prescribed-SST aquaplanet modelling environment, single and double ITCZs are simulated for the range of f_{dp} employed (section 4.3), hence, the mechanisms that determine ITCZ characteristics can be investigated. Further details of the convective parameterisation and other parameterisations in GA6.0 can be found in Walters et al. (2017).

All simulations in this thesis use an aquaplanet configuration of MetUM GA6.0, where the surface boundary is idealised as an ocean-covered Earth. Aquaplanets, previously used in a plethora of studies (e.g. Neale and Hoskins, 2001; Mobis and Stevens, 2012; Oueslati and Bellon, 2013), provide a test-bed for studying interactions between dynamics, parameterisations and boundary forcings. They retain the physics and dynamics of a full GCM whilst removing the complexities of surface inhomogeneities. Zonally-symmetric SSTs are used to remove the impact of zonal asymmetries on tropical convection (Neale and Hoskins, 2001; Adam et al., 2016b). The albedo of the sea surface is based on Barker and Li (1995). In this thesis two types of aquaplanet simulations are performed: (1) atmosphere-only prescribed-SST simulations, discussed in section 3.2; and (2) idealised atmosphere-ocean coupled simulations in which the atmosphere is coupled to a two-layer ocean with an Ekman-driven interactive OET. In the idealised coupled modelling framework, SSTs depend on surface fluxes and OET. Sections 3.3 and 6.2 discuss the idealised coupled configuration in more detail.

3.2 Atmosphere-only simulations

Chapters 4 to 6 employ atmosphere-only prescribed-SST aquaplanet simulations. Each simulation is three years in length with the first sixty days discarded as spin-up; only the final 2 years and 10 months are analysed. A perpetual diurnal cycle of insolation is employed, as the seasonal cycle of insolation is removed, only short integrations are required. All simulations are initialised from the same equilibrated prescribed-SST aquaplanet simulation which has equinoctial boundary conditions. Equinoctial boundary conditions refers to a "Qobs" prescribed-SST profile (Neale and Hoskins, 2001), employed in chapters 4 and 5, and equinox insolation. Qobs is similar to the observed zonal-mean SST distribution and is an average between the "control" and "flat" geometric functions in Neale and Hoskins (2001):

$$T_*(\lambda,\phi) = \begin{cases} 27\Big[1-\frac{1}{2}\Big(\sin^2\Big(\frac{3\phi}{2}\Big)+\sin^4\Big(\frac{3\phi}{2}\Big)\Big)\Big]\ ^\circ C : -\frac{\pi}{3} < \phi < \frac{\pi}{3} \\ 0^\circ C : \text{otherwise} \end{cases} \tag{3.3}$$

where λ and ϕ are longitude and latitude respectively (rad) and T_* is surface temperature ($^\circ$C).

In this thesis four components are changed in the atmosphere-only model configuration: (1) f_{dp} (3.1); (2) the representation of cloud-radiation interactions; (3) insolation; and (4) prescribed-SSTs. Table A.1 in the appendix gives a summary of all atmosphere-only prescribed-SST simulations employed. To accomplish the second thesis objective (section 1.3) and investigate the role of cloud-radiation interactions in the sensitivity of the ITCZ to convective mixing, cloud-radiation interactions are either interactive or prescribed. Two methods of prescribing cloud-radiation interactions is utilised; either removing cloud-radiation interactions altogether or prescribing a zonal-mean diurnal-cycle of cloudy-sky radiative fluxes at every model level. Cloudy-sky fluxes are defined as the difference between all-sky and clear-sky fluxes (equation 2.17; Slingo and Slingo, 1988). Clear-sky fluxes are diagnosed by GA6.0 by performing radiation calculations with zero cloud-liquid or cloud-ice. In chapter 5, and to achieve the third thesis objective (section 1.3), the importance of the boundary conditions on the sensitivity of the ITCZ to convective mixing is investigated through meridionally shifting the Qobs SST profile and changing insolation from equinoctial to solstitial conditions. Solstitial insolation is employed by changing the fixed solar declination angle from 0° to 23.4°N latitude. Further details on boundary condition changes are discussed in section 5.2.

Whilst prescribed-SST simulations enable the sensitivity of the tropical atmosphere to SST to be investigated (section 5.4; Hess et al., 1993; Mobis and Stevens, 2012), it is also energetically inconsistent as the ocean effectively has an infinite heat capacity and does not respond to atmospheric conditions. The impact of interactive SSTs is investigated in chapter 6 through developing an idealised atmosphere-ocean coupled modelling framework.

3.3 Coupled simulations

Chapter 6 describes the idealised coupled model employed to achieve the fourth thesis objective (section 1.3) and investigate the effect of atmosphere-ocean coupling on the sensitivity of the ITCZ to convective mixing. The atmosphere is represented by GA6.0, atmospheric physics and dynamics are the same as in atmosphere-only simulations (section 3.2), and the ocean is represented by a two-layer model with interactive Ekman-driven OET, vertical mixing, and diffusion. The model is similar to the "2-layer Ekman scheme" in Codron (2012) and is discussed in section 6.2.1.

MetUM GA6.0 is coupled to the ocean using the Ocean Atmosphere Sea Ice Soil (OASIS) coupler (Valcke et al., 2013). OASIS couples two models without substantial changes to numerical code and has been used in previous studies including Klingaman and Woolnough (2014a), Hirons et al. (2015) and Dong et al. (2017). Atmosphere-ocean coupling occurs every three hours with three one-hour ocean timesteps between each field exchange. Variables passed from the atmosphere to the ocean

include surface energy and momentum flux components, and precipitation (Thil, 1998). SSTs are passed from the ocean to atmosphere.

As in prescribed-SST atmosphere-only simulations (section 3.2), the sensitivity of the ITCZ to convective mixing in coupled simulations is investigated through changing f_{dp} (3.1). As previously stated in section 3.2, atmosphere-only simulations are energetically inconsistent as SSTs do not evolve to changes in the surface energy balance. Coupling the atmosphere to a simplified ocean with a prescribed OET is one solution to this problem and has been used in a large number of studies (e.g. Kang et al., 2008; Voigt et al., 2014; Schneider et al., 2014; Bischoff and Schneider, 2016; Voigt et al., 2016; Wei and Bordoni, 2018). However, prescribing OET fixes the net surface energy flux. Two sets of coupled simulations, with either an interactive or prescribed Ekman-driven OET, are employed in chapter 6 to understand the effect of interactive OET on the sensitivity of the tropical atmosphere to convective mixing. The prescribed Ekman-driven OET is computed from a coupled simulation with an interactive Ekman-driven OET. The model set-up, including spin-up duration and initial conditions, for these simulations are discussed in section 6.2.

Chapter 4

The role of the cloud radiative effect in the sensitivity of the ITCZ to convective mixing

Talib, J., S. J. Woolnough, N. P. Klingaman, and C. E. Holloway, 2018: The role of the cloud radiative effect in the sensitivity of the Intertropical Convergence Zone to convective mixing. *J. Climate.*, **31**, 6821–6838

4.1 Purpose of this chapter

Work in this chapter is concerned with the first two objectives of this thesis (section 1.3): (1) to understand the mechanisms responsible for the sensitivity of the ITCZ to convective mixing; (2) to isolate the role of cloud-radiation interactions in the sensitivity of the ITCZ to convective mixing. To achieve these objectives, aquaplanet simulations using variations of the Met Office Unified Model (MetUM) Global Atmosphere 6.0 (GA6.0) configuration are performed, and the CRE is prescribed as either zero or a meridionally, diurnally varying climatology.

As highlighted in section 2.5, previous studies illustrate a sensitivity of tropical precipitation to the convective parameterisation (Terray, 1998; Frierson, 2007; Wang et al., 2007; Chikira, 2010; Mobis and Stevens, 2012; Oueslati and Bellon, 2013; Bush et al., 2015; Nolan et al., 2016). Even changing individual parameters in a convection scheme can substantially impact simulated tropical precipitation (Oueslati and Bellon, 2013; Bush et al., 2015). For example, variations in the convective entrainment rate can alter the diurnal cycle of precipitation over the Maritime Continent (Wang et al., 2007) and South Asian monsoon precipitation (Bush et al., 2015). In full GCMs, complex surface characteristics and boundary conditions including land-sea contrasts, orography and zonal SST gradients, make it challenging to understand the sensitivity of tropical

precipitation to the representation of convection (Oueslati and Bellon, 2013; Bush et al., 2015). In the absence of complex surface topography, aquaplanet studies have shown that tropical precipitation characteristics, in particular the location and intensity of the ITCZ, are sensitive to the sub-gridscale treatment of convection (Hess et al., 1993; Numaguti, 1995; Chao and Chen, 2004; Liu et al., 2010; Mobis and Stevens, 2012). Mobis and Stevens (2012) studied the sensitivity of the ITCZ location to the convective parameterisation by comparing the Nordeng (1994) and Tiedtke (1989) schemes in an aquaplanet configuration of the ECHAM GCM. Nordeng (1994) and Tiedtke (1989) vary in their formulations of entrainment, detrainment and cloud base mass flux for deep convection. The Nordeng scheme, with a higher lateral entrainment rate, produced a single ITCZ, whilst the Tiedtke scheme produced a double ITCZ. Mobis and Stevens (2012) associate the ITCZ location to the maximum boundary-layer MSE; they argue that mechanisms that control the boundary-layer MSE are important to the sensitivity of the ITCZ to the representation of convection. The boundary-layer MSE distribution is predominantly controlled by the surface winds and turbulent fluxes, which are influenced by convective heating. Variations in convective heating therefore influence the ITCZ structure. Results from simulations with prescribed surface winds in the computation of the surface fluxes (Numaguti, 1995; Mobis and Stevens, 2012), also lead to the conclusion that there is a strong association between surface turbulent fluxes and the ITCZ.

CRE warms the atmosphere in the deep tropics (Tian and Ramanathan, 2002; Allan, 2011). GCM studies highlight that CRE plays a substantial role in convection, precipitation, and the atmospheric circulation in the tropics and extra-tropics (section 2.4; Slingo and Slingo, 1988; Randall et al., 1989; Sherwood et al., 1994; Crueger and Stevens, 2015). Bergman and Hendon (2000) investigated the role of clouds in a linear model of the tropical circulation forced by diabatic heating obtained from reanalysis data and radiative transfer calculations that used observed cloud properties. Through calculating the circulation response to different components of diabatic heating, latent heating and radiative forcing, and concluding that spatial variations of radiative forcing are dominated by cloudy-sky heating rates, Bergman and Hendon (2000) associate approximately 20% of the tropical circulation intensity with CRE. CRE is a major source of energy for balancing the divergence of moist static energy (MSE) by the Hadley circulation (Tian and Ramanathan, 2002). CRE is also associated with simulated regional variations of tropical convection (Wang et al., 2005; Kniffka et al., 2019).

Characteristics of the simulated ITCZ are sensitive to the representation of cloud-radiation interactions (Randall et al., 1989; Fermepin and Bony, 2014; Li et al., 2015; Harrop and Hartmann, 2016); CRE is associated with a more prominent single ITCZ (Randall et al., 1989; Crueger and Stevens, 2015; Harrop and Hartmann, 2016; Popp and Silvers, 2017). Harrop and Hartmann (2016) and Popp and Silvers (2017) investigated the association between the Hadley circulation and CRE

in a range of aquaplanet simulations with and without CRE. In all GCMs used, CRE is associated with increased equatorial rainfall, an equatorward contraction of the ITCZ, and a strengthening of the mean meridional circulation. However, the authors emphasise different mechanisms by which CRE promotes a single ITCZ. Harrop and Hartmann (2016) propose that CRE warms the tropical upper-troposphere, which reduces CAPE and restricts deep convection to the region of warmest SSTs. Popp and Silvers (2017) argue that CRE strengthens the Hadley circulation and moves the ITCZ equatorward, associated with increased MSE advection by the lower branches of the Hadley circulation. The strengthening of the mean circulation is associated with the CRE meridional gradient, as CRE heats the tropical ($\leqslant \pm 30^\circ$ latitude) atmosphere and cools the extra-tropical ($> \pm 30^\circ$ latitude) atmosphere (Allan, 2011). However, it should be noted that CRE reduces total tropical-mean precipitation due to reduced radiative cooling (Harrop and Hartmann, 2016).

Whilst the ITCZ has been shown to be sensitive to CRE (section 2.4) and the convective parameterisation (section 2.5), no study has separated these two sensitivities. For example, it is unknown whether the sensitivity of the ITCZ to the convective parameterisation is predominately due to CRE variations. In this chapter aquaplanet simulations and the AEI framework (section 2.2) are used to analyse the sensitivity of the ITCZ to convective mixing and isolate the role of CRE. Section 4.2 outlines the simulations performed and the method used to prescribe CRE. Section 4.3 describes the sensitivity of the ITCZ to convective mixing. Section 4.4 describes the role of CRE in the sensitivity of the ITCZ to convective mixing. Finally, the discussion and conclusions for this chapter are in sections 4.5 and 4.6, respectively.

4.2 Methodology

To explore the sensitivity of the ITCZ to convective mixing, five simulations are performed varying the lateral entrainment (ϵ) and detrainment (d_m) rates for diagnosed deep convection (Table 4.1). ϵ and d_m are controlled by scaling f_{dp} to five values between 0.25 and 1.5 $\times$ the default value: 0.28 (F0.28), 0.57 (F0.57), 0.85 (F0.85), 1.13 (F1.13) or 1.70 (F1.70). More details on the formulation of ϵ and d_m is given in section 3.1.

To isolate the role of CRE on the sensitivity of the ITCZ to convective mixing, a companion set of experiments with cloud-radiation interactions removed are performed: F0.28NC, F0.57NC, F0.85NC, F1.13NC and F1.70NC (Table 4.1). Cloud-radiation interactions are removed by setting the cloud liquid and cloud ice to zero in the radiation scheme; hence, only clear-sky fluxes are used for radiative heating tendencies, as in Harrop and Hartmann (2016).

Table 4.1: *Simulations varying f_{dp} with cloud-radiation interactions on (CRE-on) and off (CRE-off). F1.13 is the default integration for GA6.0.*

f_{dp}	CRE-on	CRE-off
0.28	F0.28	F0.28NC
0.57	F0.57	F0.57NC
0.85	F0.85	F0.85NC
1.13	F1.13	F1.13NC
1.70	F1.70	F1.70NC

Finally, a third set of simulations is performed with a meridionally-, diurnally-varying prescribed CRE (Table 4.2) to investigate the relative importance of f_{dp} and CRE in driving ITCZ characteristics. The four simulations have a prescribed, diurnally varying CRE vertical profile computed from a single-year simulation with f_{dp} equal to 0.57 or 1.13 (PC0.57 and PC1.13, respectively). CRE is prescribed by controlling cloudy-sky upward and downward fluxes at each model level at every model timestep, hence, radiative heating tendencies due to cloudy-sky fluxes are prescribed. The diurnally varying CRE profile is computed as a hemispherically symmetric and zonally uniform composite of the climatological diurnal cycle at each grid point, referenced to local solar time. Two of the four simulations prescribe CRE from a simulation with a different f_{dp} from that used in the simulation itself (F1.13PC0.57, F0.57PC1.13), whilst the other two simulations use CRE from a simulation with the same f_{dp} to assess the sensitivity of prescribing CRE (F1.13PC1.13, F0.57PC0.57). All simulations described in this chapter (Tables 4.1 and 4.2) use the Qobs SST profile (Neale and Hoskins, 2001) and are performed for three years; the first two months is discarded as spin-up for analysis.

Table 4.2: *Prescribed-CRE simulations; PC1.13 and PC0.57 represent the prescribed CRE computed from a one-year simulation where f_{dp} equals 1.13 or 0.57 (respectively).*

f_{dp}	PC1.13	PC0.57
1.13	F1.13PC1.13	F1.13PC0.57
0.57	F0.57PC1.13	F0.57PC0.57

4.3 Sensitivity of the ITCZ to convective mixing

Figure 4.1a shows a sensitivity of the ITCZ to f_{dp} with a single ITCZ observed at higher values (F1.13, F1.70). Reducing f_{dp} promotes a double ITCZ, with peak precipitation further away from the equator (F0.28, F0.57). F0.85 has a marginal double ITCZ with no substantial difference between equatorial and off-equatorial precipitation. Decreasing f_{dp} is associated with a weaker horizontal gradient of the mass meridional streamfunction (Fig. 4.2). Only F0.28 shows a reversed Hadley circulation in the deep tropics (Fig. 4.2e), associated with upper-level zonal-mean equatorial subsidence, typical of

a double ITCZ. F0.57 meanwhile has a typical double ITCZ structure in precipitation but not in the mass meridional streamfunction (Figs. 4.1a and 4.2d). In this thesis this scenario is referred to as a "split ITCZ": two off-equatorial precipitation maxima without any substantial zonal-mean subsidence equatorward of the precipitation maxima.

Convective mixing reduces the MSE difference between a convective plume, determined by the boundary-layer MSE, and the free-troposphere (Mobis and Stevens, 2012), which reduces the plume buoyancy. Assuming the sensitivity of the environmental saturated MSE to f_{dp} is small, the depth of convection depends on the boundary-layer MSE and f_{dp}. Decreasing f_{dp} will deepen convection for a constant boundary layer MSE, and reduce the minimum boundary-layer MSE at which deep convection occurs. Following weak temperature gradient arguments (e.g. Sobel et al., 2001) and assuming a small meridional gradient in free-tropospheric tropical temperature, and hence a small gradient in saturated MSE across the deep tropics, reduced minimum boundary-layer MSE needed for deep convection strengthens convection in off-equatorial tropical latitudes, where SSTs are cooler. Stronger off-equatorial deep convection decreases equatorward low-level winds in the deep tropics, reducing equatorial boundary layer MSE. Hence, decreasing f_{dp} is associated with a poleward ITCZ shift and promotes a double ITCZ. Similar arguments can be made for higher f_{dp} promoting a single ITCZ.

The sensitivity of the ITCZ to f_{dp} is associated with AEI changes (Fig. 4.1b); a change from a single (F1.13 and F1.70) to a double/split ITCZ (F0.28/F0.57) is associated with decreased AEI_0 (Fig. 4.3d and e). Simulations with a single ITCZ in precipitation have a positive AEI_0 whilst simulations with a double ITCZ have a negative AEI_0 (Fig. 4.1b), in agreement with Bischoff and Schneider (2016). Changes in cloudy-sky radiation and latent heat flux dominate AEI changes when varying f_{dp} (blue and orange lines respectively in Fig. 4.3). As characteristics of the Hadley circulation and ITCZ are associated with the AEI (section 2.2; Bischoff and Schneider, 2014), and CRE plays a substantial role in AEI changes when varying f_{dp}, it is hypothesised that prescribing CRE will reduce or remove the sensitivity of the AEI and ITCZ to f_{dp}. In F1.13 the total CRE peaks at approximately 60 W m^{-2} at the equator and reduces to zero around 15° latitude (blue line in Fig. 4.3b). This equatorial warming comes almost entirely from longwave CRE, which dominates the total CRE equatorward of 10° latitude (not shown). In the subtropics, 20° to 30° latitude, low clouds contribute to a negative CRE of approximately 2 W m^{-2}; longwave cooling from boundary-layer clouds is greater than shortwave heating (later shown in Fig. 4.6g). Without the CRE contribution to AEI_0 in F1.13, AEI_0 would be negative, suggesting that CRE maintains the single ITCZ, in agreement with Randall et al. (1989) and Harrop and Hartmann (2016). Removing CRE from the AEI in F1.13 would give an AEI_0 of -25.7 W m^{-2}, assuming that other AEI components remain constant. Using the Bischoff and Schneider (2016) framework (2.15) with AEI values once subtracting CRE from the total AEI in F1.13

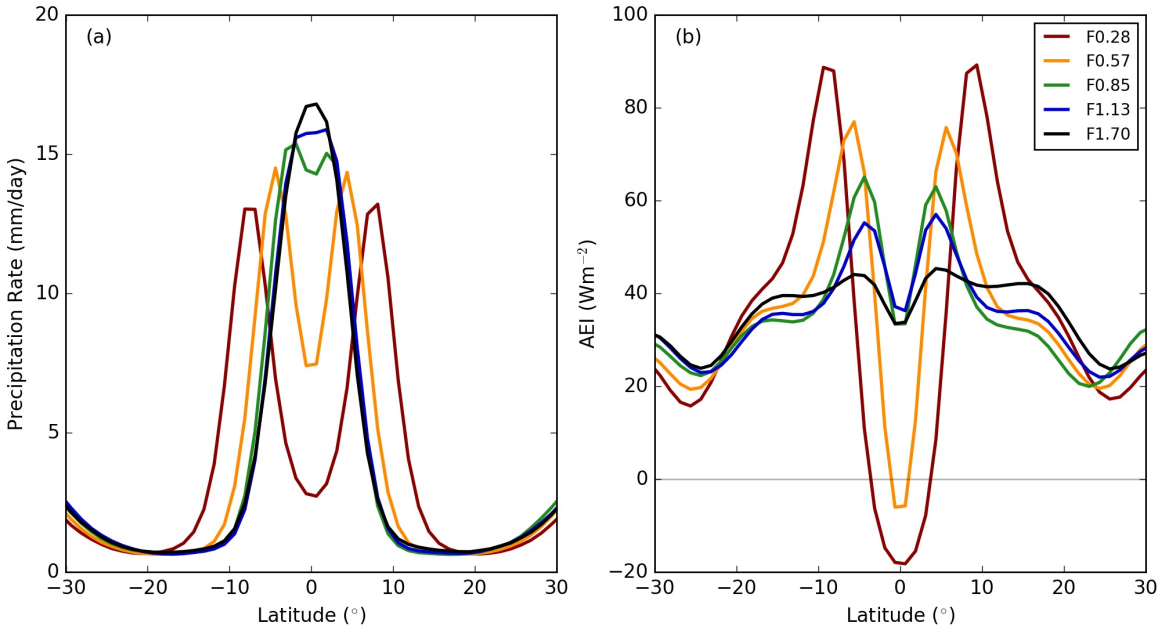

Figure 4.1: *Zonal-mean, time-mean (a) precipitation rates (mm day^{-1}) and (b) AEI (W m^{-2}) in simulations with various f_{dp}.*

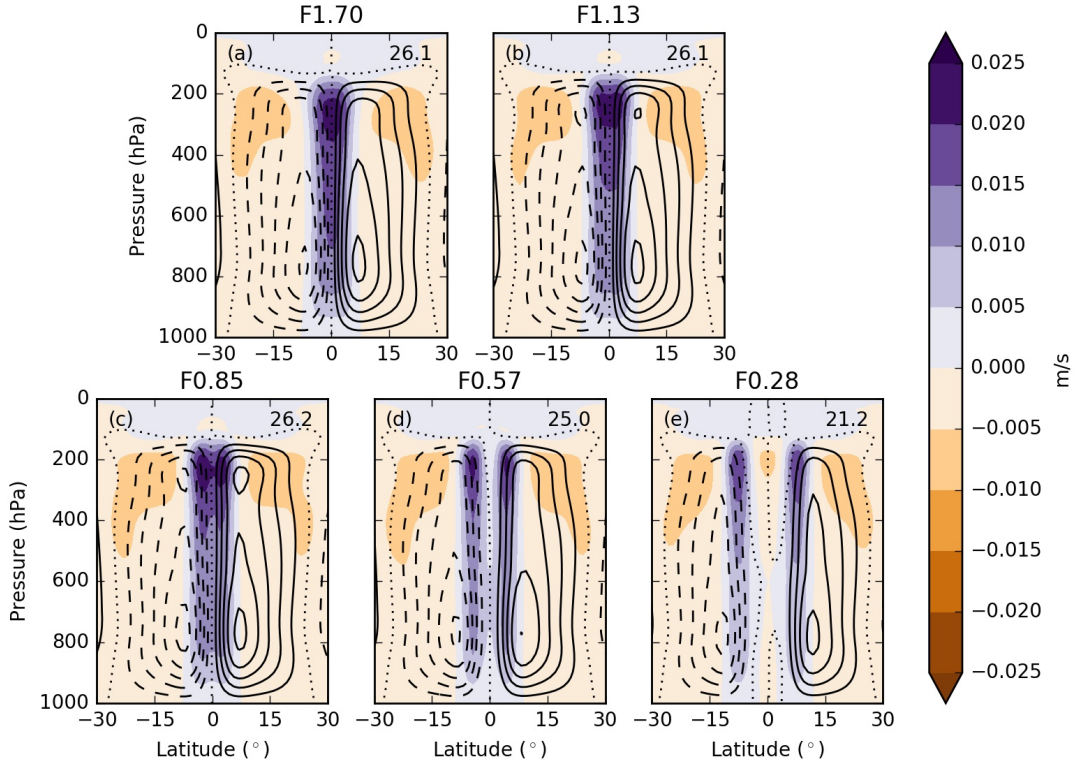

Figure 4.2: *Zonal-mean, time-mean mass meridional streamfunction (kg s^{-1}) (line contours) and vertical wind speed (m s^{-1}) (filled contours, positive upward) for (a) F1.70, (b) F1.13, (c) F0.85, (d) F0.57, (e) F0.28. Line contours are in intervals of 5×10^{10}, with dashed contours representing negative values. Positive streamfunction values indicate clockwise circulation. Dotted contour is zero value and the maximum magnitude of the mass meridional streamfunction is printed in top right-hand corner of each panel.*

and assuming that $\widehat{[\overline{vh}]}_0$ is approximately equal to 0 W m^{-1}, associated with an hemispherically symmetric atmospheric circulation, predicts a double ITCZ at $\pm$ 5.6° latitude. To explore the role of

CRE in the sensitivity of the ITCZ to f_{dp}, simulations are performed with CRE removed (section 4.4).

The change from a single to a double ITCZ in precipitation when decreasing f_{dp} from 1.13 to 0.57 is associated with a substantially reduced equatorial CRE (Fig. 4.3d). CRE profiles from simulations with f_{dp} equal to 0.57 and 1.13 are used for prescribing a meridionally-, diurnally-varying CRE (Table 4.2), as CRE profiles typical of a single and double ITCZ are observed given these two f_{dp} values. Prescribed-CRE simulations are performed to investigate the role of CRE in the sensitivity of the ITCZ to f_{dp}; analysis is shown in section 4.4.

4.4 The role of cloud-radiation interactions in the sensitivity of the ITCZ to convective mixing

4.4.1 Sensitivity of the ITCZ to convective mixing with no cloud radiative effect

In section 4.3 it is hypothesised that CRE plays a substantial role in the sensitivity of the ITCZ to f_{dp} and removing CRE when f_{dp} equals 1.13 will change the ITCZ structure from single to double. To test these hypotheses simulations without cloud-radiation interactions have been performed (Table 4.1). Figures 4.4a and 4.5 show the zonal-mean, time-mean precipitation and mass meridional streamfunction in CRE-off simulations respectively. Removing CRE when f_{dp} equals 1.13 leads to a switch from a single to a split ITCZ and an approximately 20% weakening of the Hadley circulation (Figs. 4.4a and 4.5b).

Similar to Harrop and Hartmann (2016), removing CRE cools the tropical ($\leqslant 30^{\circ}$ latitude) upper-troposphere (Fig. 4.6c), destabilizing the atmosphere and reducing the environmental saturated MSE. For a fixed boundary-layer MSE and f_{dp}, removing CRE deepens convection as the buoyancy of the convective plume increases relative to the environmental saturated MSE. Hence, removing CRE reduces the minimum boundary-layer MSE required for deep convection, strengthening off-equatorial convection over cooler SSTs. Stronger off-equatorial convection decreases equatorward low-level winds in the deep tropics (Fig. 4.6f), reducing equatorial boundary-layer MSE and promoting a double ITCZ. This mechanism is similar to that proposed for the sensitivity of the ITCZ to f_{dp} (section 4.3). However, when removing CRE changes in the environmental saturated MSE play the dominant role, whilst for the sensitivity of the ITCZ to f_{dp}, changes in the convective parcel MSE dominate.

The weaker Hadley circulation and double ITCZ in precipitation in F1.13NC is consistent with AEI changes. In F1.13NC removing CRE reduces AEI_0 by approximately 45 W m^{-2}, leading to a negative

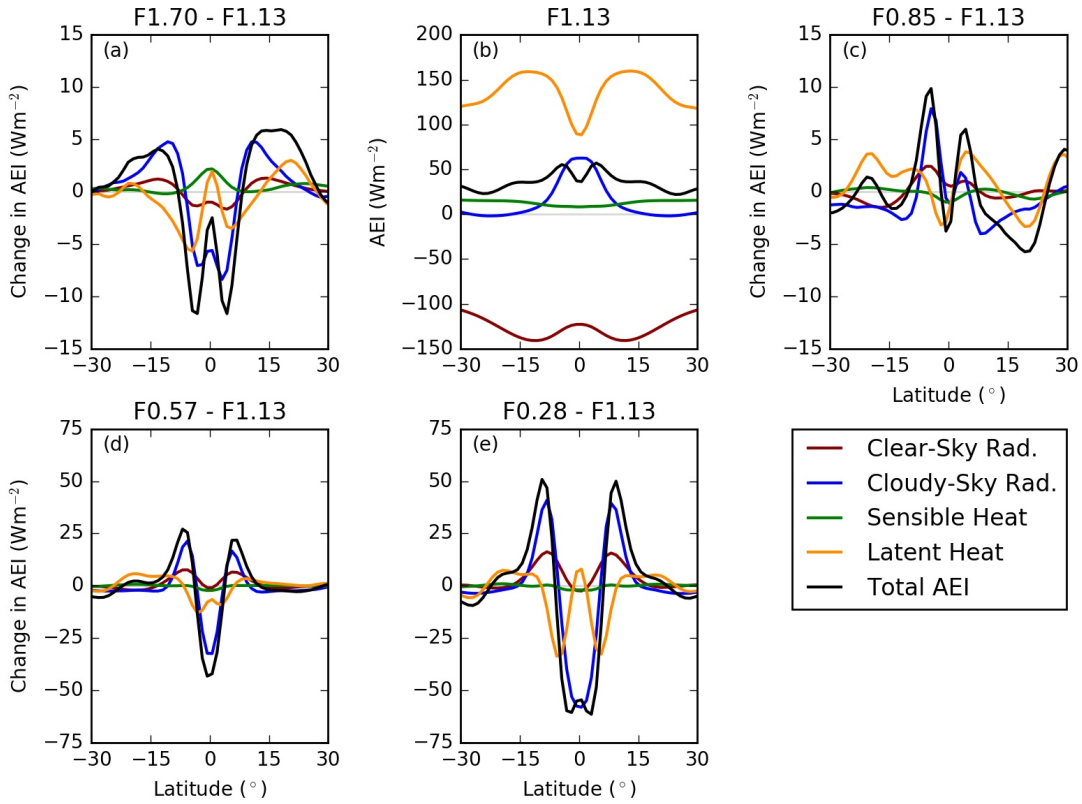

Figure 4.3: *Change in zonal-mean, time-mean AEI components (W m^{-2}) compared to F1.13 (b) for (a) F1.70; (c) F0.85, (d) F0.57, (e) F0.28. Red line is the clear-sky component, blue line is the cloudy-sky component. Green and orange lines represent the sensible and latent heat flux, respectively, and the black line is the total AEI change. Note, (a) and (c) have axis limits -15 and 15 W m^{-2}, whilst (d) and (e) have limits -75 and 75 W m^{-2}.*

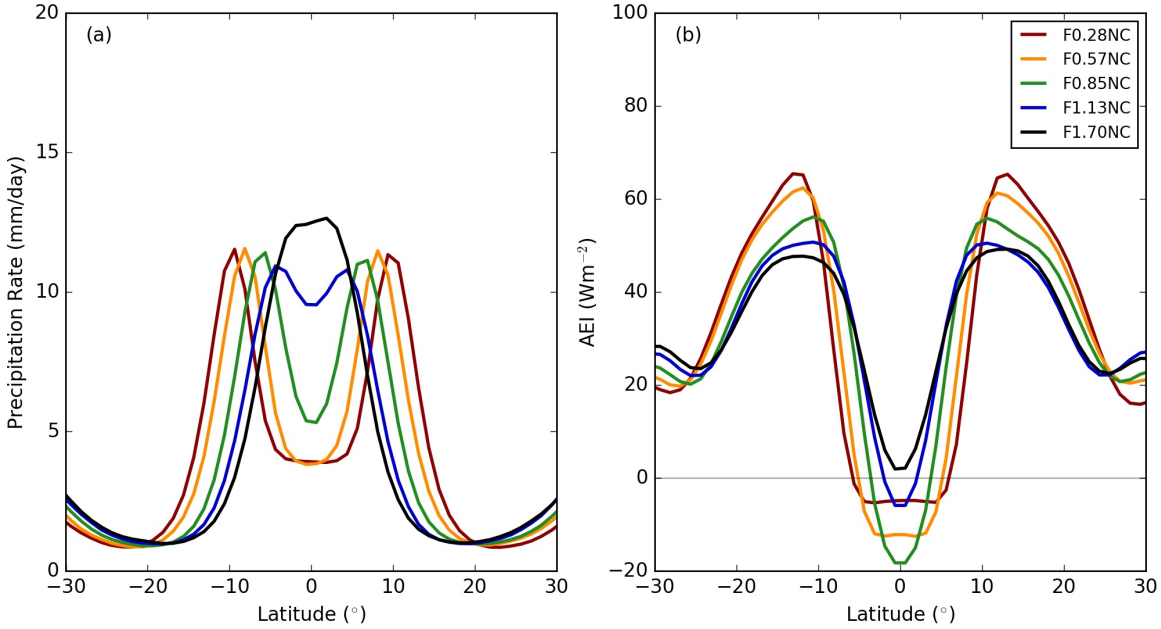

Figure 4.4: *Zonal-mean, time-mean (a) precipitation rates (mm day^{-1}) and (b) AEI (W m^{-2}) in CRE-off simulations with various f_{dp}.*

AEI$_0$ (Fig. 4.7f). Across the deep tropics the AEI change is not equal to CRE diagnosed from F1.13, due to increased turbulent and clear-sky fluxes. These increased fluxes partially offset the reduced

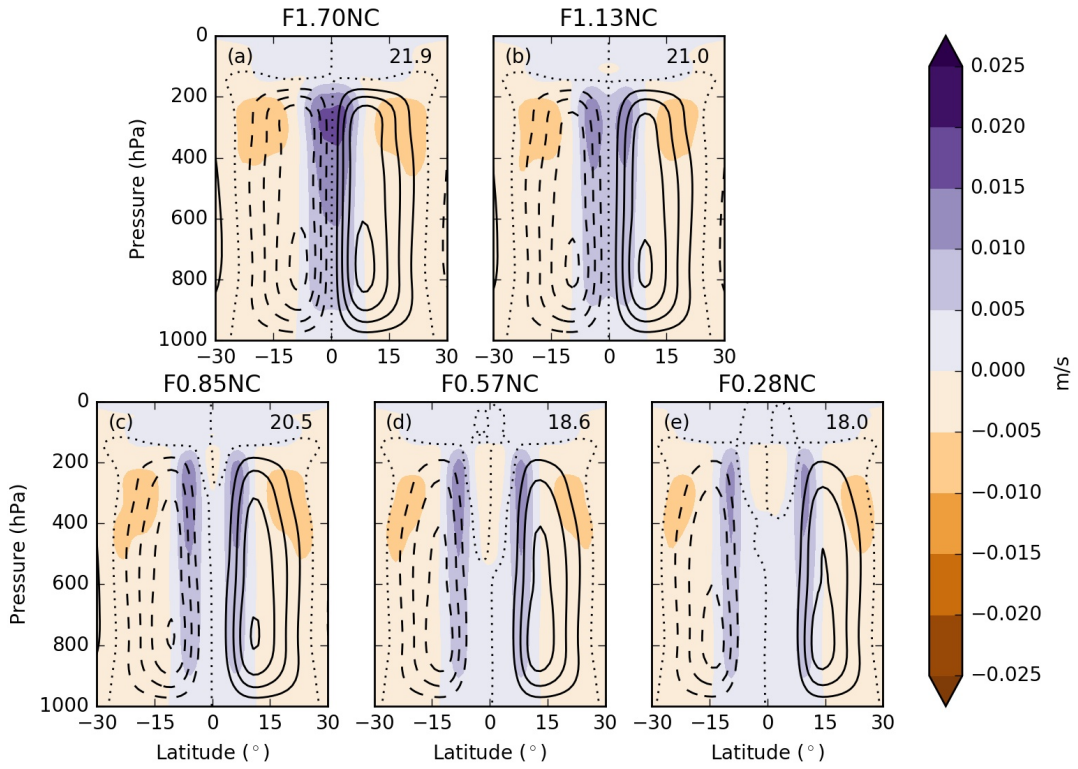

Figure 4.5: *Zonal-mean, time-mean mass meridional streamfunction (kg s^{-1}) (lined contours) and vertical wind speed (m s^{-1}) (filled contours) in (a) F1.70NC, (b) F1.13NC, (c) F0.85NC, (d) F0.57NC, (e) F0.28NC. Line contours are at intervals of 5 $\times$ 10^{10}, with dashed contours representing negative values. Positive streamfunction values indicate clockwise circulation. Dotted contour is zero value and maximum magnitude of the mass meridional streamfunction is printed in the top right-hand corner of each panel.*

AEI_0. Hence, the predicted double ITCZ location when removing CRE of $\pm$ 5.6° latitude (section 4.3) overestimated the poleward ITCZ shift. Removing CRE reduces the mean tropical AEI associated with an increased AEI at higher latitudes and a weaker Hadley circulation. Output from simulations performed are consistent with the mechanisms proposed by Popp and Silvers (2017): the ITCZ is located at the maximum boundary-layer MSE and a weaker mass meridional circulation in CRE-off simulations is associated with a reduced AEI gradient between the tropics and extratropics.

At all f_{dp} removing CRE reduces the maximum precipitation rate (comparing Figs. 4.1a and 4.4a), weakens the Hadley circulation (comparing Figs. 4.2 and 4.5) and moves the latitude of peak precipitation poleward (Fig. 4.8a). The sensitivity of the ITCZ structure to removing CRE depends on f_{dp}; either a broader single ITCZ (F1.70NC), a poleward shift of a double/split ITCZ (F0.28NC and F0.57NC), or a switch from a single to a split/double ITCZ (F0.85NC and F1.13NC). Removing CRE cools the upper troposphere (Fig. 4.6c) and reduces the boundary layer MSE required for deep convection. This increases the f_{dp} value at which the ITCZ transitions from single to double.

Removing CRE changes, but does not remove, the sensitivity of the ITCZ to f_{dp} (Fig. 4.8). Quantify-

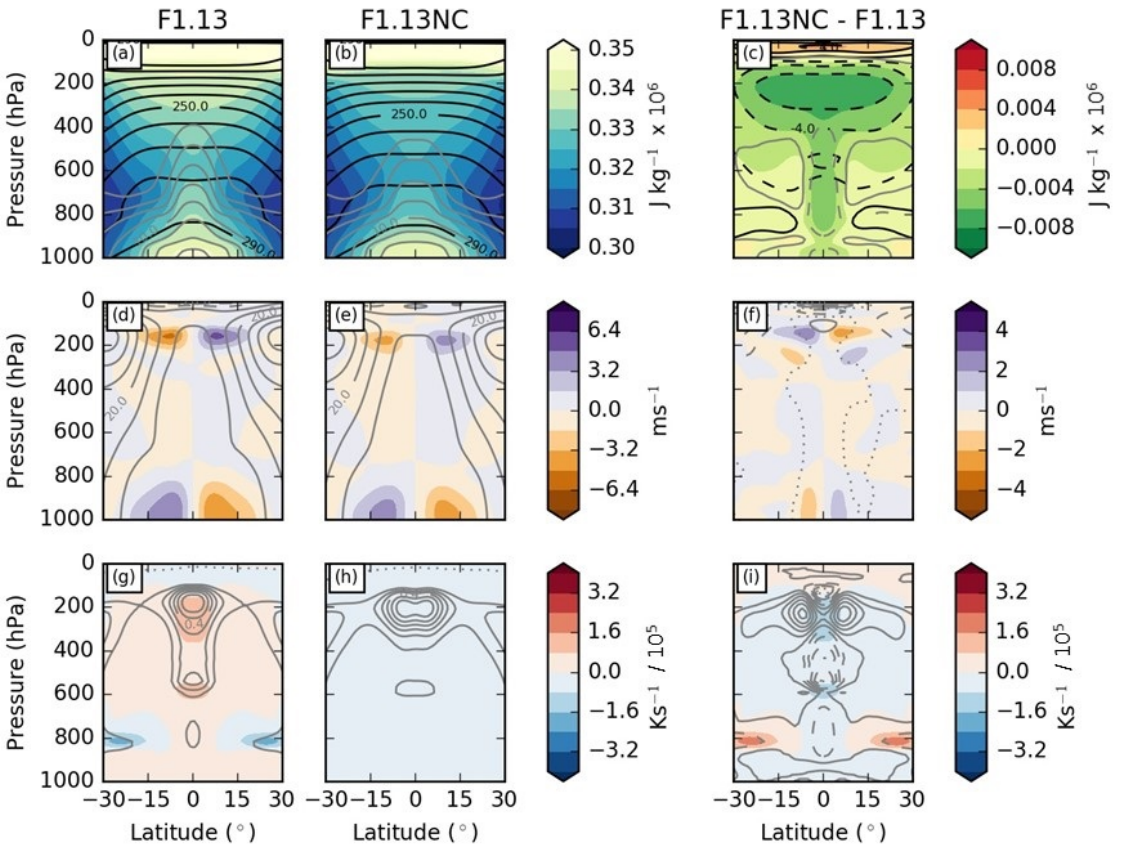

Figure 4.6: *Zonal-mean, time-mean meridional cross sections of: (a-c) MSE (J $kg^{-1}K^{-1}$, filled), temperature (K, black lines, contour spacing of 10 K) and specific humidity (g kg^{-1}, grey lines, contour spacing of 2 g kg^{-1}); (d-f) meridional (filled) and zonal (grey lines, contour spacing of 10 m s^{-1}) wind (m s^{-1}); (g-i) cloudy-sky heating rate (filled, K s^{-1}) and cloud fraction (grey lines, contour spacing of 0.1). The first column is for F1.13; the second column is for F1.13NC; the third column is the difference between F1.13NC and F1.13. For the third column, line contour spacing is reduced to (c) 2 K, 1 g kg^{-1} (black and grey lines respectively), (f) 5 m s^{-1} and (i) 0.05. Dashed and dotted contours represent negative and zero values respectively.*

ing the apparent effect of CRE on the sensitivity of the ITCZ to f_{dp} is difficult as the effect depends on both the range of f_{dp} considered and the metric used (Fig. 4.8). For an off-equatorial ITCZ in CRE-off simulations ($0.28 \leqslant f_{dp} \leqslant 1.13$), including CRE increases the sensitivity of the ITCZ location to f_{dp} by approximately 30% (comparing the slopes of the solid regression lines in Fig. 4.8a). However, because F1.70NC has a single, equatorial ITCZ, including CRE cannot shift the ITCZ further equatorward. Hence, for $0.28 \leqslant f_{dp} \leqslant 1.70$ the change in sensitivity when including CRE reduces to nearly zero (comparing the slopes of the dashed lines). The reduction in sensitivity also depends on the chosen metric. For instance, the maximum precipitation rate shows a negligible sensitivity to f_{dp} in CRE-off simulations but a substantial sensitivity in CRE-on simulations (Fig. 4.8b), highlighting that CRE enhances convection, as increased f_{dp} is associated with increased CRE (Fig. 4.9).

Increased f_{dp} is associated with increased tropical-mean CRE (legend in Fig. 4.9a), which is counter-intuitive as one might expect that increasing f_{dp} would lead to lower cloud tops and hence a reduced

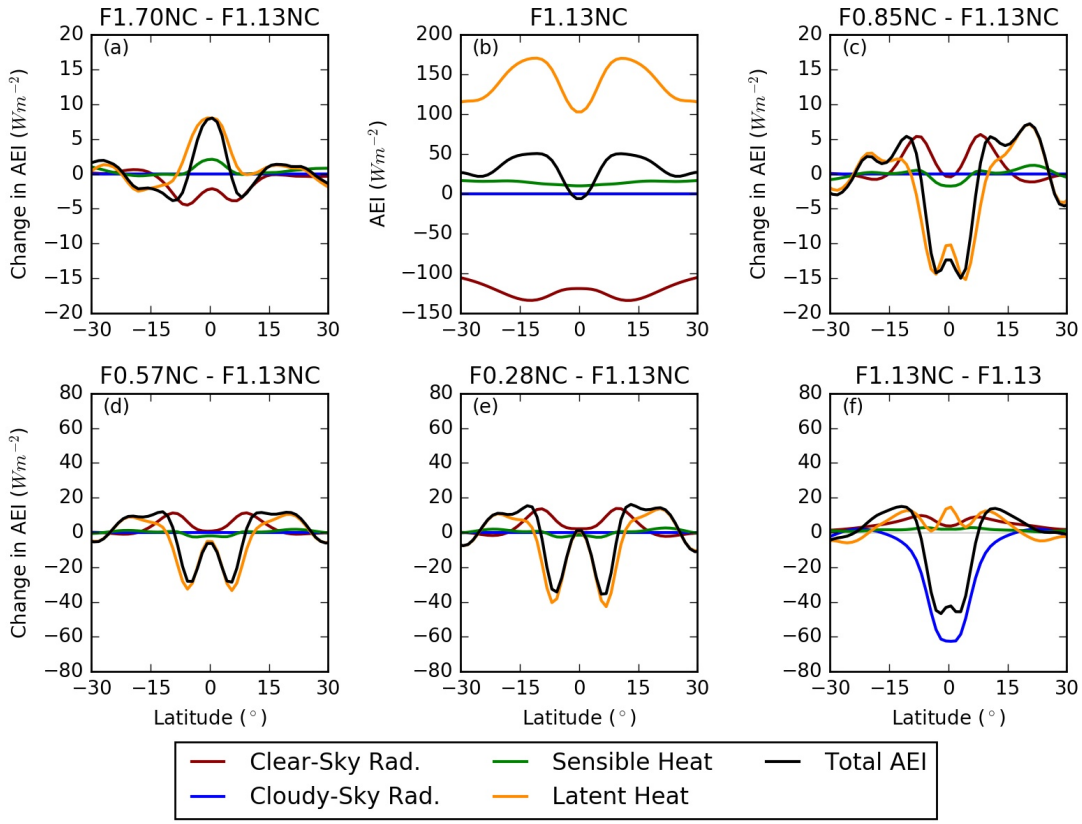

Figure 4.7: *Change in zonal-mean, time-mean AEI components (W m^{-2}) compared to F1.13NC (b) for (a) F1.70NC, (c) F0.85NC, (d) F0.57NC, (e) F0.28NC. (f) Change in AEI components when removing cloud-radiation interactions at f_{dp} equals 1.13 (F1.13NC - F1.13). Red line is the clear-sky component, blue line is the cloudy-sky component. Green and orange lines represent the sensible and latent heat flux, respectively, and the black line is the total AEI change. Note, (a) and (c) have axis limits -20 and 20 W m^{-2} whilst (d)-(f) have limits -80 and 80 W m^{-2}.*

CRE. However, the maximum cloud top height at the ITCZ is insensitive to f_{dp} (not shown), while the minimum temperature at which the cloud fraction goes to zero (cloud top temperature) is sensitive to f_{dp} in both CRE-on and CRE-off simulations (Fig. 4.9). The cloud top temperature decreases as f_{dp} increases (Fig. 4.9), associated with a cooler upper-troposphere. Furthermore, the SST increase at the ITCZ location associated with an equatorward ITCZ contraction, also contributes to an increased CRE at higher f_{dp}.

Removing CRE decreases the sensitivity of the AEI to f_{dp} (comparing Figs. 4.1b and 4.4b), associated with a reduced sensitivity of the ITCZ location (Fig. 4.8a). Latent heat flux variations account for most of the remaining AEI sensitivity to f_{dp} (Fig. 4.7). In simulations with a double ITCZ (F0.28NC, F0.57NC and F0.85NC), changes in latent heat flux and AEI have a bi-modal structure, indicating reduced latent heat flux at the location of maximum precipitation in F1.13NC (Fig. 4.7c-e). Changes in latent heat flux are predominantly controlled by alterations in near-surface wind speed rather than changes in near-surface specific humidity (not shown).

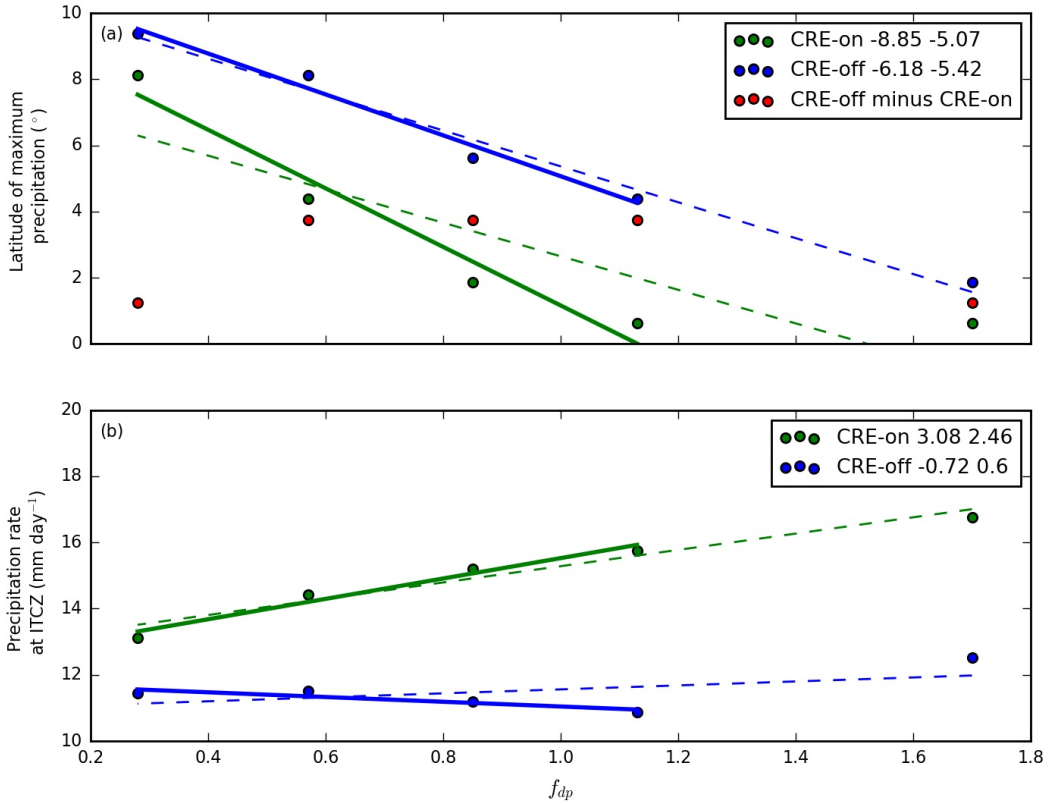

Figure 4.8: *Diagnostics for determining the sensitivity of the ITCZ to f_{dp} in CRE-on (green) and CRE-off (blue) simulations: (a) Latitude of maximum precipitation (°), and (b) maximum precipitation rate (mm day^{-1}). Four regression lines are plotted in each panel. Solid lines show regression for $0.28 \leqslant f_{dp} \leqslant 1.13$ and dashed lines show regression for $f_{dp} \leqslant 1.70$. The slope of each regression line is printed in the legend. First value shows regression for $0.28 \leqslant f_{dp} \leqslant 1.13$ and second value shows regression for $f_{dp} \leqslant 1.70$.*

The results of simulations so far agree with the association in Bischoff and Schneider (2016) between a negative AEI_0 and a double ITCZ (Figs. 4.1 and 4.4). The negative AEI_0 in F0.57 and F1.13NC requires an equatorward energy transport at low latitudes, however, the mass meridional streamfunction suggests a poleward transport of energy (Figs. 4.2d, 4.5b). In the following subsection the mechanisms for an equatorward energy transport are discussed.

4.4.2 Mechanisms responsible for an equatorward energy transport

To better understand the mean circulation response to various f_{dp} and removing CRE, the divergence of the MSE flux ($\partial_y[\widehat{\overline{vh}}]$) is partitioned into mean ($\partial_y([\hat{\overline{v}}][\hat{\overline{h}}])$) and eddy ($\partial_y([\widehat{\overline{vh}}])_{eddy}$) components (Fig. 4.10):

$$\partial_y([\widehat{\overline{vh}}])_{eddy} = \partial_y[\widehat{\overline{vh}}] - \partial_y([\hat{\overline{v}}][\hat{\overline{h}}]) \tag{4.1}$$

where square brackets denote the zonal-mean, the horizontal line denotes the time-mean, and $\hat{}$

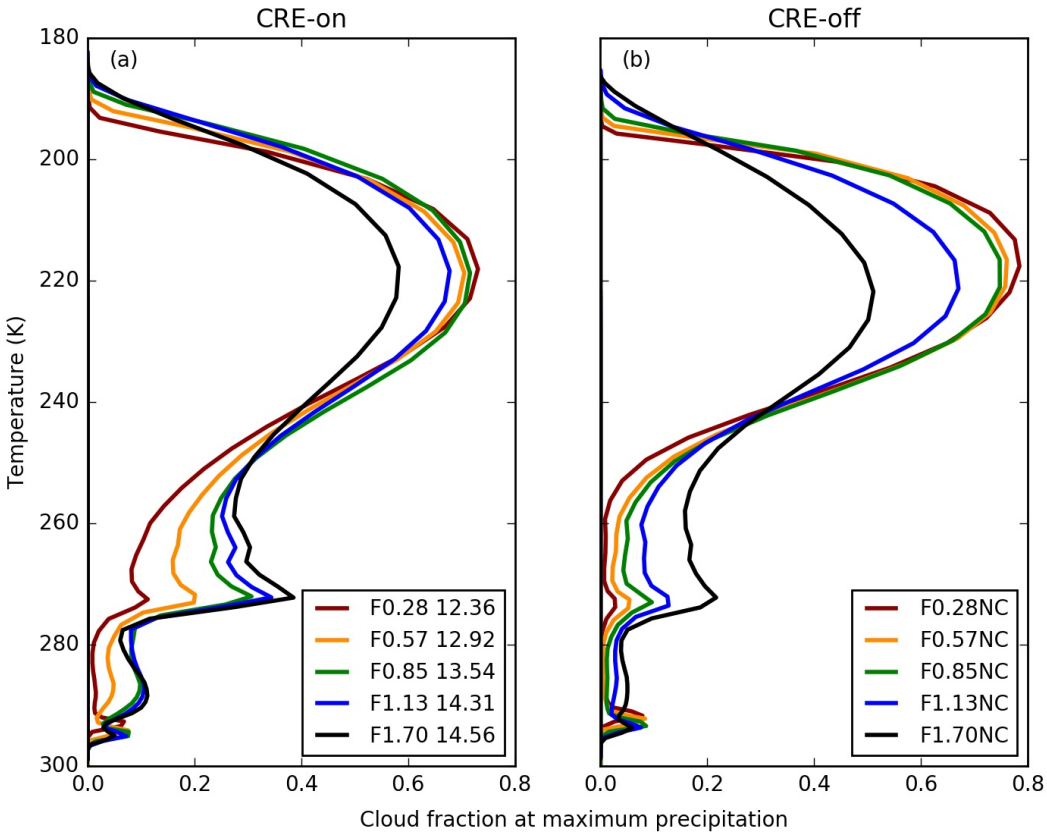

Figure 4.9: *Zonal-mean, time-mean cloud fraction against temperature (K) at the latitude of maximum precipitation for (a) CRE-on simulations and (b) CRE-off simulations. The tropical-domain average CRE (W m^{-2}) for CRE-on simulations is printed in the legend next to the simulation identifier.*

denotes the density-weighted vertical integral. In simulations in this chapter it has not been possible to close the atmospheric energy budget (2.11) due to local energy conservation issues (discussed further in section 4.5), however the sign of AEI_0 is consistent with the sign of $\partial_y[\widehat{\overline{vh}}]$ in simulations so far. In all simulations the eddy contribution to the meridional MSE flux divergence is substantial across the tropics, highlighting that the mean atmospheric circulation is not solely responsible for transporting energy. It should not necessarily be assumed that the required MSE transport is accomplished entirely by the mean meridional circulation. In simulations with a single/double ITCZ, both the mean circulation and eddies transport energy poleward/equatorward at low latitudes. In F0.57, which has a negative AEI_0 and a split ITCZ, equatorward energy transport at low latitudes is achieved solely by eddies (Fig. 4.10d). When f_{dp} equals 0.85 and 1.13, removing CRE changes the sign of $\partial_y([\hat{\overline{v}}][\hat{\overline{h}}])$ across low latitudes (comparing Fig. 4.10b and c with g and h), however there is still equatorial ascent across most of the troposphere (Fig. 4.5b, c). To understand the sensitivity of the mean circulation to removing CRE at these f_{dp} values, the change in MSE flux by the mean circulation ($[\hat{\overline{v}}][\hat{\overline{h}}]$) is partitioned into circulation changes and MSE variations.

First, the meridional mass flux, denoted by V, in F1.13NC (V_e) is partitioned into two components:

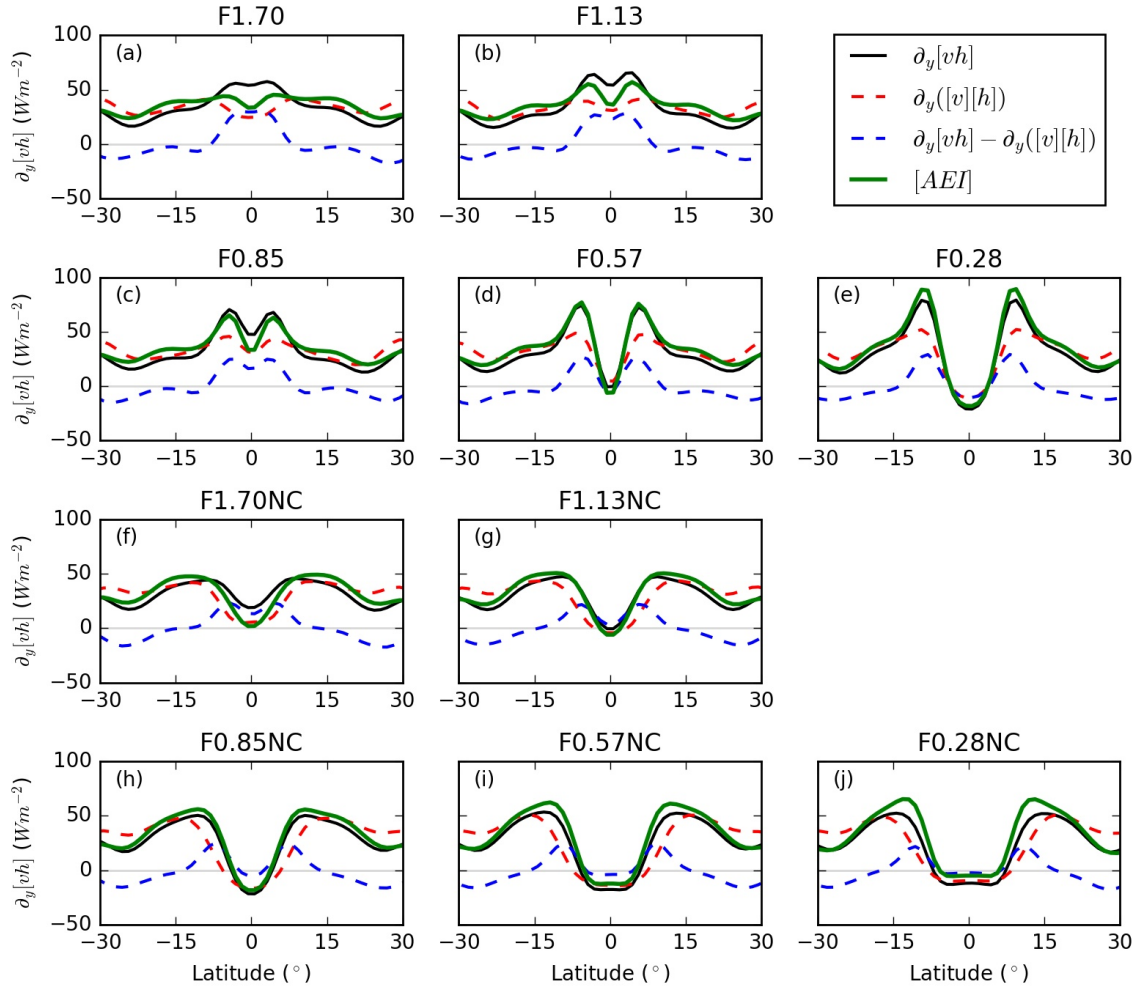

Figure 4.10: *Zonal-mean, time-mean meridional divergence of the MSE flux (W m^{-2}) for simulations with various f_{dp}. (a)-(e) CRE-on simulations, (f)-(j) CRE-off simulations. The simulation is labelled above each panel. The solid black line shows the divergence of the total MSE flux ($\partial_y[\hat{\overline{vh}}]$); the red dotted line shows the MSE flux due to the mean circulation ($\partial_y[\hat{\overline{v}}][\hat{\overline{h}}]$); and the blue line shows the eddy contribution ($\partial_y[\hat{\overline{vh}}] - \partial_y[\hat{\overline{v}}][\hat{\overline{h}}]$). The solid green line shows the zonal-mean, time-mean AEI (W m^{-2}).*

$$V_e = V_c(1+\alpha) + V_r$$
$$\text{where } \alpha = \frac{V_e \cdot V_c}{V_c \cdot V_c} - 1 \tag{4.2}$$

where subscripts c and e represent the zonal-mean, time-mean value of the control (F1.13) and experiment (F1.13NC) simulations respectively. α is a globally uniform scaling term calculated using the dot product of the meridional mass fluxes in the tropics (30°N to 30°S). In all previous calculations a density-weighted vertical integral is computed, however here, V includes density variations. $V_c(1+\alpha)$ denotes a change in the intensity of the control circulation, whilst V_r denotes a change in circulation structure. Next, MSE in the experiment simulation (h_e) is written as:

$$h_e = h_c + h_p \tag{4.3}$$

where subscript p represents the zonal-mean, time-mean difference between the two simulations. The change in MSE flux by the mean circulation between the experiment and control simulation is:

$$\begin{aligned} V_e h_e - V_c h_c = \\ \alpha V_c h_c + V_r h_c + V_c h_p + (\alpha V_c + V_r) h_p \end{aligned} \tag{4.4}$$

Each term in (4.4) represents a mechanism by which $[\hat{\overline{v}}][\hat{\overline{h}}]$ can vary: $\alpha V_c h_c$ represents circulation intensity changes; $V_r h_c$ represents changes in circulation structure; $V_c h_p$ represents MSE profile changes; and $(\alpha V_c + V_r) h_p$ represents MSE profile changes correlated with changes in circulation structure and strength.

Three of the four mechanisms are important in reducing the poleward MSE transport by the Hadley circulation in F0.85NC and F1.13NC (Fig. 4.11, only shown at f_{dp} equals 1.13): a reduction in Hadley circulation strength (Fig. 4.11e); a shallower mean circulation (Fig. 4.11f); and a reduced MSE export at the top of the Hadley circulation due to lower MSE (Fig. 4.11g). MSE profile changes correlated with changes in circulation strength and intensity, $(\alpha V_c + V_r) h_p$, are small compared to the other three mechanisms (Fig. 4.11h). As changes in circulation strength ($\alpha V_c h_c$) cannot change the direction of energy transport, the reduced upper-tropospheric MSE ($V_c h_p$) and shallower Hadley circulation ($V_r h_c$) must be responsible for the change in energy transport direction by the mean circulation. The meridional divergence of components in (4.4) highlight that at the equator circulation strength changes ($\alpha V_c h_c$) contribute approximately 16% of the reduced $\partial_y([\widehat{\overline{v}}][\widehat{\overline{h}}])$; MSE profile changes ($V_c h_p + (\alpha V_c + V_r) h_p$), including a reduced MSE export by the upper branch of the mean circulation and a shallower Hadley circulation ($V_r h_c$) contribute approximately 34% and 50% respectively (Fig. 4.12). Therefore, when f_{dp} equals 0.85 and 1.13, removing CRE is not associated with a substantial double ITCZ in the mass meridional streamfunction. However, an equatorward MSE transport is achieved by a shallower Hadley circulation and reduced upper-tropospheric MSE. Popp and Silvers (2017) also found similar behaviour in certain simulations where the zero mass meridional streamfunction contour remained at the equator even when the AEI_0 was negative.

Removing CRE and varying f_{dp} is associated with substantial AEI changes that require MSE transport variations. In the two sets of simulations discussed so far, three mechanisms have been identified to transport MSE equatorward at low latitudes when AEI_0 is negative; which mechanisms

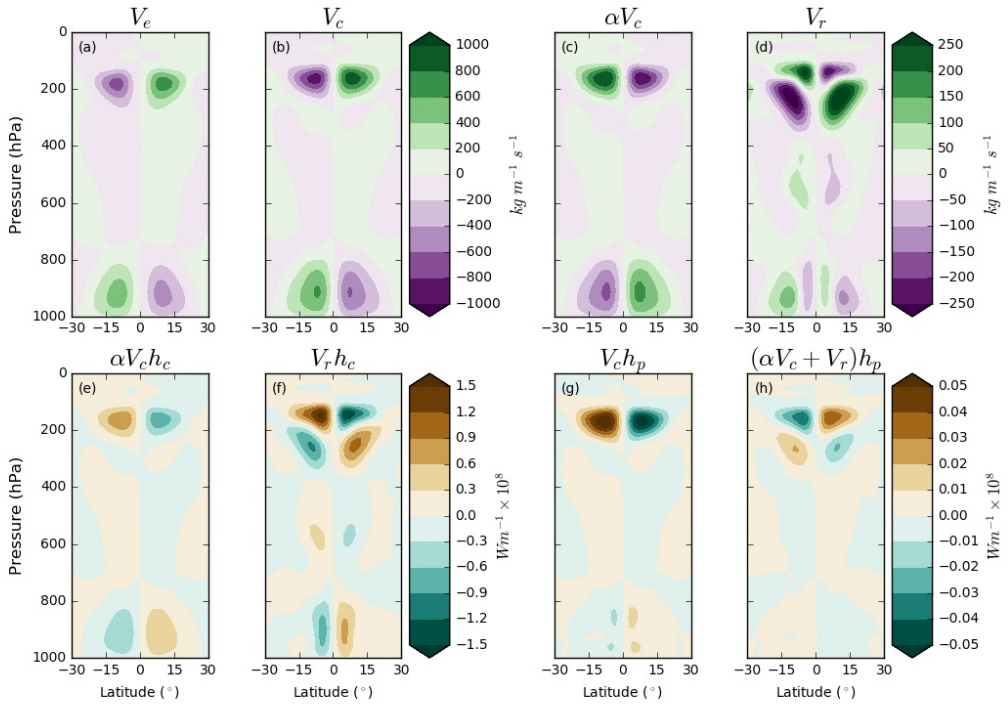

Figure 4.11: *Zonal-mean, time-mean meridional mass flux (kg m^{-1} s^{-1}) in (a) F1.13NC and (b) F1.13, (c) and (d), change in meridional mass flux due to (c) change in circulation strength and (d) change in meridional wind respectively. (e-h): Components of MSE flux change (W m^{-1}), equation 4.4, due to (e) circulation intensity changes ($\alpha V_c h_c$), (f) changes in circulation structure ($V_r h_c$), (g) MSE profile changes ($V_c h_p$), and, (h) MSE changes correlated with changes in circulation structure and strength ($(\alpha V_c + V_r)h_p$). See section 4.4 for further details.*

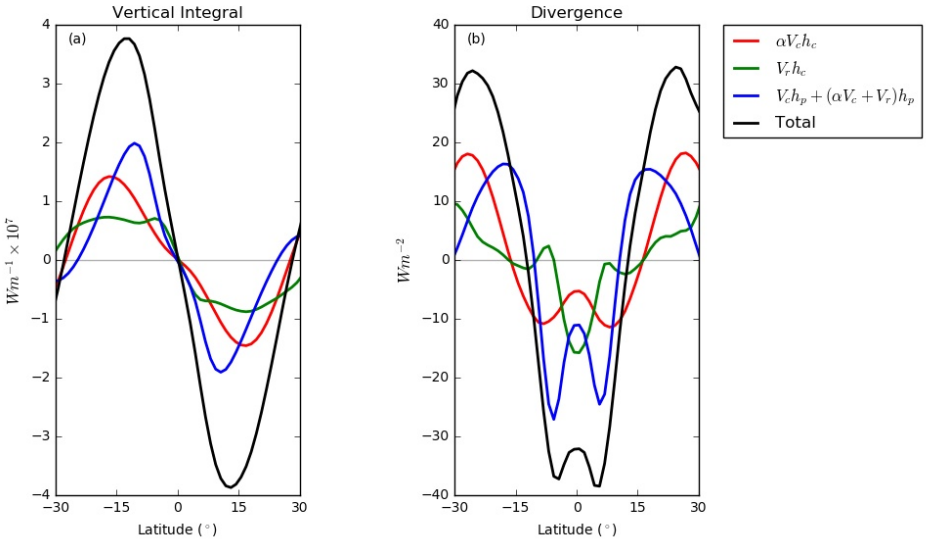

Figure 4.12: *Changes in vertically weighted-integral of (a) MSE flux (W m^{-1}) and (b) MSE flux divergence (W m^{-2}) by the mean circulation and its components as described in section 4.4, equation 4.4. F1.13 and F1.13NC are the control and experiment simulations respectively.*

dominate depends on CRE and f_{dp}. First, in F0.28, F0.28NC and F0.57NC, subsidence across the equatorial region (Figs. 4.2e and 4.5d,e) is associated with an equatorward MSE flux at low latitudes (Fig. 4.10e,j,i). Second, eddy energy transport plays a role in the equatorward MSE flux in

F0.28, F0.57, F0.28NC, F0.57NC, F0.85NC (Fig. 4.10e,d,j,i,h). Third, in F0.85NC and F1.13NC a shallower Hadley circulation and reduced upper-tropospheric MSE reduces the MSE exported in the upper branches of the mean circulation, resulting in a net equatorward MSE transport (Fig. 4.10h,g). All other simulations (F0.85, F1.13, F1.70 and F1.70NC) have a single ITCZ associated with a positive AEI_0 and poleward MSE transport at low latitudes (Fig. 4.10c,b,a,f).

4.4.3 Sensitivity of the ITCZ to convective mixing with a prescribed cloud radiative effect

To further understand the role of CRE in the sensitivity of the ITCZ to convective mixing, prescribed-CRE simulations are performed with various f_{dp} (Table 4.2). The prescribed CRE is diagnosed from single-year simulations with f_{dp} equal to 1.13 or 0.57. The effect of prescribing the diurnal cycle of CRE in a simulation with the same f_{dp} is minimal. For example, the ITCZ and Hadley circulation are similar in F1.13PC1.13 and F1.13 (comparing Figs. 4.1 with 4.13 and 4.2 with 4.14).

Similar to CRE-off simulations, the sensitivity of the ITCZ to f_{dp} is reduced when prescribing CRE (comparing Figs. 4.1a and 4.13a), associated with a reduced sensitivity of the AEI to f_{dp} (Figs. 4.13b, 4.15a,c). Prescribed CRE heating acts as a fixed MSE source; where the prescribed CRE is substantial, an increased MSE export is required and achieved through deep convection. In PC1.13 simulations CRE maximises at the equator (Fig. 4.3b), which is associated with increased equatorial convection and a single ITCZ. In PC0.57 simulations on the other hand, CRE peaks off the equator and promotes a double ITCZ. To highlight the change in sensitivity of the ITCZ and Hadley circulation to f_{dp}, the root mean square deviation (RMSD) is calculated between two simulations:

$$RMSD(\chi) = \sqrt{(\chi_e - \chi_c)^2} \tag{4.5}$$

where subscripts e and c represent the zonal-mean, time-mean value for the experiment and control simulation respectively, and χ represents the chosen diagnostic. The root mean squared deviation of the mass meridional streamfunction is density-weighted. The root mean squared deviation in tropical precipitation and the mass meridional streamfunction between prescribed-CRE simulations where f_{dp} is varied illustrates that prescribing CRE reduces the sensitivity of the ITCZ and Hadley circulation to f_{dp} by approximately 50% (Table 4.3). With F1.13PC1.13 as the control, changing either the prescribed CRE or reducing f_{dp} weakens the upper branch of the Hadley circulation (Fig. 4.14). A more intense upper branch of the mean circulation is simulated in F1.13PC0.57 compared to F0.57PC1.13 highlighting that the upper branch of the Hadley circulation is more sensitive to f_{dp} than the prescribed CRE. The higher f_{dp} value is associated with a cooler upper-troposphere (not shown), which requires an intensified upper branch of the mean circulation to maintain the same

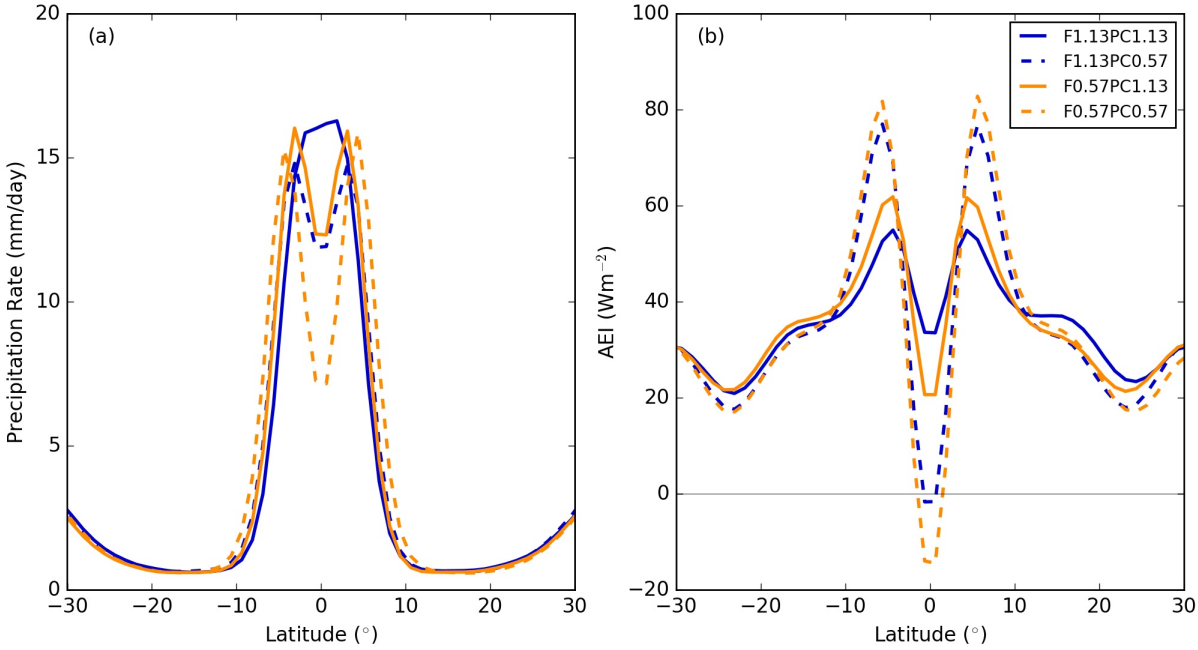

Figure 4.13: *Zonal-mean, time-mean (a) precipitation rates (mm day^{-1}) and (b) AEI (W m^{-2}) in simulations with a prescribed CRE.*

MSE transport. Whilst CRE plays a role in the sensitivity of the ITCZ to convective mixing, the ITCZ and Hadley circulation are still sensitive to f_{dp} in prescribed-CRE simulations. For example, reducing f_{dp} from 1.13 to 0.57 when using PC1.13, weakens the upper branch of the mean circulation (comparing Fig. 4.14a and c) and produces a double ITCZ in precipitation (Fig. 4.13a). The response of convection to changes in f_{dp} is partially offset by the effect of prescribing the location of CRE.

As in CRE-off simulations, AEI changes in prescribed-CRE simulations when varying f_{dp} are predominantly driven by latent heat flux variations. For example, increasing f_{dp} from 0.57 to 1.13 in PC1.13 simulations increases the equatorial latent heat flux and decreases the off-equatorial latent heat flux (Fig. 4.15a). These changes are partially offset by clear-sky radiation changes, associated with decreased TOA outgoing longwave radiation, due to increased atmospheric water vapour. As ITCZ changes are associated with AEI changes, the remaining sensitivity of the ITCZ to f_{dp} in prescribed-CRE simulations is predominately associated with latent heat flux variations. In simulations where the prescribed CRE is varied using the same f_{dp} value, AEI changes are mostly associated with cloudy-sky radiation (Fig. 4.15b, d). However, latent heat flux variations when changing the prescribed CRE are of the same order of magnitude as when varying f_{dp} (Fig. 4.15a, c). A shallower, weaker Hadley circulation is primarily responsible for changes in MSE transport by the mean circulation when reducing f_{dp} or changing the prescribed CRE from PC1.13 to PC0.57 (not shown).

F1.13PC0.57 and F0.57PC1.13 have similar, split ITCZs (Fig. 4.13a) yet very different AEI profiles (Figs. 4.13b, 4.16b and c). F0.57PC1.13 highlights that a double ITCZ in precipitation

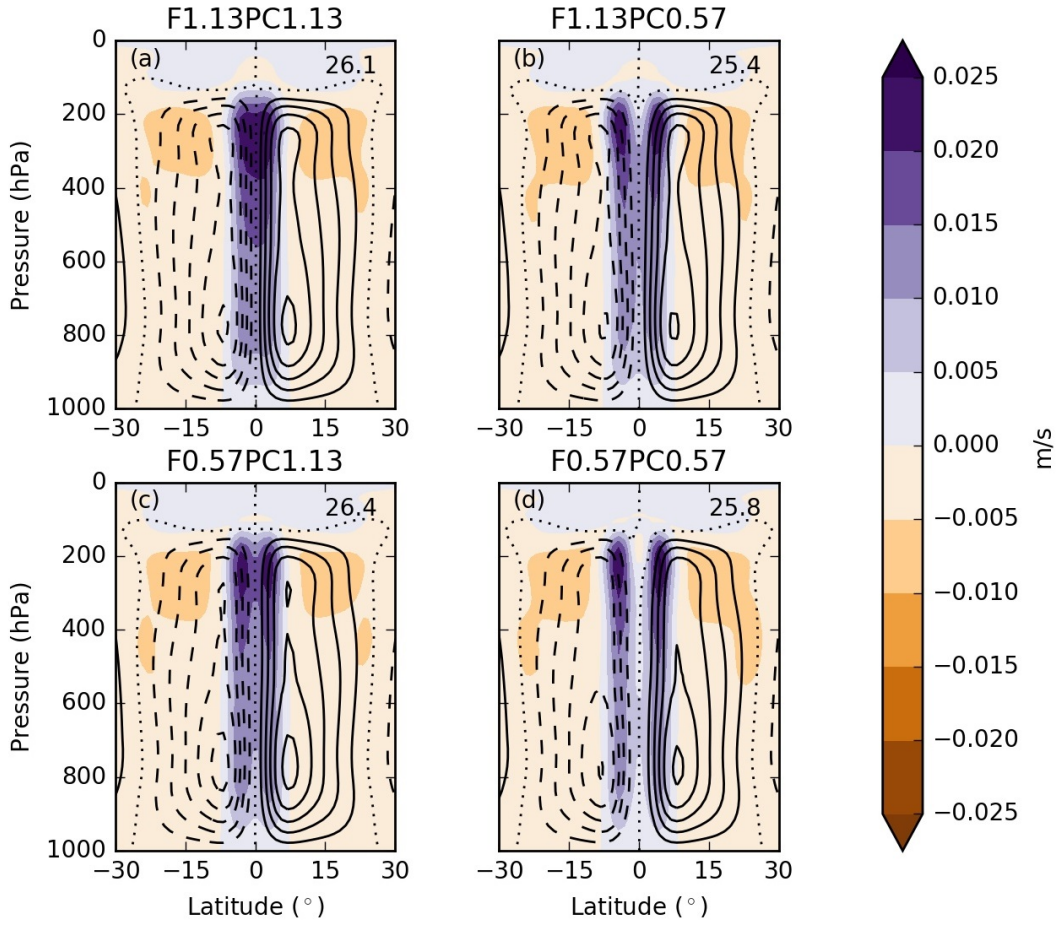

Figure 4.14: *Zonal-mean, time-mean mass meridional streamfunction (kg s^{-1}) (line contours) and vertical wind speed (m s^{-1}) (filled contours) for (a) F1.13PC1.13, (b) F1.13PC0.57, (c) F0.57PC1.13 and (d) F0.57PC0.57. Line contours are at intervals of 5 $\times$ 10^{10}, with dashed contours representing negative values. Positive streamfunction values indicate clockwise circulation. Dotted contour is zero value and the maximum magnitude of the mass meridional streamfunction is printed in the top right-hand corner of each panel.*

does not require a negative AEI_0 or an equatorward MSE transport (green and black lines respectively in Fig. 4.16c). Instead, a negative AEI_0 is a sufficient but not a necessary condition for a double ITCZ in precipitation. Due to local energy conservation issues, which are discussed further in section 4.5, it is challenging to understand F1.13PC0.57, which shows a negative AEI_0 and a positive equatorial $\partial_y[\widehat{\overline{vh}}]$ (Fig. 4.16b), contradicting equation 2.11 as steady-state has been reached.

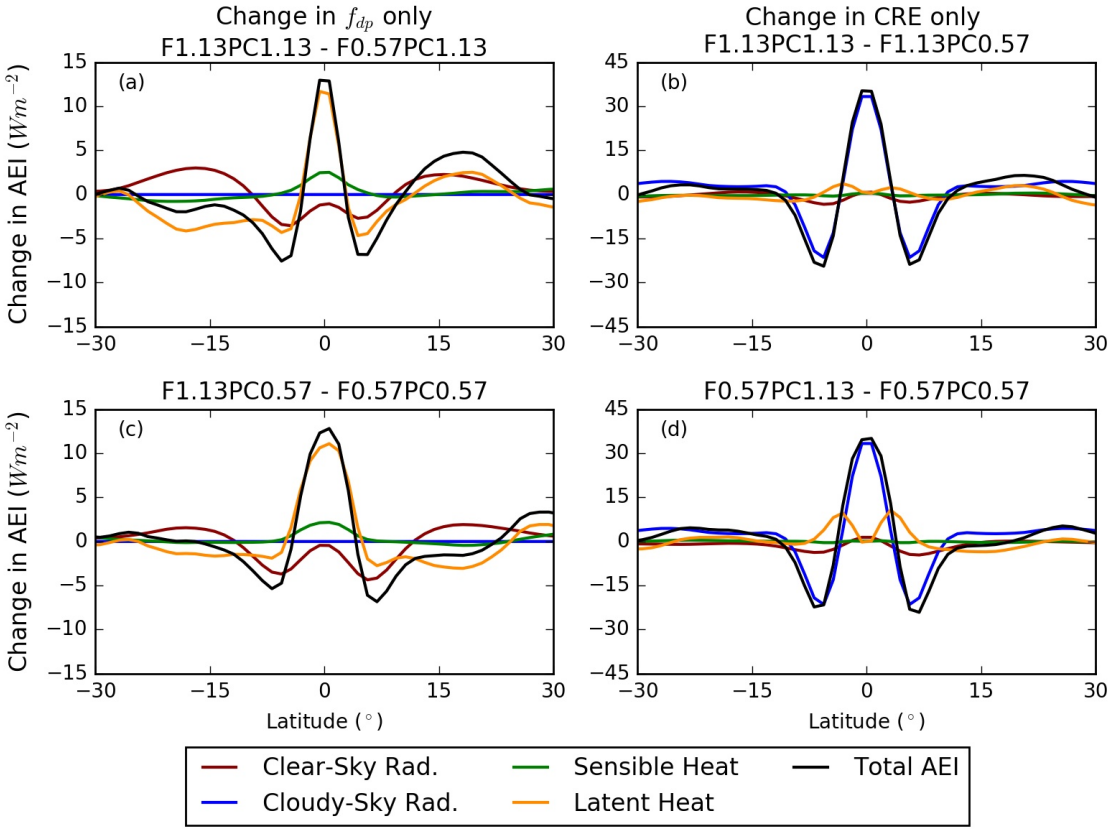

Figure 4.15: *Changes in zonal-mean, time-mean AEI contributions (W m^{-2}) for prescribed-CRE simulations. Red line is the clear-sky component, blue line is the cloudy-sky component. Green and orange lines represent the sensible and latent heat flux, respectively, and the black line is the total AEI change. Comparison of simulations with same prescribed CRE (a, c) have y-axis limits of -15 to 15 W m^{-2}, whilst those with a different f_{dp} value (b, d) have y-axis limits -45 to 45 W m^{-2}.*

Table 4.3: *Root mean squared deviation for tropical precipitation and mass meridional streamfunction between two simulations. Tropical domain defined as 30°N to 30°S. The percentage value in brackets is the reduction in sensitivity compared to F0.57 and F1.13.*

Simulations	Precipitation (mm day^{-1})	Mass Meridional Streamfunction ($\times 10^{10}$ kg s^{-1})
F0.57 & F1.13	2.84	0.76
F0.57PC1.13 & F1.13PC1.13	1.18 (58%)	0.35 (54%)
F0.57PC0.57 & F1.13PC0.57	1.65 (42%)	0.45 (41%)

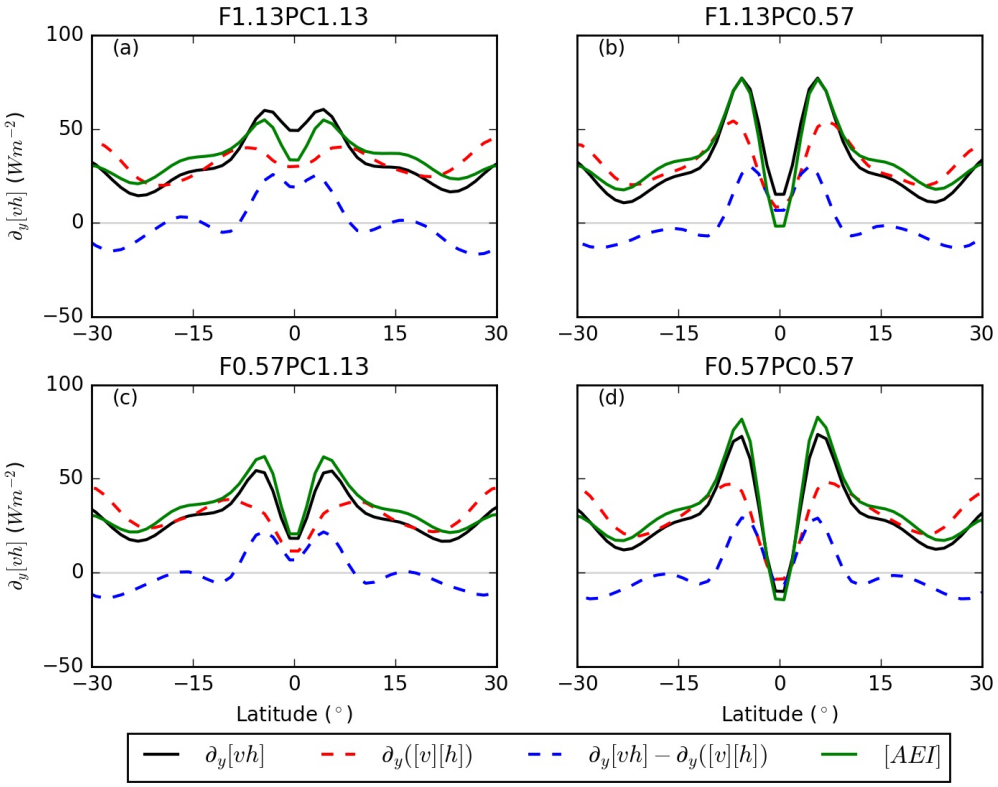

Figure 4.16: *Zonal-mean, time-mean meridional divergence of the MSE flux (W m^{-2}) and AEI for (a) F1.13PC1.13, (b) F1.13PC0.57, (c) F0.57PC1.13 and (d) F0.57PC0.57. Solid black lines denote the divergence of the total MSE flux ($\partial_y[\widehat{\overline{vh}}]$), red dotted lines denote the MSE flux due to mean circulation ($\partial_y[\hat{\overline{v}}][\hat{\overline{h}}]$), blue dotted lines denote the eddy contribution ($\partial_y[\widehat{\overline{vh}}] - \partial_y[\hat{\overline{v}}][\hat{\overline{h}}]$), and green solid lines denote the AEI.*

4.5 Discussion

Work in this chapter shows a sensitivity of the ITCZ to convective mixing in an aquaplanet modelling environment. Variations in ITCZ characteristics have been associated to AEI variations and through doing so it is shown that CRE plays an important role in the sensitivity of the ITCZ to convective mixing. In a single ITCZ scenario (F0.85, F1.13 and, F1.70) CRE is critical in maintaining a positive AEI_0; AEI_0 would be negative without the CRE in F1.13 and F1.70, associated with a double ITCZ. Changes in cloudy-sky radiation are the dominant cause of AEI changes when varying convective mixing (Fig. 4.3), leading to the hypothesis that prescribing CRE would remove or reduce the sensitivity of the ITCZ to convective mixing. The fact that a sensitivity of the ITCZ to f_{dp} remains in CRE-off and prescribed-CRE simulations highlights the importance of other AEI components, in particular the latent heat flux (Figs. 4.7 and 4.15). All simulations, with the exception of F0.57PC1.13, are consistent with the findings of Bischoff and Schneider (2016): a positive AEI_0 is associated with a single ITCZ and a negative AEI_0 is associated with a double ITCZ.

CRE-off simulations illustrate that CRE plays a substantial role in the structure and intensity of the ITCZ. Similar to Harrop and Hartmann (2016), removing CRE cools the tropical upper-troposphere (Fig. 4.6c), reducing atmospheric stability and resulting in deep convection over cooler SSTs. Stronger convection at higher latitudes reduces equatorial moisture convergence and is associated with a double ITCZ. Vishal et al. (2018) conclude, through partitioning the influence of radiative heating from low- ($\geq$ 500 hPa) and high-level ($\leq$ 500 hPa) clouds in prescribed-SST aquaplanet simulations using the Community Earth System Model, that low-tropospheric heating from upper-tropospheric clouds has the greatest impact on ITCZ characteristics. However, in Vishal et al. (2018) upper-tropospheric warming when removing all radiative heating tendencies from cloud-radiation interactions is approximately 50% weaker than in simulations in this chapter (comparing their Fig. 3a with Fig. 4.6c here); cooling rates associated with low-level subtropical clouds are approximately 50% stronger (comparing their Fig. 2i with Fig. 4.6i here). They also show that an anomalous secondary, shallow circulation is only simulated in CRE-on simulations, which is associated with a net MSE import into the ITCZ region and a stronger, narrower ITCZ. However in this chapter, a secondary shallow circulation is seen in both CRE-on and CRE-off simulations (Figs. 4.2 and 4.5). Differences in Hadley circulation and cloud characteristics across the tropics highlights a model dependence of the mechanisms responsible for ITCZ changes when removing CRE. In this chapter removing CRE also weakens the Hadley circulation by approximately 20%, agreeing with the numerical study by Bergman and Hendon (2000), and is associated with a reduced AEI gradient between the tropics and sub-tropics, in agreement with Popp and Silvers (2017). The sensitivity of the ITCZ to f_{dp} reduces when removing CRE (Fig. 4.8), agreeing with the hypothesis that

prescribing CRE would reduce the sensitivity of the ITCZ to convective mixing. Quantifying the reduction in sensitivity is a challenge as it depends on the chosen metric and range of f_{dp}. It should also be noted that when removing CRE other AEI components change, such that the AEI change is not equal to the change in CRE.

In prescribed-CRE simulations ITCZ characteristics are sensitive to both the prescribed CRE and f_{dp} (Fig. 4.13), however the sensitivity of the ITCZ to f_{dp} reduces by approximately 50% (Table 4.3). The response of convection associated with changing f_{dp} is offset by the effect of prescribing the location of CRE. Heating associated with the prescribed CRE is a MSE source, which requires stronger convection to increase MSE export. The reduced sensitivity of the ITCZ to f_{dp} when prescribing CRE compliments Voigt et al. (2014) which shows that prescribing CRE reduces the sensitivity of the ITCZ to hemispheric albedo perturbations to a similar degree. In chapter 5 work by Voigt et al. (2014) is extended by performing simulations to investigate whether CRE plays a similar role in the sensitivity of the ITCZ to hemispherically asymmetric boundary conditions (section 5.4).

In both CRE-off and prescribed-CRE simulations, latent heat flux changes, associated with circulation changes, are the predominant cause of AEI changes when varying f_{dp} (Figs. 4.7 and 4.15). Circulation changes when varying f_{dp} in CRE-off simulations are not associated with clear-sky flux variations, consistent with Harrop and Hartmann (2016), which concluded that changes in the clear-sky radiative cooling do not change the modelled circulation. Mobis and Stevens (2012) highlighted the importance of surface fluxes in reducing the sensitivity of the ITCZ to the convective parameterisation when prescribing the wind speeds in the computation of surface fluxes. Numaguti (1993) and Liu et al. (2010) also show that variations in surface evaporation are associated with the ITCZ structure. In this chapter it is highlighted that the sensitivity of the ITCZ to convective mixing is predominantly associated with surface fluxes in the absence of cloud feedbacks.

As noted in sections 4.3 and 4.4, the balance between the diagnosed AEI and $\partial_y[\widehat{\overline{vh}}]$, equation (2.11), does not hold locally in MetUM (Figs. 4.10 and 4.16). The mean amongst simulations of the maximum absolute diagnosed imbalance across the tropics is 13.4 W m^{-2}; the diagnosed equatorial energy imbalance ranges from 6.94 W m^{-2} in F0.28NC to -20.63 W m^{-2} in F1.70, with a mean absolute error of 9.89 W m^{-2}. For all simulations in this chapter apart from F1.13PC0.57, the sign of $\partial_y[\widehat{\overline{vh}}]_0$ and AEI$_0$ are the same, thus AEI$_0$ can be used as a proxy for the energy transport direction across low latitudes. However, in F1.13PC0.57 the difference between diagnosed $\partial_y[\widehat{\overline{vh}}]_0$ and AEI$_0$ is -16.9 W m^{-2}; the equatorial $\partial_y[\widehat{\overline{vh}}]$ is positive and AEI$_0$ is slightly negative (Fig. 4.16b). Whilst the local energy imbalance is a concern for F1.13PC0.57, in all other simulations

the local energy imbalance does not affect conclusions reached. There are a number of possible reasons for the localised imbalance of the AEI budget, including: non-conservation associated with the semi-Lagrangian advection scheme in MetUM; the use of dry and moist density in different components of the MetUM dynamics and physics; errors in diagnosis of the MSE budget, for example, not considering density changes within a timestep; and, using an Eulerian approach for diagnosing the energy transport, which is inconsistent with the MetUM semi-Lagrangian advection scheme. It is worth noting that other studies using the AEI framework (e.g. Donohoe et al., 2013; Bischoff and Schneider, 2014) have not shown that the MSE energy budget is locally closed; this problem may not be unique to this thesis. Nevertheless, the local energy imbalance has challenged the interpretation of some simulations, and highlights that future modelling studies using an atmospheric MSE budget should be cautious.

CRE variations when varying f_{dp} can lead to a negative AEI_0 associated with a net equatorward MSE energy transport at low latitudes. Whilst the predominant response to a negative AEI_0 is a double ITCZ associated with equatorward MSE transport at low latitudes by the mean circulation (F0.28, F0.28NC and F0.57NC), F0.57, F0.85NC and F1.13NC have shown that a net equatorward MSE transport can occur at low latitudes even with a poleward energy transport by the mean flow in the upper-troposphere. Two mechanisms may lead to this. First, the MSE flux due to eddies contributes a substantial proportion to the total MSE flux (Figs. 4.10 and 4.16), which can support equatorward MSE transport. In F0.57, the MSE flux due to eddies is responsible for a net equatorward energy transport in the deep tropics. This invalidates the assumption that the energy flux equator is associated with zero MSE transport by the mean circulation, as in Bischoff and Schneider (2016). This is also supported by the equatorward displacement of the energy flux equator diagnosed (from equations 2.13 and 2.15) relative to maximum precipitation in all simulations except for F0.85NC and F1.70NC (Table 4.4). The second mechanism for an equatorward MSE transport by the Hadley circulation even with equatorial ascent is seen in F0.85NC and F1.13NC. The direction of MSE transport by the Hadley circulation is equatorward due to a shallower Hadley circulation and a lower upper-tropospheric MSE. These changes reduce MSE export in the upper branch of the Hadley circulation, resulting in an equatorward MSE transport at low latitudes. Popp and Silvers (2017) also found equatorial ascent when AEI_0 was negative. They propose however that an intensification of a shallow circulation within the Hadley cell leads to a net-equatorward energy transport at low latitudes, rather than the entire Hadley cell becoming shallower. Recent work has also shown a reversal of the energy transport by the mean circulation in slab-ocean aquaplanet simulations with seasonally-varying insolation: the ITCZ location lags behind the energy flux equator, resulting in times where the energy flux equator and ITCZ are in opposite hemispheres (Wei and Bordoni, 2018). These times typically occur during the retreat of the winter cross-equatorial Hadley circulation from

the summer hemisphere, during which the required energy transport is achieved through changes in the vertical structure of the Hadley cell.

The proposed effects of removing CRE on the ITCZ (section 4.4) supports research on the response of the ITCZ to anthropogenic climate change (Neelin et al., 2003; Byrne and Schneider, 2016b; Byrne et al., 2018). The ITCZ weakens and broadens when removing CRE associated with upper-tropospheric cooling (section 4.4; Harrop and Hartmann, 2016). Observations and coupled GCMs show that increased greenhouse gas concentrations are associated with greater warming in the tropical upper-troposphere than the surface (Santer et al., 2008). A reduced vertical tropical temperature gradient increases atmospheric stability (Neelin et al., 2003), whilst surface warming increases atmospheric moisture; these effects combined narrow and intensify the ITCZ (Neelin et al., 2003; Byrne and Schneider, 2016b; Byrne et al., 2018). The ITCZ response to increased greenhouse gas concentrations alters the tropical hydrological cycle (Huang et al., 2013; Lau and Kim, 2015; Dunning et al., 2018). For example over Africa, anthropogenic climate change is projected to shorten and intensify wet seasons (Dunning et al., 2018). It is also shown that CRE enhances convection (section 4.4). For example, convection is favoured where CRE is substantial in prescribed-CRE simulations and the sensitivity of the ITCZ intensity to convective mixing is associated with CRE changes. Due to the influence of CRE on the sensitivity of the ITCZ to convective mixing and the tropical circulation structure, it is hypothesised that cloud-radiation interactions in the real world are associated with intensified tropical precipitation rates.

Thus far the sensitivity of the ITCZ to convective mixing and the role of CRE has only been investigated in simulations with a prescribed equatorial SST maximum and perpetual equinoctial insolation. In the real world both SST and insolation change, which has been shown to vary ITCZ characteristics in observational and modelling studies (e.g. Waliser and Gautier, 1993; Numaguti, 1995; Hoskins et al., 1999; Mobis and Stevens, 2012; Geen et al., 2018). In chapter 5 it is investigated whether changing the boundary conditions affects the role of CRE in the sensitivity of the ITCZ to convective mixing. In a prescribed-SST modelling configuration, an arbitrary and varying OET is implied to maintain the prescribed-SSTs. Thus, prescribed-SST aquaplanet experiments are energetically inconsistent. In Bischoff and Schneider (2014) and Voigt et al. (2016) OET, and hence the net-downward surface energy flux, is fixed, constraining the response of AEI components and potentially reducing the sensitivity of the ITCZ to model perturbations. In reality the ocean circulation, and thus OET, is sensitive to changes in the surface wind stress. Therefore, the SST and OET may change in response to tropical circulation changes from variations in f_{dp} or CRE. Recent work has shown that the ocean circulation plays an important role in the meridional transport of energy (Green and Marshall, 2017) and ITCZ sensitivities found in atmosphere-only simulations do not necessarily hold in a fully

coupled model (Tomas et al., 2016). For example, coupling reduces the sensitivity of the ITCZ to an interhemispheric albedo forcing (e.g. comparing Kay et al. (2016) and Hawcroft et al. (2017) to Voigt et al. (2014)). The radiative effect of clouds on surface temperature and Ekman-driven OET associated with a single ITCZ would be expected to reduce the equatorial SST gradient, which would promote a double ITCZ (Numaguti, 1995; Mobis and Stevens, 2012) and may reduce the sensitivity of the ITCZ to convective mixing. Atmosphere-ocean coupled simulations are analysed in chapter 6 to investigate the effect of coupling on the sensitivity of the ITCZ to convective mixing.

Table 4.4: *AEI_0, location of ITCZ (determined by the maximum precipitation rate) and approximate energy flux equator (δ) using equation 2.13 or 2.15 in each simulation. A single/double ITCZ is assumed when $[\overline{AEI}]_0$ is positive/negative, respectively. Not applicable (N/A) occurs when $[\overline{AEI}]_0$ and $\partial_{yy}([\overline{AEI}])_0$ are both negative and therefore the square root of $-\frac{6([\overline{AEI}])_0}{\partial_{yy}([\overline{AEI}])_0}$ has an imaginary component.*

Simulation	$[\overline{AEI}]_0$ (W m^{-2})	ITCZ location ($^\circ$)	Energy Flux Equator (δ) location ($^\circ$)
F0.28	-18.1	8.13/-8.13	6.85/-7.06
F0.57	-5.9	4.38/-4.38	0.84/-2.87
F0.85	33.4	1.88	-0.41
F1.13	36.7	0.63	0.22
F1.70	33.7	0.63	0.30
F0.28NC	-4.9	9.38/-9.38	N/A
F0.57NC	-12.2	8.13/-8.13	N/A
F0.85NC	-18.3	6.88/-5.63	6.48/-6.80
F1.13NC	-5.9	4.38/-4.38	3.21/-3.58
F1.70NC	2.0	1.88	2.73
F1.13PC1.13	33.6	0.63	0.16
F1.13PC0.57	-1.7	3.13/-3.13	0.19/-1.75
F0.57PC1.13	20.6	3.13	-0.12
F0.57PC0.57	-14.2	4.38/-4.38	2.70/-2.64

4.6 Summary and conclusions

In this chapter prescribed-SST aquaplanet simulations demonstrate a sensitivity of the ITCZ to convective mixing (Fig. 4.1a), supporting and extending previous research showing that variations in convective parameterisation can alter the simulated ITCZ (Hess et al., 1993; Numaguti, 1995; Chao and Chen, 2004; Liu et al., 2010; Mobis and Stevens, 2012). Higher convective mixing is associated with a single ITCZ, whilst lower convective mixing is associated with a double ITCZ. Decreasing convective mixing reduces the minimum boundary-layer MSE required for deep convection as convective mixing decreases the buoyancy of a convective air parcel. Increased off-equatorial convection, associated with lower convective mixing rates, inhibits equatorial convection, due to a reduced equatorward moisture flux, and promotes a double ITCZ. The sensitivity of the ITCZ to convective mixing is associated with AEI variations (Fig. 4.1b). AEI variations are predominately

caused by CRE changes (Fig 4.3), leading to the hypothesis that prescribing CRE would reduce or remove the sensitivity of the ITCZ to convective mixing. CRE plays an important role in maintaining a positive, equatorial AEI when using high convective mixing, therefore CRE is necessary for a simulated single ITCZ (consistent with Harrop and Hartmann (2016) and Bischoff and Schneider (2016)).

The response of the ITCZ to removing CRE depends on the convective mixing rate (comparing Figs. 4.1 with 4.4). At low mixing rates, for which a double ITCZ is observed with CRE, precipitation bands shift poleward. At high convective mixing, removing CRE broadens the ITCZ, whilst at certain mixing rates the ITCZ structure changes from single to double. At all mixing rates removing CRE cools the tropical upper troposphere (Fig. 4.6c), associated with a reduced minimum boundary-layer MSE required for deep convection and hence stronger off-equatorial convection over cooler SSTs. Removing CRE increases the mixing rate at which the ITCZ transitions from a single to a split/double ITCZ. Removing CRE also weakens the Hadley circulation by approximately 20% (comparing Figs. 4.2 and 4.5) and reduces the maximum precipitation rate (comparing Figs. 4.1a and 4.4a), associated with a reduced AEI gradient between the tropics and sub-tropics. Quantifying changes in sensitivity of the ITCZ to convective mixing when removing CRE is challenging, as the sensitivity depends on the range of mixing rates and the chosen metric. Two mechanisms are responsible for a net equatorward MSE transport even when no equatorial subsidence is present: MSE transport by eddies, and a reduced MSE export in the upper branch of the mean circulation due to a shallower Hadley circulation. These mechanisms highlight that caution should be taken when associating AEI changes with changes in ITCZ structure, and extends previous discussions by Popp and Silvers (2017) and Wei and Bordoni (2018).

For the mixing rates considered prescribing CRE reduces the sensitivity of the ITCZ to convective mixing by approximately 50%. Prescribed CRE heating acts a fixed MSE source promoting convection, hence, prescribing an equatorial CRE maximum promotes equatorial convection and prescribing an off-equatorial CRE maximum promotes off-equatorial convection. In simulations with CRE removed or prescribed, the ITCZ remains sensitive to convective mixing, associated with latent heat fluxes (Figs. 4.7 and 4.15a,c). Therefore, in the absence of cloud feedbacks the sensitivity of the ITCZ to convective mixing is associated with surface flux variations. Hence, simulations with fixed OETs, which constrains the net-downward surface energy flux, may underestimate the sensitivity of the ITCZ to changes in model formulation.

Work in this chapter investigated the sensitivity of the ITCZ to convective mixing when using equinoctial boundary conditions, however previous research highlights the simulated ITCZ depends on the

boundary conditions (Numaguti, 1995; Hoskins et al., 1999; Mobis and Stevens, 2012), associated with atmospheric heating variations. Work in chapter 5 investigates whether changes in the boundary conditions changes the sensitivity of the ITCZ to convective mixing and the role of CRE. Recent work has also shown that atmosphere-ocean coupling reduces the sensitivity of the ITCZ to hemispherically asymmetric atmospheric forcing, due to variations in the meridional energy transport by the ocean circulation (Green and Marshall, 2017). In chapter 6 coupled simulations are employed to investigate whether coupling changes the sensitivity of the ITCZ to convective mixing.

Chapter 5

The effect of boundary conditions on the sensitivity of the ITCZ to convective mixing

5.1 Purpose of this chapter

Work in chapter 4 shows a sensitivity of the ITCZ to convective mixing and that CRE amplifies the sensitivity. Decreasing convective mixing reduces the boundary-layer MSE required for deep convection, promoting convection over cooler SSTs and a double ITCZ. When CRE is removed or prescribed, the sensitivity of the ITCZ to convective mixing reduces, associated with changes in MSE. However, the sensitivity of the ITCZ to convective mixing and the role of CRE, has only been investigated in simulations with perpetual equinox insolation and an equatorial SST maximum. Work in this chapter extends chapter 4 and fulfils the third thesis objective (section 1.3): to determine the importance of the prescribed atmosphere boundary conditions for the sensitivity of the ITCZ to convective mixing. The mechanisms responsible for the sensitivity of the ITCZ to hemispherically asymmetric boundary conditions are also discussed (section 5.4).

When the ITCZ moves off the equator in an aquaplanet, the Hadley circulation transitions from two symmetric cells to a strong, thermally direct cross-equatorial cell in the winter hemisphere and a weak summer hemisphere cell (Merlis et al., 2013; Geen et al., 2018). These mean circulation variations, alongside hemispheric asymmetries in atmospheric heating and cloud-radiative properties, are hypothesised to change the sensitivity of the ITCZ to convective mixing and the role of CRE. For example, an off-equatorial ITCZ is associated with a non-zero cross-equatorial atmospheric energy transport (AET_0, section 2.2; Kang et al., 2008; Bischoff and Schneider, 2014). Increased convective mixing increases the mean tropical CRE in equinoctial simulations (Fig. 4.9). Hence, it

is hypothesised that increasing convective mixing will increase the hemispheric asymmetry in CRE, increase AET_0, and shift the ITCZ poleward.

Aquaplanet studies show the ITCZ is sensitive to the SST profile (Numaguti, 1995; Hoskins et al., 1999; Neale and Hoskins, 2001; Bellon and Sobel, 2010; Mobis and Stevens, 2012; Williamson et al., 2013). An off-equatorial SST maximum is commonly associated with a broader, weaker, off-equatorial ITCZ, although models simulate a range of ITCZ structures given a meridionally asymmetric SST profile (Williamson et al., 2013). The sensitivity of the ITCZ in an aquaplanet to the SST profile depends on the representation of convection (Hess et al., 1993; Mobis and Stevens, 2012). For example, Hess et al. (1993) performed simulations in an aquaplanet configuration of the National Centre for Atmospheric Research Community Climate Model (NCAR CCM1) to investigate the sensitivity of the ITCZ to the SST meridional gradient. Two convective parameterisation schemes were used: the moist convective adjustment (MCA) scheme (Williamson et al., 1987) and a modified Kuo scheme (Kuo, 1974). The MCA scheme produced a single ITCZ over the equatorial SST maximum, even when the meridional SST gradient was weak. The modified Kuo scheme produced a double ITCZ for all but the sharpest meridional SST gradients. Mobis and Stevens (2012) found that the critical meridional SST gradient for a transition from a single to a double ITCZ depends on the representation of convection.

Numaguti (1995) examined the sensitivity of the ITCZ to an off-equatorial SST maximum using three convective parameterisations: Kuo (1974), MCA and a modified Arakawa-Schubert scheme. An SST maximum at 5°N produced an equatorial ITCZ for the MCA scheme, a double ITCZ with greater SH precipitation rates for the modified Arakawa-Schubert scheme, and a single SH ITCZ for the Kuo (1974) scheme. Their results show that the sensitivity of the ITCZ to the convective parameterisation adds uncertainty to understanding the mechanisms responsible for variations in ITCZ characteristics when altering the SST distribution. However, Numaguti (1995) concluded that for any representation of convection the SST distribution plays a substantial role in driving the atmospheric boundary layer flow and the location of atmospheric convergence, thus controlling moisture availability and the ITCZ. The single SH ITCZ when using the Kuo (1974) scheme is a particularly interesting result. In both observations (Waliser and Graham, 1993) and most GCM simulations in an aquaplanet configuration (Blackburn et al., 2013), a single ITCZ is located in the same hemisphere as the SST maximum.

Cloud radiative effects cause spatiotemporal variations in atmospheric heating, which alter the large-scale atmospheric circulation and meridional energy transports (Slingo and Slingo, 1988; Randall et al., 1989; Donohoe and Battisti, 2012). Voigt et al. (2014) performed aquaplanet simulations

coupled to a slab ocean in four GCMs to study the ITCZ response to hemispherically asymmetric surface albedo forcing. A hemispheric albedo asymmetry shifted the ITCZ towards the warmer hemisphere, consistent with Kang et al. (2008) where OET is varied. Voigt et al. (2014) observed a reduced meridional ITCZ shift when removing the radiative response of clouds. Whilst the reduction depends on the choice of GCM and slab ocean depth, their study highlights that cloud-radiation interactions can have a positive feedback on ITCZ shifts.

Using a prescribed-SST aquaplanet configuration of the MetUM, this chapter investigates two sensitivities of the ITCZ: First, the sensitivity of the ITCZ to convective mixing under solstitial boundary conditions; and second, the sensitivity of the ITCZ to hemispherically asymmetric boundary conditions. The role of CRE in each of these sensitivities is also investigated. Comparing the sensitivity of the ITCZ to convective mixing under solstitial boundary conditions with results from chapter 4, determines the importance of the boundary conditions on the sensitivity of the ITCZ to convective mixing. In this chapter, section 5.2 describes the simulations performed. Section 5.3 describes the sensitivity of the ITCZ to convective mixing given solstitial boundary conditions and the role of CRE. Section 5.4 describes the mechanisms responsible for the sensitivity of the ITCZ to hemispherically asymmetric boundary conditions. Sections 5.5 and 5.6 end the chapter with discussion and conclusions.

5.2 Methodology

First, to investigate the sensitivity of the ITCZ to convective mixing under solstitial boundary conditions, five simulations are performed with f_{dp} set to 0.28 (F0.28S), 0.57 (F0.57S), 0.85 (F0.85S), 1.13 (F1.13S) and 1.70 (F1.70S), the same values employed in chapter 4 (Table 5.1). Further details on the formulation of convective mixing are in section 3.1. In this thesis "boundary conditions" refers to insolation and the prescribed-SST profile; "solstitial boundary conditions", labelled "S", refers to a model set-up with NH solstitial insolation and a prescribed-SST maximum at 10°N latitude. A "solstitial ITCZ" refers to the ITCZ simulated when using solstitial boundary conditions. "Equinoctial boundary conditions" refers to an equatorial SST maximum and equinoctial insolation.

NH solstitial insolation is prescribed by fixing the solar declination angle at 23.4°N. Fig. 5.1a illustrates the zonal-mean, time-mean insolation for both equinoctial (Eq) and solstitial (Sol) configurations. Note, the maximum zonal-mean time-mean insolation does not occur at 23.4°N in solstitial simulations due to day length variations. In the real world insolation is the only external source of heating; its seasonal cycle is associated with changes in SST and the ITCZ location (Waliser and Gau-

tier, 1993; Wei and Bordoni, 2018). However, as a prescribed-SST model configuration is used, an idealised approach is required to change SSTs. In observations (Hess et al., 1993) and slab-ocean simulations with seasonally-varying insolation (Wei and Bordoni, 2018), the SST peaks at approximately 10° latitude at solstice, hence, a prescribed-SST maximum at 10°N is used for solstitial simulations. To produce an off-equatorial SST maximum, the Qobs temperature profile (section 3.2, Neale and Hoskins, 2001) is shifted by a fixed latitude (ϕ_{max}):

$$T_*(\lambda,\phi) = \begin{cases} 27\Big[1-\frac{1}{2}\Big(\sin^2\theta+\sin^4\theta\Big)\Big]\ ^\circ C : -\frac{\pi}{3}+\phi^r_{max} < \phi < \frac{\pi}{3}+\phi^r_{max} \\ 0^\circ C : \text{otherwise} \end{cases} \tag{5.1}$$

$$\text{where } \theta = \frac{3[\phi-\phi^r_{max}]}{2}$$

where ϕ^r_{max} is the latitude of maximum SST in radians. By design (5.1) also changes the latitude at which SST equals 0°C (Fig. 5.1). Fixing the latitude where SST equals 0°C, as in Williamson et al. (2013), leads to substantial SST gradient changes. The sensitivity of the ITCZ to these SST gradient changes is minimal (not shown), hence, equation 5.1 is used to keep the simplest approach.

Table 5.1: *Solstitial simulations with various f_{dp}.*

f_{dp}	Simulation
0.28	F0.28S
0.57	F0.57S
0.85	F0.85S
1.13	F1.13S
1.70	F1.70S

Four prescribed-CRE simulations are performed to understand the relative importance of f_{dp} and the CRE in the sensitivity of the solstitial ITCZ to convective mixing (Table 5.2). Each simulation has a prescribed meridionally-, diurnally-varying CRE, computed from a single year simulation that has solstitial boundary conditions and f_{dp} equal to 1.13 or 0.57, (labeled "PC1.13S" and "PC0.57S", respectively). More details on prescribing CRE can be found in section 4.2. The procedure here is similar, expect that hemispheric asymmetries are retained. Two of the four simulations prescribe a CRE from a different f_{dp} value to that used in the simulation itself (F1.13SPC0.57S, F0.57SPC1.13S), whilst the other two simulations (F1.13SPC1.13S, F0.57SPC0.57S) are performed to assess the sensitivity of the solstitial ITCZ to prescribed cloud-radiation interactions.

Further simulations are performed to extend understanding of the mechanisms responsible for the sensitivity of the ITCZ to hemispherically asymmetric boundary conditions. Simulations are performed to isolate the effects of SST and insolation changes (Table 5.3): two simulations with equinoc-

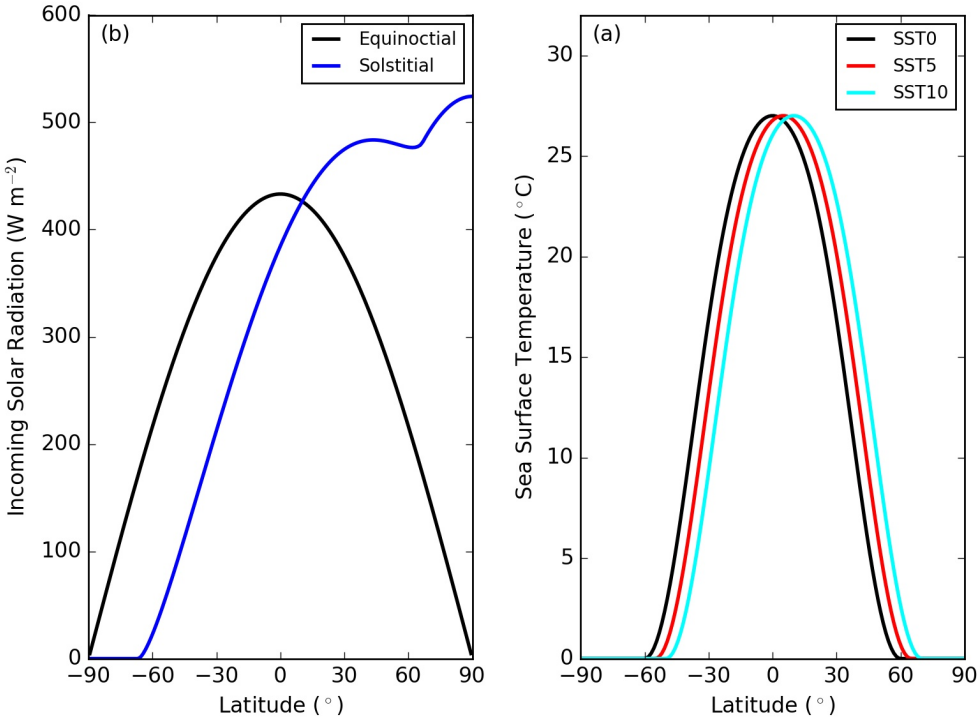

Figure 5.1: *Zonal-mean, time-mean (a) insolation (W m^{-2}) profiles for equinoctial and solstitial simulations, (b) SST (°C) for when ϕ_{max} equals 0, 5 and 10.*

Table 5.2: *Simulations with a prescribed meridionally-, diurnally-varying CRE. "PC1.13S" and "PC0.57S" denote a prescribed CRE diurnal cycle computed from a one-year simulation using solstitial boundary conditions and where f_{dp} equals 1.13 or 0.57, respectively.*

f_{dp}	PC1.13S	PC0.57S
1.13	F1.13SPC1.13S	F1.13SPC0.57S
0.57	F0.57SPC1.13S	F0.57SPC0.57S

tial insolation where ϕ_{max} equals 5 (F1.13EqSST5) and 10 (F1.13EqSST10), and two simulations with perpetual NH solstitial insolation (F1.13SolSST0, F1.13SolSST5). As highlighted in Numaguti (1995), the interpretation of the sensitivity of the ITCZ to an off-equatorial SST maximum depends on the representation of convection. To investigate whether the sensitivity of the ITCZ to hemispherically asymmetric boundary conditions depends on the convective parameterisation, simulations are repeated with f_{dp} equal to 0.57 (Table 5.3). Finally, simulations are performed to investigate the role of CRE in the sensitivity of the ITCZ to hemispherically asymmetric boundary conditions. These are explained further in section 5.4.

Table 5.3: *Simulations varying the insolation and ϕ_{max} with f_{dp} equal to 1.13 or 0.57. F1.13 and F0.57 are also shown in Table 4.1, and F1.13S and F0.57S are also shown in Table 5.1.*

f_{dp}	ϕ_{max} (°)	Equinoctial Insolation	NH Solstitial Insolation
1.13	0	F1.13	F1.13SolSST0
	5	F1.13EqSST5	F1.13SolSST5
	10	F1.13EqSST10	F1.13S
0.57	0	F0.57	F0.57SolSST0
	5	F0.57EqSST5	F0.57SolSST5
	10	F0.57EqSST10	F0.57S

5.3 The impact of boundary conditions on the sensitivity of the ITCZ to convective mixing

5.3.1 Sensitivity of solstitial ITCZ to convective mixing

Section 4.3 shows a sensitivity of the equinoctial ITCZ to convective mixing. To investigate the importance of the boundary conditions on this sensitivity, a set of solstitial simulations are performed (Table 5.1). F0.28S and F0.57S produce two precipitation peaks (Fig. 5.2a) associated with ascent (Fig. 5.3d and e): one in the deep NH tropics (0 to 5°N) and another, less intense band in the NH sub-tropics (15 to 20°N). Upper-level subsidence between the precipitation peaks is simulated (Fig. 5.3d and e), similar to equinoctial simulations with a double ITCZ such as F0.28, F0.28NC and F0.57NC (Figs. 4.1a and 4.4a). For all other f_{dp} values (F0.85S, F1.13S and F1.70S) a single ITCZ is produced with the precipitation maximum closer to ϕ_{max} as f_{dp} increases. The hemispheric asymmetry in ITCZ structure for all f_{dp} values is associated with asymmetries in Hadley circulation characteristics (Fig. 5.3). The hemispheric asymmetry in Hadley circulation is associated with an AEI hemispheric imbalance requiring a non-zero AET_0 for equilibrium (later discussed in section 5.4).

The northward ITCZ shift in response to a change from equinoctial to solstitial boundary conditions is similar across all f_{dp} values. However, its manifestation depends on f_{dp}, consistent with ITCZ structure variations seen under equinoctial boundary conditions. At $f_{dp} \leq 0.57$, off-equatorial precipitation decreases and equatorial precipitation increases, whilst when $f_{dp} \geq 0.85$, NH precipitation increases alongside decreasing SH precipitation (not shown). The sensitivity of the ITCZ to hemispherically asymmetric boundary conditions depends on the representation of convection, in agreement with Hess et al. (1993) and Mobis and Stevens (2012).

As in equinoctial simulations (section 4.3), decreasing f_{dp} under solstitial boundary conditions reduces the minimum boundary-layer MSE required for deep convection, encouraging convection to

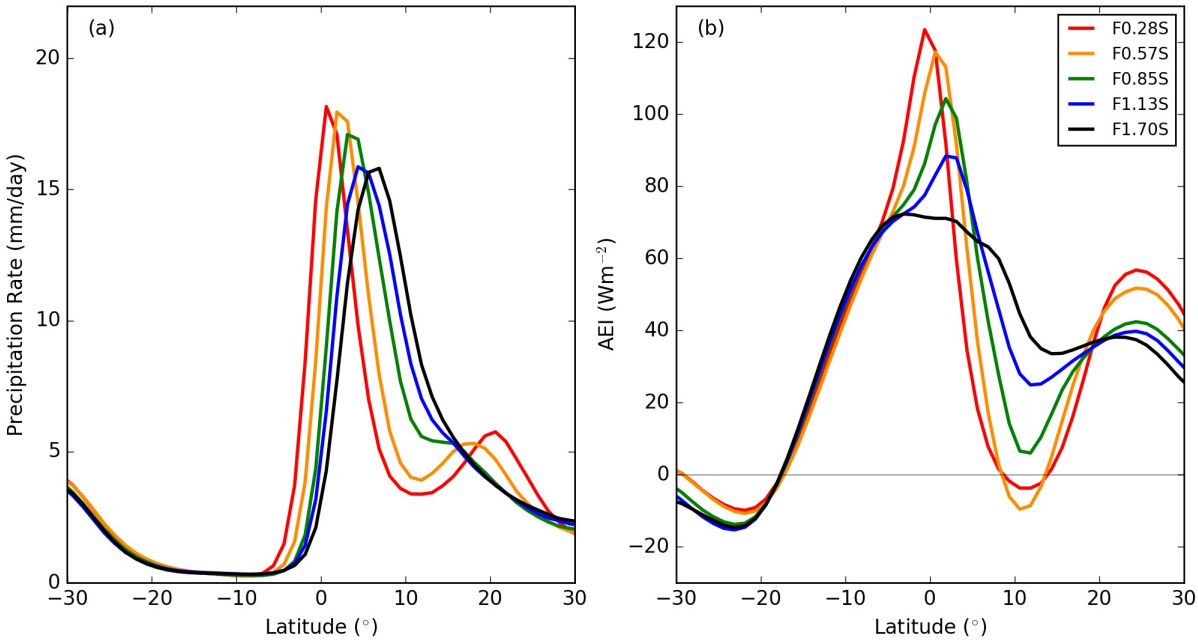

Figure 5.2: *Zonal-mean, time-mean (a) precipitation rates (mm day^{-1}) and (b) AEI (W m^{-2}) in solstitial simulations where f_{dp} is varied (Table 5.1).*

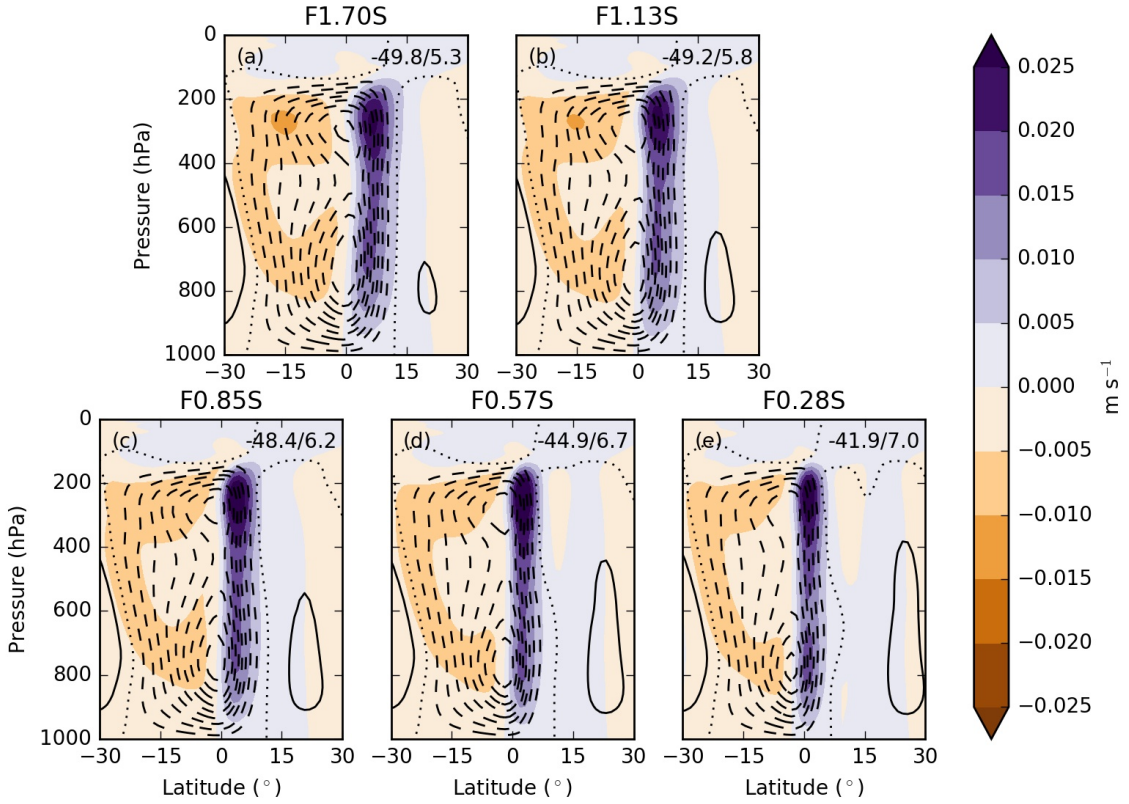

Figure 5.3: *Zonal-mean, time-mean mass meridional streamfunction (kg s^{-1}) (line contours) and vertical wind speed (m s^{-1}) (filled contours) in (a) F1.70S, (b) F1.13S, (c) F0.85S, (d) F0.57S, (e) F0.28S. Line contours are in intervals of 5×10^{10}, with dashed contours representing negative values. Positive streamfunction values indicate clockwise circulation. Dotted contour is the zero value. The maximum magnitude of the mass meridional streamfunction in the SH and NH is printed in top right-hand corner of each panel.*

occur over cooler SSTs. In solstitial simulations this leads to increased precipitation equatorward and poleward of ϕ_{max} and a reduced boundary layer moisture flux towards ϕ_{max} as f_{dp} decreases. The decrease in boundary layer moisture flux towards ϕ_{max} is associated with reduced precipitation over the warmest SSTs; decreased f_{dp} favours a double ITCZ (Figs. 4.1a and 5.2a). In equinoctial simulations decreasing f_{dp} reduces the maximum precipitation rate (Fig. 4.1a), meanwhile in solstitial simulations reducing f_{dp} increases the maximum precipitation rate when $f_{dp} \leq 0.85$ (Fig. 5.2a). Decreasing f_{dp} increases subsidence over ϕ_{max} (Fig. 5.3) associated with a reduced northern extent of the major precipitation band and an ITCZ intensification (Fig. 5.2a); the amount of tropical moisture is insensitive to f_{dp}. Increasing f_{dp} when $f_{dp} \geq 1.13$ shifts the ITCZ north; the width and intensity remain similar (Fig. 5.2a).

The sensitivity of the solstitial ITCZ to f_{dp} is further investigated using an AEI framework. Through doing so, three mechanisms are proposed by which CRE affects the sensitivity of the solstitial ITCZ to f_{dp}. The first mechanism is highlighted through partitioning AET_0 (Fig. 5.4); CRE amplifies the meridional ITCZ shifts when increasing f_{dp} (Fig. 5.2a). The ITCZ location and AET_0 are correlated in observations (Donohoe et al., 2013) and modelling studies (Kang et al., 2008; Frierson and Hwang, 2012); processes that increase the magnitude of AET_0 are associated with poleward ITCZ shifts, whilst a decreased magnitude of AET_0 is associated with an equatorward ITCZ shift. Using a similar method to Voigt et al. (2014), hemispheric differences in AEI budget components can be associated with AET_0. In this study AET_0 is partitioned into three components:

$$\text{AET}_0 = \text{AET}_0^{\text{clear}} + \text{AET}_0^{\text{cloud}} + \text{AET}_0^{\text{H}} \tag{5.2}$$

where superscripts clear, cloud and H are used to represent clear-sky radiative, cloudy-sky radiative and surface flux components of the AEI budget (respectively). Components are calculated using TOA and surface energy budgets. Figure 5.4 shows the net-southward tropical ($\leq 30^\circ$ latitude) and extratropical ($\geq 30^\circ$ latitude) AET_0 components for solstitial simulations; positive values are associated with a northward ITCZ shift and negative values are associated with a southward ITCZ shift. Under solstitial boundary conditions a hemispheric asymmetry in clear-sky radiation is introduced, associated with a southward AET_0 (red bars in Fig. 5.4). However, the imposed clear-sky radiation changes increase the SH AEI gradient between the tropics and extra-tropics and decrease the NH AEI gradient (later shown in Fig. 5.14), associated with a strengthened SH Hadley circulation and a weakened NH Hadley circulation (Fig. 5.3, Popp and Silvers, 2017). Hadley circulation intensity changes lead to increased SH tropical surface fluxes and decreased NH tropical surface fluxes, associated with a northward AET_0 (green bars in Fig. 5.4). AET_0 introduced by clear-sky radiation changes is predominately offset by changes in surface fluxes. However, as the total

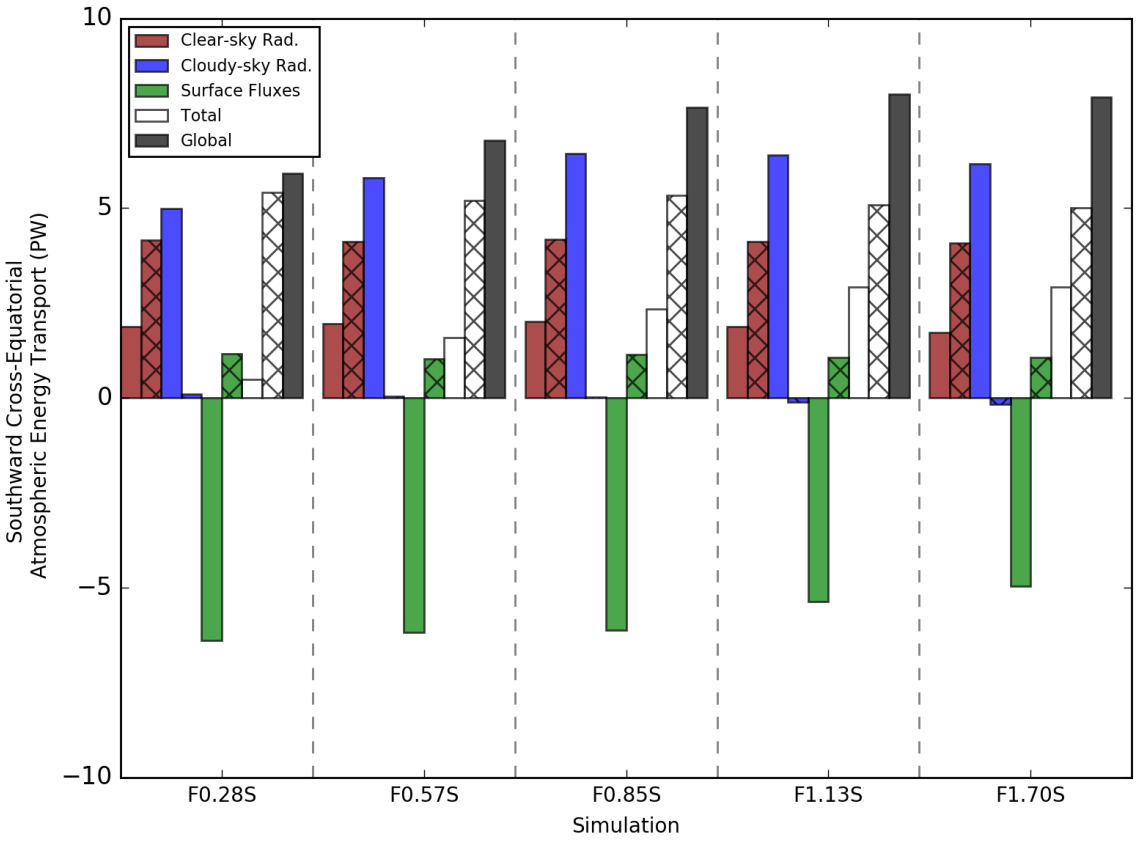

Figure 5.4: *Components of AET_0 (PW) for solstitial simulations where f_{dp} is varied (Table 5.1). Components of AET_0 are calculated using hemispheric asymmetries in AEI budget components (equation 5.2). The red bars denote clear-sky radiation contributions; the blue bars denote cloudy-sky radiation contributions; the green bars denote surface flux contributions (latent and sensible heat flux combined); and the black bars denote the total AET_0. Each component of the AET_0 is split into tropical ($\leq 30^\circ$ latitude) and extratropical components ($\geq 30^\circ$ latitude); the extratropical component is denoted by cross-hatching. The total of tropical and extratropical components is shown in white. Vertical, grey dashed lines are used to separate simulations.*

AET_0^{clear} is greater than the total AET_0^{H}, a southward AET_0 remains, associated with a NH ITCZ. The northward ITCZ shift associated with clear-sky radiation and surface flux hemispheric asymmetries, introduces a hemispheric asymmetry in CRE (blue bars in Fig. 5.4), further increasing AET_0. Hence, it is hypothesised that cloud-radiative feedbacks increase meridional ITCZ shifts associated with solstitial boundary conditions. As in equinoctial simulations (Fig. 4.9), increasing f_{dp} increases the tropical-domain CRE (not shown). As the solstitial ITCZ is located in the NH, increases in CRE increase AET_0^{cloud}, further amplifying the meridional ITCZ shift when increasing f_{dp}. Increasing f_{dp} also increases AET_0^{H}, associated with a northward shift of the southern Hadley circulation (Fig. 5.4). The second mechanism is illustrated in Figure 5.5; changes in tropical cloudy-sky radiation and latent heat fluxes play the dominante role in AEI variations when varying f_{dp}. These AEI variations lead to a negative AEI at ϕ_{max} when $f_{dp} \leq 0.57$, associated with a double ITCZ. The third mechanism is that CRE maintains the single ITCZ in F1.13S; the total AEI is approximately equal to the cloudy-sky AEI contribution (Fig. 5.5b). Hence, removing CRE from F1.13S would produce a negative or near-zero AEI at ϕ_{max}, assuming other AEI components remained constant, associated with a double ITCZ.

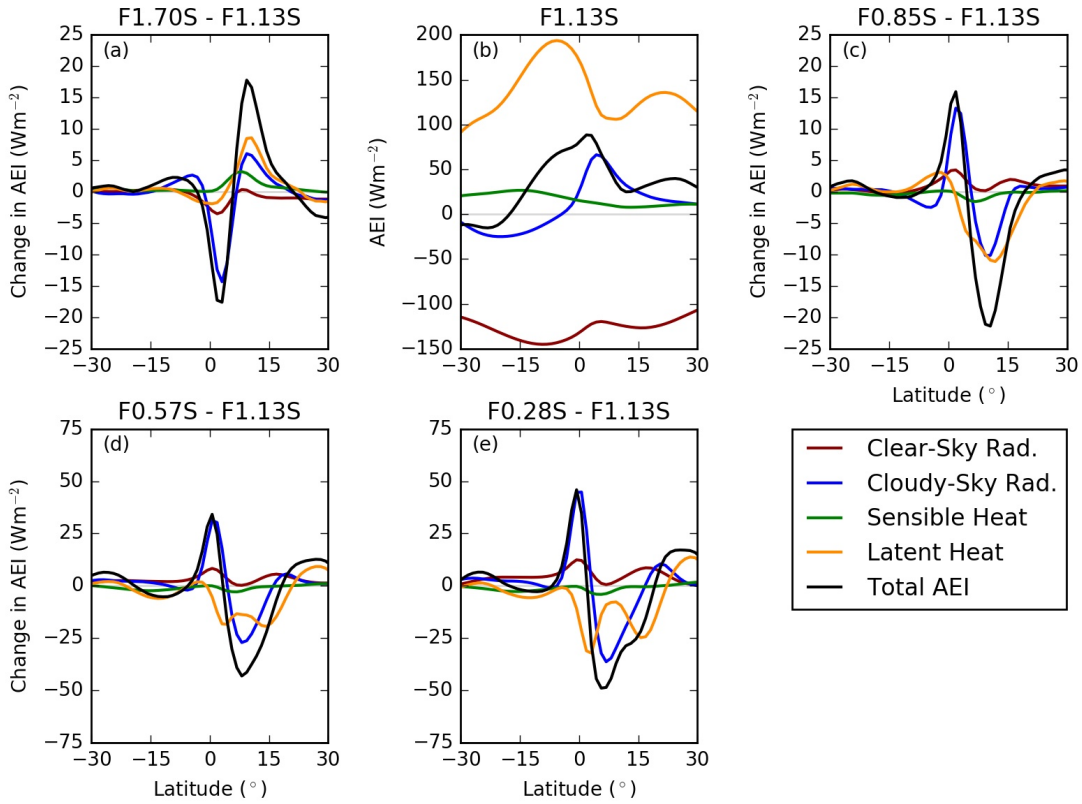

Figure 5.5: *Zonal-mean, time-mean AEI (W m^{-2}) components for (b) F1.13S, (a), (c-e) the change in AEI compared to F1.13S: (a) F1.70S, (c) F0.85S, (d) F0.57S, (e) F0.28S. Red lines denote clear-sky radiation; blue lines denote cloudy-sky radiation. Green and grey lines denote the sensible and latent heat flux (respectively) and black lines denote the total AEI.*

The concluded effect of the boundary conditions on the sensitivity of the ITCZ to f_{dp} depends on both the range of f_{dp} and the diagnostic used. Figure 5.6 shows the difference between the latitude of the ITCZ and ϕ_{max} alongside the ITCZ intensity. The difference between ϕ_{max} and the latitude of the ITCZ is used instead of the ITCZ location as increasing f_{dp} promotes the ITCZ towards ϕ_{max} in both equinoctial and solstitial simulations and allows an easier comparison of the sensitivity of the ITCZ location to f_{dp}. Considering simulations for which $f_{dp} \leq 1.13$, applying solstitial boundary conditions reduces the sensitivity of the ITCZ location to f_{dp} by approximately 45% (Fig. 5.6a). However, the reduction in sensitivity decreases to approximately 10% when $f_{dp} \leq 1.70$ due to an equatorial ITCZ in equinoctial simulations when $f_{dp} \geq 0.85$ (Fig. 4.1a) and the solstitial ITCZ shifting closer to ϕ_{max} when increasing f_{dp} across all values (Fig. 5.2a). The maximum precipitation rate also implies a reduced sensitivity of the ITCZ when applying solstitial boundary conditions (Fig. 5.6b). Increasing f_{dp} increases the equinoctial ITCZ intensity, whilst in solstitial simulations the maximum precipitation rate decreases (Fig. 5.6). The reduction in maximum precipitation in solstitial simulations is smaller than the precipitation increase in equinoctial simulations, resulting in a greater sensitivity of the ITCZ intensity to f_{dp} under equinoctial boundary conditions.

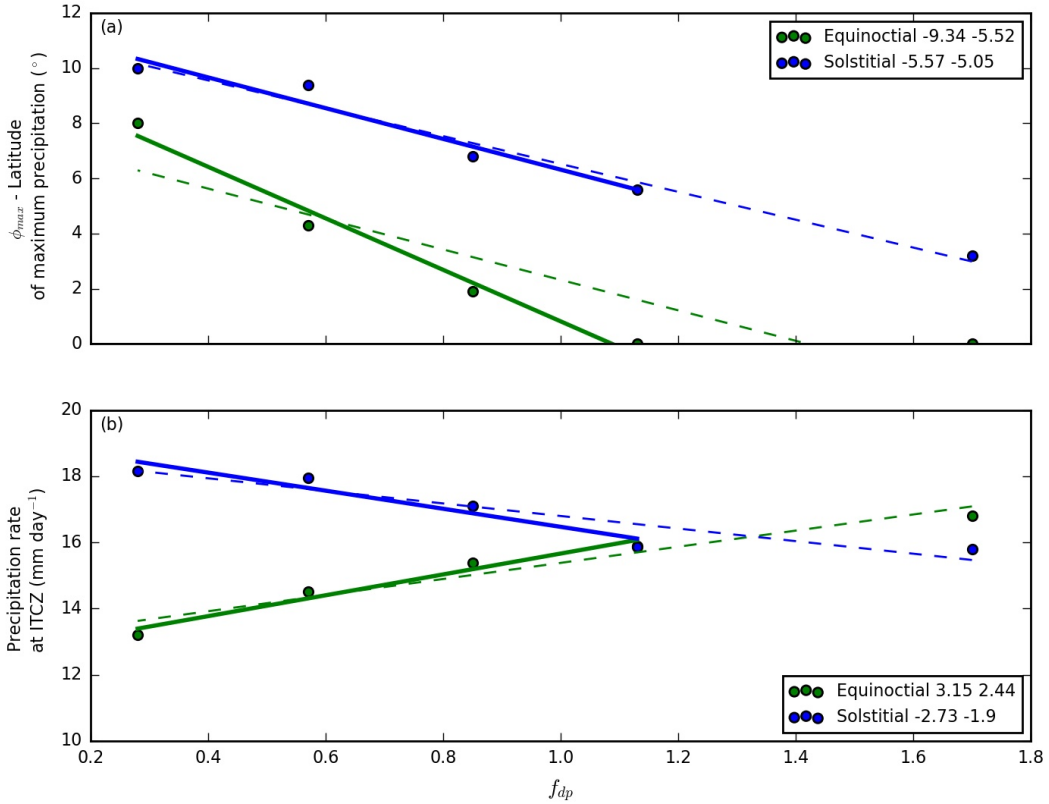

Figure 5.6: *Diagnostics for determining the sensitivity of the ITCZ to f_{dp} in equinoctial (green) and solstitial (blue) simulations. (a) ϕ_{max} minus latitude of maximum precipitation rate (°), (b) Maximum precipitation rate (mm day^{-1}). Four regression lines are plotted in each panel. Solid lines where $0.28 \leqslant f_{dp} \leqslant 1.13$ and dashed lines where $f_{dp} \leqslant 1.70$. The slope of each regression line is printed in the legend. First value where $0.28 \leqslant f_{dp} \leqslant 1.13$ and second value where $f_{dp} \leqslant 1.70$.*

Analysis of the AEI budget concludes that CRE plays a substantial role in the sensitivity of the solstitial ITCZ to f_{dp}. In the NH tropics there are substantial CRE differences between F1.13S and F0.57S (solid lines in Fig. 5.7) associated with a change from a single to a double ITCZ. As in equinoctial simulations, warming from CRE in the ITCZ region comes almost entirely from LW radiation (not shown). Outside the NH tropics similar CRE profiles are seen. The hemispheric asymmetry in extratropical ($\geq 30^\circ$ latitude) CRE is associated with higher/lower cloud fractions in the NH upper-/lower-troposphere compared to the SH (not shown). In the following subsection the effect of prescribing CRE on the sensitivity of the solstitial ITCZ to convective mixing is explored.

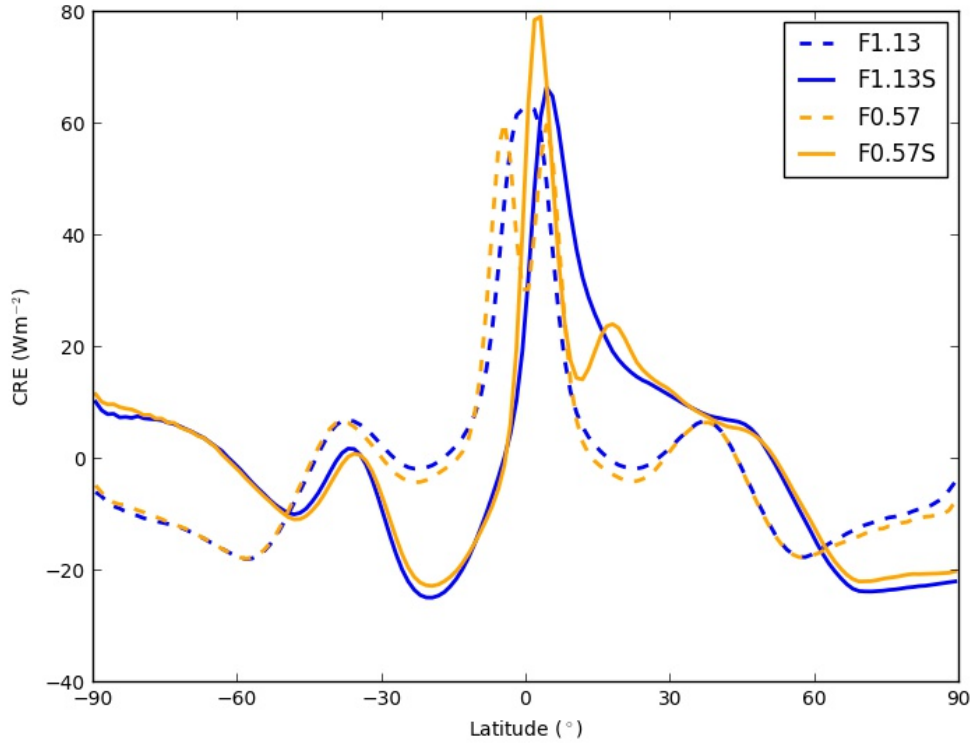

Figure 5.7: *Zonal-mean, time-mean CRE (W m^{-2}) profiles that are used for prescribed-CRE simulations in Tables 4.2, 5.2, and 5.6. Solid lines denote solstitial boundary conditions and dashed lines denote equinoctial boundary conditions. Blue lines denote when f_{dp} equals 1.13 whilst orange lines denote when f_{dp} equals 0.57.*

5.3.2 *Sensitivity of the solstitial ITCZ to convective mixing with a prescribed cloud radiative effect*

To further investigate the role of CRE in the sensitivity of the solstitial ITCZ to f_{dp}, prescribed-CRE simulations are performed with CRE profiles from F1.13S and F0.57S (Table 5.2). In equinoctial simulations, prescribing CRE from a simulation with the same f_{dp} value has a minimal effect on the mean circulation and AEI (section 4.4). However in solstitial simulations, prescribing CRE strengthens the Hadley circulation in both hemispheres. For example, the southern Hadley cell is approximately 5% stronger in F1.13SPC1.13S compared to F1.13S (Figs. 5.3b and 5.9a). Whilst the ITCZ location does not substantially change, the stronger mean circulation is associated with an increased maximum precipitation rate in F1.13SPC1.13S and F0.57SPC0.57S of approximately 3 and 1 mm day^{-1} relative to F1.13S and F0.57S respectively (comparing Figs. 5.2a and 5.8a). This implies that zonal and temporal cloudy-sky radiation variations play a role in the solstitial ITCZ intensity. In general the overall effect of prescribing CRE is small and of a similar sign in F1.13SPC1.13S and F0.57SPC0.57S, hence prescribed-CRE simulations are employed to understand the influence of CRE.

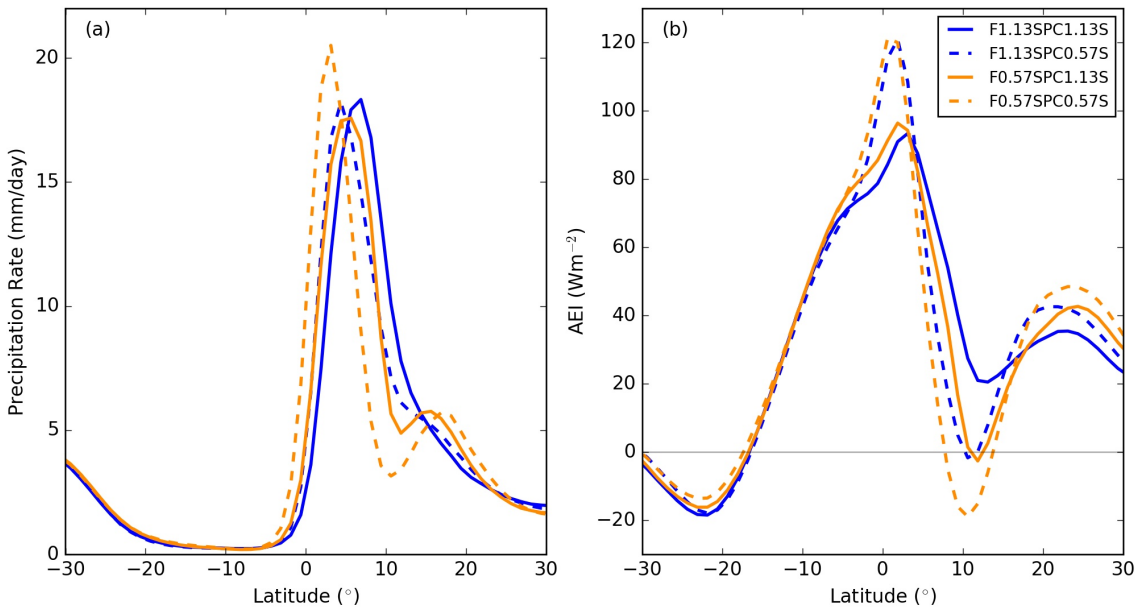

Figure 5.8: *Zonal-mean, time-mean (a) precipitation rates (mm day^{-1}) and (b) AEI (W m^{-2}), in solstitial simulations with a prescribed CRE (Table 5.2). Solid and dashed lines denote PC1.13S and PC0.57S, respectively, whilst blue and orange lines denote F1.13S and F0.57S, respectively.*

When prescribing PC1.13S and decreasing f_{dp} from 1.13 to 0.57, the double ITCZ intensity, difference between maximum precipitation and precipitation at ϕ_{max}, and the equatorward shift of the southern rainfall band reduces (Fig. 5.8a) compared to simulations with a changed prescribed CRE. The reduced sensitivity of the ITCZ to f_{dp} when prescribing CRE is associated with a reduced sensitivity of the mean circulation to f_{dp} (Fig. 5.9). For example, F0.57SPC0.57S produces stronger subsidence at 10°N than F0.57SPC1.13S (Figs. 5.9c and d). Table 5.4 shows a reduced sensitivity of the ITCZ and mean circulation to f_{dp} when prescribing CRE. However, whilst CRE plays a substantial role in the sensitivity of the ITCZ to f_{dp}, a sensitivity remains in prescribed-CRE simulations (Figs. 5.8 and 5.9). For example, a substantial sensitivity of subsidence in SH high tropical latitudes (10°S $\leq \phi \leq$ 30°S) and the upper-level structure of the mean circulation to f_{dp} remains in prescribed-CRE simulations (Fig. 5.9).

Table 5.4: *Root mean squared deviation (4.5) for tropical (30°N to 30°S) precipitation (mm day^{-1}) and mass meridional streamfunction (kg s^{-1}) between two simulations. The percentage value in brackets denotes the reduction in root mean squared deviation compared to F0.57S and F1.13S.*

Simulations	Precipitation (mm day^{-1})	Mass Meridional Streamfunction ($\times$ 10^{10} kg s^{-1})
F0.57S & F1.13S	2.75	0.57
F0.57SPC1.13S & F1.13SPC1.13S	1.60 (42%)	0.32 (44%)
F0.57SPC0.57S & F1.13SPC0.57S	2.45 (11%)	0.43 (25%)

Atmospheric heating associated with CRE promotes convection due to CRE acting as a fixed MSE source, hence, PC0.57S favours convection closer to the equator and a double ITCZ structure.

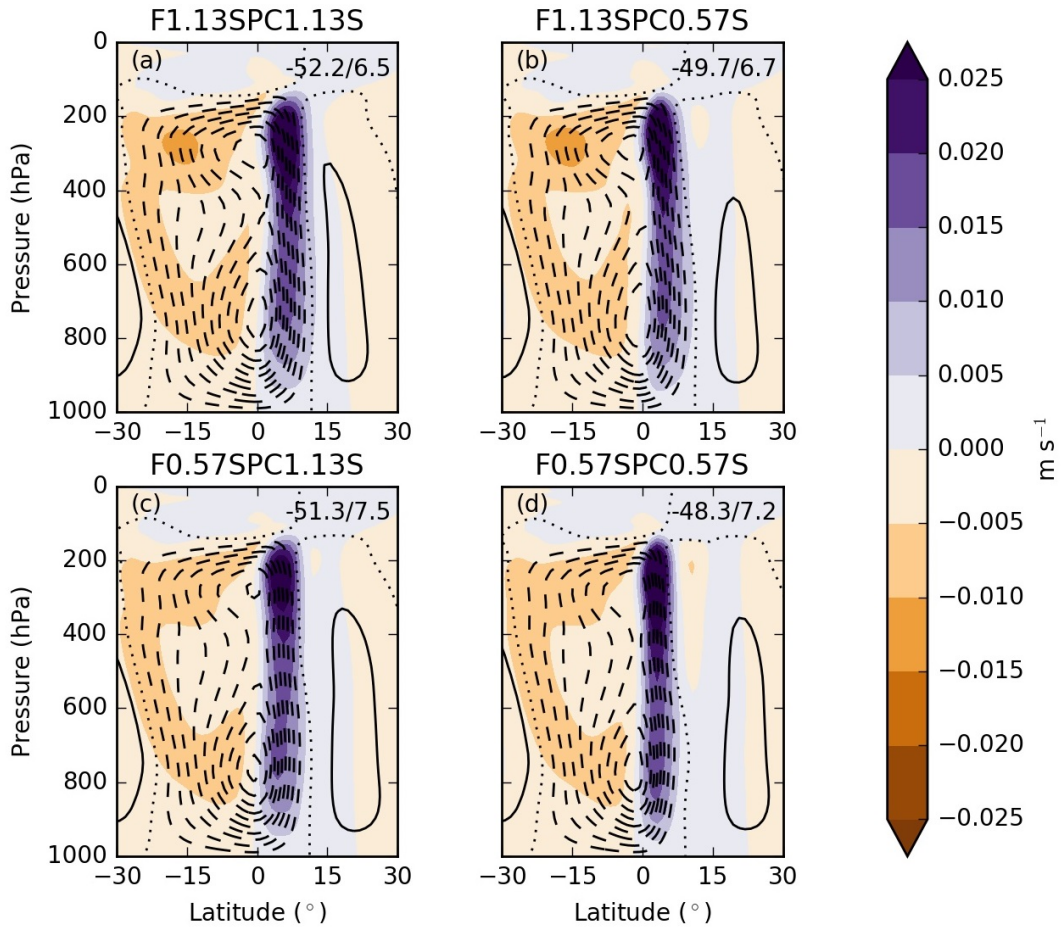

Figure 5.9: *Zonal-mean, time-mean mass meridional streamfunction (kg s^{-1}) (line contours) and vertical wind speed (m s^{-1}) (filled contours) in (a) F1.13SPC1.13S, (b) F1.13SPC0.57S, (c) F0.57SPC1.13S, (d) F0.57SPC0.57S. Line contours are in intervals of 5 $\times$ 10^{10}, with dashed contours representing negative values. Positive streamfunction values indicate clockwise circulation. The dotted contour is zero value and the maximum magnitude of the mass meridional streamfunction in the SH and NH is printed in the top right-hand corner of each panel.*

Southward of 5°N the prescribed CRE plays the dominant role in the AEI structure (Fig. 5.8b). For example, similar AEI profiles are present in F1.13SPC1.13S and F0.57SPC1.13S. Elsewhere, latent heat flux changes influence the AEI profile (Fig. 5.10a,c). For example, when prescribing the same CRE and solely changing f_{dp}, latent heat flux changes peak at approximately 25 W m^{-2} at 10°N (Figs. 5.10a,c). These latent heat flux changes play a crucial role in the sensitivity of AEI to f_{dp}.

When prescribing CRE solstitial simulations show a smaller reduction in the sensitivity of the ITCZ to f_{dp} compared to equinoctial simulations. However, the magnitude of CRE changes when varying f_{dp} is similar in both equinoctial and solstitial simulations (Fig. 4.3 and 5.5). The reduced impact of prescribing CRE is associated with a greater sensitivity of the latent heat flux to f_{dp}. For example, when decreasing f_{dp} from 1.13 to 0.57 under equinoctial boundary conditions, the maximum latent heat flux change is approximately 10 W m^{-2}; under solstitial boundary conditions this change is

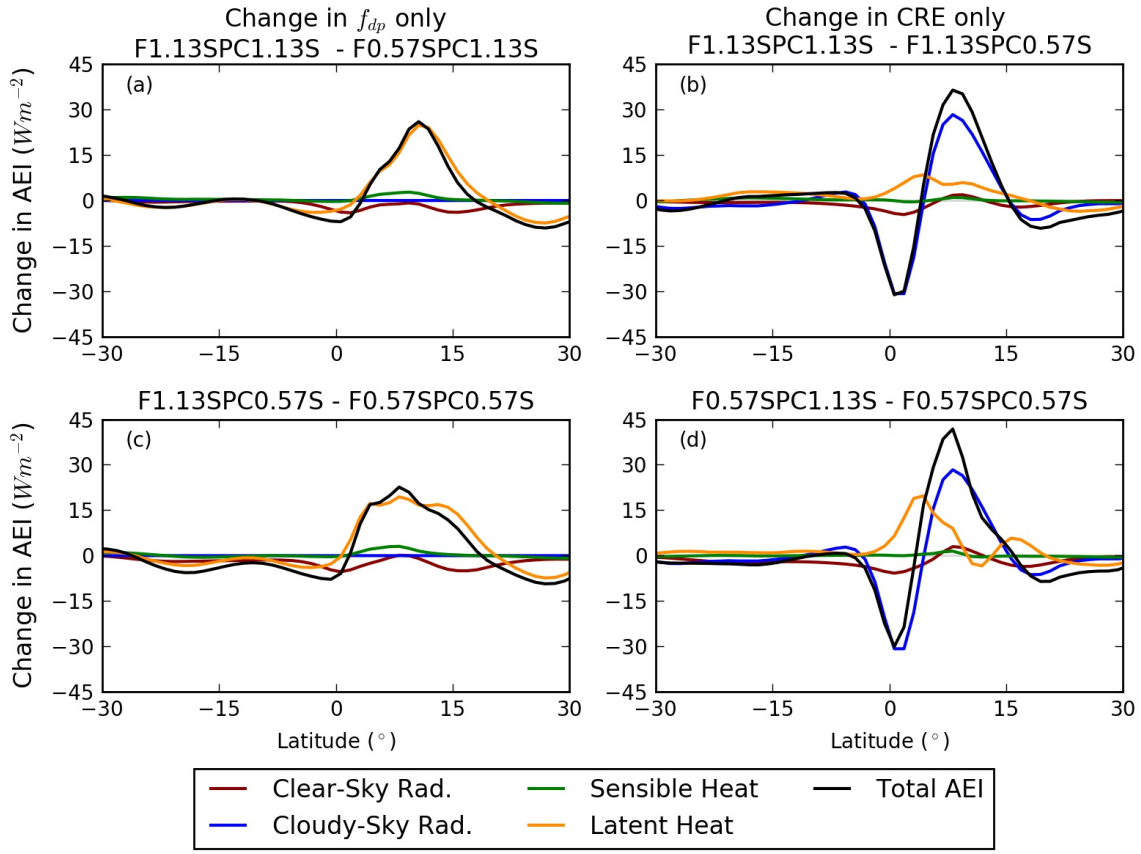

Figure 5.10: *Zonal-mean, time-mean AEI (W m^{-2}) component changes for prescribed-CRE simulations (Table 5.2). Red lines denote the clear-sky radiation component; blue lines denote the cloudy-sky radiation components. Green and grey lines denote the sensible and latent heat flux respectively, and the black line denotes the total AEI. (a) and (c) compare simulations where f_{dp} is changed whilst (b) and (d) compare simulations where the prescribed CRE is changed.*

approximately double (Figs. 4.3d and 5.5d). The sensitivity of AEI to f_{dp} given a fixed CRE is approximately double in solstitial simulations compared to equinoctial simulations, predominately due to latent heat flux variations (comparing 4.15a,c and 5.10a,c). Increased latent heat flux changes under solstitial boundary conditions are associated with greater latent heat fluxes due to an intensified Hadley circulation (Fig. 5.3). Variations in extratropical AEI components play a minimal role in the reduced sensitivity of the ITCZ to f_{dp} when prescribing CRE; there is little sensitivity of the hemispheric asymmetry in extratropical AEI components to f_{dp} (Fig. 5.4).

5.4 Sensitivity of ITCZ to hemispherically asymmetric boundary conditions

Through investigating the sensitivity of the solstitial ITCZ to convective mixing and comparing with results in chapter 4, work in section 5.3 shows the sensitivity of the ITCZ to convective mixing depends on the boundary conditions. Work in this section extends understanding the mechanisms controlling ITCZ characteristics by investigating the sensitivity of the ITCZ to hemispherically asymmetric boundary conditions. F1.13 has a single, equatorial ITCZ (Fig. 5.11a); applying solstitial

boundary conditions (F1.13S) weakens and broadens the single ITCZ with maximum precipitation equatorward of ϕ_{max} (Fig. 5.11c). Using solstitial boundary conditions strengthens the southern Hadley circulation, weakens the northern Hadley circulation (Fig. 5.12f) and shifts the ITCZ northward (Fig. 5.11c). In F1.13S a southward AET_0 is required for equilibrium (Fig. 5.4). This is predominately achieved by mean circulation changes; a strengthening and northward shift of the southern Hadley cell (comparing Fig. 5.12a and f). The intensified southern Hadley circulation is associated with the precipitation maximum being located equatorward of ϕ_{max}: The intensified circulation increases MSE transport in the lower branches of the Hadley circulation; as a result, deep convection is initiated equatorward of ϕ_{max} over cooler SSTs, as the minimum boundary-layer MSE required for deep convection is achieved equatorward of ϕ_{max}.

Applying solstitial boundary conditions introduces hemispheric asymmetries in the meridional cross-section of MSE, tropical winds and cloud properties (Fig. 5.13). The upper troposphere cools (Fig. 5.13c), associated with increased upper-level instability and a reduced minimum boundary-layer MSE required for deep convection. Fig. 5.13h shows a poleward extension of high tropical clouds in the NH, resulting in increased cloudy-sky heating over the NH tropics (Fig. 5.13i). There is little cooling from low-level, sub-tropical clouds in the NH, (approximately 800hPa, 20 to 30°N latitude), but in the SH, this cooling (and warming below) approximately doubles. In the NH extratropics ($\geq$ 30°N) high-level clouds increase and low-level clouds decrease (not shown), resulting in a substantial CRE extratropical hemispheric asymmetry (Fig. 5.7).

The northward ITCZ shift given solstitial boundary conditions results in a hemispheric asymmetry in cloudy-sky radiation and total AEI (Figs. 5.14f and 5.15). Cloudy-sky radiation increases by a maximum of approximately 40 W m^{-2} in the NH tropics whilst in the SH tropics the maximum decrease is approximately 50 W m^{-2} (blue line in Fig. 5.14f). The hemispheric asymmetry in tropical cloudy-sky radiation changes is associated with an increased southward AET_0 (Fig. 5.15), an intensified SH Hadley circulation (Fig. 5.12f), and a northward ITCZ shift (Fig. 5.11a). However, the combined effect of clear-sky and cloudy-sky radiation changes is partially offset by hemispherically asymmetric latent heat flux changes (Fig. 5.14).

Fig. 5.15 shows the net-southward tropical ($\leq 30^\circ$ latitude) and extratropical ($\geq 30^\circ$ latitude) AET_0 components for F1.13 and F1.13S. As F1.13 has hemispherically symmetric forcing, minimal AET_0 components are diagnosed. In F1.13S tropical cloudy-sky radiation plays a substantial role in the total AET_0, suggesting CRE amplifies the ITCZ shift when applying solstitial boundary conditions. Partitioning cloudy-sky radiation into SW and LW, and into high- and low-cloud, above and below

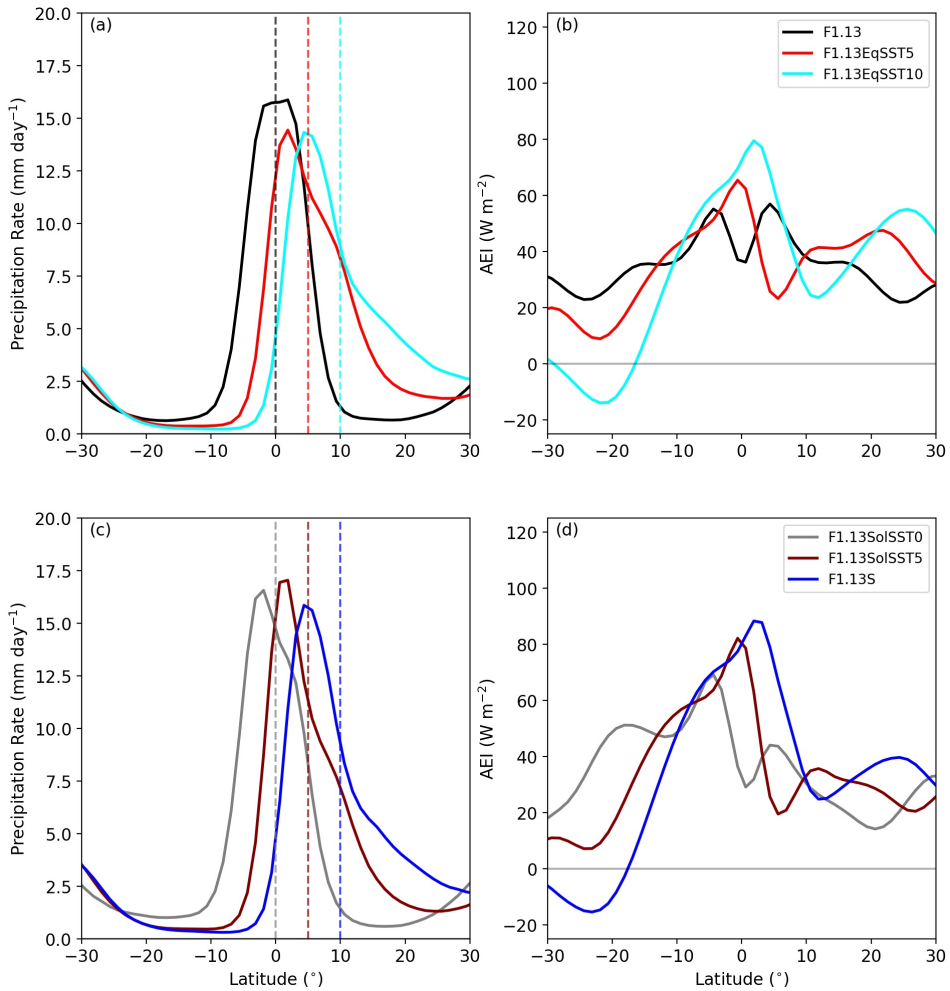

Figure 5.11: *Zonal-mean, time-mean (a), (c) precipitation rates (mm day^{-1}) and (b), (d) AEI (W m^{-2}) in F1.13 simulations where ϕ_{max} equals 0, 5 and 10. Top panels are for simulations with equinoctial insolation and bottom panels are for simulations with solstitial insolation. Vertical, dashed lines in (a) and (c) denote ϕ_{max}.*

800hPa respectively, reveals that LW cloudy-sky radiation associated with high tropical clouds plays the dominant role in the observed $\text{AET}_0^{\text{cloud}}$ (not shown). As CRE increases the hemispheric AEI asymmetry, associated with an intensified SH Hadley circulation and a northward ITCZ shift, it is hypothesised that prescribing a hemispherically symmetric CRE would reduce Hadley circulation asymmetries and the ITCZ shift observed under solstitial boundary conditions.

5.4.1 *Partitioning the sensitivity of the ITCZ to hemispherically asymmetric boundary conditions into insolation and SST forcing*

To investigate the sensitivity of the ITCZ to solstitial boundary conditions further, simulations are performed to partition the sensitivity into contributions from insolation and prescribed-SST (Table 5.3). Two simulations are performed with equinoctial insolation and a value of 5 (F1.13EqSST5) and 10 (F1.13EqSST10) for ϕ_{max}. Another two simulations are also performed with perpetual NH

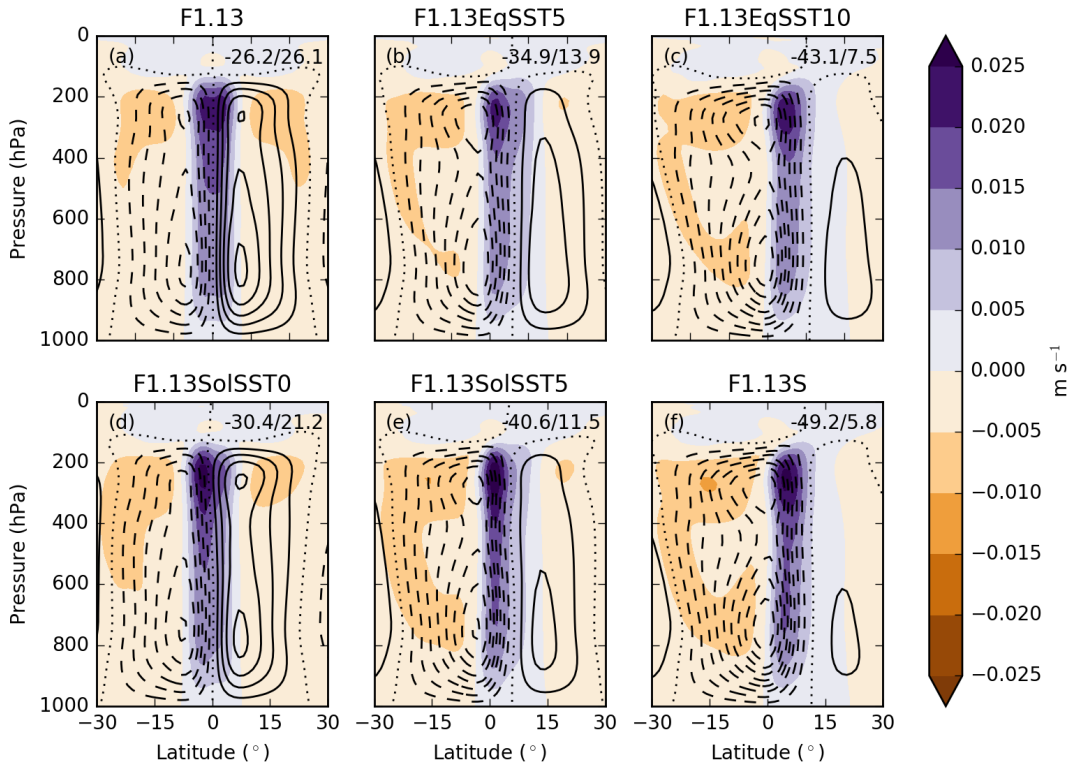

Figure 5.12: *Zonal-mean, time-mean mass meridional streamfunction (kg s^{-1}) (line contours) and vertical wind speed (m s^{-1}) (filled contours) in (a) F1.13, (b) F1.13EqSST5, (c) F1.13EqSST10, (d) F1.13SolSST0, (e) F1.13SolSST5, (f) F1.13S. Line contours are in intervals of 5 $\times$ 10^{10}, with dashed contours representing negative values. Positive streamfunction values indicate clockwise circulation. The zero contour is dotted; the maximum magnitudes of the mass meridional streamfunction in the SH and NH are printed in top right-hand corner of each panel.*

solstitial insolation (F1.13SolSST0, F1.13SolSST5) to isolate the effect of insolation variations. The mean circulation is more sensitive to ϕ_{max} than the insolation profile (Table 5.5). Whilst applying solstitial insolation when using an off-equatorial ϕ_{max} increases the maximum precipitation rate, AEI across the equatorial region (Fig. 5.11) and hemispheric asymmetry in mean circulation strength (Fig. 5.12), mean circulation variations are predominately associated with changes in ϕ_{max} (Fig. 5.12 and Table 5.5). However, using prescribed SSTs constrains the SST response to insolation changes. In the real world and simulations with varying SSTs, SST variations are driven by insolation changes (Waliser and Gautier, 1993; Wei and Bordoni, 2018), hence, the concluded importance of SSTs and insolation is an artefact of the model set-up.

A positive off-equatorial ϕ_{max} (F1.13EqSST5 and F1.13EqSST10) shifts the ITCZ northward and introduces a hemispheric asymmetry in Hadley circulation intensity. A hemispheric asymmetry in tropical cloudy-sky radiation and extratropical surface fluxes is also observed (Figs. 5.14b,c and 5.15). As in F1.13S, the increased hemispheric asymmetry in tropical cloudy-sky radiation is associated with a net-southward AET_0 (Fig. 5.15). Partitioning the role of specific humidity and

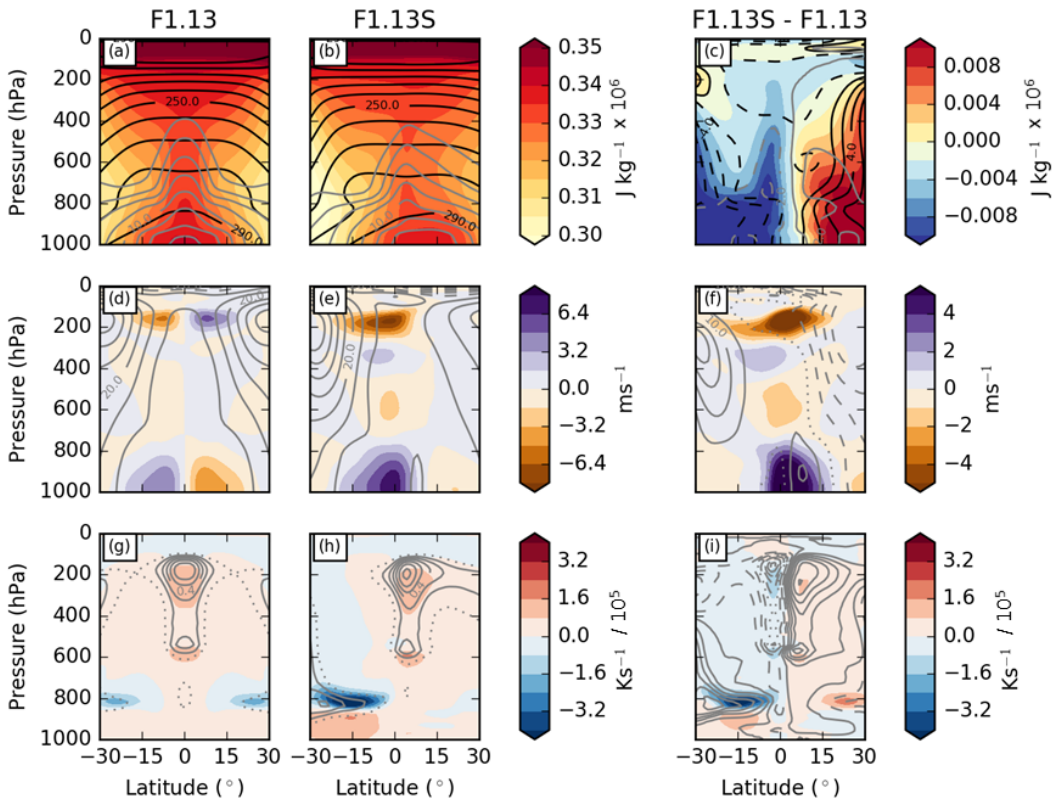

Figure 5.13: *Zonal-mean, time-mean meridional cross sections of (a-c) MSE (J kg^{-1}K^{-1}, filled), temperature (K, black lines, contour spacing of 10K) and specific humidity (g kg^{-1}, grey lines, contour spacing of 2g kg^{-1}); (d-f) meridional (filled) and zonal (grey lines, contour spacing of 10m s^{-1}) winds (m s^{-1}); (g-i) total cloudy-sky heating rates (filled, K s^{-1}) and cloud fraction (grey lines, contour spacing of 0.1). The first column is for F1.13, the second column is for F1.13S and the third column is the difference between F1.13S and F1.13. For the third column, lined contour spacing is reduced to 2K and 5m s^{-1} for black and grey lines in (c) and (f) respectively. Dashed and dotted contours represent negative and zero values respectively.*

Table 5.5: *Root mean squared deviation (4.5) for tropical (30°N to 30°S) precipitation (mm day^{-1}) and mass meridional streamfunction (kg s^{-1}) between two simulations.*

Forcing Change	Simulations	Precipitation (mm day^{-1})	Mass Meridional Streamfunction ($\times$ 10^{10} kg s^{-1})
SST and Insolation	F1.13S & F1.13	5.58	11.9
SST	F1.13EqSST10 & F1.13	5.53	10.9
Insolation	F1.13SolSST0 & F1.13	1.09	1.8
SST and Insolation	F0.57S & F0.57	4.58	9.1
SST	F0.57EqSST10 & F0.57	4.68	8.7
Insolation	F0.57SolSST0 & F0.57	2.11	2.1

absolute wind variations in latent heat flux changes, shows that changes in extratropical latent heat fluxes (approximately 40 to 60° latitude, Fig. 5.14b,c) are associated with SST and zonal-wind changes (not shown).

Whilst a positive off-equatorial ϕ_{max} produces an NH ITCZ, applying solstitial insolation and

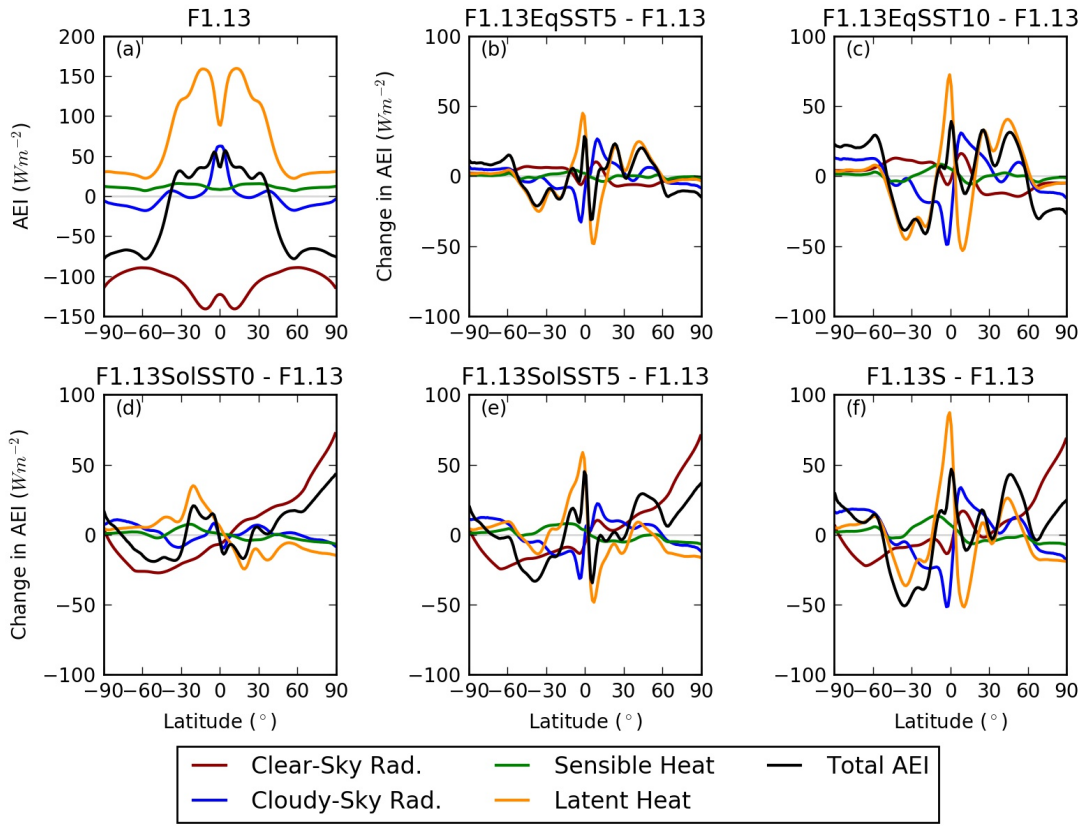

Figure 5.14: *Zonal-mean, time-mean AEI (W m^{-2}) components. (a) F1.13, (b)-(f) change in AEI components compared to F1.13, (b) F1.13EqSST5; (c) F1.13EqSST10, (d) F1.13SolSST0, (e) F1.13SolSST5, (f) F1.13S. The red lines denote clear-sky radiation; the blue lines denote cloudy-sky radiation. Green and grey lines denote sensible and latent heat flux (respectively) and black line is the total AEI.*

an equatorial SST maximum (F1.13SolSST0) produces an SH ITCZ (Fig. 5.11a,c). The Hadley circulation intensifies in the SH and weakens in the NH by approximately 20% (Fig. 5.12d). An SH ITCZ in F1.13SolSST0 is counter-intuitive. From an AEI perspective one would expect an NH ITCZ: if all other AEI components remained unchanged, increasing NH insolation would lead to a hemispheric energy imbalance that would require a southward AET_0 and an associated NH ITCZ (Kang et al., 2008; Donohoe et al., 2013). In F1.13SolSST0 however, a more intense SH Hadley circulation (Fig. 5.12d) is accompanied by higher tropical SH precipitation (Fig. 5.11c). The hemispheric Hadley circulation intensity asymmetry increases SH surface turbulent fluxes and decreases NH surface turbulent fluxes (Figs. 5.14d and 5.15). However, surface turbulent flux changes do not fully compensate the southward AET_0 associated with the hemispheric asymmetry in clear-sky radiation (Fig. 5.15). Hence, further investigation is required to explain how a southward AET_0 and an SH ITCZ arises in F1.13SolSST0.

To better understand the ITCZ response when shifting from equinoctial to solstitial insolation, an ensemble of twenty-six 60-day simulations (Sol_{ens}) is performed. Each ensemble member is initiated from separate initial conditions from F1.13, has a fixed solar declination angle of 23.4°N, and an f_{dp}

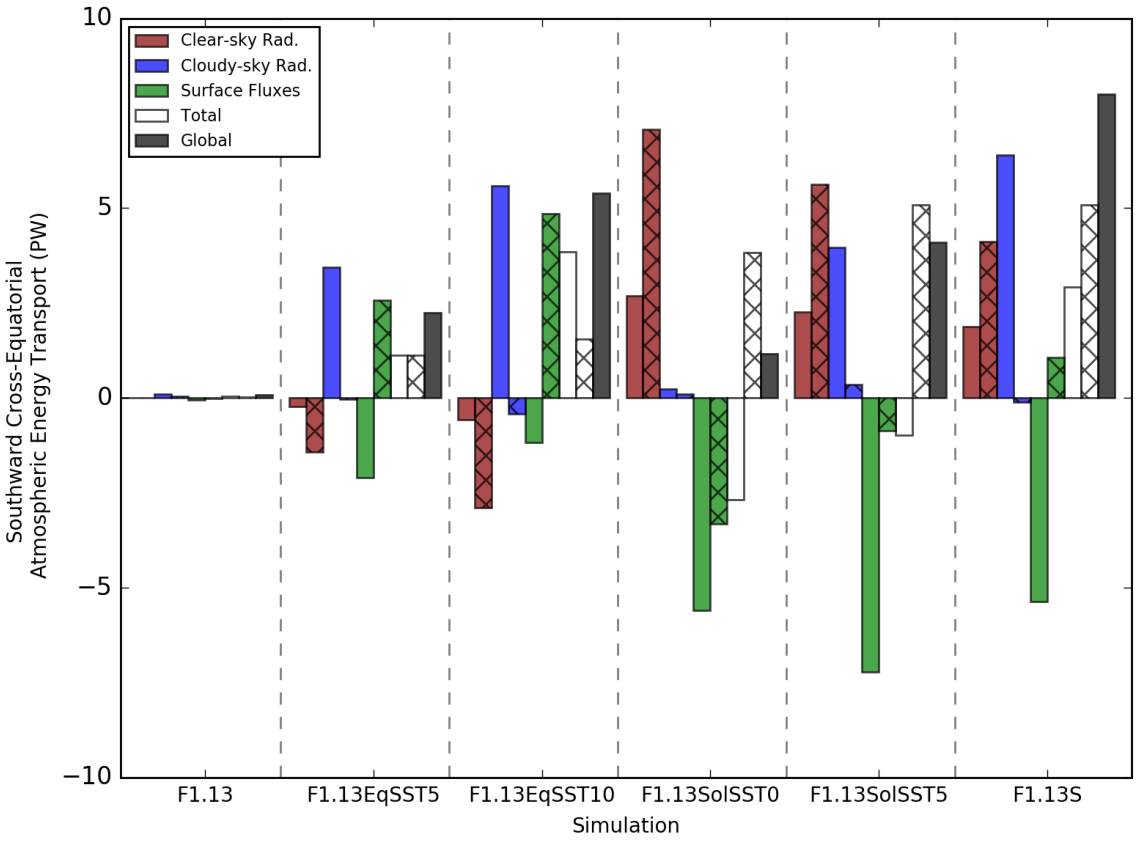

Figure 5.15: *Components of AET_0 (PW) for simulations where ϕ_{max} and insolation is varied. Components of AET_0 are calculated using hemispheric asymmetries in AEI budget components (section 5.3). The red bars denote clear-sky radiation; the blue bars denote cloudy-sky radiation; green bars denote surface flux contributions (latent and sensible heat flux combined); and the black bars denote the total AET_0. Each component of AET_0 is split into tropical ($\leq 30^\circ$ latitude) and extratropical components ($\geq 30^\circ$ latitude) where the extratropical component is denoted by cross hatching. Total of tropical and extratropical components are shown in white. Positive values indicate a greater contribution to the NH AEI compared to the SH AEI, associated with a southward AET_0 and a NH ITCZ.*

value of 1.13. As observed in F1.13SolSST0, the ensemble mean of Sol_{ens} has an SH precipitation maximum (Fig. 5.16) associated with a hemispheric asymmetry in Hadley circulation intensity (not shown). The initial AEI change results from increased NH clear-sky fluxes and decreased SH clear-sky fluxes (Fig. 5.17b). The AEI gradient between the tropics and extratropics increases in the SH and decreases in the NH, associated with an intensified SH Hadley circulation and a weakened NH Hadley circulation (Popp and Silvers, 2017). Variations in Hadley circulation intensity lead to latent heat flux changes that take approximately 10 days to develop (Fig. 5.17). Meanwhile, the boundary-layer MSE meridional profile remains unchanged throughout the 60 days of simulation (not shown), primarily due to prescribed-SSTs. As the ITCZ is typically observed near the point of maximum boundary layer MSE (Mobis and Stevens, 2012), the tropical rainbelt remains in the equatorial region but with higher SH precipitation. As in F1.13SolSST0, even with the hemispheric asymmetry in surface turbulent fluxes, a southward AET_0 is required. Further simulations, in which insolation is gradually shifted from equinoctial to solstitial conditions over 90 days, shows a minimal

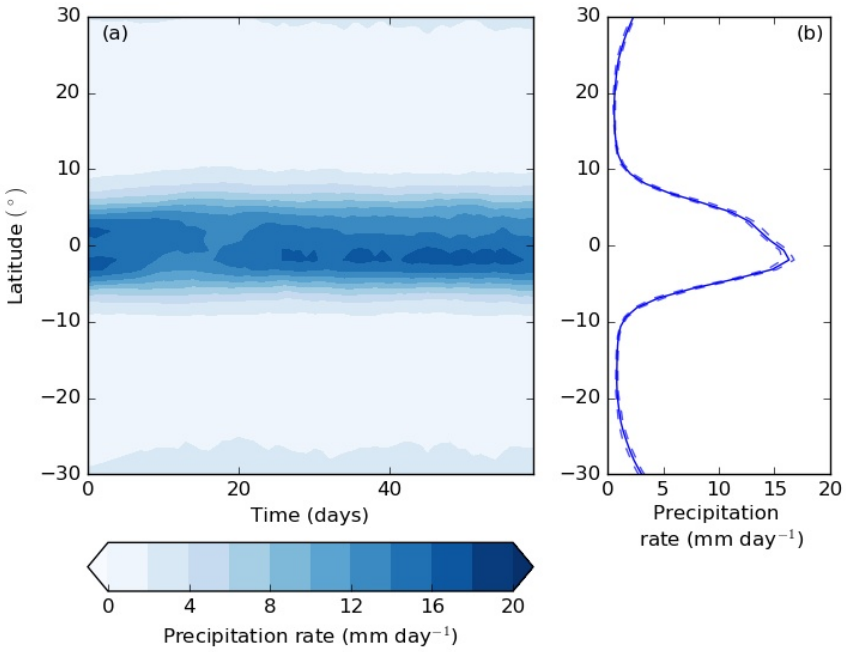

Figure 5.16: *Zonal-mean precipitation rates (mm day^{-1}) in (a) ensemble-mean of Sol$_{ens}$, (b) time-mean, ensemble-mean of Sol$_{ens}$ over the last 30 days. Dashed blue lines in (b) denote the ensemble 10th and 90th percentiles in Sol$_{ens}$.*

role of the timescale of insolation changes (not shown). Further analysis is therefore required to understand how the ensemble mean of Sol$_{\text{ens}}$ and F1.13SolSST0 both have an SH ITCZ and a southward AET$_0$.

To investigate how a southward AET$_0$ is achieved in F1.13SolSST0, the mass meridional streamfunction (Ψ) is partitioned into hemispherically symmetric (Ψ_{Sym}) and asymmetric (Ψ_{Asym}) components:

$$\begin{aligned} \Psi(\phi) &= \Psi_{Sym}(\phi) + \Psi_{Asym}(\phi), \\ \Psi_{Sym}(\phi) &= \frac{1}{2}[\Psi(\phi) - \Psi(-\phi)], \\ \Psi_{Asym}(\phi) &= \frac{1}{2}[\Psi(\phi) + \Psi(-\phi)] \end{aligned} \tag{5.3}$$

where ϕ denotes latitude. As Ψ_{Sym} cannot transport energy across the equator, Ψ_{Asym} is entirely responsible for the AET$_0$ by the mean circulation (Green and Marshall, 2017). Two circulations are identified in Ψ_{Asym} of F1.13SolSST0 (Fig. 5.18a); first, a shallow upper-tropospheric cross-equatorial circulation (approximately 150 to 550hPa); and second, a broad cross-equatorial circulation in the lower- and mid-troposphere (below approximately 550hPa). The hemispheric symmetry in Ψ_{Asym} (Fig. 5.18a) is associated with the hemispheric asymmetry in Hadley circulation intensity (Fig. 5.12d). A southward cross-equatorial MSE flux, associated with these circulations, is seen between

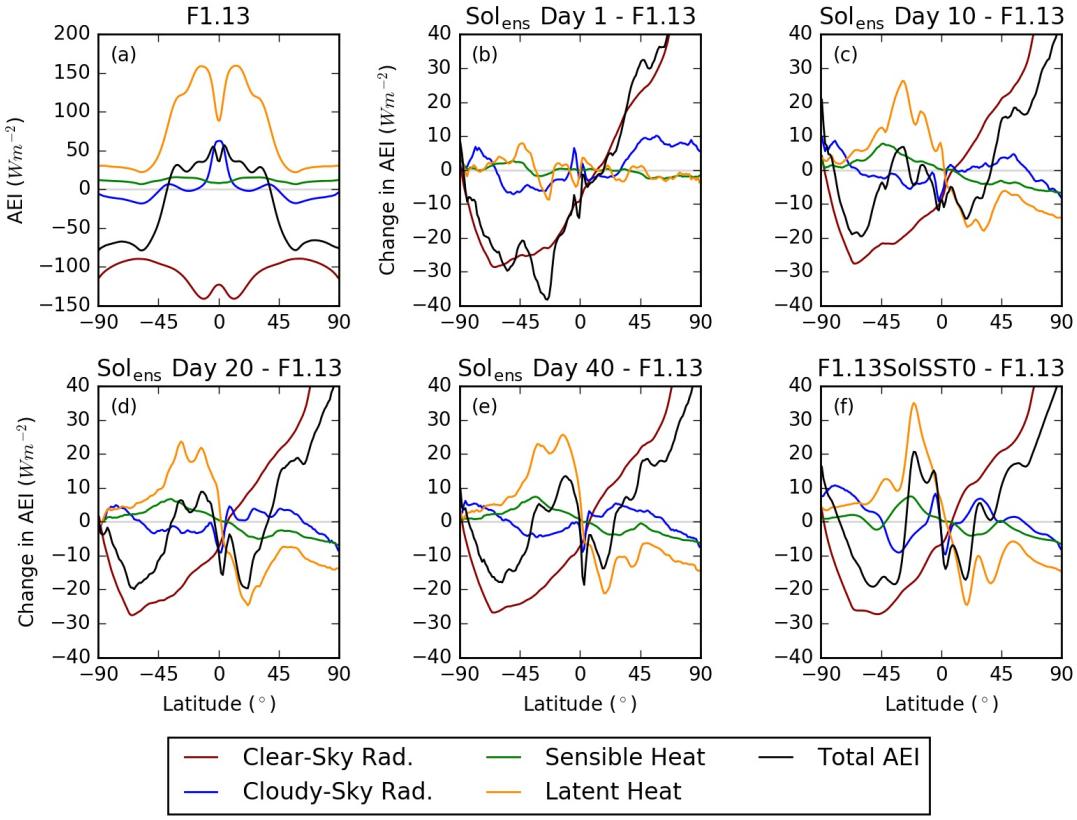

Figure 5.17: *Zonal-mean, time-mean AEI components (Wm^{-2}). a) F1.13, (b)-(e) change in AEI components compared to F1.13 for ensemble-mean of Sol_{ens} at day (b) 1, (c) 10, (d) 20 and (e) 40. (f) Change in AEI components comparing F1.13SolSST0 with F1.13. Red lines are the clear-sky radiation component; blue lines are the cloudy-sky radiation components. Green and grey lines are the sensible and latent heat flux (respectively) and black line is the total AEI.*

approximately 200 and 650hPa. The southward cross-equatorial MSE flux is greater than the northward cross-equatorial MSE flux observed below 650hPa and above 200hPa (Fig. 5.18b). Ψ_{Asym} in F1.13SolSST0 illustrates how a southward AET_0 is achieved even though an SH ITCZ is present. F1.13SolSST0 highlights that the sign of AET_0 is not always indicative of the ITCZ location.

To investigate the cause of Hadley circulation asymmetries, the mass meridional streamfunction associated with the temperature tendency of each MetUM physics scheme is computed following a similar method to Holloway and Woolnough (2016):

$$\Psi_i^{heat}(z) = \Psi_{i-1}^{heat}(z) + \{\rho(z)\} \left| \frac{Q'}{\{\prod\}\frac{\partial\theta}{\partial z}} \right|_{i-\frac{1}{2}} (z) \tag{5.4}$$

where Ψ^{heat} is the computed mass meridional streamfunction associated with the temperature tendency, $\{\}$ is the tropical-domain ($30°N \leq \phi \leq 30°N$) average, Q' is horizontal anomaly of the temperature tendency from each MetUM physics scheme, $\prod$ is the Exner function ($\frac{\theta}{T}$) and θ is the potential temperature. As $\frac{\partial\theta}{\partial z}$ is small in the boundary layer, $\frac{Q'}{\{\prod\}\frac{\partial\theta}{\partial z}}$ is set as zero at the

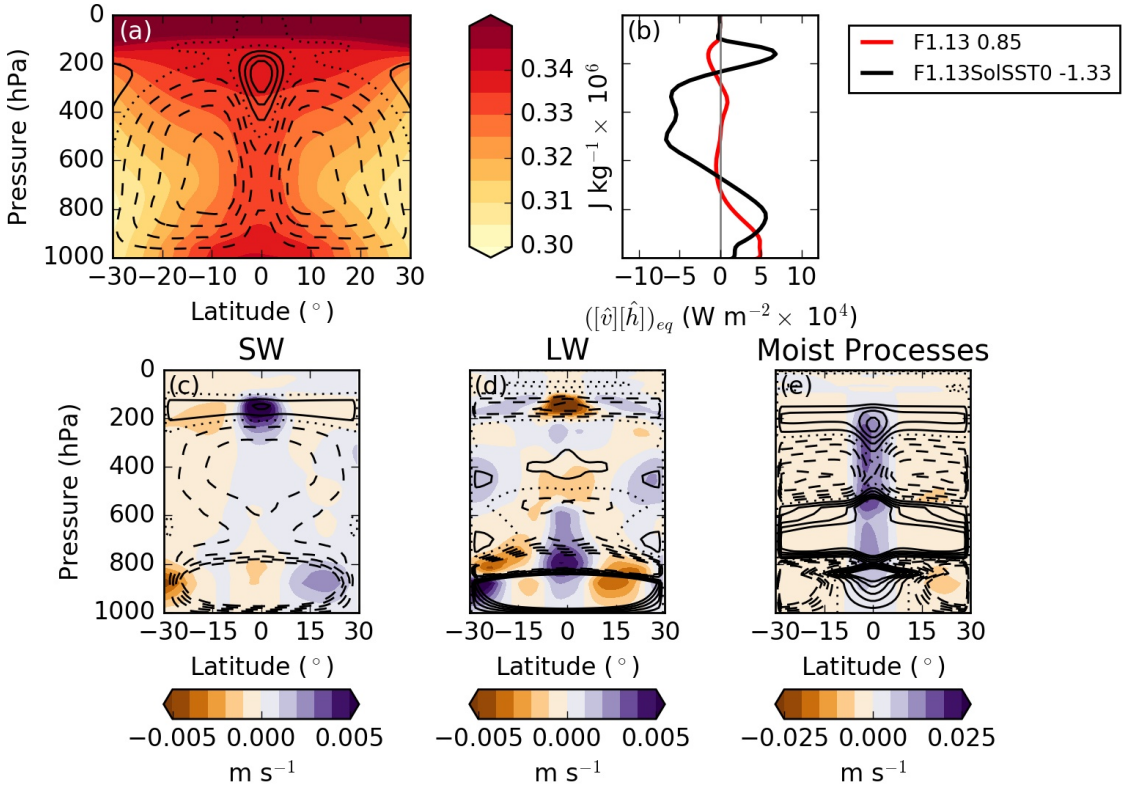

Figure 5.18: *(a) Zonal-mean, time-mean MSE (filled, J kg^{-1}) and Ψ_{Asym} (line, kg s^{-1}) in F1.13SolSST0. (b) Vertical profile of the time-mean, zonal-mean ($[\overline{v}]\widehat{[\overline{h}]}$) (W m^{-2}). In (b) the red line denotes F1.13 and the black line denotes F1.13SolSST0. Negative values indicate a southward cross-equatorial energy transport. Printed in legend next to each label identifier is the vertical integral of each profile in PW. (c)-(e) Vertical wind speed (filled, m s^{-1}) and Ψ^{heat}_{Asym} (line, kg s^{-1}) diagnosed from the temperature tendency outputted from the (c) shortwave radiation parameterisation, (d) longwave radiation parameterisation, and (e) moist processes including large-scale rainfall and convection parameterisation. Filled contours in intervals of 0.001 m s^{-1} for (c) and (d), and 0.005 m s^{-1} for (e). All streamfunction contours in (a) and (c-e) are in intervals of 10 × 10^9, with dashed contours representing negative values. The zero contour is dotted. Positive streamfunction values indicate clockwise circulation.*

lowest model level (10m) and linearly interpolated to the value at approximately 950m (10th model level). Equation 5.4 assumes a weak temperature gradient across the tropical free-troposphere (Sobel et al., 2001) and describes the circulation that would develop if the free-tropospheric horizontal anomalous heating, associated with each MetUM physics scheme, is balanced by vertical advection of dry static energy (Holloway and Woolnough, 2016). Ψ^{heat} is then partitioned into symmetric (Ψ^{heat}_{Sym}) and asymmetric (Ψ^{heat}_{Asym}) components (5.3). Figure 5.18c-e shows Ψ^{heat}_{Asym} associated with the SW radiation scheme, LW radiation scheme, and moist processes including large-scale rainfall and convective parameterisation. Unfortunately, due to the linear interpolation of $\frac{Q'}{\{\Pi\}\frac{\partial\theta}{\partial z}}$ below approximately 950m it is challenging to interpret the circulation dignosed below approximately 800hPa. The structure of Ψ_{Asym} in F1.13SolSST0 (Fig. 5.18a) is associated with temperature tendencies from the SW radiation scheme and moist processes (Fig. 5.18c,e). Temperature tendencies from the SW radiation scheme lead to a broad cross-equatorial circulation in the mid-,

upper-troposphere (Fig. 5.18c); temperature tendencies from the SW radiation scheme are associated with ascent in the NH, descent in the SH, and a southward AET_0. The upper-tropospheric clockwise circulation in Ψ_{Asym} (Fig. 5.18a) is predominantly associated with moist processes (Fig. 5.18e). The hemispheric asymmetry in Hadley circulation intensity leads to higher temperatures tendencies from the convective parameterisation in the SH compared to the NH, associated with substantial ascent in the SH upper-troposphere and descent in the NH upper-troposphere. As characteristics of Ψ_{Asym} in F1.13SolSST0 are associated with the convective parameterisation (Fig. 5.18e), it is hypothesised that the observed Ψ_{Asym} when shifting from equinoctial to solstitial insolation is sensitive to the representation of convection.

Numaguti (1995) illustrated that the sensitivity of the ITCZ to the boundary conditions depends on the representation of convection, hence, simulations are performed to investigate the sensitivity of the ITCZ to hemispherically asymmetric boundary conditions with f_{dp} equal to 0.57 (Table 5.3). Changing from equinoctial to solstitial boundary conditions when f_{dp} equals 0.57 (F0.57S) intensifies the SH Hadley circulation, weakens the NH Hadley circulation (Fig. 5.19f) and shifts the ITCZ northward (Fig. 5.20c). A double ITCZ with greater precipitation associated with the southern rainfall belt is observed for all values of ϕ_{max} (Fig. 5.20). Hemispherically asymmetric boundary conditions produce the same response at both f_{dp} values: Applying a non-zero ϕ_{max} introduces a hemispherically asymmetric AEI associated with an increased AET_0 and a stronger, meridionally-shifted SH Hadley circulation. The ITCZ response to solstitial insolation is also similar when f_{dp} equals 0.57: greater SH precipitation is observed even though a southward AET_0 is required (Fig. 5.20a). A broad cross-equatorial circulation, associated with temperature tendencies from the SW radiation scheme, leads to a southward AET_0 (not shown). As hypothesised, Ψ^{heat}_{Asym} associated with moist processes is sensitive to the convective parameterisation. When f_{dp} equals 0.57, heating tendencies from the convective parameterisation are associated with a deeper, broader upper-level circulation compared to that seen when f_{dp} equals 1.13 (not shown). However, whilst tropical mean-state changes are seen when reducing f_{dp} to 0.57 from 1.13, the mechanisms responsible for the sensitivity of the ITCZ to hemispherically asymmetric boundary conditions are similar for both values of f_{dp}.

5.4.2 *Sensitivity of the ITCZ to hemispherically asymmetric boundary conditions with a prescribed cloud radiative effect*

When shifting from equinoctial to solstitial boundary conditions the SH Hadley circulation intensifies and shifts northwards (Fig. 5.12f); a NH ITCZ is observed (Fig. 5.11c). Associated with

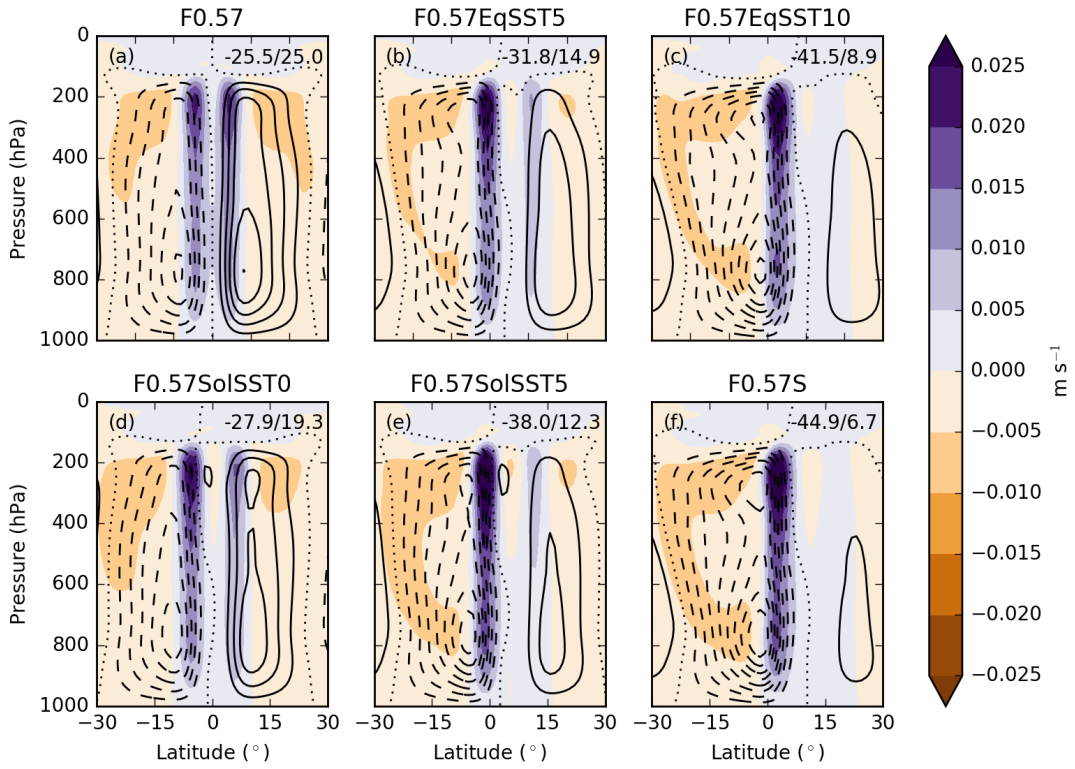

Figure 5.19: *Zonal-mean, time-mean mass meridional streamfunction (kg s^{-1}) (line contours) and vertical wind speed (m s^{-1}) (filled contours) in (a) F0.57, (b) F0.57EqSST5, (c) F0.57EqSST10, (d) F0.57SolSST0, (e) F0.57SolSST5, (f) F0.57S. Line contours are in intervals of 5 $\times$ 10^{10}, with dashed contours representing negative values. Positive streamfunction values indicate clockwise circulation. The zero contour is dotted and the maximum magnitudes of the mass meridional streamfunction in the SH and NH are printed in top right-hand corner of each panel.*

the northward ITCZ shift, CRE increases the NH tropics and decreases in the SH tropics (Fig. 5.14f), increasing both the hemispheric asymmetry in AEI and AET_0. It is hypothesised that CRE enhances meridional ITCZ shifts and without CRE the meridional ITCZ shift would be reduced. To improve understanding of the role of CRE in the sensitivity of the ITCZ to solstitial boundary conditions, prescribed-CRE simulations are performed. Equinoctial or solstitial boundary conditions are employed along with a diurnally-varying prescribed CRE computed from a single-year simulation with either equinoctial or solstitial boundary conditions (Table 5.6, prescribed CRE profiles shown in Fig. 5.7). Two sets of prescribed-CRE simulations are performed, where f_{dp} equals 1.13 or 0.57, to investigate whether the role of CRE depends on the representation of convection. Precipitation and AEI profiles for prescribed-CRE simulations in Table 5.6 are shown in Figure 5.21.

Prescribing CRE reduces the sensitivity of the ITCZ to the boundary conditions; for example, prescribing an equinoctial CRE and applying solstitial boundary conditions (F1.13SPC1.13 and F0.57SPC0.57) reduces the intensification and shift of the southern Hadley cell compared to simulations with a solstitial prescribed CRE (F1.13SPC1.13S and F0.57SPC0.57S, Figs. 5.22 and

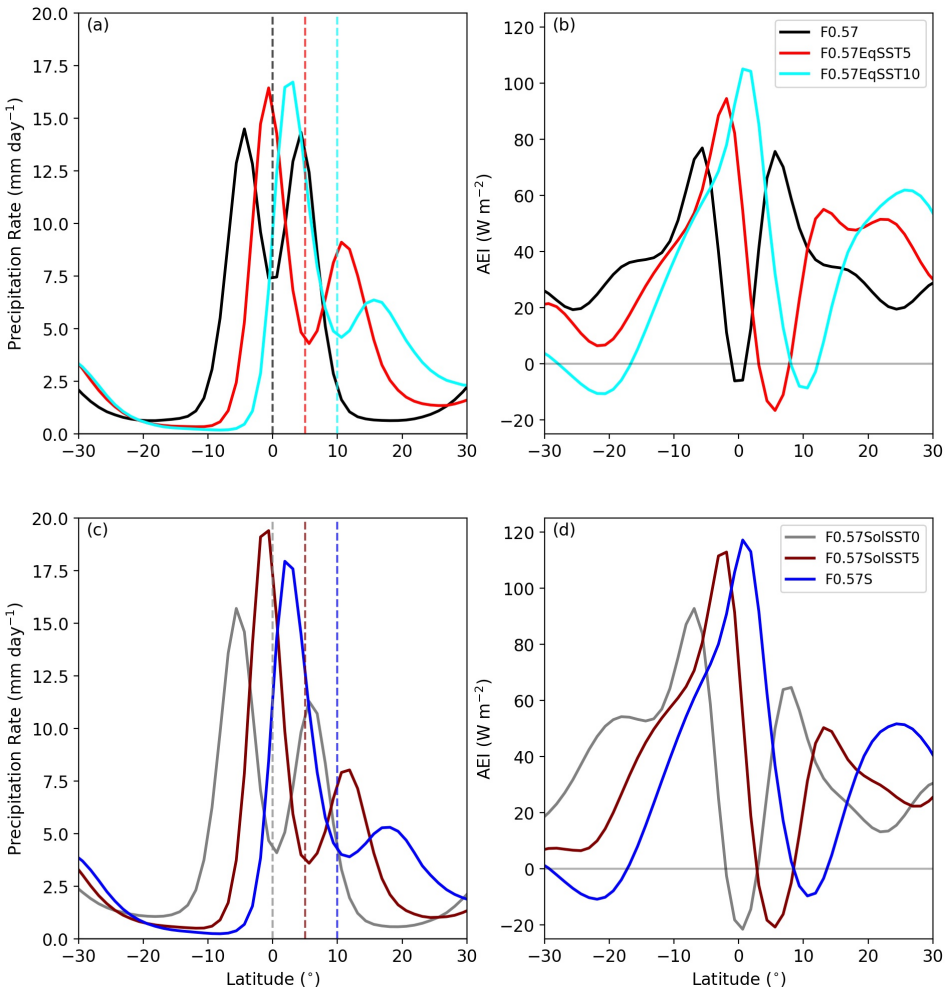

Figure 5.20: *Zonal-mean, time-mean (a), (c) precipitation rates (mm day^{-1}) and (b), (d) AEI (W m^{-2}), in F0.57 simulations where ϕ_{max} equals 0, 5 and 10. Top panels show simulations with equinoctial insolation and bottom panels show simulations with solstitial insolation. Vertical, dashed lines in (a) and (c) denote ϕ_{max}.*

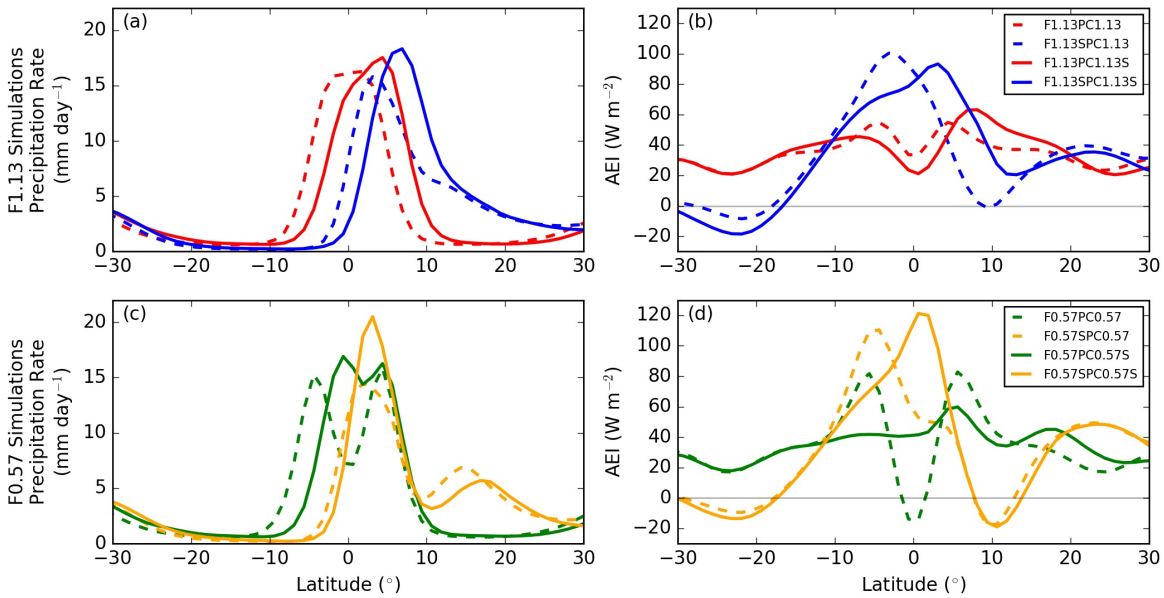

Figure 5.21: *Zonal-mean, time-mean (a),(c) precipitation rates (mm day^{-1}) and (b),(d) AEI (W m^{-2}), for prescribed-CRE simulations (Table 5.6). Top panels show F1.13 simulations and bottom panels show F0.57 simulations.*

Table 5.6: *Two sets of four prescribed-CRE simulations with f_{dp} equal to either 1.13 or 0.57. Boundary conditions are either equinoctial or solstitial, whilst the prescribed CRE is computed from a single year simulation with either equinoctial or solstitial boundary conditions. F1.13PC1.13 and F0.57PC0.57 are also shown in Table 4.2, and F1.13SPC1.13S and F0.57SPC0.57S are shown in Table 5.2*

	F1.13		F0.57	
SST and Insolation	PC1.13	PC1.13S	PC0.57	PC0.57S
Equinoctial	F1.13PC1.13	F1.13PC1.13S	F0.57PC0.57	F0.57PC0.57S
Solstitial	F1.13SPC1.13	F1.13SPC1.13S	F0.57SPC0.57	F0.57SPC0.57S

.

5.23). The precipitation centroid (P_{cent}), used in previous studies (Frierson and Hwang, 2012; Donohoe et al., 2013; Voigt et al., 2014), shows that constraining the cloud response given a change in boundary conditions reduces the meridional ITCZ shift (Fig. 5.23). P_{cent} is the median of tropical precipitation between 20°S and 20°N. To calculate P_{cent} precipitation is interpolated to a 0.1° grid to allow variations smaller than grid spacing (1.25°). Prescribing an equinoctial CRE reduces the hemispheric asymmetry in AEI, associated with an approximately 20% reduction in meridional ITCZ shift (Fig. 5.23) and an approximately 50% reduction in AET_0 (not shown). Whilst prescribing CRE reduces the sensitivity of the ITCZ to hemispherically asymmetric boundary conditions, a substantial sensitivity still remains (Fig. 5.21a,c). For example, applying solstitial boundary conditions and a equinoctial CRE produces a substantial poleward ITCZ shift (Fig. 5.21) and weakens the NH Hadley cell (Fig. 5.22). Mean circulation changes simulated when constraining CRE are associated with hemispheric asymmetries in AEI. Variations in AEI are predominantly due to latent heat flux changes which are similar to simulations with an interactive CRE.

Whilst the ITCZ is approximately 40% more sensitive to the boundary conditions than the prescribed CRE (Table 5.7), and the ITCZ only broadens when changing the boundary conditions (Fig. 5.21), the ITCZ is sensitive to the prescribed CRE. Changing the prescribed CRE from an equinoctial to a solstitial structure shifts the ITCZ poleward, towards the location of maximum prescribed CRE (Fig. 5.21a,c). The prescribed CRE acts as an MSE source, hence increasing the required MSE export. For example, convection intensifies in the NH given equinoctial boundary conditions and a solstitial CRE (F1.13PC1.13S and F0.57PC0.57S), as an increased MSE export is required in the NH. This leads to increased NH precipitation and a stronger southern Hadley circulation (Figs. 5.21a, and 5.22a,c). When changing either the prescribed CRE or the boundary conditions, changes in the meridional MSE flux are predominately due to mean circulation changes; changes in eddy transport are small (not shown).

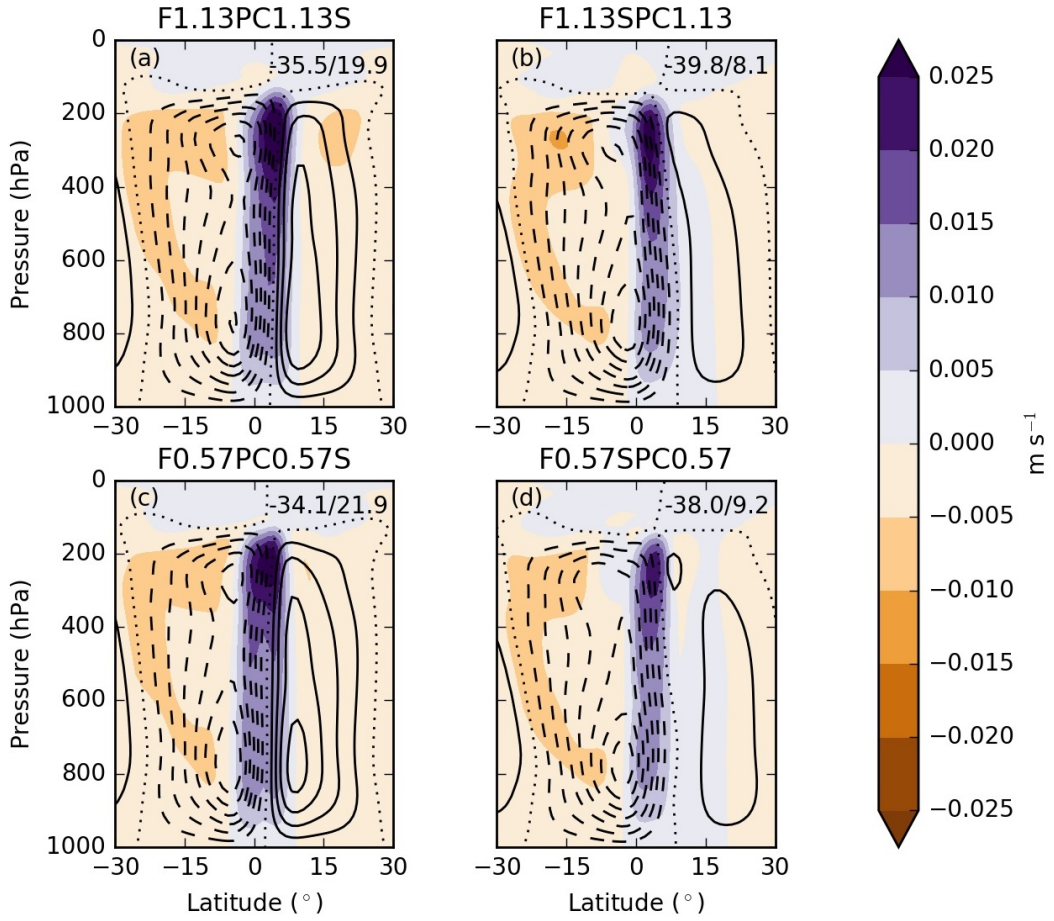

Figure 5.22: *Zonal-mean, time-mean mass meridional streamfunction (kg s^{-1}) (line contours) and vertical wind speed (m s^{-1}) (filled contours) for (a) F1.13PC1.13S, (b) F1.13SPC1.13, (c) F0.57PC0.57S and (d) F0.57SPC0.57. Line contours are at intervals of 5 $\times$ 10^{10}, with dashed contours representing negative values. Positive streamfunction values indicate clockwise circulation. Dotted contour is zero value. Maximum magnitude of the mass meridional streamfunction in the SH and NH is printed in the top right-hand corner of each panel. For other simulations in Table 5.6 the mass meridional streamfunction is shown in Figure 4.14 (F1.13PC1.13 and F0.57PC0.57) or Figure 5.9 (F1.13SPC1.13S and F0.57SPC0.57S).*

Table 5.7: *Root mean squared deviation (4.5) for tropical (30°N to 30°S) precipitation (mm day^{-1}) and mass meridional streamfunction (kg s^{-1}) between two simulations. First and last four rows are for F1.13 and F0.57 simulations respectively. BC stands for boundary conditions.*

Forcing Change	Simulations	Precipitation (mm day^{-1})	Mass Meridional Streamfunction ($\times$ 10^{10} kg s^{-1})
Change BC	F1.13SPC1.13 & F1.13PC1.13	4.76	3.36
Change BC	F1.13SPC1.13S & F1.13PC1.13S	4.65	3.24
Change CRE	F1.13PC1.13S & F1.13PC1.13	3.04	2.31
Change CRE	F1.13SPC1.13S & F1.13SPC1.13	2.72	2.09
Change BC	F0.57SPC0.57 & F0.57PC0.57	4.44	2.86
Change BC	F0.57SPC0.57S & F0.57PC0.57S	3.71	2.38
Change CRE	F0.57PC0.57S & F0.57PC0.57	3.15	1.69
Change CRE	F0.57SPC0.57S & F0.57SPC0.57	1.70	1.07

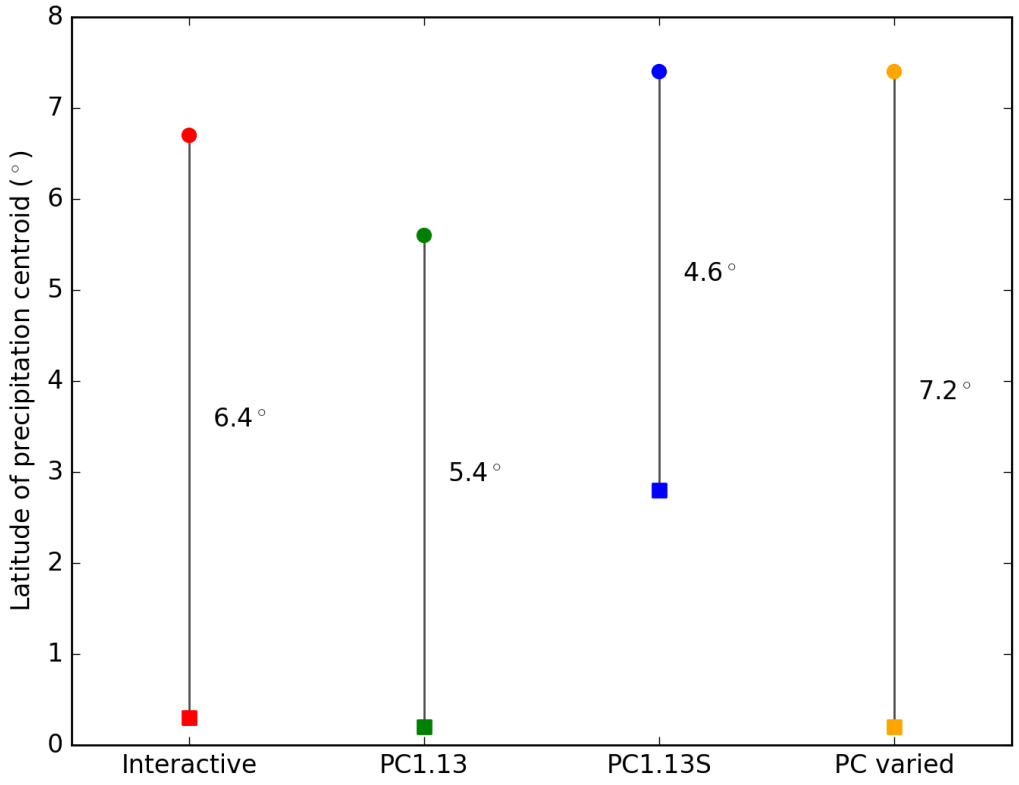

Figure 5.23: *Change in zonal-mean, time-mean precipitation centroid, (°, precipitation centroid explained in section 5.4), when changing from equinoctial (squares) to solstitial boundary conditions (dots). Red points denote interactive CRE changes (F1.13 and F1.13S), green points have a prescribed CRE typical of an equatorial ITCZ (F1.13PC1.13 and F1.13SPC1.13), blue points have a prescribed CRE typical of a solstitial ITCZ (F1.13PC1.13S and F1.13SPC1.13S), yellow points have the same prescribed-CRE as the boundary conditions (F1.13PC1.13 and F1.13SPC1.13S). Total shift of precipitation centroid printed adjacent to line connecting each pair of simulations.*

5.5 Discussion

The sensitivity of the tropical circulation to hemispherically asymmetric boundary conditions discussed in this chapter agrees with previous aquaplanet studies: solstitial boundary conditions are associated with a poleward ITCZ shift and a stronger winter hemisphere Hadley circulation (section 5.4; Neale and Hoskins, 2001; Bellon and Sobel, 2010; Mobis and Stevens, 2012; Williamson et al., 2013). Partitioning the influence of boundary conditions into insolation and SST variations shows that SSTs play the dominant role in varying the structure of the tropical atmosphere; SSTs exert a substantial control on boundary-layer convergence (Lindzen and Nigam, 1987; Numaguti, 1995). However, it is nontrivial to predict the ITCZ location given a meridional SST shift. For example, when an equatorial ITCZ is observed given equatorial boundary conditions (F1.13 and F1.70, section 4.3), it should not be assumed that the ITCZ will remain over the SST maximum when applying solstitial boundary conditions. Profile changes of $\widehat{[\overline{vh}]}$ and AEI occur when applying solstitial boundary conditions, associated with changes in ITCZ characteristics (Bischoff and Schneider, 2014). For example, increased equatorial surface turbulent fluxes, associated with the strengthening and northward shift of the southern Hadley circulation given solstitial boundary conditions, increase AEI_0 and reduce the meridional ITCZ shift. Variations in AEI and $\widehat{[\overline{vh}]}$ show that SSTs are not the only controlling factor in ITCZ characteristics; this point is further emphasised by the sensitivity of the ITCZ to the representation of convection (sections 4.3 and 5.3; Mobis and Stevens, 2012).

Work in chapter 4 and previous literature (Numaguti, 1995; Chao and Chen, 2004; Liu et al., 2010; Mobis and Stevens, 2012) is extended here by investigating the effect of the boundary conditions on the sensitivity of the ITCZ to convective mixing. Low convective mixing produce two precipitation peaks in the NH alongside subsidence at 10°N (F0.28S and F0.57S), whilst high convective mixing produce a single NH ITCZ (F0.85S, F1.13S and F1.70S). As observed in Bush et al. (2015), increasing convective mixing intensifies the summer-hemisphere Hadley circulation. The sensitivity of the solstitial ITCZ is associated with the sign of AEI at 10°N: single ITCZs are associated with a positive AEI, whilst double ITCZs are associated with a negative AEI. Negative AEI requires energy convergence at equilibrium: the mean circulation in all solstitial simulations transports energy towards the latitude of negative AEI (Fig. 5.24). Bischoff and Schneider (2016) proposed that a negative AEI_0 is associated with a double ITCZ, as the energy flux across the tropics no longer increases monotonically with latitude. Solstitial simulations highlight that a double ITCZ can be associated with a negative AEI at any latitude in the deep tropics ($\pm 10^\circ$ latitude), even if AEI_0 is positive.

The manifestation of the sensitivity of the ITCZ location to convective mixing depends on the

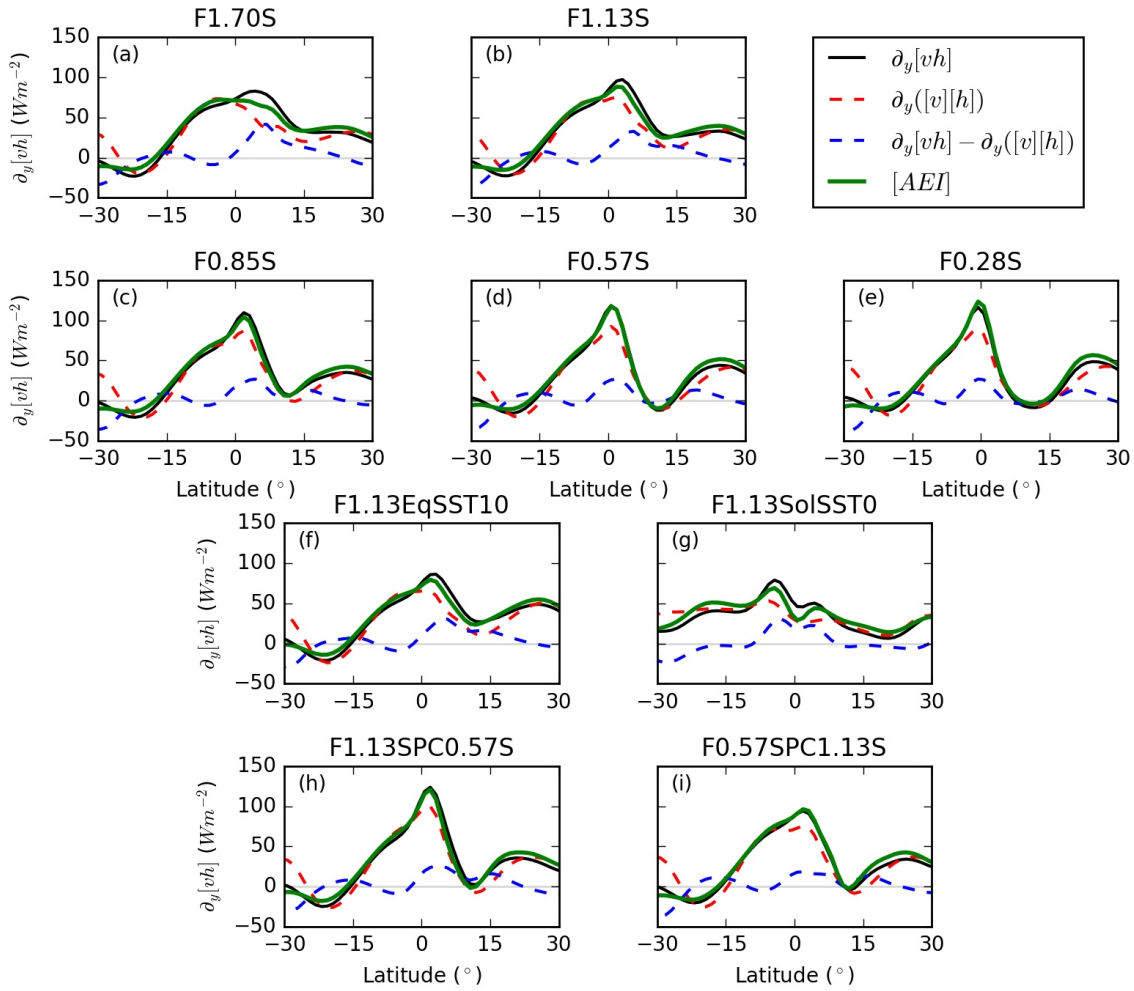

Figure 5.24: *Zonal-mean, time-mean divergence of the MSE flux and its components (W m^{-2}). (a)-(e) CRE-on solstitial simulations with various f_{dp}, (f) F1.13EqSST10, (g) F1.13SolSST0, (h)-(i) prescribed-CRE simulations, F1.13SPC0.57S and F0.57SPC1.13S. The corresponding simulation is labelled above each panel. The solid black line shows the divergence of the total MSE flux ($\partial_y[\overline{vh}]$); the red dotted line shows the MSE flux due to the mean circulation ($\partial_y[\overline{v}][\overline{h}]$); and the blue line shows the eddy contribution ($\partial_y[\overline{vh}] - \partial_y[\overline{v}][\overline{h}]$). The solid green line shows zonal-mean, time-mean AEI.*

boundary conditions; even though the same mechanisms are responsible for the sensitivity under both sets of boundary conditions. In solstitial and equinoctial simulations the minimum boundary-layer MSE needed for deep convection reduces as convective mixing decreases. At high convective mixing in equinoctial simulations a single equatorial ITCZ is produced; the minimum boundary-layer MSE required for deep convection is achieved close to the equator, the location of SST maximum. Hence, increasing convective mixing further leads to no change in the ITCZ location. Meanwhile under solstitial boundary conditions, the ITCZ is simulated equatorward of the SST maximum for all convective mixing rates used; further increasing convective mixing leads to a poleward ITCZ shift. A poleward shift of the summer hemisphere Hadley circulation towards the summer hemsiphere pole is also observed when increasing convective mixing in an atmosphere-only configuration of HadGEM3 (Bush et al., 2015). The sensitivity of the ITCZ location to f_{dp} at low convective mixing rates depends on the boundary conditions; the equatorial ITCZ shifts poleward when decreasing

convective mixing whilst the solstitial ITCZ is restricted to the NH. Blackburn et al. (2013) show an ITCZ equatorward of an off-equatorial SST maximum in a range of prescribed-SST aquaplanet GCMs with an SST maximum at 5°N. The solstitial ITCZ over cooler SSTs is associated with a reduced upper-tropospheric MSE, increased upper-level instability and reduced minimum boundary-layer MSE required for deep convection. The association between upper-tropospheric MSE and the minimum boundary-layer MSE required for deep convection has already been shown in simulations without CRE (section 4.4; Harrop and Hartmann, 2016). Neelin et al. (2003) investigated reduced precipitation at the margins of convergence zones in global warming simulations. They proposed a similar association between the minimum boundary layer MSE required for deep convection and upper-tropospheric MSE: a warmer atmosphere, hence greater upper-tropospheric MSE, requires higher boundary-layer MSE for deep convection. The solstitial ITCZ simulated equatorward of the SST maximum is also associated with an intensified southern Hadley circulation and increased surface evaporation and moisture contribution to boundary-layer MSE. Increased moisture reduces the dry static energy required to achieve the same MSE and allows the minimum boundary-layer MSE required for deep convection to be achieved equatorward of the SST maximum. The influence of moisture on ITCZ characteristics shows the importance of surface evaporation (Numaguti, 1993; Chao and Chen, 2004; Mobis and Stevens, 2012). Previous research has emphasised the role of surface evaporation on ITCZ characteristics by removing the dependence of surface evaporation on the wind speed (Numaguti, 1993, 1995; Mobis and Stevens, 2012).

The sensitivity of the ITCZ to convective mixing depends on the convective mixing rates used, the chosen diagnostic, and the boundary conditions. For example, the solstitial ITCZ location is sensitive to convective mixing for all convective mixing rates used (section 5.3), whilst the equinoctial ITCZ is only sensitive to convective mixing for a subset of f_{dp} values ($f_{dp} \leq 0.85$, section 4.3). The sensitivity of the ITCZ intensity also depends on the boundary conditions; increasing f_{dp} increases the equinoctial ITCZ intensity but decreases the solstitial ITCZ intensity. The response of the solstitial ITCZ is contradictory to previous literature which concludes that increasing convective mixing increases deep convection in convergence zones (Terray, 1998; Oueslati and Bellon, 2013). As the manifestation of the sensitivity of the ITCZ to convective mixing depends on the boundary conditions, future work investigating sensitivities of the ITCZ in a prescribed-SST modelling environment should take into consideration the prescribed boundary conditions. As well as this, predicting the sensitivity of tropical precipitation to the representation of convection in full GCMs remains a challenge. For example, different meridional SST profiles exist over the West and East Pacific Ocean, hence, zonal variations in the response of tropical precipitation to changes in the representation of convection is expected in full GCMs. Oueslati and Bellon (2013) illustrate that the sensitivity of tropical precipitation to convective mixing is different in the Central and Eastern Pacific

in both atmosphere-only and coupled GCMs.

Changing from equinoctial to solstitial boundary conditions reduces the role of CRE in the sensitivity of the ITCZ to convective mixing. Prescribed-CRE simulations show that atmospheric heating associated with CRE promotes convection as it acts as a fixed MSE source. However in solstitial simulations, latent heat fluxes plays a greater role in the sensitivity of the AEI to convective mixing, reducing the impact of prescribing CRE. Hence, the role of CRE in sensitivities of the ITCZ depend on the prescribed boundary conditions. This dependence is highlighted when comparing Chao and Chen (2004) and Harrop and Hartmann (2016). Both studies perform atmosphere-only aquaplanet simulations with and without CRE. In Chao and Chen (2004), who use a globally-uniform prescribed-SST, the ITCZ location is similar with and without CRE. Harrop and Hartmann (2016) on the other hand, who use the Qobs SST profile, show a substantial ITCZ poleward expansion when removing CRE. Section 4.4 and Harrop and Hartmann (2016) also show the ITCZ response to removing CRE depends on the representation of convection and choice of GCM. The different ITCZ responses to the representation of CRE across studies illustrates that the sensitivity of the ITCZ to cloud-radiation interactions depends on the boundary conditions and choice of GCM.

The role of CRE is also investigated in the sensitivity of the ITCZ to hemsipherically asymmetric boundary conditions as our current understanding of the importance of clouds in driving the large-scale atmospheric circulation is insufficient (Bony et al., 2015). Numaguti (1995) performed simulations in which the radiation scheme only included clear-sky longwave radiative transfer, hence neglecting the radiative effect of clouds and shortwave radiation. The authors show an SH ITCZ given an SST maxima at 5 and 10°N and the Kuo (1974) convective parameterisation scheme (Numaguti, 1995). It is hypothesised that excluding shortwave radiation and cloud-radiation interactions influences the ITCZ location, especially given that most other studies find an ITCZ in the same hemisphere as the SST maximum (Hess et al., 1993; Williamson et al., 2013). When prescribing an equinoctial CRE and applying solstitial boundary conditions, the meridional ITCZ shift reduces by approximately 20%, associated with an approximately 50% reduction in AET_0. Prescribed-CRE simulations illustrate a non-linear relationship between AET_0 and the ITCZ location, contrary to the linear relationship in Donohoe et al. (2013), who analysed the seasonal cycle of the ITCZ using NCEP reanalysis and precipitation climatology from the NOAA Climate Prediction Center. Voigt et al. (2014), who imposed hemispheric surface albedo asymmetries in four atmospheric GCMs, also found a reduced meridional ITCZ shift when prescribing CRE in slab-ocean simulations. Clouds amplify the meridional ITCZ shift, however, the model response to prescribing CRE depends on the atmospheric GCM and slab ocean depth (Voigt et al., 2014). Inter-model variability in clouds under a hemispherically symmetric surface albedo is responsible for approximately half of the inter-model

variability in ITCZ response to hemispherically asymmetric surface albedo forcing (Voigt et al., 2014).

The sensitivity of the ITCZ to insolation alone in a prescribed-SST aquaplanet modelling environment has not been considered in previous studies; in the real world insolation changes drive SST variations. Investigating the sensitivity of the ITCZ to insolation highlights issues with the AEI framework (Kang et al., 2008; Donohoe et al., 2013). Given NH solstitial insolation and an equatorial SST maximum, an SH ITCZ and a net-southward AET_0 is observed. This outcome does not support theory by Kang et al. (2008), Donohoe et al. (2013) and others, who propose that the net-southward AET_0 is correlated with a northward ITCZ shift. In the prescribed-SST model setup used this chapter, the ITCZ is restricted by the prescribed-SST profile, as SSTs substantially control the boundary-layer MSE (Mobis and Stevens, 2012). The southward AET_0 required to balance insolation changes cannot be achieved by meridional shifts of the mean circulation, instead a net-southward AET_0 is achieved through changes in the equatorial meridional wind profile, in particular, southward cross-equatorial winds are observed between 220 and 600hPa associated with a broad cross-equatorial circulation. Wei and Bordoni (2018) investigated the ITCZ response in slab-ocean aquaplanet simulations to seasonally-varying insolation. They concluded that on subseasonal timescales the energy flux equator leads the ITCZ; during certain periods the sign of AET_0 does not indicate the hemisphere in which the ITCZ is located. For example, during the retreat phase of the winter hemisphere cross-equatorial Hadley circulation, the energy flux equator resides in the opposite hemisphere to the ITCZ. Wei and Bordoni (2018) conclude that whilst the seasonal cycle of the energy flux equator is in phase with the seasonally varying insolation, the atmospheric circulation is constrained by surface thermodynamics and cannot adjust as quickly as the energy flux equator. Our prescribed-SST simulation with solstitial insolation is consistent with Wei and Bordoni (2018); the surface response to a change in insolation is constrained, resulting in the energy flux equator and ITCZ to reside in opposite hemispheres. Work by Wei and Bordoni (2018) also illustrate an increased SST maximum and a weaker SST meridional gradient under solstitial boundary conditions (Wei and Bordoni, 2018); neither of these changes have been considered in the "solstitial" SST profile. The sensitivity of the ITCZ to insolation highlights the importance of SSTs in constraining the ITCZ location (Hess et al., 1993; Numaguti, 1995; Mobis and Stevens, 2012) and that caution should be taken when associating AET_0 to the ITCZ location (Wei and Bordoni, 2018).

Work in chapters 4 and 5 have investigated sensitivities of the ITCZ using prescribed-SST atmosphere-only simulations. However, recent modelling studies have shown that simulated ITCZ shifts, associated with AEI variations, in atmosphere-only simulations are damped when the atmosphere is coupled to a dynamical ocean (Green and Marshall, 2017; Hawcroft et al., 2017). As well

as this, a prescribed SST model setup is energetically inconsistent and influences the atmospheric response to model perturbations. In the real world and atmosphere-ocean coupled simulations, the SST depends on the surface energy budget. It is hypothesised that using free-varying SSTs will change the sensitivity of the ITCZ to convective mixing and hemispherically asymmetric boundary conditions. For example, the SH ITCZ observed when using perpetual NH solstitial insolation may not be observed if SSTs were free to vary; a NH SST maximum may develop and promote a NH ITCZ. Future work should investigate sensitivities of the ITCZ, such as convective mixing and the boundary conditions, in a coupled modelling environment. Coupled simulations also allow variations in ocean circulation. The tropical poleward energy transport is dominated by the oceanic energy flux (Green and Marshall, 2017; Schneider, 2018), hence an interactive oceanic energy transport may reduce sensitivities of the ITCZ and the role of CRE. Work in chapter 6 investigates changes in the sensitivity of the ITCZ to convective mixing when coupling the atmosphere to an idealised ocean model that includes an energy transport that responds to the tropical atmospheric circulation.

5.6 Summary and conclusions

The tropical mean state in an aquaplanet model is sensitive to insolation and prescribed SSTs (section 5.4), supporting and extending previous research (Hess et al., 1993; Mobis and Stevens, 2012; Blackburn et al., 2013). Using an off-equatorial prescribed-SST maximum and perpetual solstitial insolation produces an off-equatorial ITCZ, associated with an hemispherically asymmetric Hadley circulation and a cross-equatorial atmospheric energy transport. The minimum boundary-layer MSE required for deep convection is achieved over cooler SSTs; an intensified cross-equatorial winter hemisphere Hadley circulation increases the moisture contribution to the boundary-layer MSE. The increased role of surface evaporation in achieving the minimum boundary-layer MSE needed for deep convection affects both the sensitivity of the ITCZ to convective mixing and the role of CRE. Simulations with solstitial insolation and an equatorial SST maximum show that the sign of the cross-equatorial energy transport is not always indicative of the hemisphere in which the ITCZ resides.

In agreement with chapter 4, reducing convective mixing decreases the minimum boundary-layer MSE needed for deep convection and promotes a double ITCZ. In a double ITCZ scenario the diagnosed hemispheric AEI asymmetry under solstitial boundary conditions is associated with a stronger SH Hadley circulation and a weaker NH Hadley circulation, leading to greater precipitation in the southern rainfall band. However, whilst the mechanisms responsible for the sensitivity of the ITCZ to convective mixing are insensitive to the boundary conditions, the manifestation of

the sensitivity depends on the boundary conditions. For example, increased convective mixing is associated with an intensified equinoctial ITCZ but a weakened solstitial ITCZ. Future work should therefore be cautious that concluded sensitivities of the ITCZ are not dependent on the chosen boundary conditions.

As in equinoctial simulations, the sensitivity of the solstitial ITCZ to convective mixing is associated with AEI changes. Cloudy-sky radiation plays a substantial role in this sensitivity. However, the role of CRE in the sensitivity of the ITCZ to convective mixing depends on the boundary conditions. Changing from equinoctial to solstitial boundary conditions reduces the role of CRE by approximately 20%, predominately due to an increased sensitivity of latent heat fluxes. Prescribing CRE also reduces the meridional ITCZ shift when changing from equinoctial to solstitial boundary conditions, associated with a reduced hemispheric AEI asymmetry and a decreased cross-equatorial atmospheric energy transport. It is concluded that CRE plays a substantial role in meridional ITCZ shifts.

Chapter 6

The impact of atmosphere-ocean coupling on the sensitivity of the ITCZ to convective mixing

6.1 Purpose of this chapter

Work in chapters 4 and 5 explore the sensitivity of the ITCZ to convective mixing in a prescribed-SST aquaplanet modelling configuration: reducing convective mixing promotes a double ITCZ associated with AEI changes. However, using prescribed SSTs is energetically inconsistent and prohibits interactions between SSTs and surface fluxes. One solution to this problem, used by several studies, is to couple the atmosphere to a slab ocean with a prescribed ocean energy transport (OET) (e.g. Merlis et al., 2013; Schneider et al., 2014; Wei and Bordoni, 2018). However, whilst using a slab ocean with a prescribed OET is energetically consistent, it prohibits any dynamic ocean response. Previous studies show that the ocean circulation response to changes in atmospheric circulation reduces the sensitivity of the ITCZ to hemispherically asymmetric forcings (Kay et al., 2016; Tomas et al., 2016; Green and Marshall, 2017; Hawcroft et al., 2017). Atmosphere-ocean coupling reduces the sensitivity of the ITCZ to convective mixing in the full GCM configuration of CNRM-CM5 (Oueslati and Bellon, 2013). Oueslati and Bellon (2013) propose the reduced sensitivity is associated with coupled atmosphere-ocean feedbacks, but do not hypothesise which processes are important. In this chapter an idealised atmosphere-ocean coupled model, with an interactive OET based on the meridional Ekman-driven ocean circulation, is developed to fulfil the final objective of this thesis (section 1.3); to quantify the effect of atmosphere-ocean coupling on the sensitivity of the ITCZ to convective mixing.

Green and Marshall (2017) introduce hemispherically asymmetric surface albedo in two configurations of a coupled atmosphere-ocean version of MITgcm (Marshall et al., 1997). The atmosphere is coupled to either a full dynamical ocean or a slab ocean with a prescribed OET. The prescribed OET used in the slab ocean configuration is calculated from the surface heat fluxes simulated when using the dynamical ocean model and a hemispherically symmetric albedo. Coupling the atmosphere to a dynamical ocean rather than a slab ocean reduces the sensitivity of the ITCZ location to a hemispherically asymmetric surface albedo by approximately 75%; an interactive OET enables both the atmosphere and ocean to respond to imposed AEI changes. The full dynamical ocean model produces a cross-equatorial OET, reducing the cross-equatorial AET required to balance the imposed hemispherically asymmetric surface albedo, and hence also reducing the ITCZ shift (Green and Marshall, 2017). Coupling the atmosphere to a dynamical ocean instead of a slab ocean with a prescribed OET also reduces the sensitivity of the ITCZ location to projected Arctic sea ice loss over the twenty-first century (Tomas et al., 2016). Changing the prescribed Arctic sea ice concentration from observations during the end of the twentieth century to simulated values at the end of the twenty-first century, decreases the present-day northward cross-equatorial OET and leads to hemispherically symmetric warming across high latitudes. Coupling the atmosphere to a slab ocean with a prescribed OET meanwhile, constrains the ocean response to atmospheric changes and substantial warming is only simulated in the NH extratropics ($\geq$30° latitude; Tomas et al., 2016). Hwang and Frierson (2013) argue that in coupled and atmosphere-only GCMs a Southern Ocean shortwave radiation bias leads to cross-equatorial AET biases associated with tropical precipitation biases. Across the Southern Ocean too much shortwave radiation is absorbed at the surface, associated with cloud cover biases (Trenberth and Fasullo, 2010; Haynes et al., 2011; Hwang and Frierson, 2013), which leads to a southward bias of the ITCZ location. However, artificially removing the Southern Ocean shortwave radiation bias in a model configuration where the atmosphere is coupled to a dynamical ocean does not remove the double ITCZ bias; energy transport changes associated with hemispherically asymmetric forcing are mostly accomplished by the ocean (Kay et al., 2016; Hawcroft et al., 2017).

In the tropics the majority of meridional OET is associated with the Ekman-driven ocean circulation (Levitus, 1987; Codron, 2012). Surface frictional stress decrease near-surface atmospheric winds and leads to an Ekman mass flux in the near-surface ocean layer (Schneider, 2018). Poleward and equatorward oceanic Ekman mass fluxes are associated with easterly and westerly near-surface zonal winds, respectively. Due to mass conservation, the near-surface oceanic Ekman mass flux forms the upper-branch of an overturning ocean circulation, with a return flow at depth (Schott et al., 2004). The heat transport associated with the overturning ocean circulation can be computed as the product of the mass flux and temperature difference between the two flows (Held, 2001; Codron, 2012). Coupling the atmosphere to a two-layer ocean that resolves the Ekman circulation substantially

impacts the structure and intensity of the simulated ITCZ (section 2.6; Pike, 1971; Codron, 2012). A set of numerical schemes to represent the Ekman-driven heat transport is introduced in Codron (2012). The coupled atmosphere-ocean modelling framework developed in this chapter is similar to the "2-layer Ekman scheme" in Codron (2012). The 2-layer Ekman scheme produces the structure of an Ekman-driven circulation, is computationally cheaper than coupling the atmosphere to a full dynamical ocean model, and is energetically consistent. It is also easier to understand the effect of the wind-driven circulation in the idealised modelling framework; in fully coupled models partitioning the effect of different components of the ocean circulation is challenging. The modelling framework is discussed in detail in sections 6.2.1 and 6.2.2. Kang et al. (2018) show that coupling the atmosphere to a slab ocean that includes Ekman advection reduces the sensitivity of the ITCZ to hemispherically asymmetric extratropical forcing (Kang et al., 2018). However, Kang et al. (2018) do not consider changes in Ekman upwelling and downwelling; instead, a constant temperature difference is prescribed between the two layers.

In this chapter an idealised atmosphere-ocean coupled model is developed to investigate the impact of atmosphere-ocean coupling on the sensitivity of the ITCZ to convective mixing. The ocean is represented by a two-layer model that resolves the Ekman-driven ocean circulation; OET depends on the atmospheric circulation. This is the first aquaplanet study to investigate a sensitivity of the ITCZ to an atmospheric process or forcing in such a modelling framework. It is hypothesised that coupling will substantially reduce the sensitivity of the ITCZ to convective mixing, as previous studies have shown that coupling the atmosphere to a full dynamical ocean reduces the sensitivity of the ITCZ to hemispherically asymmetric forcing (Green and Marshall, 2017). As well as investigating the impact of atmosphere-ocean coupling on the sensitivity of the ITCZ to convective mixing, prescribed-OET simulations are performed to examine the effects of an interactive OET. Comparing interactive and prescribed OET simulations shows the role of OET in changes in the sensitivity of the ITCZ to convective mixing when coupling.

Section 6.2 discusses the idealised atmosphere-ocean coupled modelling framework (6.2.1), the method used to achieve equilibrium (6.2.2), and simulations employed in this chapter (6.2.3). Section 6.3 describes the characteristics of the tropical atmosphere and ocean when coupling. Section 6.4 discusses the sensitivity of the ITCZ to convective mixing. Due to substantial mean-state changes when coupling, prescribed-SST simulations are performed with SSTs from interactive-OET simulations. Prescribed-SST simulations along with prescribed-OET simulations are discussed in section 6.5. Sections 6.6 and 6.7 end the chapter with discussion and conclusions.

6.2 Methodology

6.2.1 Coupled atmosphere-ocean modelling framework

A coupled modelling framework is developed in which the atmosphere is coupled to an idealised axisymmetric two-layer ocean model with an Ekman-driven circulation. The top layer, denoted by subscript m, represents the ocean mixed layer, whilst the bottom layer, denoted by subscript d, represents the deep ocean. SSTs are the same as the temperature in the ocean mixed layer. The zonal-mean zonal surface wind stress (τ_x, kg m^{-1} s^{-2}) determines the meridional Ekman ocean current in the mixed layer (v_{ek_m}, m s^{-1}):

$$[v_{ek\_m}] = \frac{-[\tau_x]}{\rho f H_m} \tag{6.1}$$

where ρ is a fixed density of 1030 kg m^{-3}, f is the Coriolis parameter (rad s^{-1}), [ ] represents the zonally-averaged value, and H_m is the ocean mixed layer depth (30m). Within $\pm 2.5^\circ$ latitude of the equator, f at 2.5° latitude is prescribed to ensure that v_{ek_m} is not unrealistically large close to the equator. To achieve vertical mass conservation, an equal but opposite-signed mass flux is computed in the deep layer (v_{ek_d}):

$$[v_{ek\_d}] = -[v_{ek\_m}]\frac{H_m}{H_d} \tag{6.2}$$

where H_d is the depth of the deep ocean layer (970m). The meridional Ekman-driven currents are calculated at the grid-points. Meridional Ekman currents at the cell boundaries are given using the average Ekman current at the two grid points either side of the boundary (Fig. 6.1):

$$[v_{ek}]_{i+\frac{1}{2}} = \frac{1}{2}([v_{ek}]_{i+1} + [v_{ek}]_i) \tag{6.3}$$

where both $[v_{ek\_m}]$ and $[v_{ek\_d}]$ are zero at the poles. The vertical Ekman-driven current (w_{ek}, m s^{-1}) is calculated using the meridional divergence of the meridional currents in the mixed layer:

$$[w_{ek}] = \partial_y([v_{ek\_m}])H_m \tag{6.4}$$

where ∂_y represents the meridional divergence. All calculations are performed in spherical coordinates. The vertical and meridional Ekman currents are then multiplied by the upcurrent temperature to calculate the associated heat fluxes. The temperature tendencies at each grid point are calculated using the meridional divergence of the horizontal heat flux ($-\partial_y(v_{ek\_m}[T_m])$, $-\partial_y(v_{ek\_d}[T_d])$) and the vertical heat flux divided by the layer depth ($\frac{w_{ek}[T^*]}{H_m}$, $\frac{w_{ek}[T^*]}{H_d}$, later shown in

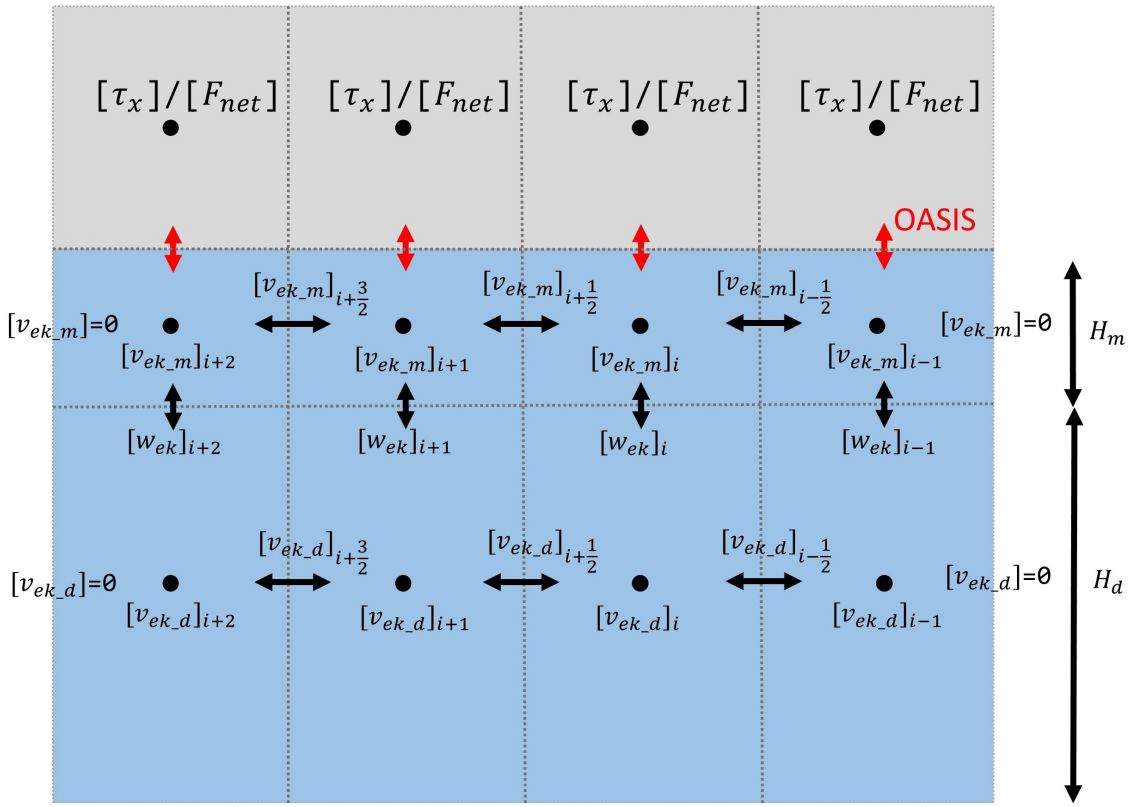

Figure 6.1: *Schematic (not to scale) of the numerical scheme used for the two-layer ocean model. Grid points are denoted by filled circles. Ocean cell boundaries, where heat fluxes are computed, are denoted by black double-pointed arrows. The atmosphere-ocean boundary, where atmosphere-ocean fluxes are exchanged via OASIS (section 3.3), are denoted by double-pointed red arrows. H_m and H_d denote the mixed and deep layer depths respectively. Further explanation on notation is given in section 6.2.*

[6.5] and [6.6]). A prescribed ocean heat transport (OHT_p, W m^{-1}, Fig. 6.2a) is also imposed to represent other dynamical features such as barotropic gyres and large-scale density currents. The meridional divergence of OHT_p (Fig. 6.2b, W m^{-2}), which is only substantial poleward of 25° latitude, is referred to as the "prescribed extratropical q-flux" following Voigt et al. (2016). The prescribed extra-tropical q-flux warms the high latitudes ($>$ 50° latitude) and cools the sub-tropics (25° to 50° latitude). All atmosphere-ocean fluxes are zonally-averaged to ensure axisymmetric SSTs.

In initial experiments with ocean temperature tendencies that depended on the Ekman circulation, prescribed extra-tropical q-flux, and surface fluxes, the mid-latitude (40 to 60° latitude) deep ocean became warmer than the mixed layer (not shown); mixed-layer cooling from Ekman transport was greater than warming from surface fluxes. To remove this, a temperature tendency associated with vertical mixing was added at all grid-points. If $[T_\mathrm{d}]$ is greater than $[T_\mathrm{m}]$, then this vertical mixing behaves like convection and ensures the deep ocean remains cooler than the mixed layer. If however $[T_\mathrm{m}]$ is greater than $[T_\mathrm{d}]$, this mixing acts like vertical diffusion. A scalar (C^*) is used to change the amount of heat transport associated with convection and vertical diffusion; larger heat transports are associated with convection. Finally, horizontal diffusion in the deep layer removes substantial

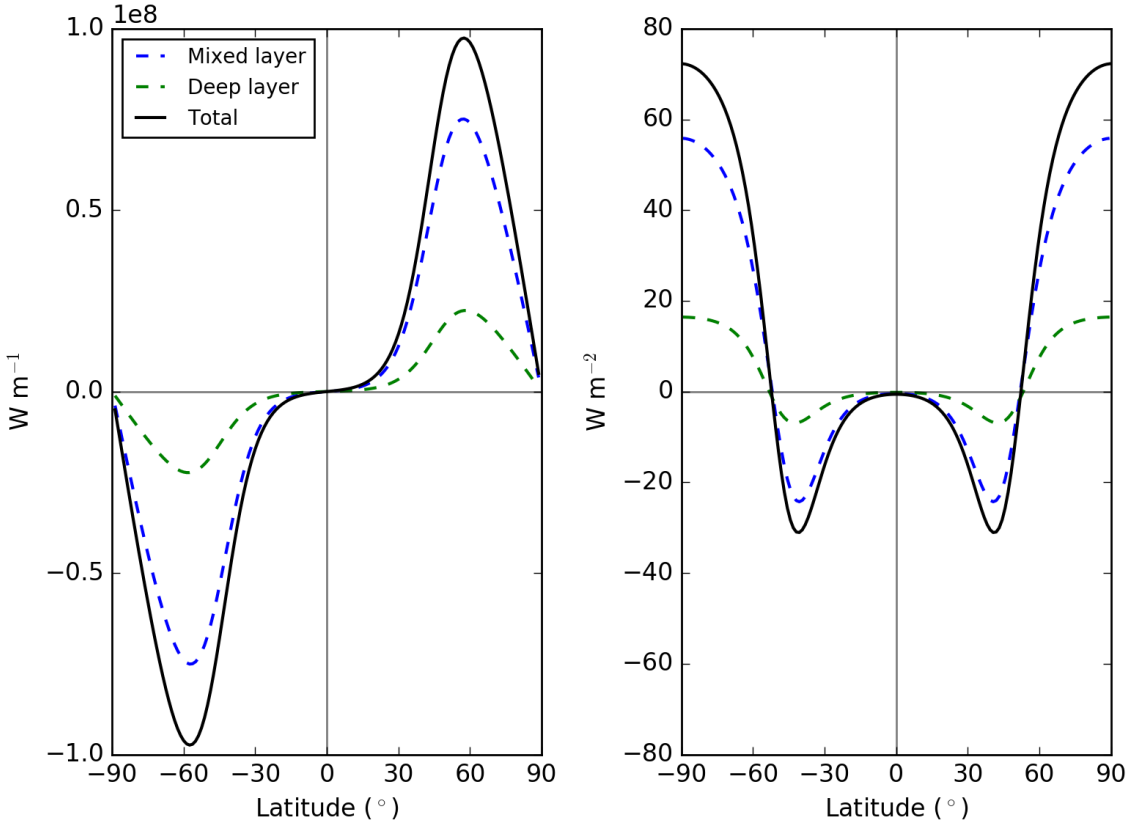

Figure 6.2: *Prescribed (a) northward meridional ocean energy transport (OET_p, W m^{-1}) and (b) extratropical q-flux ($\partial_y(OET_p)$, W m^{-2}) in interactive-OET and prescribed-OET simulations (Table 6.1). Blue and green dashed lines denote mixed and deep ocean layers respectively. The black line denotes the sum of both layers.*

horizontal temperature gradients. The final temperature tendency equations for the mixed and deep ocean layers are:

$$\frac{\partial [T_m]}{\partial t} = -\partial_y(v_{ek\_m}[T_m]) + \frac{w_{ek}[T^*]}{H_m} + \frac{1}{\rho C_p H_m}\Big[[F_{net}] - \partial_y(OHT_p)\Big] + \frac{C^*([T_d]-[T_m])}{H_m} \quad (6.5)$$

$$\frac{\partial [T_d]}{\partial t} = -\partial_y(v_{ek\_d}[T_d]) - \frac{w_{ek}[T^*]}{H_d} - \frac{\partial_y(OHT_p)}{\rho C_p H_d} - \frac{C^*([T_d]-[T_m])}{H_d} + D\partial_{yy}[T_d] \quad (6.6)$$

where F_{net} is the net-downward surface energy flux (W m^{-2}); C_p is a fixed specific heat capacity of 4000 J kg^{-1} K^{-1}; T is temperature (K) with T^* the upcurrent temperature; C^* is a scalar for vertical mixing (m s^{-1}), 100.0 or 0.001 for upward or downward vertical mixing, respectively; and D is a diffusion constant, 1.0 m^2 s^{-1}.

To spin up the ocean model efficiently "accelerated coupling" is used. Once atmosphere-ocean fluxes

are exchanged via OASIS (section 3.3), the ocean model is integrated for thirty hours and the atmosphere is integrated for three hours. The atmosphere-ocean fluxes are then exchanged again. Accelerated coupling is computational cheaper than running both models at the same speed as it reduces the computational time required for the ocean to equilibrate. Using accelerated coupling should not affect conclusions reached in this chapter. All simulation lengths, regardless of simulation technique, are stated in "atmospheric years", e.g. a 10 year simulation using accelerated coupling refers to 10 years of atmosphere and 100 years of ocean.

6.2.2 Achieving equilibrium

After running the model for 30 years of accelerated coupling, equilibrium is still not reached. The global-mean net-downward surface energy flux remains positive (Fig. 6.3a), associated with increasing ocean temperatures (Fig. 6.3b). The diminishing rate at which the global-mean net-downward surface energy flux decreases (Fig. 6.3a) makes it difficult to predict the timescale to achieve a zero global-mean net-downward surface energy flux. Even if equilibrium was achieved, SSTs would be unrealistically warm. For example, after 30 years tropical SSTs already peak at approximately 33.5°C (red lines in Fig. 6.4). To estimate the equilibrated SST profile, a line of best fit between the globally-integrated net-downward surface energy flux and ocean temperature after 15 years is calculated at each latitude. A global-mean ocean temperature of 20.3°C, a mean tropical SST of 30.8°C, and a maximum tropical SST of 35.0°C are predicted at equilibrium (Fig. 6.5). These SSTs are unrealistically warm. Between 2003 and 2010 the average tropical Pacific SST was approximately 27.0°C and the global mean ocean temperature was approximately 17°C (NCAR, 2014).

To enforce equilibrium and achieve a more realistic ocean heat content and SST, a globally uniform temperature tendency is applied:

$$\frac{\partial[T]}{\partial t} = \frac{-F_{corr}}{\rho C_p (H_m + H_d)} \tag{6.7}$$

where F_{corr} is a prescribed energy flux correction term applied to all grid points (W m^{-2}). In all coupled simulations F_{corr} is prescribed at 4 W m^{-2} and initial conditions are taken from 15 years of the spin-up simulation, after which the meridional structure of SST (Fig. 6.4a) and the temperature difference between the mixed and deep layers (Fig. 6.3b) remain similar. SSTs are more realistic at this point in the spin-up simulation (black line in Fig. 6.4); the tropical-mean and global-mean SSTs are 27.0 and 20.3°C respectively. Using a spatio-temporal uniform energy flux correction permits SST changes when changing atmospheric model components, is energetically consistent, and produces a more realistic equilibrium SST profile.

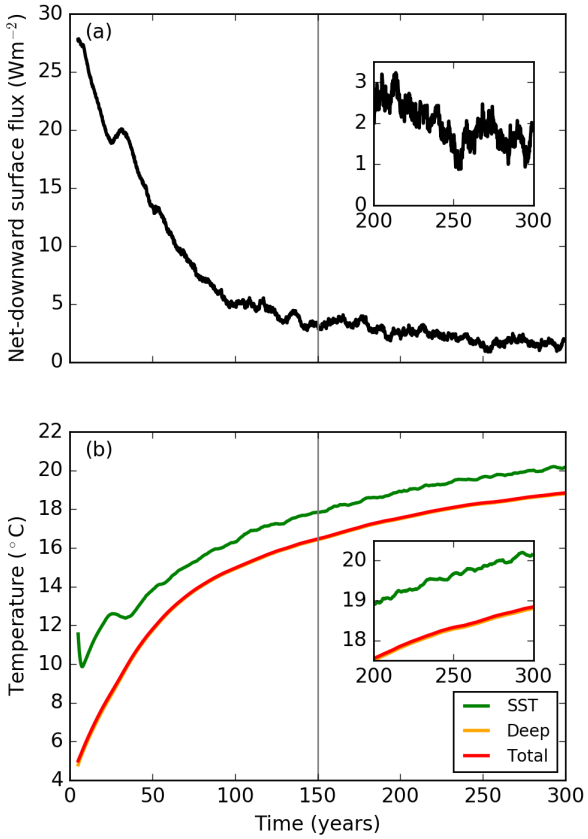

Figure 6.3: *Six-month running mean of the temporal evolution of globally-averaged (a) net-downward surface flux (W m^{-2}), (b) SST (green), deep-layer ocean temperature (orange) and ocean temperature ($^\circ$C, red) from initial 30-year simulation. Deep-layer temperatures are nearly identical to the total ocean temperatures. The vertical grey line denotes the point at which initial conditions were taken for interactive-OET simulations. In each panel an inset zooms into the last 100 years of simulation.*

6.2.3 Experiment design

Using the coupled modelling framework introduced in sections 6.2.1 and 6.2.2, three MetUM GA6.0 aquaplanet simulations are performed to explore the sensitivity of the ITCZ to convective mixing; f_{dp} is set to 0.5, 1.0 and 1.5 $\times$ the default value: 0.57 (C0.57), 1.13 (C1.13) and 1.70 (C1.70), respectively (Table 6.1). The role of f_{dp} in the formulation of convective mixing is discussed in section 3.1. For each simulation, 20 years of accelerated coupling is followed by 10 years of simulation. An equilibrated ocean state is achieved in all simulations during the first 20 years of accelerated coupling. The final 5 years of simulation are analysed. Coupled simulations are denoted by the label "C" followed by the given value of f_{dp}. Coupled simulations with an interactive Ekman-driven q-flux are referred to as "interactive-OET" simulations.

To investigate the role of atmosphere-ocean coupling on the sensitivity of the ITCZ to convective mixing, nine three-year atmosphere-only prescribed-SST simulations are performed. A simulation

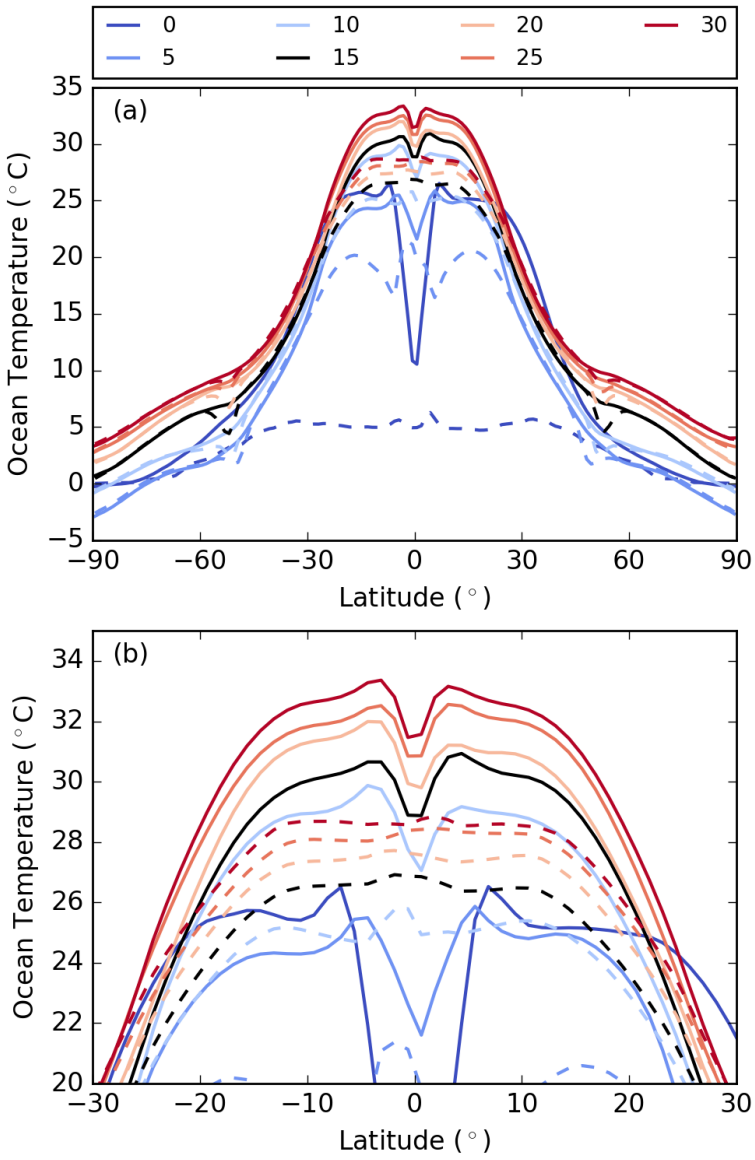

Figure 6.4: *(a) Annual-mean, zonal-mean mixed (solid) and deep (dashed) ocean temperatures (°C) at regular intervals of the initial spin-up simulation. The year at which the annual-mean is taken is printed in the legend. The black line denotes ocean temperature profiles at 15 years, the time position where initial conditions are taken from for interactive-OET simulations. (b) As in (a), but zooming into the tropics (± 30° latitude).*

length of three years is chosen to be consistent with all previous atmosphere-only simulations (chapters 4 and 5). The first two months of simulation is discarded as spin-up; the remaining two years and ten months are analysed. Zonal-mean, time-mean SSTs from interactive-OET simulations are used for the prescribed SST profiles. These are labelled "PS" (prescribed SST) followed by the interactive-OET simulation from which the prescribed SSTs are computed. For each prescribed SST profile (PS0.57, PS1.13 and PS1.70), three simulations are performed with f_{dp} varied to 0.57, 1.13 and 1.70 (Table 6.2), the same values used in the interactive-OET simulations (Table 6.1).

Finally, to explore the effect of interactive OET on the sensitivity of the ITCZ to convective mixing,

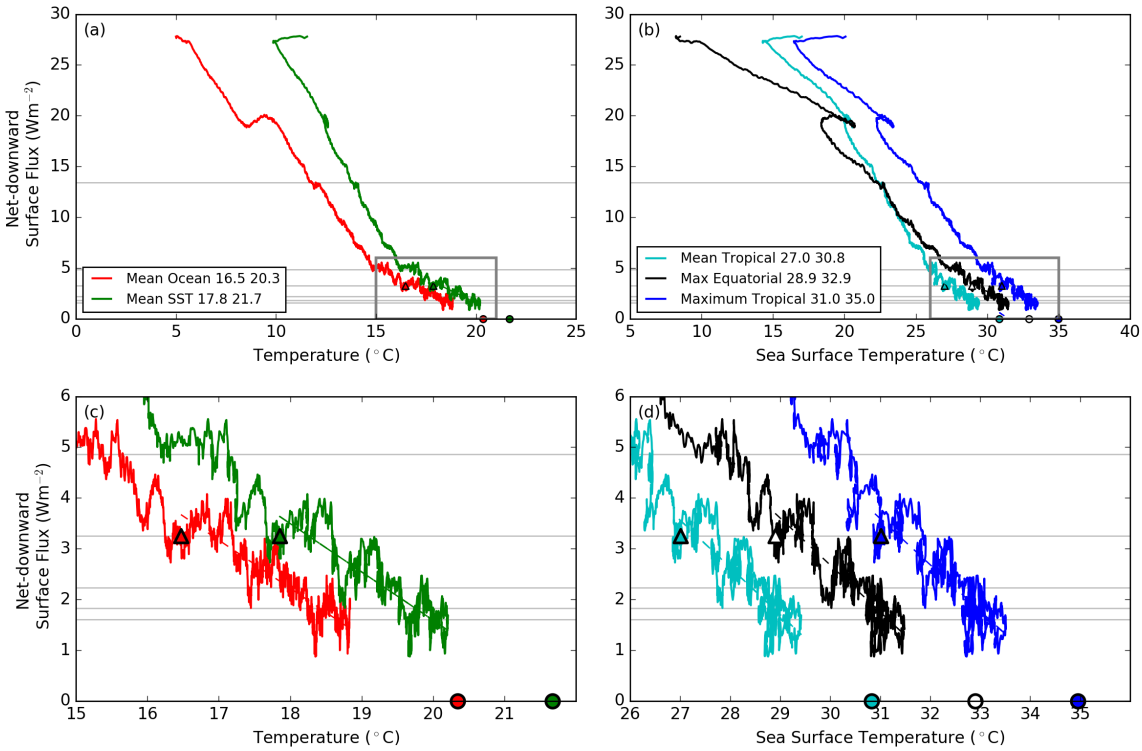

Figure 6.5: *(a) Global-averaged ocean temperature (red), global-mean SST (°C, green), (b) mean tropical SST (cyan, ± 30° latitude), maximum equatorial SST (black, ± 0.625° latitude) and maximum tropical SST (°C, blue) against net-downward surface energy flux (W m^{-2}). Solid lines denote simulated values whilst dashed lines denote lines of best fit after discarding the first 15 years of simulation. Triangles denote the value of each variable at 15 years, the time at which initial conditions are taken for interactive-OET simulations (Table 6.1). The value is also printed in the legend next to the line identifier. Circles denote the linear extrapolated values of each variable to a zero global-mean net-downward surface energy flux. These values are the second values printed next to each simulation identifier in the legend. Grey horizontal lines represent the net-downward surface energy flux every 5 years. (c) and (d), as in (a) and (b) respectively, zoom into where the net-downward surface energy flux is less than 6 W m^{-2}, visualised by the grey outline in (a) and (b).*

simulations are performed with a prescribed Ekman-driven q-flux (Table 6.1). The Ekman-driven q-flux is added to the extra-tropical q-flux (section 6.2.1). To prescribe the Ekman-driven q-flux, zonal-mean, time-mean temperature tendencies associated with the Ekman-driven circulation in an interactive-OET simulation are applied in the ocean mixed layer at all latitudes. Temperature tendencies associated with vertical mixing are also prescribed, decoupling the two ocean layers and reducing the time to achieve equilibrium. The temperature tendencies used to prescribe the Ekman-driven q-flux are denoted with "PQ" (prescribed q-flux), followed by the value of f_{dp} used in the interactive-OET simulation from which temperature tendencies are computed. Three "prescribed-OET" simulations are performed with a prescribed Ekman-driven q-flux from C1.13, with f_{dp} set to the values used in interactive-OET simulations; C0.57PQ1.13, C1.13PQ1.13, and C1.70PQ1.13. The prescribed-OET simulations are initialised from the end of C1.13. Ten years of accelerated coupling is followed by 10 years of simulation; the final 5 years are analysed.

Table 6.1: *Interactive-OET and prescribed-OET coupled simulations.*

Simulation	f_{dp}	Ekman-driven q-flux
C0.57	0.57	Interactive
C1.13	1.13	Interactive
C1.70	1.70	Interactive
C0.57PQ1.13	0.57	Prescribed PQ1.13
C1.13PQ1.13	1.13	Prescribed PQ1.13
C1.70PQ1.13	1.70	Prescribed PQ1.13

Table 6.2: *Prescribed-SST simulations using simulated zonal-mean, time-mean SSTs from interactive-OET simulations (Table 6.1).*

		Prescribed SSTs		
		PS0.57	PS1.13	PS1.70
f_{dp}	0.57	F0.57PS0.57	F0.57PS1.13	F0.57PS1.70
	1.13	F1.13PS0.57	F1.13PS1.13	F1.13PS1.70
	1.70	F1.70PS0.57	F1.70PS1.13	F1.70PS1.70

6.3 Climatology of idealised coupled simulation

The atmospheric mean state is substantially different in the coupled configuration compared to atmosphere-only prescribed-SST simulations (Fig. 6.6). This section describes the mean-state climate in the interactive-OET simulation where f_{dp} equals 1.13 (C1.13). C1.13 produces a double ITCZ (Fig. 6.6a) associated with an equatorial local SST minimum (Fig. 6.6c) and a negative AEI_0 (Fig. 6.6b). Easterly zonal wind stresses (Fig. 6.6d) drive a poleward oceanic mass flux in the surface layer, leading to equatorial oceanic upwelling and an SST minimum across the equatorial region (Fig. 6.6c). Cooler equatorial SSTs decrease the boundary-layer MSE (not shown), restricting equatorial convection and promoting a double ITCZ. Negative AEI_0 is associated with an equatorward AET across low latitudes (Figs. 6.7 and 6.8a). However, whilst equatorial subsidence is seen through the whole troposphere (later shown in Fig. 6.12b), the mean circulation plays a minimal role in the equatorward AET across low latitudes (Fig. 6.8a).

Fig. 6.8 illustrates components of AET and OET in C1.13; h_o denotes energy at each ocean grid-point (C_pT). The meridional divergence of the meridional ocean energy flux ($\partial_y\widehat{[\overline{v}\overline{h_o}]}$) is partitioned into two components: the Ekman-driven component ($\partial_y\widehat{[\overline{v_{ek}}\overline{h_o}]}$) and the component associated with diffusion and the prescribed extra-tropical q-flux ($D\partial_{yy}(T_D) + \partial_y(OHT)_p$). OEI, the net-downward surface energy flux, is also shown. By experimental design (section 6.2.1), the Ekman-driven energy transport ($\partial_y\widehat{[\overline{v_{ek}}\overline{h_o}]}$) is responsible for most of the tropical OET (Fig. 6.8b). Partitioning Ekman-driven OET into mean ($\partial_y\widehat{[\overline{v_{ek}}][\overline{h_o}]}$) and eddy ($\partial_y\widehat{[\overline{v_{ek}}\overline{h_o}]}$ - $\partial_y\widehat{[\overline{v_{ek}}][\overline{h_o}]}$) components shows that the mean Ekman-driven circulation is predominantly responsible for tropical OET (not shown). Partitioning AET into mean circulation ($\partial_y(\widehat{[\overline{v}][\overline{h}]})$) and eddy components ($\partial_y\widehat{[\overline{v}\overline{h}]}$ - $\partial_y(\widehat{[\overline{v}][\overline{h}]})$),

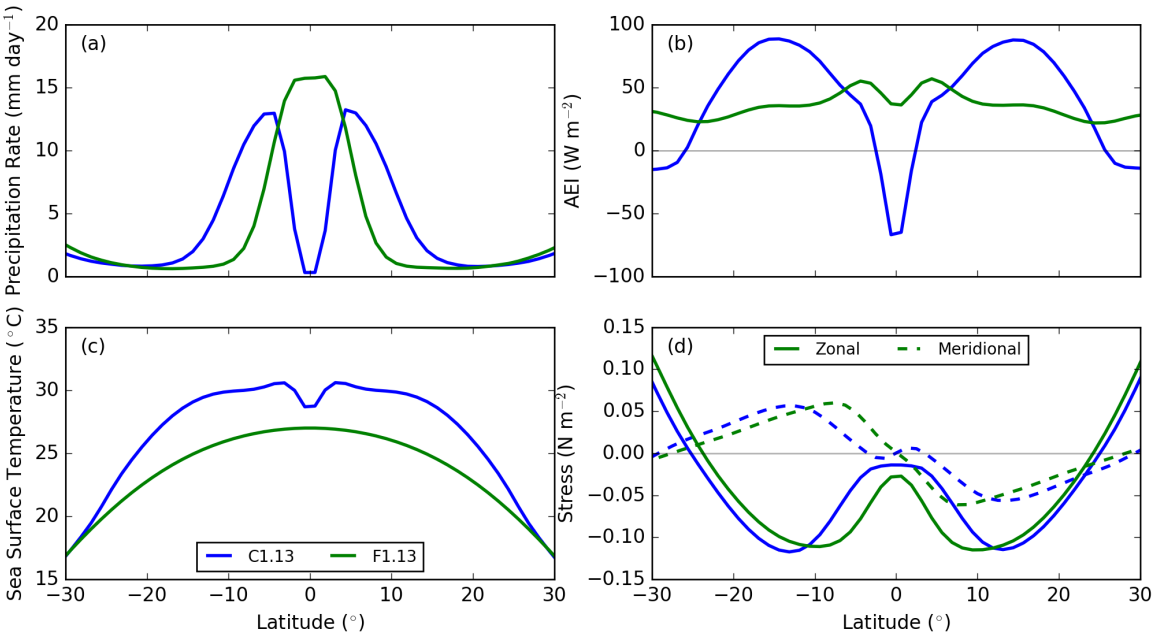

Figure 6.6: *Zonal-mean, time-mean tropical (a) precipitation (mm day^{-1}), (b) AEI (W m^{-2}), (c) SSTs (°C) and (d) zonal (solid) and meridional (dashed) surface wind stresses (N m^{-2}) in C1.13 (blue) and F1.13 (green, chapter 4).*

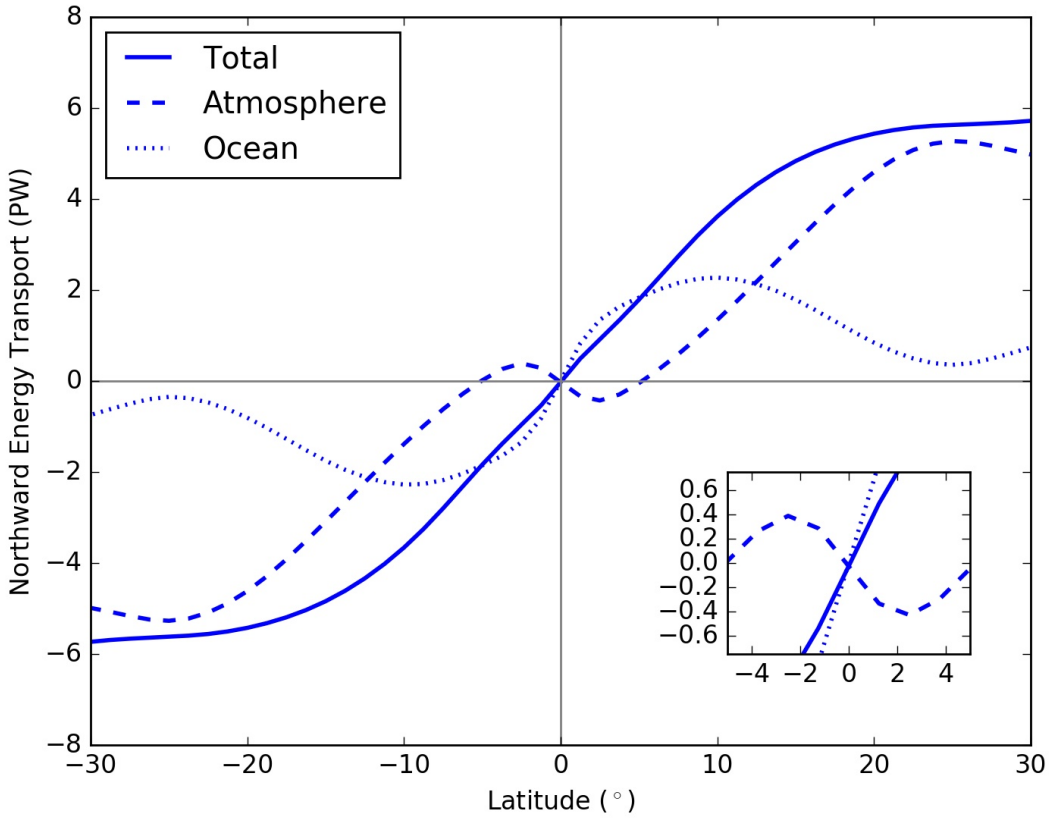

Figure 6.7: *Zonal-mean, time-mean total (solid), atmospheric (dashed) and oceanic (dotted) energy transports (PW) in C1.13. The inset on the bottom right zooms into the equatorial region.*

highlights that eddies play the dominant role in low-latitude equatorward AET in C1.13 (Fig. 6.8a). AET is investigated further for two reasons. First, the role of eddies is much greater in C1.13

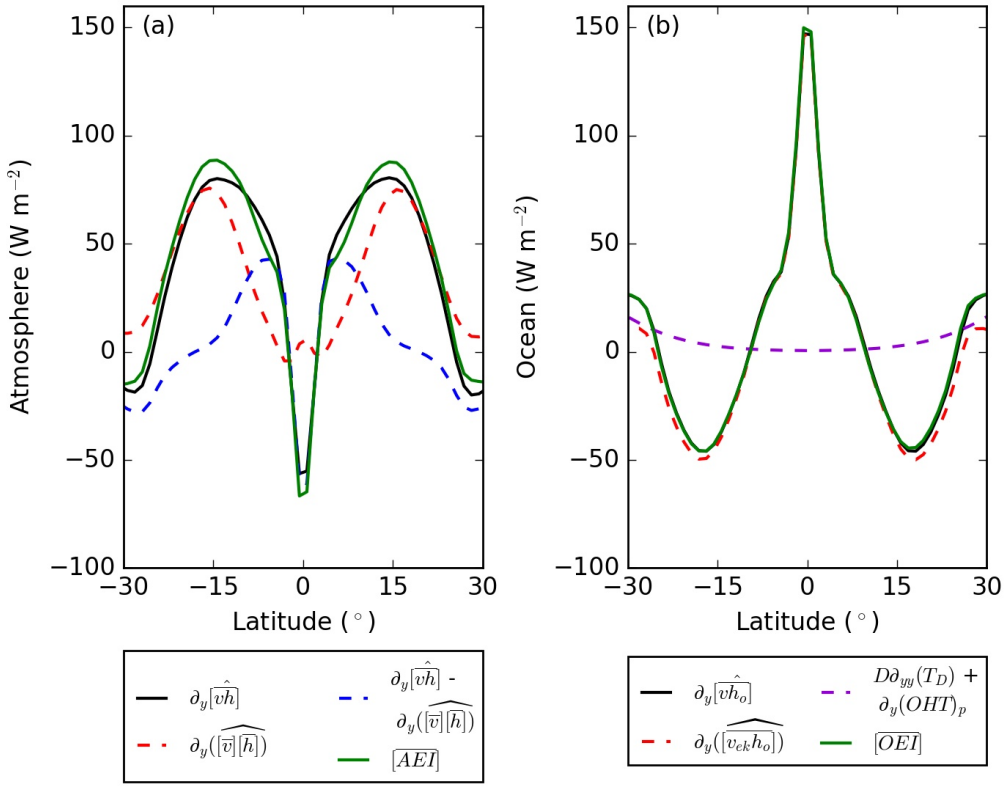

Figure 6.8: *(a) Components of meridional divergence of atmospheric MSE flux and AEI (W m^{-2}) in C1.13. The solid black line denotes meridional divergence of total MSE flux ($\partial_y[\hat{\overline{vh}}]$); the red dotted line denotes meridional divergence of MSE flux due to mean circulation ($\partial_y(\widehat{[\overline{v}][\overline{h}]})$); the blue dotted line denotes meridional divergence of MSE flux due to eddies ($\partial_y[\hat{\overline{vh}}] - \partial_y(\widehat{[\overline{v}][\overline{h}]})$); and the solid green line denotes zonal-mean, time-mean AEI. (b) Components of meridional divergence of ocean energy flux (W m^{-2}) and OEI (W m^{-2}) in C1.13. The solid black line denotes meridional divergence of total energy flux and includes extra-tropical prescribed q-flux and diffusion ($\partial_y[\hat{\overline{vh_o}}]$); the red dotted line denotes meridional divergence of ocean energy flux due to the mean Ekman-driven circulation ($\partial_y(\widehat{[\overline{v_{ek}}][\overline{h_o}]})$); the violet dotted line denotes meridional divergence of ocean energy flux due to diffusion and extra-tropical prescribed q-flux; and the solid green line denotes zonal-mean, time-mean OEI.*

compared to atmosphere-only simulations with a similar negative AEI_0 (Figs. 4.10d,e,g-i, 5.24d,e,h,i and 6.8a). Second, Bischoff and Schneider (2016) propose that a double ITCZ is associated with an equatorward AET by the mean circulation; C1.13, and other interactive-OET simulations (not shown), illustrate that this is not always the case.

To investigate the equatorward AET by eddies, the MSE flux is further partitioned. As in chapter 4, the MSE energy flux by eddies ($\partial_y(\widehat{[\overline{vh}]})_{eddy}$, W m^{-2}) is calculated from the difference between total MSE flux ($\partial_y[\hat{\overline{vh}}]$) and the MSE flux by the mean circulation ($\partial_y(\widehat{[\overline{v}][\overline{h}]})$, equation 4.1). To gain greater insight into the MSE components responsible for the equatorward AET, the same calculation is performed except that h is replaced with dry static energy ($C_pT + gZ$, denoted s) or latent energy (L_vq, denoted l). This reveals that equatorward AET across low latitudes is achieved by the flux of

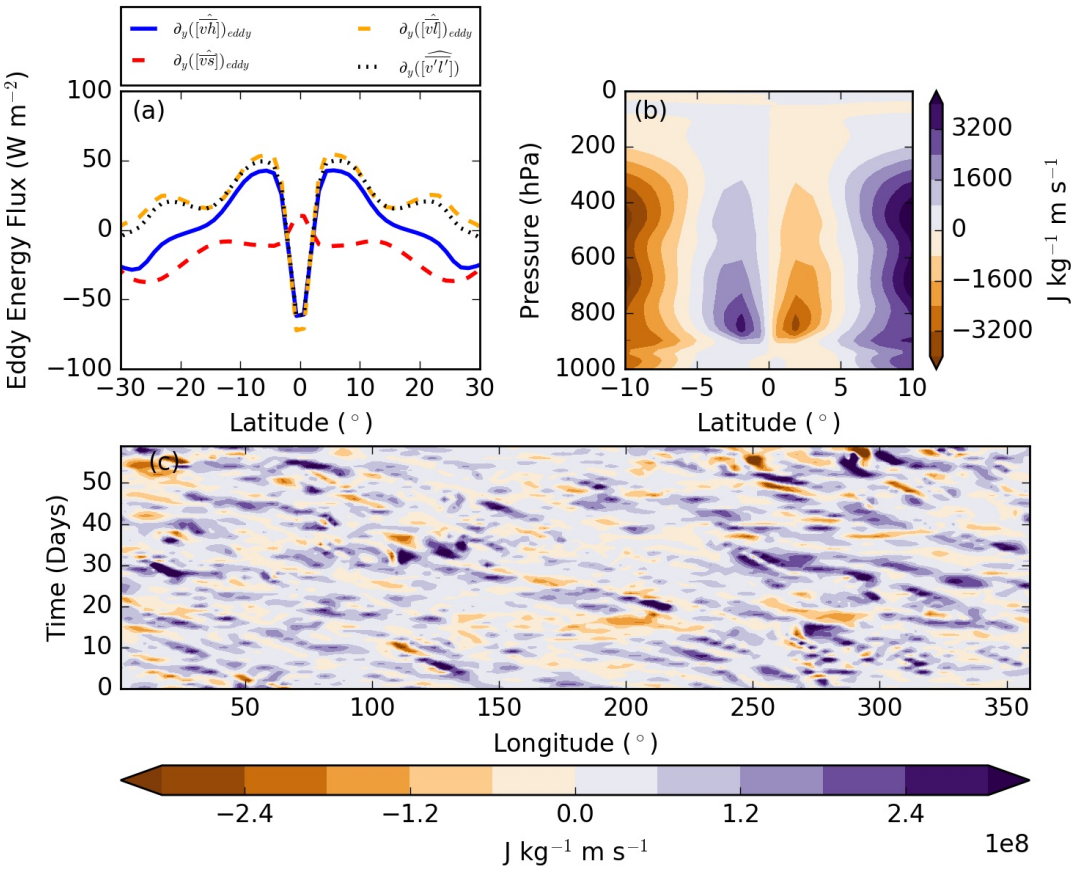

Figure 6.9: *Meridional divergence (W m^{-2}) of (a) $[\widehat{\overline{vl}}]_{eddy}$ (solid blue line), $[\widehat{\overline{vs}}]_{eddy}$ (dashed red line), $[\widehat{\overline{vl}}]_{eddy}$ (dashed yellow line) and $[\widehat{\overline{v'l'}}]$ (dotted black line) in C1.13. (b) $[\widehat{\overline{v'l'}}]$ (J kg^{-1} m s^{-1}) across ±10° latitude in C1.13. (c) Hovmöller of the vertically-integrated total equatorward latent energy flux by $\widehat{v'l'}$ between 5°S and the equator for the first 60 days.*

moisture associated with eddies (yellow line in Fig. 6.9a); dry static energy eddy flux is small across the equatorial region (red line in Fig. 6.9a). To understand the mechanisms responsible for the eddy moisture flux, $\partial_y([\widehat{\overline{vl}}])_{eddy}$ is partitioned further:

$$\partial_y([\widehat{\overline{vl}}])_{eddy} = \partial_y(\widehat{[\overline{v}]'[\overline{l}]'}) + \partial_y([\widehat{\overline{v}^*\overline{l}^*}]) + \partial_y([\widehat{\overline{v'l'}}]) \tag{6.8}$$

where * denotes deviations from the zonal-mean and $'$ denotes deviations from the time-mean. $\partial_y(\widehat{[\overline{v}]'[\overline{l}]'})$ is the moisture eddy flux due to correlated fluctuations of the zonal-mean. $\partial_y([\widehat{\overline{v}^*\overline{l}^*}])$ and $\partial_y([\widehat{\overline{v'l'}}])$ are contributions from stationary and transient eddies respectively; $\partial_y([\widehat{\overline{v'l'}}])$ is shorthand for $\partial_y([\widehat{\overline{v'^*l'^*}}])$ following James (1995). $\partial_y(\widehat{[\overline{v}]'[\overline{l}]'})$ and $\partial_y([\widehat{\overline{v}^*\overline{l}^*}])$ are small across the tropics (not shown); the eddy-associated latent energy flux across low latitudes is dominated by transient eddies (black dotted line in Fig. 6.9a). The latent energy flux associated with transient eddies is substantial between approximately 900 and 400hPa and is only equatorward between ±5° latitude (Fig. 6.9b). A Hovmöller of the vertically-integrated total latent energy flux by transient moisture eddies between 5°S and the equator identifies that westward propagating disturbances with a phase speed of approximately 5.5 m s^{-1} are responsible for the equatorward latent energy

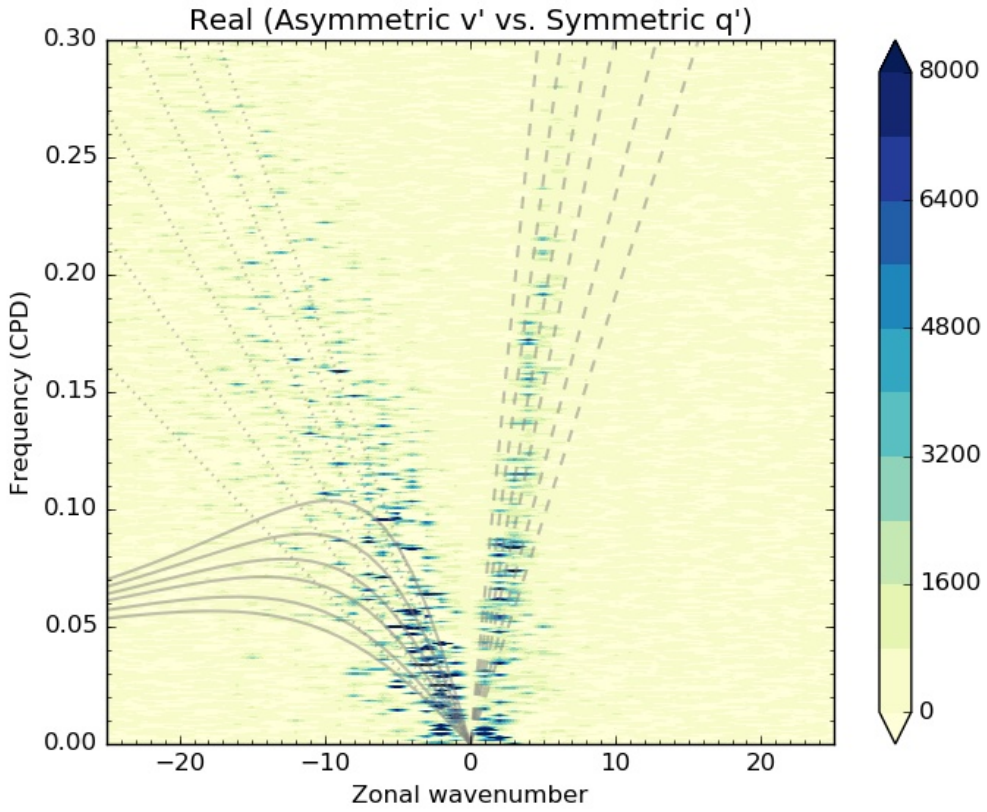

Figure 6.10: *Real components of the cross-power spectrum between v' and q' in C1.13. Grey lines illustrate dispersion curves for equatorial n=1 Rossby (solid) and Kelvin (dashed) waves with equivalent depths of 8.0, 12.0, 20.0, 30.0, 50.0 and 90.0m. Grey dotted lines indicate constant phase speeds of 3.0, 4.0, 5.0, 6.0, 7.0 and 8.0 m s^{-1}.*

flux (Fig. 6.9c). The equatorward latent energy flux in C1.13 is associated with an equatorial minimum and substantial meridional gradient in specific humidity (not shown) and SST (Fig. 6.6). In atmosphere-only simulations with a double ITCZ (F0.28 and F0.57, chapter 4), the difference in specific humidity and SST between the equator and low tropical latitudes is much smaller, associated with a reduced equatorward latent energy flux by transient eddies.

To further investigate the mechanisms responsible for the equatorward latent energy transport by transient eddies, a cross-power spectra of v' and q' is computed. v' and q' at 800hPa is partitioned into equatorially symmetric and antisymmetric components across the equatorial band 5°S to 5°N. At this height and between these latitudes the equatorward eddy-associated latent energy transport is at its greatest (Fig. 6.9b). Temporal anomalies of v' and q' are then obtained by subtracting the time-mean. Figure 6.10 shows the real component of the cross-power spectra associated with symmetric q' and asymmetric v'. Equatorward eddy-associated latent energy transport is associated with westward moving disturbances with zonal wavenumbers of 2 to 6 and phase speeds of 5 to 20 m s^{-1}, consistent with equatorial Rossby-waves where n=1 (solid grey lines in Fig. 6.10). There is also substantial power associated with Kelvin waves, however due to the structure of Kelvin waves,

these cannot contribute to the equatorward latent energy transport.

6.4 Sensitivity of ITCZ to convective mixing

Coupling substantially changes the mean state (section 6.3). Tropical SSTs are considerably warmer and a local equatorial SST minimum promotes a double ITCZ (Fig. 6.6). This section discusses the sensitivity of the ITCZ to f_{dp} in interactive-OET simulations. All values of f_{dp} produce a double ITCZ (Figs. 6.11a and 6.12) associated with negative AEI_0 (Fig. 6.11b). Decreasing f_{dp} intensifies the ITCZ and expands it poleward (Fig. 6.11a). Similar to the argument proposed for the sensitivity of the ITCZ to f_{dp} in atmosphere-only simulations (sections 4.3 and 5.3), reducing f_{dp} decreases the minimum boundary-layer MSE needed for deep convection and encourages deep convection over cooler SSTs. Deep convection at higher tropical latitudes broadens the ITCZ and reduces the equatorward moisture flux at low latitudes. Decreasing f_{dp} also increases the temperature difference between the equatorial and maximum tropical SST (Fig. 6.11c), associated with a broader region centered on the equator with minimal precipitation (Fig. 6.11a) and increased equatorward eddy-associated latent energy transport at low latitudes.

The MSE argument proposed for the ITCZ broadening when decreasing f_{dp} does not explain the sensitivity of the ITCZ intensity (Fig. 6.11a). The intensified ITCZ when decreasing f_{dp} (Fig. 6.11a) is likely due to warmer tropical SSTs (Fig. 6.11c) associated with increased surface latent heat fluxes (Fig. 6.13d) and atmospheric moisture (not shown); there are minimal changes in moisture export out of the tropics (not shown). Decreased f_{dp} increases TOA radiative cooling (Fig. 6.13a) which is balanced by increased latent heat fluxes (Fig. 6.13d) and precipitation (Fig. 6.11a) to ensure radiative-convective equilibrium. The sensitivity of tropical SSTs to f_{dp} is investigated by partitioning the globally-integrated net-downward surface energy flux into clear-sky and cloudy-sky radiative fluxes and surface turbulent fluxes. Figure 6.14a shows the difference in the temporal evolution of net-downward surface energy flux components between C0.57 and C1.70 during the entire simulation including the accelerated coupling period. Both simulations are commenced from the same initial conditions (section 6.2.2). Initially, C0.57 produces more net-downward surface energy flux (grey line in Fig. 6.14a) due to cloudy-sky radiation differences (blue line in Fig. 6.14a). Below approximately 500hPa, decreasing f_{dp} increases downward SW cloudy-sky radiation (filled contours in Fig. 6.14b) associated with decreased cloud-ice and cloud-liquid concentration in convective regions (filled and lined contours respectively in Fig. 6.14c). The effect of decreased cloud-ice and cloud-liquid concentration on downward SW cloudy-sky radiation at the surface is greater than the effect associated with increased upper-tropospheric (approximately 150hPa) cloud

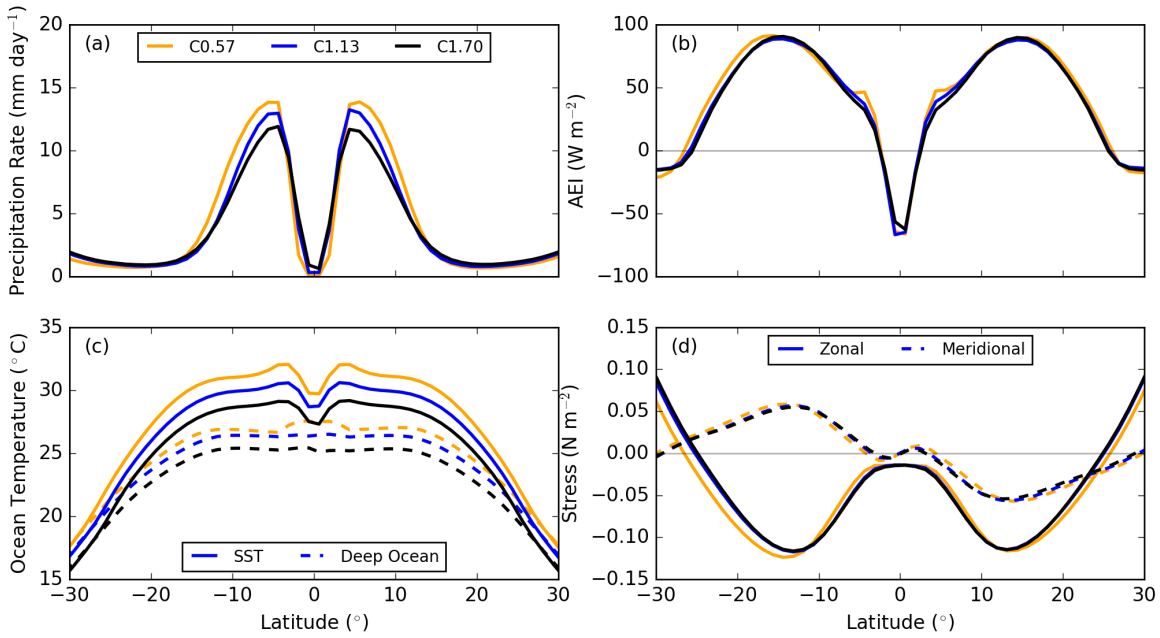

Figure 6.11: *Zonal-mean, time-mean tropical (a) precipitation (mm day^{-1}), (b) AEI (W m^{-2}), (c) ocean temperatures (°C), where solid lines denote SSTs and dashed lines denote deep ocean layer temperatures, and (d) zonal (solid) and meridional (dashed) surface wind stresses (N m^{-2}) in C0.57 (orange), C1.13 (blue) and C1.70 (black).*

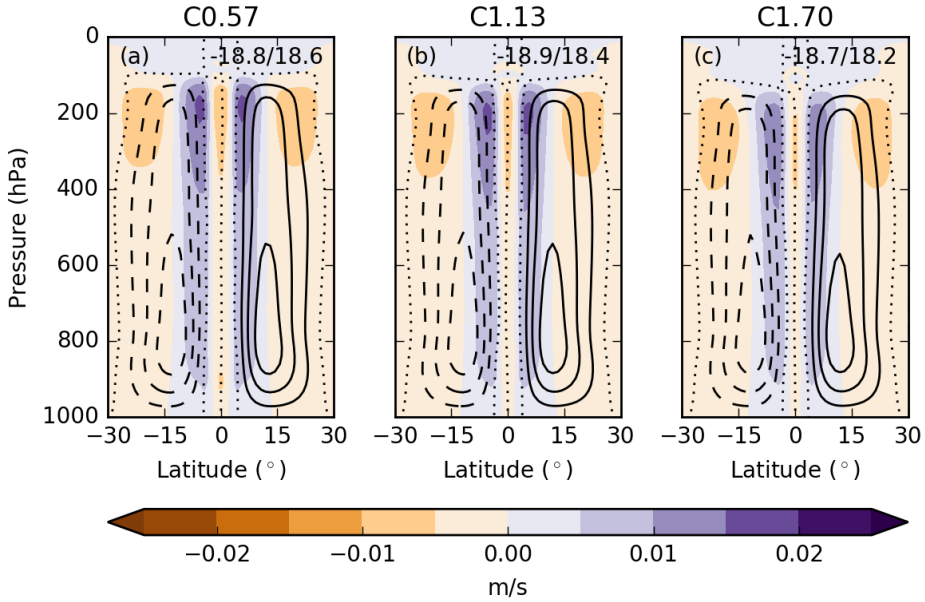

Figure 6.12: *Zonal-mean, time-mean mass meridional streamfunction (kg s^{-1}) (line contours) and vertical wind speed (m s^{-1}) (filled contours) for (a) C0.57, (b) C1.13 and (c) C1.70. Line contours are in intervals of 5 $\times$ 10^{10}, with dashed and dotted contours representing negative and zero values respectively. Positive streamfunction values indicate clockwise circulation. Maximum magnitude of the mass meridional streamfunction in the SH and NH is printed in the top right-hand corner of each panel.*

fraction and cloud ice (Fig. 6.14b,c). Decreased f_{dp} is associated with increased plume buoyancy and less moisture gained by the environment from convective plumes in the lower- and mid-troposphere. At lower f_{dp} more convective plumes reach the tropopause where forced detrainment increases upper-tropospheric moisture content. Other components of the net-downward surface energy flux

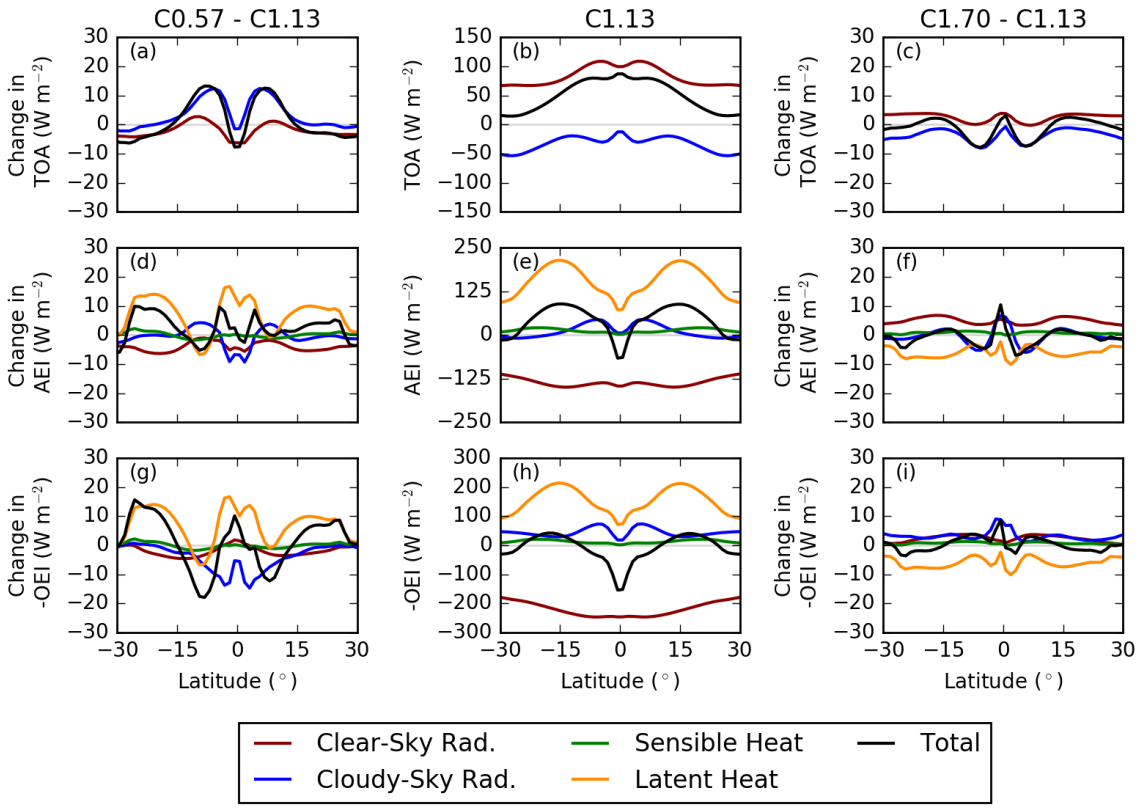

Figure 6.13: *Zonal-mean, time-mean of components of (a-c) net-downward TOA flux (W m^{-2}) (d-f) AEI (W m^{-2}) and, (g-i) -OEI (W m^{-2}). Panels in first and third column show the change in components when decreasing and increasing f_{dp} to 0.57 and 1.70 respectively from 1.13. Panels in second column show C1.13. The red lines denote clear-sky radiation; the blue lines denote cloudy-sky radiation. The green and orange lines denote sensible and latent heat fluxes, respectively; the black lines denote the total of all components.*

respond on longer timescales (Fig. 6.14a). For example, increased SSTs (Fig. 6.11c), associated with SW cloudy-sky radiation changes, increase surface latent heat fluxes (Figs. 6.13d) and reduce the difference in net-downward surface energy flux (Fig. 6.14a). Surprisingly, even with increased SST as f_{dp} decreases (Fig. 6.11c), the sensible heat flux contribution to the net-downward surface energy flux increases (green line in Fig. 6.14a). Further analysis reveals that the near-surface air temperature warms more the surface temperature (not shown). The equilibrated ocean heat content is achieved when cloudy-sky radiation changes are balanced by other surface energy flux components.

Across the tropics total energy transport is largely insensitive to f_{dp} (Fig. 6.15). The sum of AEI and OEI is positive across the tropics, indicative of a poleward total energy transport. However, the contributions of total energy transport from atmospheric and oceanic components depends on latitude and f_{dp}. Across the equatorial region both AET and OET are insensitive to f_{dp}, however in the mid-tropics (10 to 25° latitude), decreasing f_{dp} decreases AET and increases OET. Decreased f_{dp} warms tropical-mean SSTs (Fig. 6.11c), associated with increased moisture content, increased MSE transport in lower branches of the Hadley circulation, and a reduced poleward AET (dashed

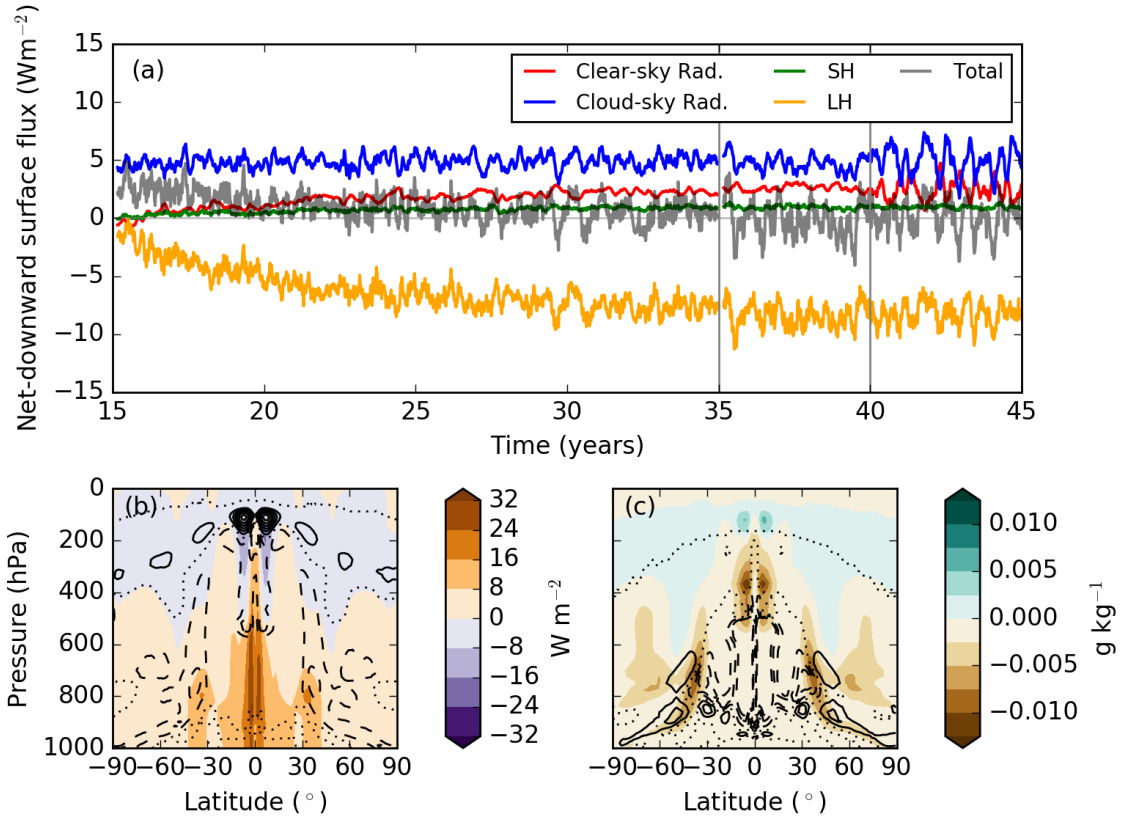

Figure 6.14: *C0.57 minus C1.70 for (a) zonal-mean evolution of the globally-averaged net-downward surface energy flux and its components (W m^{-2}). In (a) a 60-day running mean is shown. The first and second vertical grey lines indicate the end of accelerated coupling and the analysis period respectively. Red line denotes the clear-sky component, blue line denotes the cloudy-sky component. Green and orange lines denotes the sensible and latent heat flux, respectively; the grey line is the total AEI change. (b) and (c), zonal-mean, time-mean differences during the analysis period (final five years); (b) cloud fraction (lined, %), downward SW cloud radiative flux (W m^{-2}); (c) cloud-liquid (lined, g kg^{-1}) and cloud-ice concentrations (filled, g kg^{-1}). Line contours in (b) and (c) in intervals of 5% and 0.002 g kg^{-1} respectively. Dashed and dotted contours represent negative and zero values respectively.*

lines in Fig. 6.15). Decreased AET is compensated by increased OET, leading to minimal in total energy transport change. OET is the product of the vertically-integrated mass flux multiplied by the vertical temperature gradient (Held, 2001). Changes in the vertical temperature gradient play the dominant role in OET changes between 10° and 25° latitude (not shown). However, several processes controlling the temperature difference between the two layers are not well represented by the ocean model (section 6.2.1). For example, tropical deep-layer ocean temperatures are partly determined by sub-tropical ocean temperatures (approximately 30° latitude) which are associated with processes at higher latitudes ($\geq$ 30° latitude) that are represented by a prescribed OET.

AEI$_0$ is highly insensitive to f_{dp} in interactive-OET simulations (Fig. 6.11b), consistent with the minimal sensitivity of AET across low latitudes (Fig. 6.15). To better understand this lack of sensitivity, the net-downward TOA flux and the AEI and OEI budgets are calculated (Fig. 6.13). The negative of OEI is shown (Fig. 6.13g-i) so that all energy budgets are considered from an

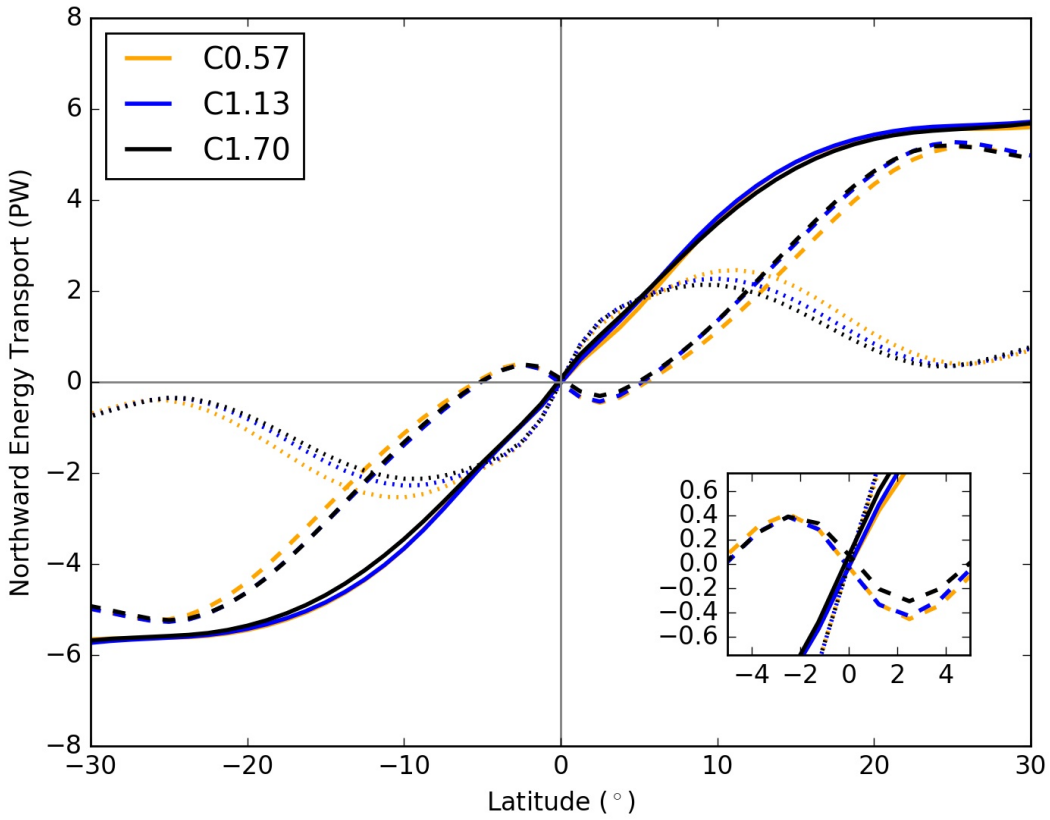

Figure 6.15: *Zonal-mean, time-mean total (solid), atmospheric (dashed) and oceanic (dotted) energy transports (PW) in C0.57 (orange), C1.13 (blue) and C1.70 (black). The inset on the bottom right zooms into the equatorial region.*

atmospheric perspective, i.e. positive values indicate an energy flux into the atmosphere. As in atmosphere-only prescribed-SST Qobs simulations (Fig. 4.3), latent heat fluxes and cloudy-sky radiative fluxes show the largest sensitivities to f_{dp} (Fig. 6.13d,f). Decreasing f_{dp} from 1.13 to 0.57 decreases equatorial cloudy-sky AEI_0 (Fig. 6.13d) associated with the preference of off-equatorial convection (Fig. 6.11a). The AEI_0 decrease due to cloudy-sky radiation is offset by increased latent heat fluxes (Fig. 6.13d) associated with increased SSTs (Fig. 6.11c). As a result a minimal sensitivity of AEI_0 to f_{dp} exists in interactive-OET simulations due to interactive SSTs.

Interactive-OET simulations show a substantial sensitivity of the net-downward TOA flux and OEI to f_{dp} (Fig. 6.13a,c,g,i). For example, decreasing f_{dp} from 1.13 to 0.57 increases the cloudy-sky radiation flux contribution to the net-downward TOA flux across the ITCZ region (Fig. 6.13a) associated with reduced cloud-liquid and cloud-ice concentration across the majority of the troposphere (Fig. 6.14c) and decreased reflection of SW radiation by clouds. Increased TOA cloudy-sky radiative flux is also associated with an intensified ITCZ (Fig. 6.11a) which increases LW radiation absorption by clouds (Fig. 6.13d) and reduces upward TOA cloudy-sky flux. OEI is more sensitive than AEI to f_{dp} across the tropics (Fig. 6.13d,f,g,i). For example, when decreasing f_{dp} from 1.13 to 0.57,

the maximum AEI change across the tropics is approximately 15 W m^{-2} (Fig. 6.13d) whilst the maximum OEI change is just below 20 W m^{-2} (Fig. 6.13g). A greater sensitivity of OEI than AEI to f_{dp} suggests that OET changes are partly responsible for the reduced sensitivity of the ITCZ to f_{dp} when coupling.

Comparing atmosphere-only simulations in section 4.3 to interactive-OET simulations suggests that coupling substantially reduces the sensitivity of the ITCZ to f_{dp} (Figs. 4.1a and 6.11a). However, it difficult to conclude that coupling is primarily responsible for the reduced sensitivity as substantial SST changes occur when coupling (Fig. 6.6c). In the following section atmosphere-only simulations with prescribed SSTs from interactive-OET simulations are analysed to isolate the effect of coupling on the sensitivity of the ITCZ to f_{dp}.

6.5 The impact of atmosphere-ocean coupling on the sensitivity of the ITCZ to convective mixing

6.5.1 The effect of prescribing SST on the sensitivity of the ITCZ to convective mixing

Due to changes in the mean state when coupling (section 6.3) it is inappropriate to compare the sensitivity of the ITCZ to f_{dp} in Qobs atmosphere-only simulations (chapter 4) with interactive-OET simulations. Hence, to explore the effect of coupling on the sensitivity of the ITCZ to f_{dp}, nine three-year prescribed-SST aquaplanet simulations are performed (Table 6.2). For each SST profile from the three interactive-OET simulations (Fig. 6.11c), three simulations are performed with f_{dp} set to 0.57, 1.13 and 1.70 (Table 6.2). All prescribed-SST simulations produce a double ITCZ with negligible equatorial precipitation (Fig. 6.16a,c,e), associated with negative AEI_0 (Fig. 6.16b,d,f) and equatorial subsidence (Fig. 6.17). The ITCZ contracts equatorward as f_{dp} increases for every prescribed SST profile (Fig. 6.16a,c,e and Fig. 6.18a). Assuming that the sensitivity of tropical free-tropospheric MSE to f_{dp} is small, increased f_{dp} increases the amount of boundary-layer MSE required for deep convection, weakening convection over cooler SSTs and leading to an equatorward ITCZ contraction. Similar behaviour is seen for the Qobs SST profile (section 4.3, Fig. 4.1a).

However, as in chapter 5, the sensitivity of the ITCZ to f_{dp} depends on the SST profile and diagnostic used. Figure 6.18 illustrates the maximum precipitation rate, precipitation centroid (P_{cent}), and the ITCZ width in prescribed-SST simulations. Following Hwang and Frierson (2010) and Byrne and Schneider (2016a) respectively, P_{cent} is the median of zonal-mean precipitation between 0° and 20°N and the ITCZ width is defined as the meridional distance between the ascending branch of

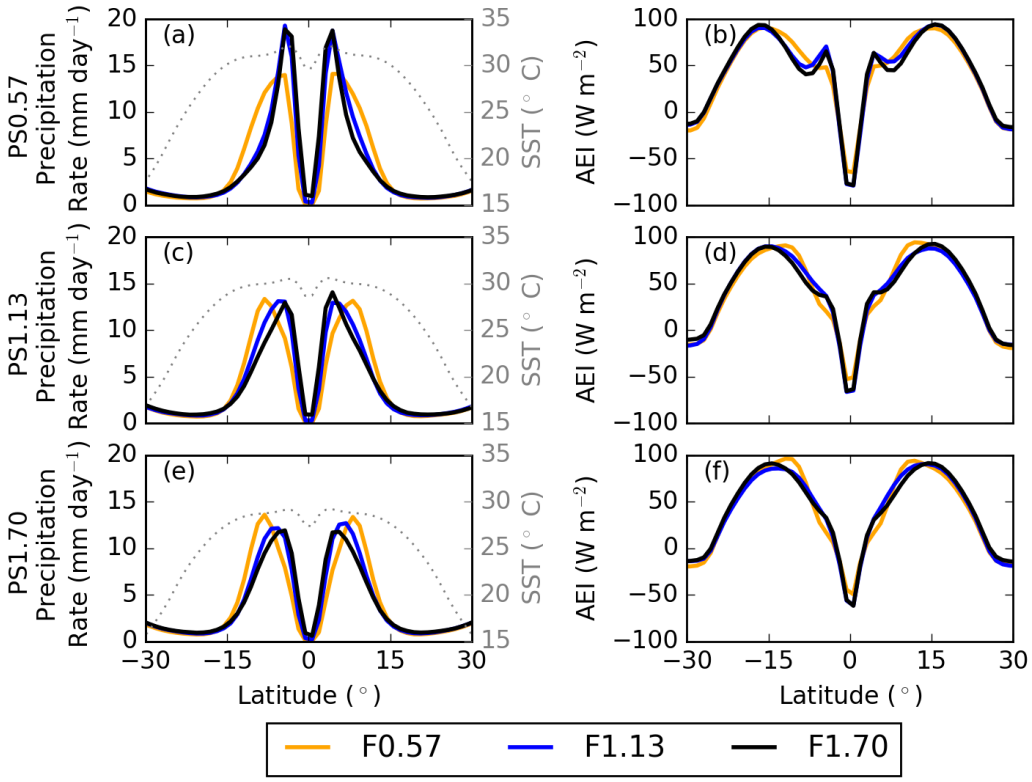

Figure 6.16: *Zonal-mean, time-mean (a), (c), (e) precipitation rates (solid lines, mm day^{-1}) and prescribed SSTs (grey dotted, °C), and (b), (d), (f) AEI (W m^{-2}) in PS0.57, PS1.13 and PS1.70 simulations respectively. Orange, blue and black lines denote f_{dp} equals 0.57, 1.13 and 1.70 respectively.*

the Hadley circulation and the local maximum in mass meridional streamfunction. Both diagnostics are interpolated to a 0.1° grid. Increasing f_{dp} from 0.57 to 1.70 contracts the ITCZ equatorward for all prescribed-SST profiles (Figs. 6.16a,c,e and 6.18b). However, under PS0.57 the equatorward ITCZ contraction is accompanied by increased maximum precipitation (Fig. 6.16a). The same ITCZ response in PS0.57 simulations to increased f_{dp} is seen on the equator when using Qobs (Fig. 4.1a). Due to the closer proximity of the ITCZ to the SST maximum in F0.57PS0.57 compared to F0.57PS1.13 and F0.57PS1.70 (yellow lines in Figs. 6.16a,c,e), the ITCZ reaches the latitude of SST maximum at a lower f_{dp} under PS0.57. As a result, the ITCZ cannot contract equatorward when increasing f_{dp} from 1.13 to 1.70 due to equatorial subsidence (Fig. 6.17). As the precipitation maxima are not collocated with the SST maxima for the range of f_{dp} used in PS1.13 and PS1.70 simulations (Fig. 6.16c,e); it is proposed that even larger f_{dp} is needed to simulate an ITCZ over the SST maxima for these SST profiles. In agreement with previous work (Hess et al., 1993; Bellon and Sobel, 2010; Mobis and Stevens, 2012), it is hypothesised that difference in ITCZ location is associated with a larger meridional SST gradient across the deep tropics ($\pm 10^\circ$ latitude) for PS0.57 than PS1.13 and PS1.70 (not shown). When using PS0.57 the minimum boundary-layer MSE needed for deep convection is achieved closer to the equator, resulting in a more equatorward ITCZ.

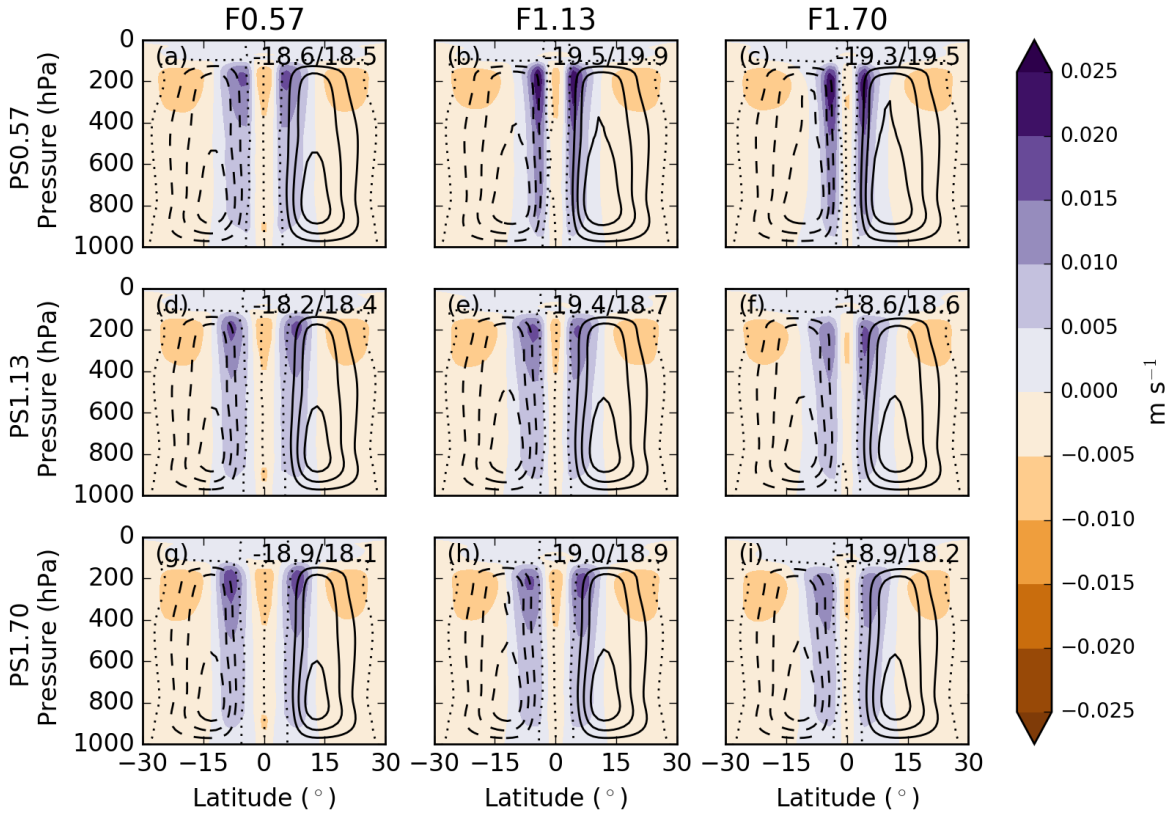

Figure 6.17: *Zonal-mean, time-mean mass meridional streamfunction (kg s^{-1}) (line contours) and vertical wind speed (m s^{-1}) (filled contours) for (a-c) PS0.57, (d-f) PS1.13 and (g-i) PS1.70 simulations. F0.57, F1.13 and F1.70 simulations are shown in the first, second and third columns respectively. Line contours are in intervals of 5 $\times$ 10^{10}, with dashed and dotted contours representing negative and zero values respectively. Positive streamfunction values indicate clockwise circulation. Maximum magnitude of the mass meridional streamfunction in the SH and NH is printed in the top right-hand corner of each panel.*

The sensitivity of the ITCZ intensity also depends on the prescribed SSTs (Figs. 6.16a,c,e and 6.18a). In PS0.57 simulations the sensitivity is similar to Qobs simulations (section 4.3); the ITCZ intensifies as f_{dp} increases (Figs. 6.16a and 6.18a), associated with the ITCZ narrowing and becoming collocated with the SST maxima when $f_{dp} \geq 1.13$. However in PS1.13 simulations, maximum precipitation remains similar for all values of f_{dp}, and in PS1.70 simulations, maximum precipitation decreases as f_{dp} increases (Figs. 6.16c,e and 6.18a). Regardless of prescribed SSTs, increasing f_{dp} reduces the tropical-mean latent heat flux (Fig. 6.19). Under PS1.13, reduced latent heat flux is associated with a narrower ITCZ and a similar ITCZ intensity for values of f_{dp} used (Fig. 6.18a,c). However under PS1.70, the sensitivity of the ITCZ width to f_{dp} is reduced, hence, the ITCZ intensity reduces to balance the latent heat flux decrease. The dependence of the sensitivity of the ITCZ intensity on prescribed SSTs is also seen in section 5.3; the solstitial ITCZ weakened (Fig. 5.2a) and the equatorial ITCZ intensified (Fig. 4.1a) with increased f_{dp}.

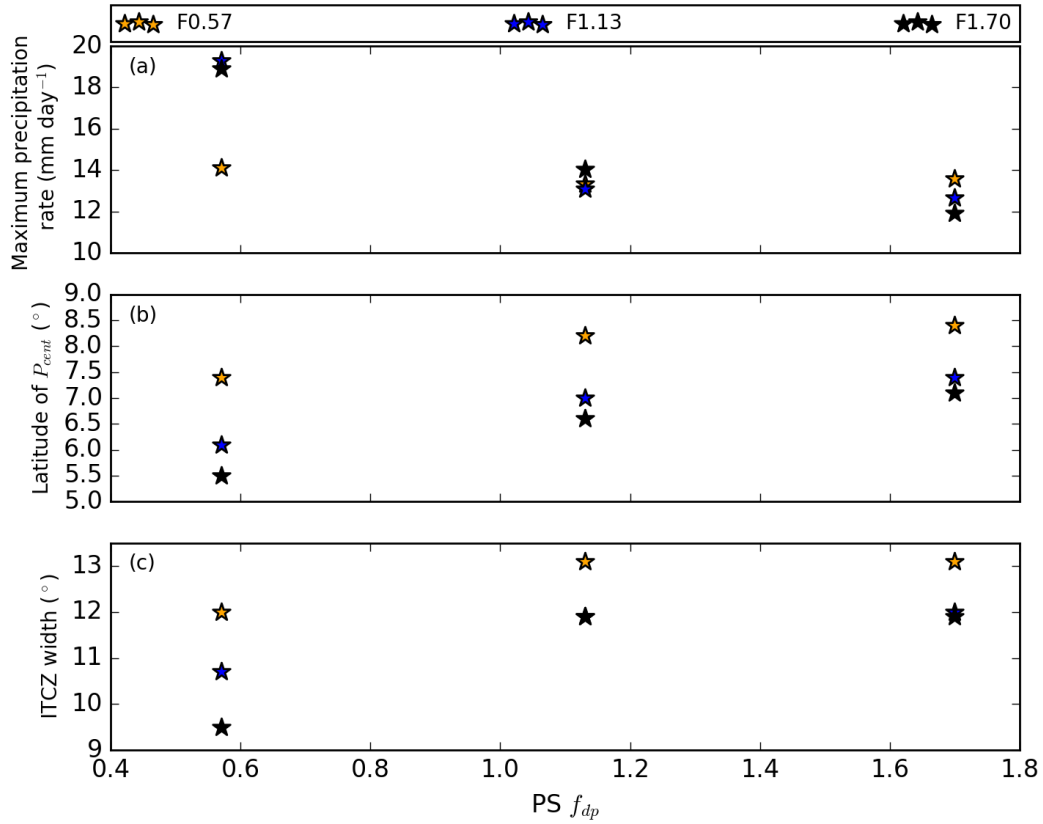

Figure 6.18: *Zonal-mean, time-mean (a) maximum precipitation rate (mm day^{-1}), (b) latitude of P_{cent} and (c) ITCZ width (°) in prescribed-SST simulations. Orange, blue and black stars denote simulations where f_{dp} equals 0.57, 1.13 and 1.70. The x-axis corresponds to the f_{dp} value used in the coupled simulation in which the prescribed SSTs are taken from. In (c) when PS1.13 is used, F1.13 and F1.70 are identical.*

As in chapters 4 and 5, the sensitivity of the ITCZ to f_{dp} in prescribed-SST simulations is explored using an AEI framework. Across the equatorial region the sensitivity of AEI to f_{dp} depends on cloudy-sky radiation and latent heat flux (Fig. 6.19). Decreased f_{dp} decreases equatorial cloudy-sky radiation (Fig. 6.19a,d,g). The reduced equatorial MSE input from cloud-radiation interactions is associated with reduced equatorial convection and a double ITCZ. However, AEI_0 does not reduce when decreasing f_{dp}, due to increased equatorial latent heat fluxes associated with a greater difference between the surface saturation humidity and the specific humidity at the lowest model level. Increased AEI_0 when decreasing f_{dp} is consistent with reduced equatorward AET at low latitudes (dotted yellow line in Fig. 6.21d).

Prescribed-SST simulations in this chapter illustrate two reasons why the AEI framework (section 2.2) should be used with caution to understand the tropical atmosphere. First, increased AEI_0 is not associated with an equatorward contraction of the double ITCZ for all prescribed-SST profiles (Fig. 6.16). For example, when decreasing f_{dp} under PS0.57, AEI_0 increases but the ITCZ shifts poleward. Increased AEI_0 is predominantly associated with latent heat fluxes (Fig. 6.19) and a drier equatorial lower atmosphere. Second, as in interactive-OET simulations (section 6.4), equatorward

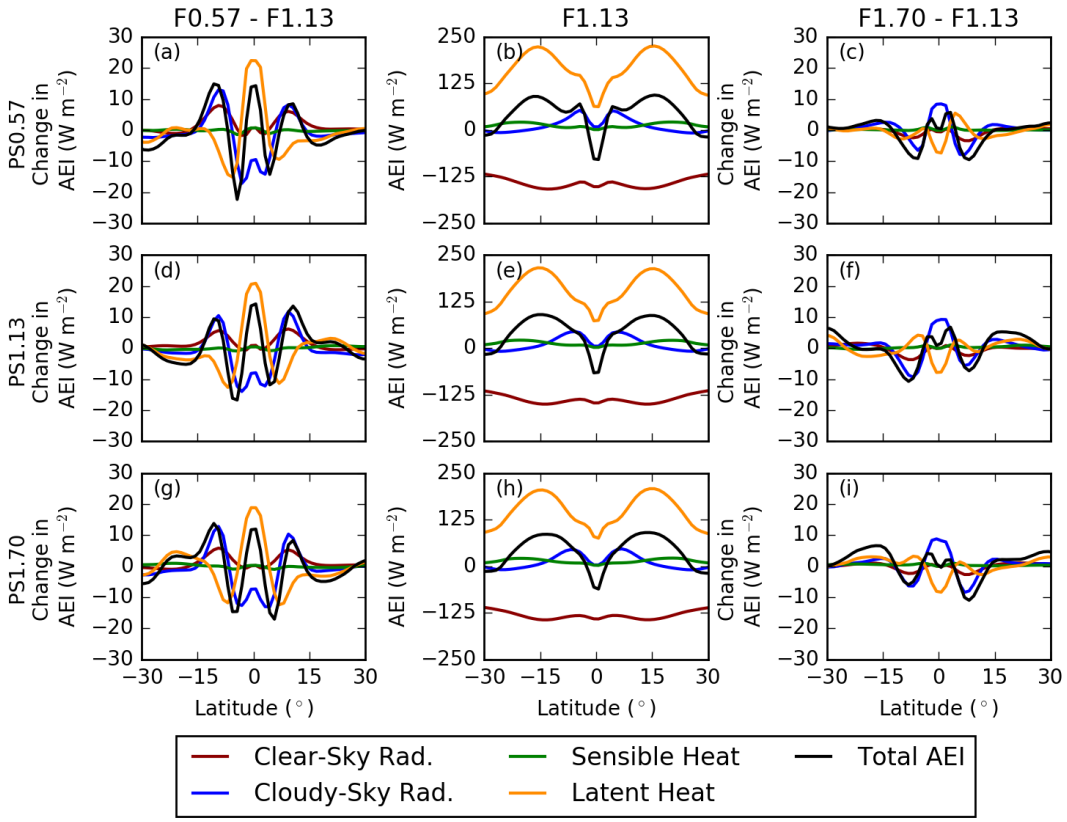

Figure 6.19: *Zonal-mean, time-mean AEI (W m^{-2}) budgets in (a-c) PS0.57 (d-f) PS1.13 and (g-i) PS1.70 simulations. Panels in first and third column show change in AEI components when changing f_{dp} to 0.57 and 1.70 respectively from 1.13. Panels in second column show F1.13 simulations. The red lines denote clear-sky radiation component; the cyan lines denote cloudy-sky radiation component. Green and orange lines denote sensible and latent heat fluxes respectively and black lines denote the total of all components.*

AET at low latitudes is predominantly achieved by eddies (Fig. 6.20b,e,h). Hence, it appears that the increased role of eddies in prescribed-SST simulations in this chapter and interactive-OET simulations (Fig. 6.20) are associated with the equatorial SST minimum and double ITCZ (Fig. 6.16a,c,e). As in interactive-OET simulations (section 6.4), it is proposed that the increased role of eddies in equatorward AET at low latitudes is associated with an equatorial minimum in specific humidity (not shown). Changes in MSE flux when changing f_{dp} are also predominantly associated with eddies. In prescribed-SST simulations with Qobs (section 4.3), MSE flux changes are associated with changes in both eddies and the mean circulation (Fig. 4.10).

Comparing the sensitivity of the ITCZ to f_{dp} in interactive-OET (section 6.4) and prescribed-SST simulations reveals that coupling changes the sensitivity of the ITCZ to f_{dp} (Figs. 6.21a and 6.22). Changes in ITCZ location and width when decreasing f_{dp} from 1.70 to 0.57 are greater in prescribed-SST simulations (Fig. 6.21a and 6.22b,c). However, whilst Figure 6.22a indicates that coupling increases the sensitivity of the ITCZ intensity to f_{dp} (Fig. 6.22a), it should be noted that ITCZ intensity changes are associated with the mean tropical SST (section 6.4). Atmosphere-ocean

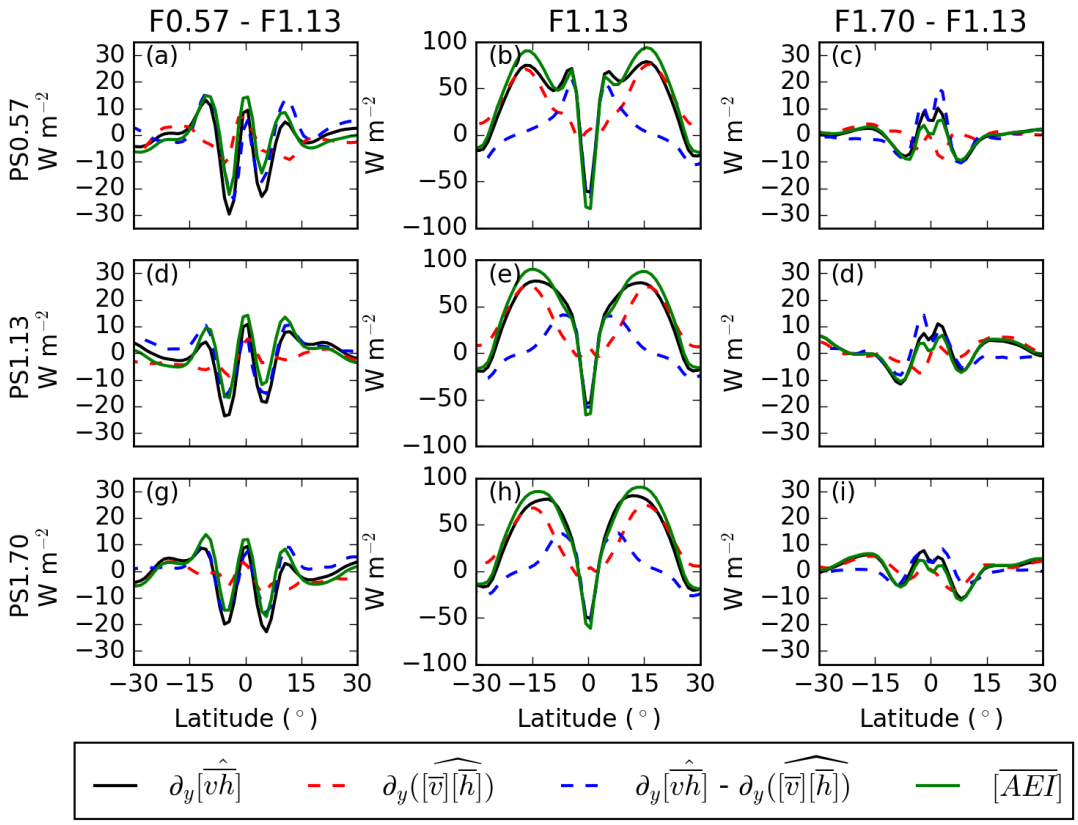

Figure 6.20: *Components of meridional divergence of atmospheric MSE flux and AEI (W m^{-2}) in prescribed-SST simulations. Solid black lines denote meridional divergence of total MSE flux ($\partial_y[\overline{v}\overline{h}]$), red dotted lines denote meridional divergence of MSE flux due to mean circulation ($\partial_y[\overline{v}][\overline{h}]$), blue dotted lines denote meridional divergence of MSE flux due to eddies ($\partial_y[\overline{v}\overline{h}] - \partial_y[\overline{v}][\overline{h}]$), solid green line denote zonal-mean, time-mean AEI. Panels in first and third columns show the change in energy transport components when changing f_{dp} to 0.57 and 1.70 respectively from 1.13. Panels in second column show F1.13 simulations.*

coupling decreases the sensitivity of AEI and AET across the equatorial and ITCZ region ($\leq$10° latitude; Fig. 6.21b,f), associated with a reduced response of cloudy-sky radiation and latent heat fluxes (Fig. 6.21d,e). Poleward of 10°, AEI changes when decreasing f_{dp} are greater in interactive-OET simulations due to changes in SST (Fig. 6.11c) and latent heat fluxes (Fig. 6.21e).

The reduced sensitivity of the ITCZ location to f_{dp} when coupling is associated with meridional SST gradient changes. Decreasing f_{dp} in interactive-OET simulations increases the meridional SST gradient between the tropical SST maximum and approximately $\pm$15° latitude (Fig. 6.11c) and promotes convection equatorward. Assuming that circulation changes are minimal when changing f_{dp} and the SST profile plays the dominant role in determining the boundary-layer MSE, an increased SST gradient increases the gradient of boundary-layer MSE. An increased gradient of boundary-layer MSE is associated with deep convection at lower latitudes as the minimum boundary-layer MSE required for deep convection is surpassed at a lower latitude. The reduced boundary-layer MSE required for deep convection when decreasing f_{dp} (chapter 4) is offset by changes in tropical SSTs.

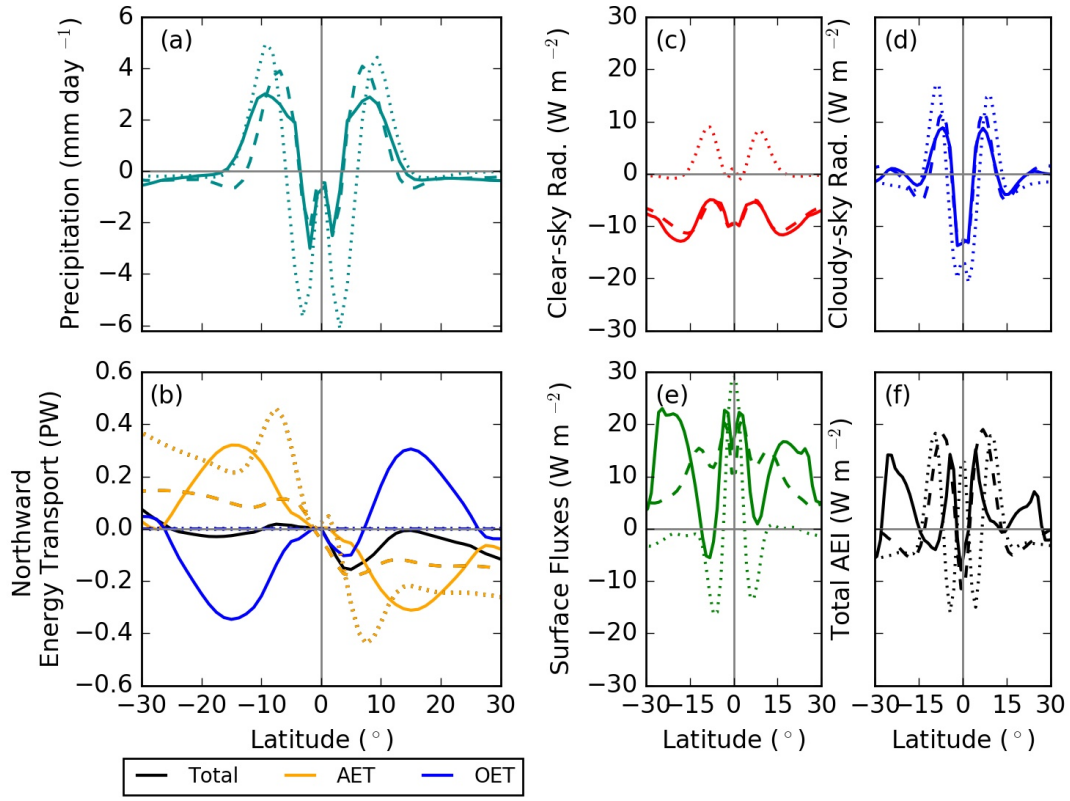

Figure 6.21: *Differences in (a) precipitation (mm day^{-1}), (b) total (black), atmospheric (yellow) and oceanic (blue) energy transports (PW), (c) clear-sky radiation AEI, (d) cloudy-sky radiation AEI, (e) surface fluxes AEI (including surface and latent heat fluxes) and (f) total AEI, when decreasing f_{dp} from 1.70 to 0.57. Solid lines denote interactive-OET simulations, dotted lines denote prescribed-SST simulations (PS1.13) and dashed lines denote prescribed-OET simulations. In (b) total energy transport change is only shown for coupled simulations. In (e) surface flux changes are predominantly associated with latent heat fluxes.*

To further investigate the change in ITCZ sensitivity to f_{dp} when coupling, changes in the vertical tropical temperature profile are analysed. It was first hypothesised that the reduced sensitivity of the ITCZ to f_{dp} when coupling was associated with changes in upper-tropospheric temperature. Decreasing f_{dp} increases the temperature difference between the upper- and lower-troposphere in interactive-OET simulations (Fig. 6.23), indicating increased atmospheric stability. However, changes in tropical temperature are predominantly associated with changes in the moist adiabat, hence, changes in atmospheric stability can not be inferred (Fig. 6.23). Whilst upper-tropospheric warming is stronger than changes in the moist adiabat, due to changes in cloud fraction at approximately 150 to 200hPa (Fig. 6.14b), similar changes are observed in prescribed-SST simulations. Therefore, it is unlikely that increased upper-tropospheric CRE when decreasing f_{dp} is responsible for the reduced sensitivity of the ITCZ to convective mixing when coupling.

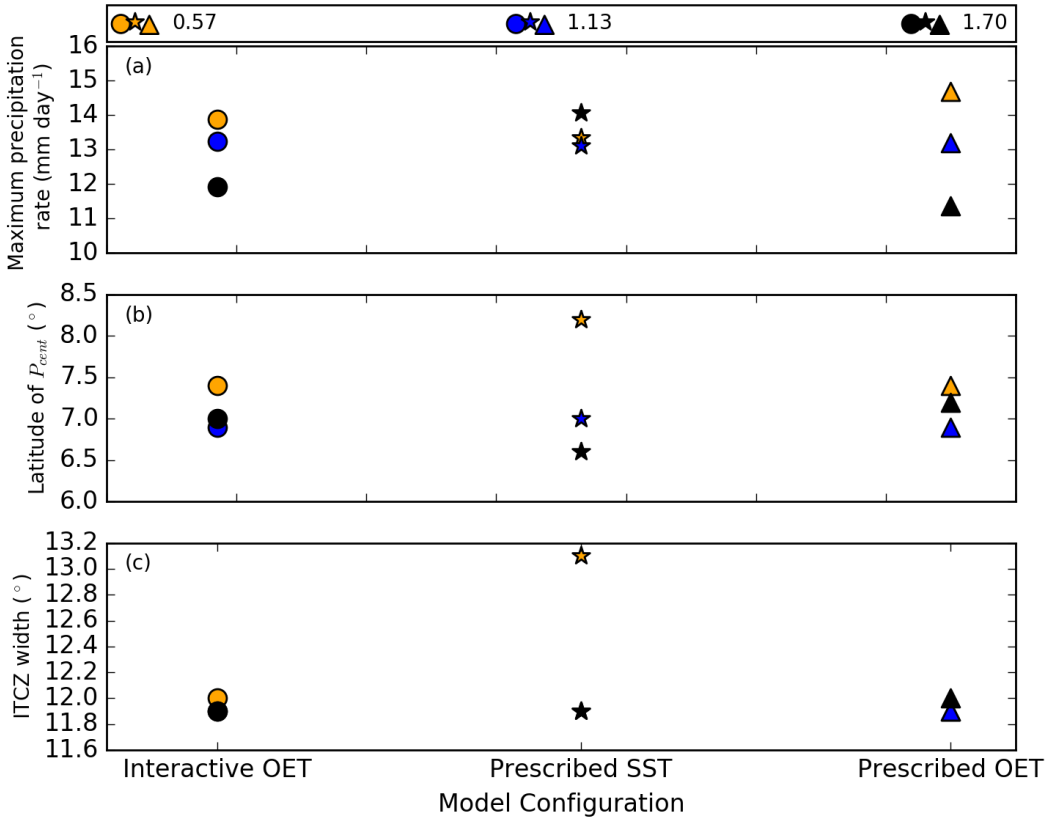

Figure 6.22: *Zonal-mean, time-mean (a) maximum precipitation rate (mm day^{-1}), (b) latitude of P_{cent} and (c) ITCZ width (°). Orange, blue and black symbols denote simulations where f_{dp} equals 0.57, 1.13 and 1.70 respectively. Circles, stars and triangles denote interactive-OET, prescribed-SST (PS1.13) and prescribed-OET simulations respectively. The ITCZ width (c) in interactive-OET and prescribed-SST simulations are identical when f_{dp} equals 1.13 and 1.70, whilst prescribed-OET simulations are identical when f_{dp} equals 0.57 and 1.13.*

6.5.2 *Sensitivity of the ITCZ to convective mixing with a prescribed ocean energy transport*

Previous research illustrates that interactive OET plays a substantial role in the reduced sensitivity of the ITCZ to hemispherically asymmetric forcing when coupling (Tomas et al., 2016; Hawcroft et al., 2017; Green and Marshall, 2017). To isolate the effect of interative OET in the reduced sensitivity of the ITCZ to f_{dp} when coupling, simulations with a prescribed Ekman-driven q-flux are analysed (prescribed-OET simulations, Table 6.1). The prescribed Ekman-driven q-flux is calculated using zonal-mean, time-mean values from C1.13; more details on prescribing the Ekman-driven q-flux can be found in section 6.2.3. Three simulations are performed (Table 6.1) with f_{dp} equal to 0.57 (C0.57PQ1.13), 1.13 (C1.13PQ1.13) and 1.70 (C1.70PQ1.13). C1.13 and C1.13PQ1.13 have a similar mean-state (comparing blue lines in Figs. 6.11 and 6.24), demonstrating that prescribing the time-mean Ekman-driven q-flux does not introduce substantial changes in the mean tropical atmosphere. Section 6.4 shows a substantial sensitivity of OEI to f_{dp} in interactive-OET simulations; therefore, it is hypothesised that prescribing the Ekman-driven q-flux will increase the sensitivity of

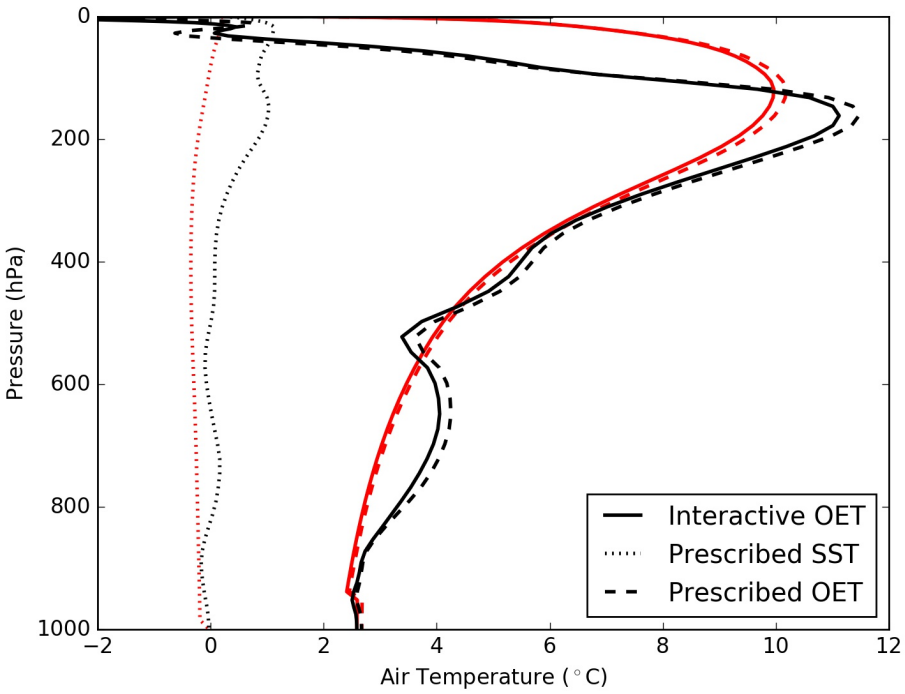

Figure 6.23: *Differences in air temperature (black) and temperature of parcel ascent (red, °C) in convective regions (precipitation is greater than 5 mm day^{-1}) when decreasing f_{dp} from 1.70 to 0.57. Solid lines denote interactive-OET simulations, dotted lines denote prescribed-SST simulations (PS1.13) and dashed lines denote prescribed-OET simulations. To compute the parcel ascent zonal-mean, time-mean surface temperature and specific humidity across convective regions (tropical [$\leq \pm 30°$ latitude] latitudes with precipitation greater than 5 mm day^{-1}) are used. The parcel follows the dry adiabat to lifting condensation level and then the moist adiabat.*

AEI and the ITCZ to f_{dp} due to a constrained OET and OEI.

As in interactive-OET and prescribed-SST simulations (Figs. 6.11a and 6.16a,c,e), all three prescribed-OET simulations produce a double ITCZ (Fig. 6.24a), negative AEI_0 (Fig. 6.24b), equatorial subsidence (Fig. 6.25), and an equatorward AET at low latitudes (Fig. 6.26). The prescribed Ekman-driven q-flux produces an equatorial SST minimum (Fig. 6.24c) associated with a equatorial minimum in boundary-layer MSE and convection. As in interactive-OET simulations (section 6.4), the mean circulation plays a minimal role in the equatorward AET across low latitudes (not shown). Latent energy transport associated with transient eddies plays the dominant role in equatorward AET at low latitudes.

As required at equilibrium, prescribing the Ekman-driven OET requires a constant OEI (Fig. 6.27). Decreasing f_{dp} reduces reflection of SW radiation by clouds (Fig. 6.14) and increases surface absorption of cloudy-sky radiation (Fig. 6.27g). As OEI is constrained by the prescribed Ekman-driven OET, other components of the net-downward surface energy flux respond to offset cloudy-sky radiation changes. Latent heat fluxes play the dominant role and increase across the

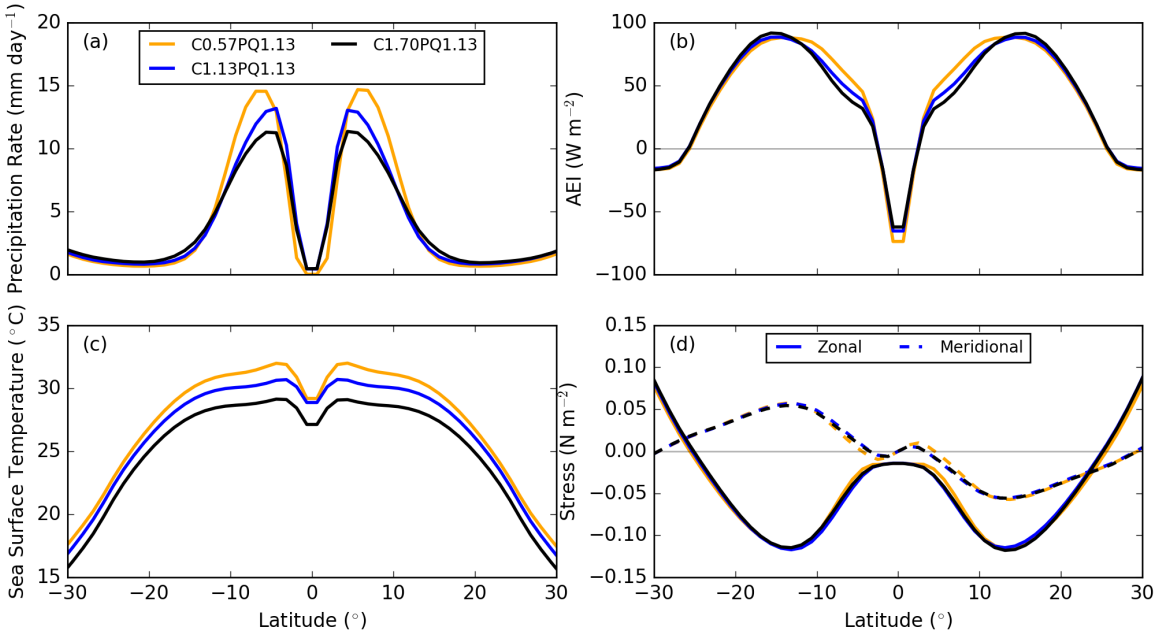

Figure 6.24: *Zonal-mean, time-mean tropical (a) precipitation (mm day^{-1}), (b) AEI (W m^{-2}), (c) SSTs (°C), and (d) zonal (solid) and meridional (dashed) wind stresses (N m^{-2}) in prescribed-OET simulations (Table 6.1).*

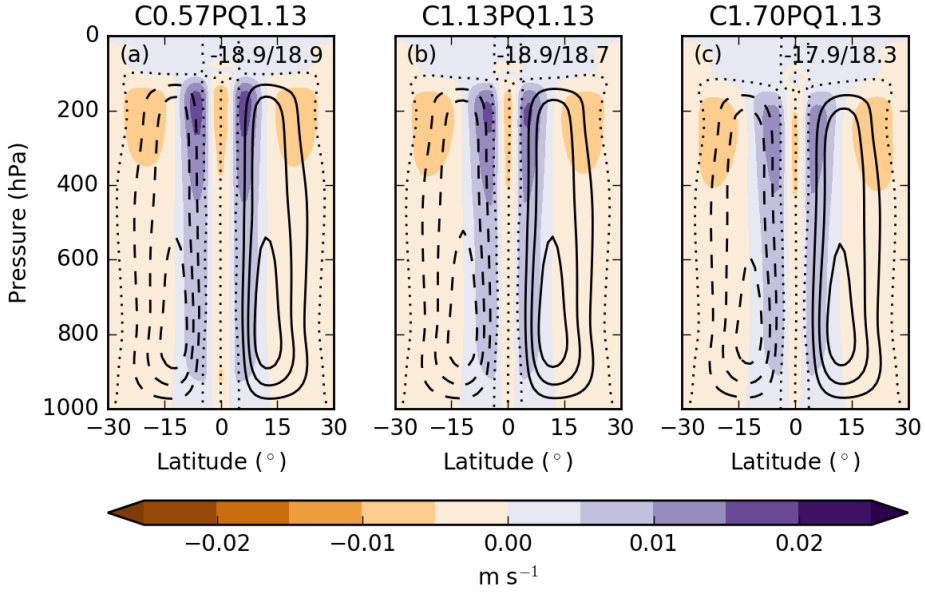

Figure 6.25: *Zonal-mean, time-mean mass meridional streamfunction (kg s^{-1}) (line contours) and vertical wind speed (m s^{-1}) (filled contours) for (a) C0.57PQ1.13, (b) C1.13PQ1.13 and (c) C1.70PQ1.13. Line contours are in intervals of 5 × 10^{10}, with dashed and dotted contours representing negative and zero values respectively. Positive streamfunction values indicate clockwise circulation. Maximum magnitude of the mass meridional streamfunction in the SH and NH is printed in the top right-hand corner of each panel.*

tropics (Fig. 6.27g). Comparing the sensitivity of energy budgets to f_{dp} between interactive-OET and prescribed-OET simulations (Figs. 6.13 and 6.27) reveals that prescribing OET increases the sensitivity of AEI to f_{dp} equatorward of 10° (Fig. 6.21f). For example, prescribed-OET simulations show a stronger decrease in AEI$_0$ by 5 W m^{-2} when decreasing f_{dp} from 1.70 to 0.57 (Fig. 6.21f). Across the ITCZ region, latent heat flux increases when decreasing f_{dp} are greater in prescribed-OET

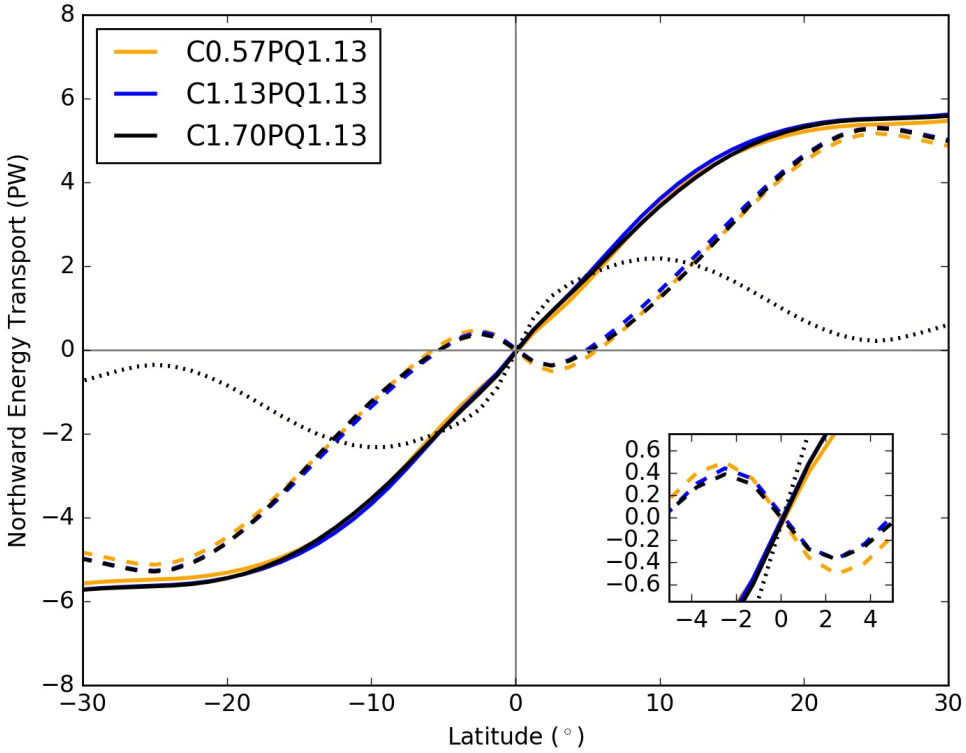

Figure 6.26: *Zonal-mean, time-mean total (solid), atmospheric (dashed) and oceanic (dotted) energy transports (PW) in C0.57PQ1.13 (orange), C1.13PQ1.13 (blue) and C1.70PQ1.13 (black). The inset on the bottom right zooms into the equatorial region.*

simulations than interactive-OET simulations (Figs. 6.21e). The sensitivity of the net-downward TOA flux to f_{dp} is similar in interactive-OET and prescribed-OET simulations (Figs. 6.13a,c and 6.27a,c); the change in sensitivity of AEI to f_{dp} when prescribing OET is not associated with net-downward TOA flux changes.

Prescribing OET increases the sensitivity of AEI to f_{dp} (Fig. 6.22f), therefore, a reduced sensitivity of the ITCZ to f_{dp} is expected in interactive-OET simulations compared to prescribed-OET simulations. However, the change in sensitivity depends on the chosen metric (Fig. 6.22). The sensitivity of the ITCZ location and width to f_{dp} are similar in interactive-OET and prescribed-OET simulations (Fig. 6.22b,c). Decreasing f_{dp} may decrease AEI_0 more in prescribed-OET simulations, which requires a more equatorward AET, but increased AET is predominantly achieved by eddies. Therefore, the ITCZ location does not change. Prescribing OET increases the sensitivity of ITCZ intensity to f_{dp} (Fig. 6.22a). Increased tropical latent heat fluxes when decreasing f_{dp} are greater in prescribed-OET simulations (Fig. 6.21e) as the increased surface absorption of cloudy-sky radiation (Fig. 6.27g) can not be partly offset by OET changes. Increased tropical latent heat fluxes intensify the ITCZ (Fig. 6.24). Whilst the apparent change in the sensitivity of the ITCZ to f_{dp} when prescribing the Ekman-driven OET depends on the chosen metric, prescribed-OET simulations reveal that the

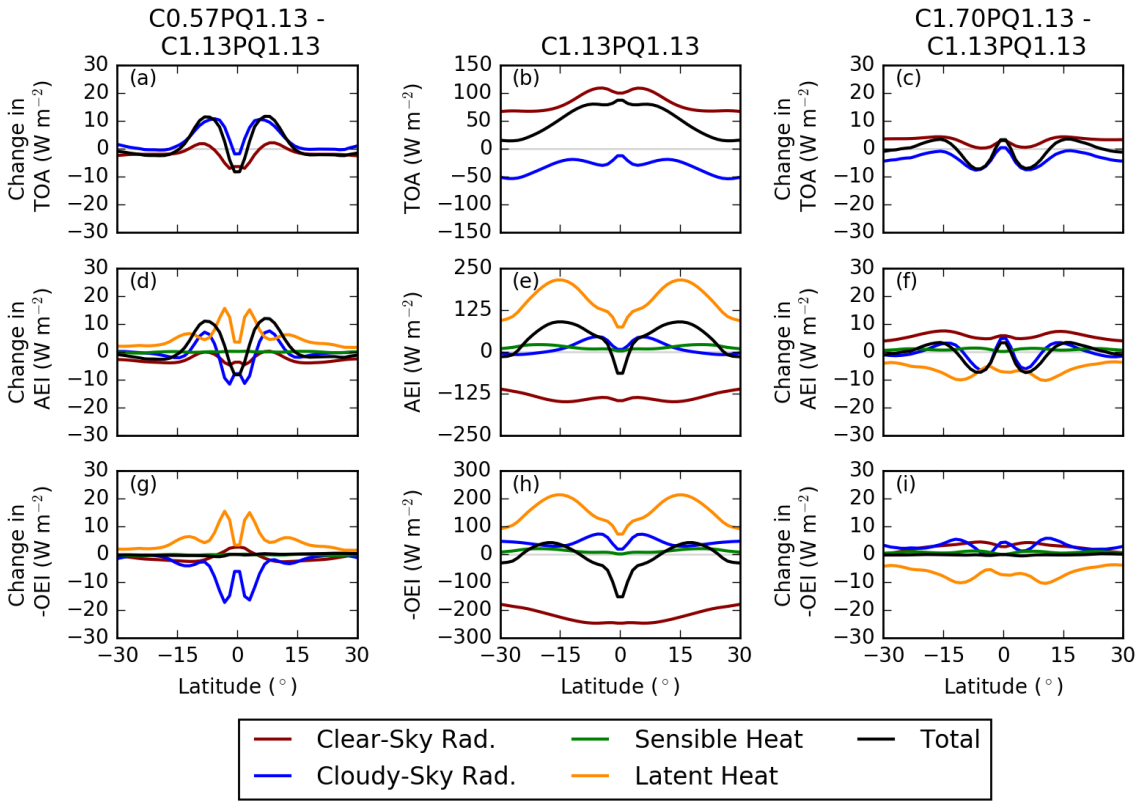

Figure 6.27: *Zonal-mean, time-mean components of (a-c) net-downward TOA flux (W m^{-2}) (d-f) AEI (W m^{-2}), (g-i) -OEI (W m^{-2}). Panels in first and second columns show the difference between C0.57PQ1.13 and C1.13PQ1.13, respectively, with C1.70PQ1.13. Panels in third column show observed values in C1.70PQ1.13. Red line is the clear-sky radiation component; blue line is the cloudy-sky radiation component. Green and orange lines are the sensible and latent heat flux (respectively) and black line is the total of all components.*

sensitivity of the ITCZ to a change in an atmospheric process or feedback cannot be assumed to be the same in a model configuration with interactive OET. Caution should be taken in interpreting sensitivities of the ITCZ in a model configuration without interactive OET.

6.6 Discussion

Coupling the atmosphere to an idealised two-layer ocean model with an interactive Ekman-driven OET simulates a double ITCZ for all convective mixing rates used. Ekman-driven oceanic upwelling reduces equatorial boundary-layer MSE and promotes a double ITCZ (Pike, 1971; Codron, 2012). It is hypothesised that a double ITCZ and negative AEI_0 would be simulated at any convective mixing rate due to small equatorial surface fluxes associated with the equatorial SST minimum. Coupling reduces the sensitivity of the ITCZ location and width to convective mixing and is an example of a reduced sensitivity of the ITCZ to an atmospheric process or forcing when coupling (Oueslati and Bellon, 2013; Tomas et al., 2016; Green and Marshall, 2017). Whilst previous studies argue that OET changes reduce the sensitivity of the ITCZ to hemispherically asymmetric forcing (i.e. Green and Marshall, 2017; Kang et al., 2018), here a reduced sensitivity of the ITCZ to convective mixing when coupling is due to interactive SSTs. Decreasing convective mixing increases tropical-mean SST and the meridional SST gradient across low latitudes. An increased meridional SST gradient promotes convection at lower latitudes (Fig. 2.6; Mobis and Stevens, 2012). The poleward ITCZ expansion associated with decreased convective mixing in prescribed-SST simulations (chapter 4) is offset by the effect of meridional SST gradient changes. It is hypothesised that the reduced sensitivity of the ITCZ to convective mixing when coupling in Oueslati and Bellon (2013, Fig. 2.9) is partly due SST changes. In this study coupled simulations reveal that sensitivities of the ITCZ to an atmospheric forcing or process in atmosphere-only simulations may not apply to the real world.

Coupling the atmosphere to an ocean with an interactive OET reduces the sensitivity of the ITCZ to hemispherically asymmetric forcing (Kay et al., 2016; Tomas et al., 2016; Green and Marshall, 2017; Hawcroft et al., 2017). In this study, an interactive OET has a minimal impact on the sensitivity of the ITCZ location and width to convective mixing; the reduced sensitivity associated with coupling is predominantly due to thermodynamic processes. The sensitivity of OET to convective mixing is small, hence, prescribing OET has a minimal impact on the ITCZ location and width. However, an interactive OET decreases the sensitivity of the ITCZ intensity to convective mixing. Prescribing OET constrains the total OEI at equilibrium. As a result, the increased latent heat flux associated with decreased convective mixing is larger when prescribing OET. Increased latent heat fluxes lead to an intensified ITCZ. The increased sensitivity of the ITCZ intensity to convective mixing in prescribed-OET simulations highlights that caution should be taken when using prescribed-OET simulations to understand the sensitivity of the real-world ITCZ to modified atmospheric forcings or processes.

The AEI framework (section 2.2; Kang et al., 2008; Bischoff and Schneider, 2014, 2016) breaks down

when applied to simulations in this chapter. It cannot be used to explain the sensitivity of the ITCZ to convective mixing in interactive-OET simulations, nor the reduced sensitivity when coupling. Whilst in all experiments a double ITCZ and negative AEI_0 is diagnosed, in agreement with Bischoff and Schneider (2016), equatorward AET is achieved by transient eddies transporting latent energy, not by the mean circulation. As the mean circulation plays a minimal role in equatorward AET, the AEI framework is not useful at diagnosing the ITCZ location. For example, in prescribed-SST simulations decreased convective mixing increases AEI_0 (Table 6.3), typically associated with an equatorward contraction of the double ITCZ (Bischoff and Schneider, 2016). However, the ITCZ expands poleward and changes in the diagnosed energy flux equator are negligible (Table 6.3). Future work to understand the double ITCZ bias in GCMs (section 1.2) and real world ITCZ characteristics must consider the AET by eddies.

Table 6.3: *$[\overline{AEI}]_0$ ($W\ m^{-2}$), location of P_{cent} ($^\circ$) and approximate energy flux equator (δ, $^\circ$) using equation 2.13 or 2.15 in each simulation.*

Simulation	$[\overline{AEI}]_0$ (W m^{-2})	P_{cent} ($^\circ$)	Energy Flux Equator (δ) location ($^\circ$)
C0.57	-65.2	7.4	4.2/-4.2
C1.13	-65.7	6.9	4.3/-4.2
C1.70	-59.4	7.0	4.2/-4.4
F0.57PS1.13	-51.7	8.2	4.4/-4.1
F1.13PS1.13	-65.6	7.0	4.3/-4.3
F1.70PS1.13	-64.4	6.6	4.3/-4.0
C0.57PQ1.13	-73.6	7.4	4.3/-4.3
C1.13PQ1.13	-65.3	6.9	4.2/-4.3
C1.70PQ1.13	-62.1	7.2	4.3/-4.3

The conclusions reached in this chapter depend on the design of the two-layer ocean model. Prescribed SST simulations reveal that the sensitivity of the ITCZ to convective mixing depends on SSTs (sections 5.3 and 6.5). Hence, any change in model design that affects SST may change the sensitivity of the ITCZ to convective mixing. Changes in model design that may affect SST include: changes in prescribed OET; introducing zonal asymmetries in SST and surface fluxes; inserting continental land; changing the point in the spin-up simulation where an energy correction is applied; and changing the latitude where the Coriolis parameter is fixed.

Changing the extra-tropical q-flux in interactive-OET simulations will change SSTs and hence change the sensitivity of SSTs and the ITCZ to convective mixing. For example, the tropical meridional SST gradient might weaken if the prescribed extratropical OET (Fig. 6.2) were expanded equatorward or a prescribed OET were imposed from the equator to the subtropics. A reduced meridional tropical SST gradient would promote convection at higher latitudes (section 6.5; Mobis and Stevens, 2012). The response of SSTs and the ITCZ to prescribed extra-tropical q-flux changes

depends on the Ekman-driven OET and surface energy fluxes; further investigation is required to understand the sensitivity of the ITCZ to the prescribed OET.

The design of an axisymmetric ocean model removes zonal SST asymmetries. A zonally symmetric SST is consistent with prescribed SSTs in previous atmosphere-only simulations (chapters 4 and 5). As the sensitivity of the ITCZ to convective mixing in CNRM-CM5 varies zonally (Oueslati and Bellon, 2013) and introducing zonal SST asymmetries in an aquaplanet varies the structure and intensity of the ITCZ in a zonal direction (Neale and Hoskins, 2001; Nakajima et al., 2013), it is hypothesised that zonal SST asymmetries will change the sensitivity of the ITCZ to convective mixing. In the real world zonally-varying tropical SSTs affect the ITCZ and the influence of Ekman-driven upwelling on SSTs. For example, over the Pacific Ocean easterly trade winds develop SST gradients between the West and East Pacific (Bjerknes, 1969). Zonal tropical SST variations change the tropical rainfall structure (Dai, 2006), the influence of Ekman-driven upwelling, and the sensitivity of tropical rainfall to atmospheric forcing and parameterisation (Oueslati and Bellon, 2013; Tomas et al., 2016; Hawcroft et al., 2017). GCM experiments in this chapter have also disregarded zonal and meridional surface temperature asymmetries associated with land. Real world continental land and topography will lead to asymmetries in surface properties and affect both the mean-state and zonal variations of ITCZ characteristics. Codron (2012) performed GCM experiments with continental land and the atmosphere coupled a two-layer ocean model that resolves the Ekman-driven OET. Introducing land resulted in zonal variations in ITCZ characteristics and changes the mean state (Codron, 2012).

The position chosen in the spin-up simulation at which a constant energy flux correction is applied ensures realistic SSTs. Previous GCM experiments that couple the atmosphere to an ocean model that resolves the Ekman-driven OET equilibrate to SSTs warmer than observations (Codron, 2012; Kang et al., 2018). However, a change in sensitivity of the ITCZ to convective mixing may be simulated if a different time position was chosen. For example, if the energy flux correction was applied at a later time, warmer SSTs and an intensified ITCZ would be simulated and may be associated with a changed sensitivity of the ITCZ to convective mixing.

To ensure the computed meridional Ekman-driven current in the mixed ocean layer (6.1) is not unrealistically large across the equatorial region, f at 2.5° latitude is used for latitudes smaller than 2.5°. The simulated Ekman-driven ocean circulation depends on the chosen Coriolis parameter across low latitudes (Codron, 2012). Changes in the latitude at which f becomes fixed is hypothesised to change the mean state climate and the sensitivity of the ITCZ to convective mixing. However, hypothesising the ITCZ response is challenging. For example, whilst increasing the latitude at which f becomes

fixed weakens the Ekman-driven upwelling (Codron, 2012), reducing cooling temperature tendencies at the equator and promoting equatorial atmospheric convection, the region of Ekman-driven upwelling and minimum tropical SST will also broaden, shifting the ITCZ to higher tropical latitudes.

Increasing ocean model complexity is also likely to change the sensitivity of the ITCZ to convective mixing. For example, coupling the atmosphere to a global ocean GCM, such as NEMO (Nucleus for European Modelling of the Ocean; Madec et al., 2017), will increase the number of factors controlling OET. In a full ocean GCM, a thermally-direct ocean circulation affects the tropical OET (Tomas et al., 2016; Green and Marshall, 2017). Tomas et al. (2016) find a reduced sensitivity of the ITCZ to projected Arctic sea ice conditions due to OET changes associated with the thermally-direct circulation. It remains to be answered whether changes in OET associated with the thermally-direct circulation affect the sensitivity of the ITCZ to convective mixing. Increased horizontal ocean resolution will introduce an OET associated with mesoscale eddies (Iovino et al., 2016). The effect of mesoscale eddies is often parameterised in ocean model. Here, the effect of mesoscale eddies on OET has only been considered in the prescribed extra-tropical q-flux. The contributions of OET by mesoscale eddies and the thermally-direct circulation will affect the sensitivity of the ITCZ to convective mixing. Increasing ocean model vertical resolution reduces the influence of Ekman-driven upwelling on equatorial SSTs (Iovino et al., 2016; Green and Marshall, 2017) and will likely change the sensitivity of the ITCZ to convective mixing.

This study has investigated the impact of atmosphere-ocean coupling on the sensitivity of the ITCZ to convective mixing when using hemispherically symmetric boundary conditions. Hemispherically symmetric boundary conditions simulate a symmetric ITCZ centered on the equator (chapter 4; Neale and Hoskins, 2001; Codron, 2012; Mobis and Stevens, 2012). As discussed in chapter 5, the ITCZ response to hemispherically asymmetric boundary conditions affects the sensitivity of the ITCZ to convective mixing. Therefore, further work is required to investigate whether the effect of coupling on the sensitivity of the ITCZ to convective mixing depends on the boundary conditions. Several techniques could be used to impose a hemispherically asymmetric ITCZ, including imposing a cross-equatorial OET (Kang et al., 2008; Bischoff and Schneider, 2014; Voigt et al., 2016; Kang et al., 2018) or introducing a hemispherically asymmetric surface albedo (Voigt et al., 2014; Green and Marshall, 2017). Whilst Green and Marshall (2017) and Kang et al. (2018) reveal that an interactive OET reduces the meridional ITCZ shift associated with a hemispherically asymmetric surface albedo or a cross-equatorial OET, hemispherically asymmetric forcing can still lead to an off-equatorial ITCZ. As the influence of Ekman-driven upwelling on SSTs is minimal in Green and Marshall (2017) and not considered in Kang et al. (2018), the sensitivity of the ITCZ to hemispherically asymmetric boundary conditions in a coupled model where Ekman-driven upwelling

affects SST remains to be answered. Prescribing a cross-equatorial OET may shift the ITCZ poleward and promote a single ITCZ. However, shifting the ITCZ poleward also shifts the location of Ekman-driven SST cooling (Schneider, 2018), which may damp the ITCZ shift. Alongside changes in tropical Ekman-driven OET, changes in the prescribed extra-tropical q-flux also need to be considered if prescribing a hemispherically asymmetric boundary forcing; previous studies illustate a seasonal cycle of extratropical OET in the real world (Fasullo and Trenberth, 2008).

Coupling the atmosphere to an ocean model with an interactive OET is hypothesised to reduce the simulated sensitivity of the ITCZ to insolation in prescribed-OET slab ocean simulations (Merlis et al., 2013; Wei and Bordoni, 2018; Voigt et al., 2016). An interactive OET enables OET changes and reduces the cross-equatorial AET and ITCZ shift associated with hemispherically asymmetric boundary conditions (Green and Marshall, 2017). Shifting the ITCZ poleward also shifts the region of Ekman-driven upwelling (Schneider, 2018) and is associated with an intensified cross-equatorial Hadley circulation (chapter 5). Both will warm SSTs equatorward of the ITCZ, hence, the ITCZ will be favoured towards the equator. Codron (2012) apply a seasonal cycle of insolation in an aquaplanet model with an Ekman-driven OET. Equatorial Ekman-driven upwelling prevents an equatorial ITCZ and the ITCZ jumps from one hemisphere to another (Codron, 2012). Interestingly, even though a hemispherically symmetric seasonal cycle of insolation is applied, SH precipitation is greater than NH precipitation (Codron, 2012). Further investigation is required to understand the hemispherically asymmetric ITCZ when applying a seasonal cycle of insolation.

Understanding what controls ITCZ characteristics remains a fundamental question in climate science (Bony et al., 2015) and has motivated several model intercomparison projects including prescribed-SST aquaplanet simulations in CMIP5 (Voigt and Shaw, 2015) and TRACMIP (Tropical Rain belts with an Annual cycle and a Continent), aquaplanet simulations coupled to a slab ocean with a prescribed q-flux (Voigt et al., 2016). As previous studies reveal that an interactive OET reduces the sensitivity of the ITCZ to atmospheric forcing or parameterisation (Tomas et al., 2016; Green and Marshall, 2017), an idealised model intercomparison project with an interactive OET is planned in the foreseeable future (Kucharski et al., 2018). The model intercomparison project will investigate whether interactive OET changes the inter-model variability of tropical circulation. Here it is shown that an interactive OET does not substantially change the sensitivity of the ITCZ to convective mixing (section 6.5), therefore, it is hypothesised that the effect of an interactive OET on the inter-model variability will be minimal. However, the effect of interactive OET will depend on the ocean model design; here, the model design favours a double ITCZ. Further idealised experiments are required before commencing a model intercomparison project in an aquaplanet configuration with an interactive OET.

6.7 Conclusions

Work in chapters 4 and 5 illustrate a sensitivity of the ITCZ to convective mixing in prescribed-SST simulations. However, not only are prescribed SSTs energetically inconsistent, but several studies reveal that coupling the atmosphere to an ocean model with an interactive ocean energy transport reduces the sensitivity of the ITCZ to hemispherically asymmetric forcing (i.e. Green and Marshall, 2017; Kang et al., 2018) and convective mixing (Oueslati and Bellon, 2013). In this chapter an idealised coupled modelling framework is developed to quantify the effect of coupling on the sensitivity of the ITCZ to convective mixing.

Coupling the atmosphere to an ocean model that resolves the Ekman-driven ocean energy transport promotes a double ITCZ. Ekman-driven equatorial upwelling leads to an equatorial SST minimum, decreased equatorial boundary-layer MSE, and reduced equatorial convection. Previously, a double ITCZ and negative equatorial atmospheric energy input were associated with equatorward energy transport at low latitudes by the mean circulation (chapter 4 and Bischoff and Schneider, 2016). However in coupled simulations in this study, transient eddies transporting latent energy predominantly accomplish the equatorward atmospheric energy transport associated with a double ITCZ. The substantial role of eddies is associated with SSTs and the meridional gradient in specific humidity. As the mean circulation plays a minimal role in changes in equatorward atmospheric energy transport when changing convective mixing, the AEI framework (Kang et al., 2008; Bischoff and Schneider, 2014, 2016) breaks down.

Atmosphere-ocean coupling reduces the sensitivity of the ITCZ to convective mixing. The reduced sensitivity is predominantly associated with meridional SST profile changes; the sensitivity of ocean energy transport to convective mixing is minimal. Decreased convective mixing increases the meridional SST gradient in the deep tropics ($\pm 10^\circ$ latitude), associated with reduced off-equatorial boundary-layer MSE and a more equatorward latitude at which deep convection is initiated. The promotion of equatorial convection when decreasing convective mixing in coupled simulations offsets the favouring of off-equatorial convection seen in prescribed-SST simulations associated with a reduced boundary-layer moist static energy required for deep convection (chapters 4 and 5). The reduced ITCZ response to convective mixing in coupled simulations reveals the importance of SST feedbacks in determining ITCZ characteristics. Sensitivities of the ITCZ to an atmospheric process or forcing in prescribed-SST experiments may not hold in atmosphere-ocean coupled simulations or the real world.

Chapter 7

Conclusions

To improve understanding of the mechanisms that control ITCZ characteristics the sensitivity of the ITCZ to convective mixing is analysed in an aquaplanet modelling configuration (chapters 4 to 6). In this chapter section 7.1 reviews key conclusions from this thesis with respect to the thesis objectives (section 1.3). Section 7.2 discusses the implications of the presented research, and section 7.3 ends the chapter with limitations of the work performed and possible approaches for future research.

7.1 Key findings

The first objective of this thesis is "to understand the mechanisms responsible for the sensitivity of the ITCZ to convective mixing" (section 1.3). Previous studies show the ITCZ is sensitive to convective mixing in atmosphere-only and coupled GCMs with topography and land (Terray, 1998; Oueslati and Bellon, 2013; Bush et al., 2015), yet these studies did not identify the key mechanisms responsible for this sensitivity. A greater insight into these mechanisms is gained through investigating the sensitivity of the ITCZ to convective mixing in an atmosphere-only prescribed-SST aquaplanet configuration (section 4.3). Prescribed-SST aquaplanet simulations show the ITCZ is sensitive to convective mixing (chapters 4 and 5). Decreasing convective mixing reduces the minimum boundary-layer MSE required for deep convection which favours off-equatorial convection, decreases equatorward moisture flux at low latitudes, and promotes a double ITCZ (section 4.3). This proposed mechanism supports previous research that emphasises the substantial role of boundary-layer MSE in determining the ITCZ location (Liu et al., 2010; Mobis and Stevens, 2012).

The second objective of this thesis is "to isolate the role of cloud-radiation interactions in the

sensitivity of the ITCZ to convective mixing" (section 1.3). This thesis is the first study to investigate the role of cloud-radiation interactions in the sensitivity of the ITCZ to convective mixing. The AEI framework was initially used to isolate the role of cloud-radiation interactions. Previous studies emphasise that ITCZ characteristics are determined by the meridional AEI profile (Kang et al., 2008; Bischoff and Schneider, 2014). For example, a single ITCZ is associated with a positive equatorial AEI whilst a double ITCZ is associated with a negative equatorial AEI (Bischoff and Schneider, 2016). Section 4.3 shows that the sensitivity of AEI to convective mixing is predominantly associated with cloudy-sky radiation, hence CRE plays a substantial role in the sensitivity of the ITCZ to convective mixing. The AEI framework also reveals that cloud-radiation interactions maintain the single ITCZ at high convective mixing rates; without cloudy-sky radiation the equatorial AEI would be negative and a double ITCZ would form.

To further investigate the role of cloud-radiation interactions in the sensitivity of the ITCZ to convective mixing two sets of prescribed-SST simulations are performed (section 4.4): (1) with CRE removed; (2) with a prescribed meridionally-, diurnally-varying CRE. In agreement with Harrop and Hartmann (2016), removing CRE cools the upper-troposphere due to reduced longwave radiation absorption, associated with reduced atmospheric stability and a decreased boundary-layer MSE required for deep convection. Removing CRE therefore promotes off-equatorial convection and a double ITCZ. Removing CRE reduces the sensitivity of the ITCZ to convective mixing, however quantifying the precise reduction depends on the chosen metric and range of convective mixing rates. The ITCZ response to removing CRE (section 4.4) and the sensitivity of the ITCZ to convective mixing (section 4.3) shows that processes that modify the boundary-layer MSE and free-tropospheric temperature play a role in determining tropical circulation characteristics. Prescribing CRE reduces the sensitivity of the ITCZ to convective mixing by approximately 50%. The prescribed CRE acts as a fixed MSE source; where the prescribed CRE is substantial, deep convection is favoured due to CRE heating. Applying the AEI framework to simulations with CRE prescribed, reveals that CRE plays a substantial role in determining tropical circulation characteristics. However, the ITCZ remains sensitive to convective mixing without interactive CRE; this sensitivity is predominantly associated with surface-flux feedbacks. The importance of surface fluxes for tropical circulation characteristics is also emphasised in Numaguti (1995) and Mobis and Stevens (2012), where prescribing the surface wind in the computation of surface fluxes reduces the sensitivity of the ITCZ to the representation of convection.

The third objective of this thesis is "to determine the importance of the boundary conditions on the sensitivity of the ITCZ to convective mixing" (section 1.3). A similar role of the boundary-layer MSE in determining the ITCZ structure is observed when comparing the sensitivity of the ITCZ to

convective mixing in aquaplanets with equinoctial and solstitial boundary conditions (section 5.3). However, the manifestation of this sensitivity depends on the chosen boundary conditions due to mean-state differences. For example, in solstitial simulations the ITCZ remains equatorward of the SST maximum for all convective mixing rates, whilst in equinoctial simulations, the ITCZ lies at the equator (over the SST maximum) at high convective mixing. As a result, increasing convective mixing shifts the solstitial ITCZ towards the SST maximum for all convective mixing rates, whilst in equinoctial simulations the ITCZ remains at the equator. Quantifying the difference in sensitivity between equinoctial and solstitial simulations is challenging as it depends on the chosen metric and range of convective mixing rates.

The sensitivity of the mean state to the boundary conditions affects not only the sensitivity of the ITCZ to convective mixing but also the role of CRE (section 5.3). The intensified cross-equatorial overturning circulation associated with solstitial boundary conditions (section 5.4) increases latent heat fluxes due to stronger winds over the warmest SSTs. Using solstitial boundary conditions increases the sensitivity of the latent heat flux to convective mixing. Therefore, whilst the sensitivity of cloudy-sky radiation to convective mixing remains similar for both sets of boundary conditions, the increased sensitivity of the latent heat flux reduces the role of CRE. Due to the important role of cloud-radiation interactions in the sensitivity of the ITCZ to convective mixing (sections 4.4 and 5.3), the role of CRE in the sensitivity of the ITCZ to hemispherically asymmetric boundary conditions was also investigated (section 5.4). Prescribing CRE with cloud-radiation interactions from equinoctial simulations reduces the sensitivity of the ITCZ location to hemispherically asymmetric boundary conditions by approximately 20%. The reduced ITCZ shift is associated with a reduced hemispheric AEI asymmetry and an increased likelihood of deep convection in regions of substantial CRE.

The final objective of this thesis is to "quantify the effect of atmosphere-ocean coupling on the sensitivity of the ITCZ to convective mixing" (section 1.3) as previous studies show that coupling reduces the sensitivity of the ITCZ to an atmospheric parameterisation or forcing (Oueslati and Bellon, 2013; Green and Marshall, 2017). To investigate the effect of coupling, an idealised two-layer ocean model with an Ekman-driven OET is developed (section 6.2). Upon coupling Ekman-driven upwelling cools equatorial SSTs, decreasing equatorial boundary-layer MSE and promoting a double ITCZ (section 6.3). A minimal sensitivity of the ITCZ location to convective mixing is concluded in coupled simulations (section 6.4). Although, decreasing convective mixing broadens and intensifies the ITCZ. Similar to the argument proposed for the sensitivity of the ITCZ location to convective mixing in atmosphere-only prescribed-SST simulations (sections 4.3 and 5.3), it is hypothesised that decreasing convective mixing reduces the minimum boundary-layer MSE required for deep convection, thereby promoting convection over cooler SSTs and broadening the ITCZ. However,

the MSE argument cannot explain the intensified ITCZ when decreasing convective mixing. The intensification of the ITCZ is associated with warmer tropical SSTs. Decreased convective mixing increases surface absorption of shortwave radiation due to reduced mid-tropospheric cloud cover, associated with increased tropical SSTs and latent heat fluxes.

Due to substantial mean-state differences between coupled and atmosphere-only "Qobs" simulations (section 6.3), prescribed-SST simulations with SSTs from the coupled experiments are performed (section 6.5). Comparing coupled and prescribed-SST simulations reveals that coupling substantially changes the sensitivity of the ITCZ to convective mixing (section 6.5). However, the precise value of the sensitivity change depends on the chosen metric. For example, coupling substantially reduces the sensitivity of the ITCZ location and width, whilst increasing the sensitivity of the ITCZ intensity. To partition the impact of coupling into the effect of interactive SSTs and interactive OET, prescribed-OET simulations are employed. An interactive OET has a minimal effect on the sensitivity of the ITCZ location and width to convective mixing due to small OET changes when changing convective mixing; the reduced sensitivity when coupling is predominately due to interactive SSTs. However, prescribing OET increases the sensitivity of the ITCZ intensity to convective mixing. Prescribing OET fixes the total net-downward surface energy flux, thereby constraining surface energy flux components. Decreased convective mixing increases surface absorption of shortwave radiation (section 6.4) which is offset by increased latent heat fluxes associated with an intensified ITCZ (section 6.5).

In this thesis two key deficiencies in the AEI framework (Kang et al., 2008; Bischoff and Schneider, 2016) are shown, highlighting that in some circumstances the AEI framework cannot be used to understand the mechanisms controlling the tropical circulation. First, the AEI framework assumes that tropical AET is mostly achieved by the mean circulation. However, in atmosphere-only and coupled simulations in this thesis, eddies contribute substantially to the tropical AET. For example, in several atmosphere-only prescribed-SST simulations, where the equatorial AEI is negative, and all coupled simulations, equatorward AET at low latitudes is achieved by atmospheric eddies (sections 4.3 and 6.3). In coupled simulations latent energy transport associated with transient eddies dominates the equatorward AET at low latitudes (section 6.4). The substantial role of eddies prohibits using the AEI framework to diagnose the sensitivity of the ITCZ to convective mixing. For example, in interactive OET simulations decreasing f_{dp} decreases the equatorial AEI, which is associated with a poleward expansion of the double ITCZ (Bischoff and Schneider, 2016). However, whilst the ITCZ broadens, changes in the energy flux equator are negligible (Table 6.3).

The second deficiency of the AEI framework is that it assumes that a poleward AET is associated with equatorial ascent. Several simulations show equatorial ascent with an equatorward AET by the mean circulation at low latitudes (section 4.4). Reduced upper-tropospheric MSE and a shallower Hadley circulation decrease the MSE transport in the upper branch of the Hadley circulation and lead to an equatorward AET. The direction of AET by the mean circulation also changes when investigating the sensitivity of the ITCZ to the seasonal cycle of insolation (Wei and Bordoni, 2018). During the retreat phase of the over-turning winter hemisphere Hadley circulation the energy flux equator and ITCZ reside in opposite hemispheres, associated with a change in the AET direction by the mean circulation (Wei and Bordoni, 2018).

Throughout this thesis ITCZ characteristics are predominantly determined by cloud-radiation interactions and latent heat fluxes (chapters 4 to 6). On the other hand, cloud-radiation interactions and latent heat fluxes are determined by the ITCZ itself. The association between AEI components and the ITCZ makes it challenging to determine causality. Therefore, whilst the AEI framework is useful for diagnosing ITCZ characteristics in certain circumstances, such as in paleoclimate studies (Haug et al., 2001), it struggles to predict the ITCZ location without a priori knowledge of changes in AEI components. For example, removing CRE at the default convective mixing rate produces a double ITCZ at approximately $\pm 4.4^\circ$ latitude (section 4.3). However, simply removing CRE from the total AEI in the model configuration with cloud-radiation interactions and using the AEI framework (Bischoff and Schneider, 2016) predicts a double ITCZ location at $\pm 5.6^\circ$ latitude. The poleward bias in the predicted ITCZ location is associated with increased equatorial latent heat fluxes when removing CRE. As AEI components are sensitive to atmospheric forcings and model parameters, the AEI framework can not be used to predict the sensitivity of the ITCZ to the same factors.

7.2 Implications

As shown in previous studies the ITCZ is sensitive to the representation of convection (sections 4.3, 5.3 and 6.4; Terray, 1998; Mobis and Stevens, 2012; Song and Zhang, 2018). Unique to this study, sections 4.4 and 5.3 highlight that cloud-radiation interactions play a substantial role in this sensitivity. The role of cloud-radiation interactions in driving the atmospheric circulation implies the accurate representation of cloud-radiative effects must be a priority in convective scheme development. Using an AEI framework and employing simulations without CRE, section 4.4 shows that cloud-radiation interactions play a crucial role in determining the mean-state; small changes in cloud-radiation interactions can lead to substantial tropical precipitation changes. In the real world and more complex GCM simulations, cloud-radiation interactions are expected to be important for

determining the observed and simulated large-scale tropical circulation. To understand the ITCZ response to anthropogenic climate change a consideration of changes in CRE is required. The sensitivity of the ITCZ to convective mixing emphasises the importance of boundary-layer MSE in determining the large-scale circulation. To support climate model development and the predicted ITCZ response to anthropogenic climate change, processes controlling boundary-layer MSE need to be understood.

Coupling substantially reduces the sensitivity of the ITCZ location and width to convective mixing (section 6.5). Comparing interactive and prescribed OET simulations reveals that the reduced sensitivity is predominantly due to interactive SSTs. Therefore, to evaluate and develop climate models, coupled, not atmosphere-only simulations, should be used to investigate the sensitivity of the ITCZ to an atmospheric forcing or parameterisation. Several studies include interactive SSTs by coupling the atmosphere to a slab ocean with a prescribed OET (e.g. Bischoff and Schneider, 2014; Voigt et al., 2016; Wei and Bordoni, 2018). However, prescribing OET fixes the net-downward surface energy flux, constraining the response of surface energy flux components to changes in forcing. This thesis demonstrates several reasons for why model configurations with constrained surface fluxes should not be used as proxies to study the real-world ITCZ. First, surface fluxes play an important role in the sensitivity of the ITCZ to the representation of convection (sections 4.4 and 5.3; Numaguti, 1995; Mobis and Stevens, 2012); and second, the sensitivity of the ITCZ intensity to convective mixing is greater with a prescribed OET (section 6.5). Prescribing OET limits surface-atmosphere interactions thereby possibly damping the sensitivity of the ITCZ to an atmospheric forcing or parameterisation. To fully understand the impact of anthropogenic climate change on ITCZ dynamics, simulations with interactive surface-atmosphere interactions should be performed.

This thesis demonstrates two reasons why the AEI framework cannot always be used to understand ITCZ dynamics (Kang et al., 2008; Bischoff and Schneider, 2014). First, in several simulations both equatorward atmospheric energy transport and equatorial ascent are diagnosed; second, in the majority of simulations a substantial proportion of atmospheric energy transport is associated with eddies. The sensitivity of the ITCZ to insolation (section 5.4) also shows that an ITCZ can reside in the opposite hemisphere to the energy flux equator. As the sensitivity of the ITCZ to the representation of convection, cloud-radiation interactions, and boundary conditions depends on AEI components, such as cloudy-sky radiation and latent heat flux, the AEI framework is only useful when diagnosing ITCZ characteristics. The AEI framework should be avoided when predicting the ITCZ response to a change in atmospheric parameterisation or forcing.

In this study ITCZ dynamics have only been explored using an AEI framework (Kang et al., 2008; Bischoff and Schneider, 2014). It may be the case that other theoretical frameworks better diagnose changes in ITCZ characteristics. Several studies propose that tropical convection is determined by local vertical profiles in temperature and moisture (Sobel and Neelin, 2006). This, in conjunction with the weak temperature gradient approximation (Sobel et al., 2001), has led to theories that correctly construct tropical convergence and precipitation from surface conditions (Neelin and Held, 1987; Sobel and Bretherton, 2000). Considering these theories, Lambert et al. (2017) and Todd et al. (2018) use near-surface relative humidity and temperature to diagnose tropical precipitation changes associated with anthropogenic climate change and ENSO. For example, through ranking grid point values of surface air temperature and relative humidity in ERA-Interim, Todd et al. (2018) show that tropical precipitation shifts associated with ENSO are strongly correlated with surface conditions. Surface temperature and relative humidity are strongly associated to the boundary-layer MSE. Therefore, using surface conditions may explain the sensitivity of the ITCZ to convective mixing and boundary conditions (chapters 4 to 6). Using a framework based on surface conditions will also support the argument that meridional SST gradient changes are responsible for the reduced sensitivity of the ITCZ to convective mixing when coupling (section 6.4). However, a framework that solely depends on surface conditions excludes free-tropospheric radiative processes, including the cloud radiative effect, which have been shown to affect ITCZ dynamics (section 4.4; Allen and Sherwood, 2011; Harrop and Hartmann, 2016; Popp and Silvers, 2017). The boundary-layer momentum budget has also been used to understand ITCZ dynamics (Lindzen and Nigam, 1987; Waliser and Somerville, 1994). Pressure gradients associated with tropical SST can substantially impact boundary-layer flow, convergence and ITCZ dynamics (Lindzen and Nigam, 1987; Back and Bretherton, 2009). However, using a boundary-layer momentum budget approach that is strongly dependent on SSTs to understand sensitivities of the ITCZ in a prescribed-SST modelling framework would be purely diagnostic. As in other frameworks that solely rely on surface conditions, it would also exclude free-tropospheric processes.

7.3 Limitations and future work

Prescribed-SST simulations are important to investigate climate dynamics and support the development of climate models. However, the lack of interactive SSTs may overemphasise the sensitivity of the tropical circulation to an atmospheric process compared to coupled simulations or the real world. The difference in sensitivity of the ITCZ to an atmospheric process or forcing when coupling (section 6.5; Oueslati and Bellon, 2013; Tomas et al., 2016) highlights that caution should taken when applying conclusions from prescribed-SST simulations (sections 4.3, 5.3 and 5.4; Hess et al., 1993; Neale and Hoskins, 2001) to the real world. In prescribed-SST simulations CRE plays a

substantial role in the sensitivity of the ITCZ to convective mixing; it remains to be determined whether interactive SSTs alter this role. In the real world CRE associated with the ITCZ reduces the net-downward surface energy flux (Allan, 2011), cooling SSTs, decreasing boundary-layer MSE, and inhibiting convection. Therefore, whilst CRE promotes convection in prescribed-SST simulations (chapters 4 and 5; Harrop and Hartmann, 2016), in coupled simulations, the surface effect of CRE may restrict convection. Future work is required to understand the effect of coupling on the role of CRE in determining tropical circulation characteristics.

Introducing land into the model design would also affect the sensitivity of the ITCZ to convective mixing. In the real world and simulations with continents, thermal contrasts between land and ocean affect ITCZ characteristics. For example, meridional ITCZ migrations are much greater in ocean basins with large adjacent tropical land masses (Waliser and Gautier, 1993; Schneider et al., 2014). It is hypothesised that introducing land will decrease tropical latent heat fluxes and reduce the sensitivity of the latent heat flux to convective mixing. In chapter 5 changing from equinoctial to solstitial boundary conditions reduced the role of CRE in the sensitivity of the ITCZ to convective mixing due to larger latent heat flux variations when changing convective mixing. Hence, as the sensitivity of the latent heat flux to convective mixing is expected to be smaller over land, the role of CRE is proposed to be greater in simulations with land. However, the role of CRE in driving the tropical circulation will depend on the influence of CRE on surface temperatures. If CRE substantially reduces surface temperatures, thereby reducing the boundary-layer MSE and prohibiting convection, then the role of CRE will be minimal.

Introducing real world topography and land would also create zonal surface temperature asymmetries. Further investigation is required to understand whether zonal SST variations affect the influences of cloud-radiation interactions and atmosphere-ocean coupling on the sensitivity of the ITCZ to the representation of convection. Introducing surface temperature zonal asymmetries in an aquaplanet leads to zonal variations in ITCZ characteristics, the formation of zonally-orientated circulations, and mean-state changes (Neale and Hoskins, 2001; Nakajima et al., 2013). ITCZ characteristics and the sensitivity of the ITCZ to an atmospheric parameterisation depend on the boundary conditions (sections 5.4 and 6.5). For example, the sensitivity of the ITCZ to convective mixing differs substantially between experiments with SSTs from coupled simulations and "Qobs" (section 6.5). Hence, it is hypothesised that zonal SST asymmetries will affect the sensitivity of the ITCZ to an atmospheric parameterisation or forcing. Zonally-orientated circulations, partly driven by zonal SST asymmetries, also prohibit using the AEI framework to diagnose the ITCZ. In the West Pacific the Walker circulation transports atmospheric energy zonally, leading to a disparity between AEI and the meridional transport associated with the Hadley circulation (Adam

et al., 2016a). As zonally-orientated circulations affect the AET associated with the mean meridional circulation, it is hypothesised that zonally asymmetric boundary conditions will change the role of CRE in determining the tropical circulation structure. For example, removing CRE in a zonally symmetric prescribed-SST simulation promotes a double ITCZ due to the requirement of equatorward atmospheric energy transport by the meridional circulation. When removing CRE from a zonally-orientated circulation changes in the zonal circulation may compensate the reduced AEI. This thesis shows the importance of cloud-radiation interactions in driving the atmospheric circulation. A more complete understanding of the role of CRE in determining ITCZ characteristics requires further studies using more sophisticated models. Zonally-orientated circulations and zonal SST asymmetries will also influence the effect of Ekman-driven upwelling on tropical SSTs. For example in the real world, Ekman-driven upwelling is much stronger over the East Pacific than the West.

Model resolution is another aspect of model design which may affect the sensitivity of the ITCZ to convective mixing. In an aquaplanet configuration the ITCZ is sensitive to horizontal resolution (Williamson, 2008; Mobis and Stevens, 2012; Benedict et al., 2017; Retsch et al., 2019). Increasing horizontal resolution is hypothesised to increase the latitude at which the minimum boundary-layer MSE needed for deep convection is achieved, thereby promoting off-equatorial convection and a double ITCZ. However, previous studies highlight an inter-model variability in the sensitivity of the ITCZ to model resolution; decreasing grid spacing has been shown to expand the ITCZ poleward (Benedict et al., 2017; Retsch et al., 2019) and equatorially contract the ITCZ (Williamson, 2008; Mobis and Stevens, 2012; Blackburn et al., 2013; Benedict et al., 2017). For example, Benedict et al. (2017) found that increasing horizontal resolution in the Community Atmosphere Model version 4 (CAM4) led to an ITCZ contraction. Meanwhile in CAM5.3 the ITCZ expanded poleward. Several atmospheric components of the two configurations are identical including the dynamics and deep convective parameterisation scheme. However, differences in the representation of shallow convection, microphysics, and radiation are hypothesised to be responsible for changes in the sensitivity of the ITCZ to horizontal resolution. Not only does the impact of model resolution on the sensitivity of the ITCZ to convective mixing remain to be investigated, but future work should also aim to understand the influence of convective mixing on the sensitivity of the ITCZ to model resolution.

In this thesis the role of CRE in sensitivity of the ITCZ to convective mixing is only investigated using the MetUM. However conclusions may be model-dependent. For example, simulated tropical CRE varies amongst GCMs, particularly the vertical structure (Voigt and Shaw, 2015; Harrop and Hartmann, 2016). Dixit et al. (2018) show that in an aquaplanet configuration of the Community Climate System Model (CESM) version 1.2.2, lower-tropospheric CRE plays a more important

role in determining ITCZ characteristics than upper-tropospheric CRE. Meanwhile in section 4.4 and Harrop and Hartmann (2016), upper-tropospheric temperature changes when removing CRE play a greater role in determining the ITCZ structure than lower-tropospheric CRE changes. The inter-model variability in the proposed mechanisms is associated with the simulated CRE vertical structure: in CESM 1.2.2 tropical upper-tropospheric warming is approximately half of that simulated in MetUM (section 4.3; Dixit et al., 2018). Due to the substantial inter-model variability of CRE in aquaplanets (Voigt and Shaw, 2015), greater work is required to understand how the vertical structure of CRE affects the role of cloud feedbacks on the sensitivity of the ITCZ to the representation of convection across models.

Another conclusion from this study that may be model dependent is that OET is insensitive to convective mixing (section 6.4). As a result the reduced sensitivity of the ITCZ to convective mixing when coupling is mostly associated with interactive SSTs (section 6.5). However, the reduced sensitivity of the ITCZ to convective mixing and minimal role of OET in coupled simulations most likely depends on the mean state in the coupled model configuration. Coupling introduces equatorial Ekman-driven upwelling, which cools equatorial SSTs, reduces the equatorial boundary-layer MSE, and inhibits equatorial convection (section 6.3). The substantial equatorial SST minimum results in a persistent double SST peak associated with a double ITCZ. Reducing equatorial upwelling may reduce the effect of coupling on the sensitivity of the ITCZ to convective mixing. Several techniques could be used to reduce the effects of equatorial upwelling including: imposing a seasonally-varying insolation (Codron, 2012); prescribing a cross-equatorial OET; or introducing zonally asymmetric land to reduce the influence of Ekman-driven upwelling at certain longitudes. The importance of atmosphere-ocean coupling in determining ITCZ characteristics in this study motivates further work to understand the impact of atmosphere-ocean feedbacks on ITCZ characteristics in more complex model configurations.

Cloud-radiation interactions play a substantial role in the sensitivity of the mean-state to the representation of convection (sections 4.4 and 5.3). Further studies are required to isolate the role of CRE in the sensitivity of other aspects of the tropical climate to the representation of convection. The diurnal cycle of tropical precipitation over land (Wang et al., 2007), the intensity and propagation of the MJO (Bechtold et al., 2008; Hannah and Maloney, 2011; Klingaman and Woolnough, 2014a), and the Indian monsoon (Bush et al., 2015) are all sensitive to the representation of convection. Yet, it remains to be determined what role CRE plays in any of these sensitivities. Kniffka et al. (2019) show that the simulated diurnal cycle of precipitation during the West African monsoon is influenced by CRE associated with low tropical clouds that form during the night and persist throughout the day. Increasing the optical thickness of these low tropical clouds reduces simulated biases in the timing

and intensity of the diurnal cycle of precipitation for both parameterised and explicit representations of convection, associated with reduced surface temperatures, atmospheric instability, and convection. Improving our understanding and simulation of cloud-radiative interactions is essential to reduce spatio-temporal tropical precipitation biases in GCM simulations.

Through performing idealised GCM experiments this thesis emphasises the role of cloud-radiation interactions and atmosphere-ocean feedbacks in determining ITCZ characteristics. Whilst GCMs are a useful tool to understand the climate system, it is often difficult to translate mechanisms from GCM experiments to the real world. To gain a greater insight into the role of cloud-radiation interactions and atmosphere-ocean feedbacks in driving the atmospheric circulation, improved observations in the tropics are required. For example, observing the vertical structure of CRE across the tropics will enhance understanding of the role of cloud-radiation interactions in driving the large-scale circulation. There is also substantial uncertainty in the tropical precipitation response to anthropogenic climate change (Chadwick et al., 2013; Voigt and Shaw, 2015). Even in aquaplanets with zonally symmetric prescribed-SSTs, the tropical circulation response to an uniform 4K surface warming varies substantially amongst models (Voigt and Shaw, 2015). In aquaplanet slab-ocean simulations with a prescribed q-flux, the inter-model variability of climate sensitivities is just as large as the standard coupled and atmosphere-only CMIP5 simulations (Voigt et al., 2016). This study motivates future work to attribute the inter-model variability of the ITCZ response to anthropogenic climate change to the representation of convection and changes in the vertical profile of MSE. Coupled simulations (chapter 6) also motivate further research to understand the association between convective mixing and climate sensitivity. Understanding the response of tropical precipitation to anthropogenic climate change is vital for future adaptation policies. The important roles of cloud-radiation interactions and atmosphere-ocean feedbacks in driving the tropical circulation revealed here, emphasises the requirement of enhanced understanding of the response of cloud-radiative effects and atmosphere-ocean interactions to anthropogenic climate change.

Chapter A

Appendix

A.1 Simulations performed

Table A.1: *Three-year aquaplanet prescribed-SST simulations employed in chapters 4 to 6. From left to right columns show the simulation label, chapter(s) in which the simulation is employed, f_{dp} value used, representation of cloud-radiation interactions and the insolation and prescribed-SST profiles. The description of SSTs is given as either the location of ϕ_{max} (for simulations in chapters 4 and 5) or the coupled simulation which SSTs are computed from (for simulations in chapter 6). Horizontal lines are used to partition the simulations discussed in each chapter.*

Simulation	Chapter	f_{dp}	CRE	Insolation	SST
F0.28	4/5	0.28	Interactive	Equinoctial	0
F0.57	4/5	0.57	Interactive	Equinoctial	0
F0.85	4/5	0.85	Interactive	Equinoctial	0
F1.13	4/5	1.13	Interactive	Equinoctial	0
F1.70	4/5	1.70	Interactive	Equinoctial	0
F0.28NC	4	0.28	Removed	Equinoctial	0
F0.57NC	4	0.57	Removed	Equinoctial	0
F0.85NC	4	0.85	Removed	Equinoctial	0
F1.13NC	4	1.13	Removed	Equinoctial	0
F1.70NC	4	1.70	Removed	Equinoctial	0
F1.13PC1.13	4/5	1.13	Prescribed, PC1.13	Equinoctial	0
F1.13PC0.57	4	1.13	Prescribed, PC0.57	Equinoctial	0
F0.57PC1.13	4	0.57	Prescribed, PC1.13	Equinoctial	0
F0.57PC0.57	4/5	0.57	Prescribed, PC0.57	Equinoctial	0
F1.13EqSST5	5	1.13	Interactive	Equinoctial	5
F1.13EqSST10	5	1.13	Interactive	Equinoctial	10
F1.13SolSST0	5	1.13	Interactive	Solstitial	0
F1.13SolSST5	5	1.13	Interactive	Solstitial	5
F1.13S	5	1.13	Interactive	Solstitial	10
F0.57EqSST5	5	0.57	Interactive	Equinoctial	5
F0.57EqSST10	5	0.57	Interactive	Equinoctial	10
F0.57SolSST0	5	0.57	Interactive	Solstitial	0
F0.57SolSST5	5	0.57	Interactive	Solstitial	5
F0.57S	5	0.57	Interactive	Solstitial	10
F0.28S	5	0.28	Interactive	Solstitial	10
F0.85S	5	0.85	Interactive	Solstitial	10
F1.70S	5	1.70	Interactive	Solstitial	10
F1.13SPC1.13S	5	1.13	Prescribed, PC1.13S	Solstitial	10
F0.57SPC1.13S	5	0.57	Prescribed, PC1.13S	Solstitial	10
F1.13SPC0.57S	5	1.13	Prescribed, PC0.57S	Solstitial	10
F0.57SPC0.57S	5	0.57	Prescribed, PC0.57S	Solstitial	10
F1.13PC1.13S	5	1.13	Prescribed, PC1.13S	Equinoctial	0
F1.13SPC1.13	5	1.13	Prescribed, PC1.13	Solstitial	10
F0.57PC0.57S	5	0.57	Prescribed, PC0.57S	Equinoctial	0
F0.57SPC0.57	5	0.57	Prescribed, PC0.57	Solstitial	10
F0.57PS0.57	6	0.57	Interactive	Equinoctial	C0.57
F0.57PS1.13	6	0.57	Interactive	Equinoctial	C1.13
F0.57PS1.70	6	0.57	Interactive	Equinoctial	C1.70
F1.13PS0.57	6	1.13	Interactive	Equinoctial	C0.57
F1.13PS1.13	6	1.13	Interactive	Equinoctial	C1.13
F1.13PS1.70	6	1.13	Interactive	Equinoctial	C1.70
F1.70PS0.57	6	1.70	Interactive	Equinoctial	C0.57
F1.70PS1.13	6	1.70	Interactive	Equinoctial	C1.13
F1.70PS1.70	6	1.70	Interactive	Equinoctial	C1.70

Table A.2: *Interactive and prescribed OET coupled simulations employed in chapter 6*

Simulation	f_{dp}	Ekman-driven q-flux
C0.57	0.57	Interactive
C1.13	1.13	Interactive
C1.70	1.70	Interactive
C0.57PQ1.13	0.57	Prescribed PQ1.13
C1.13PQ1.13	1.13	Prescribed PQ1.13
C1.70PQ1.13	1.70	Prescribed PQ1.13

A.2 Acroynms and Abbreviations

Acroynm and Abbreviation	Definition
AEI	Atmospheric Energy Input
AET	Atmospheric Energy Transport
AM2	Atmosphere Model version 2
AR4	Fourth Assessment Report
BC	Boundary Conditions
CAM	Community Atmosphere Model
CAPE	Convective Available Potential Energy
CCM	Community Climate Model
CCSM	Community Climate System Model
CEA	Central Electric Authority
CESM	Community Earth System Model
CMIP	Coupled Model Intercomparison Project
CNRM	Centre National de Recherches Météorolqiques
CRE	Cloud Radiative Effect
DSE	Dry Static Energy
ECMWF	European Centre for Medium-Range Weather Forecasts
ENSO	El Niño Southern Oscillation
ECMWF	European Centre for Medium-Range Weather Forecasts
ENDGame	Even Newer Dynamics for General atmospheric modelling of the environment
ENSO	El Niño Southern Oscillation
FAO	Food and Agriculture Organisation of the United Nations
GA	Global Atmosphere
GC	Global Coupled
GCM	General Circulation Model
GDP	Gross Domestic Product
GFDL	Geophysical Fluid Dynamics Laboratory
GloSea	Global Seasonal forecasting system
GPCC	Global Precipitation Climatology Project
HadGEM	Hadley Centre Global Environment Model
IPCC	Intergovernmental Panel on Climate Change
IPSL	Institute Pierre Simon Laplace
ITCZ	Intertropical Convergence Zone

LW	Longwave
MCA	Moist Convective Adjustment
MetUM	Met Office Unified Model
MIT	Massachusetts Institute of Technology
MJO	Madden Julian Oscillation
MPI-ESM	Max Planck Institute for Meteorology Earth System Model
MSE	Moist Static Energy
NCAR	National Centre for Atmospheric Research
NCEP	National Centers for Environmental Prediction
NEMO	Nucleus for European Modelling of the Ocean
NH	Northern Hemisphere
NOAA	National Oceanographic and Atmospheric Administration
NWP	Numerical Weather Prediction
OASIS	Ocean Atmosphere Sea Ice Soil
OET	Ocean Energy Transport
POP	Parallel Ocean Program
RCP	Representation Concentration Pathway
RH	Relative Humidity
SFC	Surface
SH	Southern Hemisphere
SPCZ	South Pacific Convergence Zone
SST	Sea Surface Temperature
SW	Shortwave
TOA	Top of the Atmosphere
TRMM	Tropical Rainfall Measuring Mission

A.3 Mathematical notation

Notation	Definition
x_0	Equatorial value of x
x_δ	Value of x at energy flux equator
x_*	Surface value of x
x_d	Value of x in ocean deep layer
x_{eddy}	Eddy component of x
x_m	Value of x in ocean mixed layer

x_{max}	Value of x at maximum sea surface temperature
x^*	Deviations of x from the zonal-mean
x'	Deviations of x from the time-mean
$[x]$	Zonal-mean of x
$\bar{x}$	Time-mean of x
$\hat{x}$	Vertical integral of x
$^\circ$	Degrees
$^\circ$C	Degrees Celsius
α	Scaling term used in section 4.4
∂	Partial differential
∂_y	Meridional divergence
∂_{yy}	Second meridional divergence
χ	Parameter when working out root mean squared deviation
δ	Energy flux equator
ϵ	Lateral entrainment rate
η	Parameter used to control "Qobs" SST gradient in Mobis and Stevens (2012)
θ	Potential temperature
$\prod$	Exner function ($\frac{\theta}{T}$)
ρ	Density
ϕ	Latitude
ϕ_H	Latitude of Hadley circulation edge
ϕ_{max}	Latitude of maximum SST (degrees)
ϕ^r_{max}	Latitude of maximum SST (radians)
Ψ	Mass meridional streamfunction
Ψ_{Asym}	Hemispherically asymmetric component of mass meridional streamfunction
Ψ_{Sym}	Hemispherically symmetric component of mass meridional streamfunction
Ψ^{heat}	Mass meridional streamfunction associated with temperature tendency
τ_x	Zonal surface wind stress
Ω	Rotation rate of Earth
AEI	Atmospheric energy input
AET	Atmospheric energy transport
$\text{AET}^{\text{clear}}$	Atmospheric energy transport associated with clear-sky radiation
$\text{AET}^{\text{cloud}}$	Atmospheric energy transport associated with cloudy-sky radiation
AET^{H}	Atmospheric energy transport associated with surface energy fluxes
a	Radius of Earth
a_p	Convective plume fractional area

as	All-sky
BL	Boundary layer
C^*	Scalar used for vertical mixing in ocean model
C_E	Coefficient between entrainment rate and buoyancy in Song and Zhang (2018) spectral cloud model
C_p	Specific heat capacity
cls	Clear-sky
CRE	Cloud radiative effect
D	Diffusion constant in ocean model
d_m	Lateral detrainment rate
f	Coriolis parameter
F_{corr}	Surface energy correction term
F_{net}	Net-downward surface energy flux
f_{dp}	Constant used to control convective mixing
$\mathcal{F}_x$	Zonal surface stress
g	Gravitational constant
H	Atmospheric energy input from surface turbulent fluxes
H_d	Depth of idealised ocean model deep layer
H_{HC}	Height of Hadley circulation
H_m	Depth of idealised ocean model mixed layer
h	Moist static energy
h_o	Oceanic energy
L	Top of the atmosphere net-incoming longwave radiative flux
l	Latent energy
LW	Atmospheric energy input from longwave radiation
L_v	Latent heat of vaporisation
M	Mass flux
M_A	Specific angular momentum
O	Net-downward surface radiative flux
OET	Ocean energy transport
OET_p	Prescribed ocean energy transport
p	Pressure
P_{cent}	Precipitation centroid
Q'	Horizontal anomaly of temperature tendency
q	Specific humidity
R_o	Rossby number

R^2	Coefficient of determination
RH	Relative humidity
$RMSD$	Root mean squared deviation
S	Top of the atmosphere net-incoming shortwave radiative flux
s	Dry static energy
SFC	Surface
SW	Atmospheric energy input from shortwave radiation
T	Temperature
T^*	Upcurrent temperature
TOA	Top of the atmosphere
u	Zonal wind
V	Density-weighted meridional wind
v	Meridional wind
v_{ek_m}	Mixed-layer meridional Ekman-driven ocean current
v_{ek_d}	Deep-layer meridional Ekman-driven ocean current
w	Vertical current/wind
w_p	Convective plume upward velocity
w_{ek}	Vertical Ekman-driven current
Z	Geopotential height
z	Height

References

Adam, O., T. Bischoff, and T. Schneider, 2016a: Seasonal and interannual variations of the energy flux equator and ITCZ. Part I: Zonally averaged ITCZ position. *J. Climate.*, **29**, 3219–3230.

— 2016b: Seasonal and interannual variations of the energy flux equator and ITCZ. Part II: Zonally varying shifts of the ITCZ. *J. Climate.*, **29**, 7281–7293.

Allan, R. P., 2011: Combining satellite data and models to estimate cloud radiative effect at the surface and in the atmosphere. *Meteorol. Apps*, **18**, 324–333.

Allen, R. J. and S. C. Sherwood, 2011: The impact of natural versus anthropogenic aerosols on atmospheric circulation in the community atmosphere model. *Clim. Dyn.*, **36**, 1959–1978.

Arakawa, A. and V. R. Lamb, 1977: Computational design of the basic dynamical processes of the UCLA general circulation model. *General Circulation Models of the Atmosphere*, **17**, 173–265.

Arakawa, A. and W. H. Schubert, 1974: Interaction of a cumulus cloud ensemble with the large-scale environment, part I. *J. Atmos. Sci.*, **31**, 674–701.

Back, L. E. and C. S. Bretherton, 2009: On the relationship between sst gradients, boundary layer winds, and convergence over the tropical oceans. *J. Climate.*, **22**, 4182–4196.

Bacmeister, J. T., M. J. Suarez, and F. R. Robertson, 2006: Rain reevaporation, boundary layer–convection interactions, and pacific rainfall patterns in an AGCM. *J. Atmos. Sci.*, **63**, 3383–3403.

Bain, C. L., J. De Paz, J. Kramer, G. Magnusdottir, P. Smyth, H. Stern, and C.-c. Wang, 2011: Detecting the ITCZ in instantaneous satellite data using spatiotemporal statistical modeling: ITCZ climatology in the east Pacific. *J. Climate.*, **24**, 216–230.

Barker, H. W. and Z. Li, 1995: Improved simulation of clear-sky shortwave radiative transfer in the CCC-GCM. *J. Climate.*, **8**, 2213–2223.

Basu, B., 2005: Some characteristics of model-predicted precipitation during the summer monsoon over india. *J. of Appl. Meteorol.*, **44**, 324–339.

Bechtold, P., M. Köhler, T. Jung, F. Doblas-Reyes, M. Leutbecher, M. J. Rodwell, F. Vitart, and G. Balsamo, 2008: Advances in simulating atmospheric variability with the ECMWF model: from synoptic to decadal time-scales. *Q. J. Roy. Meteor. Soc.*, **134**, 1337–1351.

Bellon, G. and A. H. Sobel, 2010: Multiple equilibria of the Hadley circulation in an intermediate-complexity axisymmetric model. *J. Climate.*, **23**, 1760–1778.

Bellucci, A., S. Gualdi, and A. Navarra, 2010: The double-ITCZ syndrome in coupled general circulation models: the role of large-scale vertical circulation regimes. *J. Climate.*, **23**, 1127–1145.

Benedict, J. J., E. D. Maloney, A. H. Sobel, D. M. Frierson, and L. J. Donner, 2013: Tropical intraseasonal variability in version 3 of the GFDL atmosphere model. *J. Climate.*, **26**, 426–449.

Benedict, J. J., B. Medeiros, A. C. Clement, and A. G. Pendergrass, 2017: Sensitivities of the hydrologic cycle to model physics, grid resolution, and ocean type in the aquaplanet community atmosphere model. *J. Adv. Model. Earth Sy.*, **9**, 1307–1324.

Bergman, J. W. and H. H. Hendon, 2000: Cloud radiative forcing of the low-latitude tropospheric circulation: linear calculations. *J. Atmos. Sci.*, **57**, 2225–2245.

Berry, G. and M. J. Reeder, 2014: Objective identification of the Intertropical Convergence Zone: Climatology and trends from the ERA-Interim. *J. Climate.*, **27**, 1894–1909.

Birch, C. E., D. Parker, J. Marsham, D. Copsey, and L. Garcia-Carreras, 2014: A seamless assessment of the role of convection in the water cycle of the West African monsoon. *J. Geophys. Res-Atmos.*, **119**, 2890–2912.

Bischoff, T. and T. Schneider, 2014: Energetic constraints on the position of the Intertropical Convergence Zone. *J. Climate.*, **27**, 4937–4951.

— 2016: The equatorial energy balance, ITCZ position, and double-ITCZ bifurcations. *J. Climate.*, **29**, 2997–3013, and corrigendum, 29(19), 7167–7167.

Bjerknes, J., 1969: Atmospheric teleconnections from the equatorial Pacific. *Mon. Weat. Rev.*, **97**, 163–172.

Blackburn, M., D. L. Williamson, K. Nakajima, W. Ohfuchi, Y. O. Takahashi, Y.-Y. Hayashi, H. Nakamura, M. Ishiwatari, J. L. McGregor, H. Borth, et al., 2013: The aqua-planet experiment (APE): control SST simulation. *J. Meteorol. Soc. Jap.*, **91**, 17–56.

Bony, S., B. Stevens, D. M. Frierson, C. Jakob, M. Kageyama, R. Pincus, T. G. Shepherd, S. C. Sherwood, A. P. Siebesma, A. H. Sobel, et al., 2015: Clouds, circulation and climate sensitivity. *Nat. Geosci.*, **8**, 261–268.

Bordoni, S. and T. Schneider, 2008: Monsoons as eddy-mediated regime transitions of the tropical overturning circulation. *Nat. Geosci.*, **1**, 515.

Bretherton, C. S., P. N. Blossey, and M. Khairoutdinov, 2005: An energy-balance analysis of deep convective self-aggregation above uniform SST. *J. Atmos. Sci.*, **62**, 4273–4292.

Broccoli, A. J., K. A. Dahl, and R. J. Stouffer, 2006: Response of the ITCZ to Northern Hemisphere

cooling. *Geophys. Res. Lett.*, **33**.

Bush, S., A. Turner, S. Woolnough, G. Martin, and N. Klingaman, 2015: The effect of increased convective entrainment on Asian monsoon biases in the MetUM general circulation model. *Q. J. Roy. Meteor. Soc.*, 311–326.

Byrne, M. P., A. G. Pendergrass, A. D. Rapp, and K. R. Wodzicki, 2018: Response of the Intertropical Convergence Zone to climate change: location, width, and strength. *Current Climate Change Reports*, **4**, 355–370.

Byrne, M. P. and T. Schneider, 2016a: Energetic constraints on the width of the Intertropical Convergence Zone. *J. Climate.*, **29**, 4709–4721.

— 2016b: Narrowing of the ITCZ in a warming climate: Physical mechanisms. *Geophys. Res. Lett.*, **43**.

CEA, 2018: Review of performance of hydropower stations 2017-18. Technical report, Central Electric Authority, Government of India, Ministry of Power, New Delhi.

Chadwick, R., I. Boutle, and G. Martin, 2013: Spatial patterns of precipitation change in CMIP5: Why the rich do not get richer in the tropics. *J. Climate.*, **26**, 3803–3822.

Chao, W. C. and B. Chen, 2004: Single and double ITCZ in an aqua-planet model with constant sea surface temperature and solar angle. *Clim. Dyn.*, **22**, 447–459.

Charney, J. G., 1971: Tropical cyclogenesis and the formation of the Intertropical Convergence Zone. Lectures in applied mathmatics, 13, Providence, RI. *Amer. Math. Soc.*, 355–368.

Charney, J. G. and A. Eliassen, 1964: On the growth of the hurricane depression. *J. Atmos. Sci.*, **21**, 68–75.

Charney, J. G. and N. Phillips, 1953: Numerical integration of the quasi-geostrophic equations for barotropic and simple baroclinic flows. *Journal of Meteorology*, **10**, 71–99.

Chiang, J. C., M. Biasutti, and D. S. Battisti, 2003: Sensitivity of the Atlantic Intertropical Convergence Zone to last glacial maximum boundary conditions. *Paleoceanography*, **18**, 1094–1112.

Chiang, J. C. and C. M. Bitz, 2005: Influence of high latitude ice cover on the marine Intertropical Convergence Zone. *Clim. Dyn.*, **25**, 477–496.

Chiang, J. C., Y. Kushnir, and A. Giannini, 2002: Deconstructing Atlantic Intertropical Convergence Zone variability: Influence of the local cross-equatorial sea surface temperature gradient and remote forcing from the eastern equatorial Pacific. *J. Geophys. Res-Atmos.*, **107**, pp. ACL–3, 1–19.

Chikira, M., 2010: A cumulus parameterization with state-dependent entrainment rate. Part II: Impact on climatology in a general circulation model. *J. Atmos. Sci.*, **67**, 2194–2211.

Codron, F., 2012: Ekman heat transport for slab oceans. *Clim. Dyn.*, **38**, 379–389.

Collins, W., N. Bellouin, M. Doutriaux-Boucher, N. Gedney, P. Halloran, T. Hinton, J. Hughes, C. Jones, M. Joshi, S. Liddicoat, et al., 2011: Development and evaluation of an Earth-System model - HadGEM2. *Geosci. Model. Dev.*, **4**, 1051–1075.

Crueger, T. and B. Stevens, 2015: The effect of atmospheric radiative heating by clouds on the Madden-Julian Oscillation. *J. Adv. Model. Earth Sy.*, **7**, 854–864.

Dai, A., 2006: Precipitation characteristics in eighteen coupled climate models. *J. Climate.*, **19**, 4605–4630.

de Rooy, W. C., P. Bechtold, K. Frhlich, C. Hohenegger, H. Jonker, D. Mironov, A. Pier Siebesma, J. Teixeira, and J.-I. Yano, 2013: Entrainment and detrainment in cumulus convection: An overview. *Q. J. Roy. Meteor. Soc.*, **139**, 1–19.

De Rooy, W. C. and A. P. Siebesma, 2008: A simple parameterization for detrainment in shallow cumulus. *Mon. Weat. Rev.*, **136**, 560–576.

De Szoeke, S. P. and S.-P. Xie, 2008: The tropical eastern Pacific seasonal cycle: Assessment of errors and mechanisms in IPCC AR4 coupled ocean–atmosphere general circulation models. *J. Climate.*, **21**, 2573–2590.

Del Genio, A. D. and R. J. Suozzo, 1987: A comparative study of rapidly and slowly rotating dynamical regimes in a terrestrial general circulation model. *J. Atmos. Sci.*, **44**, 973–986.

Derbyshire, S., A. Maidens, S. Milton, R. Stratton, and M. Willett, 2011: Adaptive detrainment in a convective parametrization. *Q. J. Roy. Meteor. Soc.*, **137**, 1856–1871.

Derbyshire, S. H., I. Beau, P. Bechtold, J.-Y. Grandpeix, J.-M. Piriou, J.-L. Redelsperger, and P. M. M. Soares, 2004: Sensitivity of moist convection to environmental humidity. *Q. J. Roy. Meteor. Soc.*, **130**, 3055–3079.

Dixit, V., O. Geoffroy, and S. C. Sherwood, 2018: Control of ITCZ width by low-level radiative heating from upper-level clouds in aquaplanet simulations. *Geophys. Res. Lett.*, **45**, 5788–5797.

Dong, B., R. T. Sutton, L. Shaffrey, and N. P. Klingaman, 2017: Attribution of forced decadal climate change in coupled and uncoupled ocean–atmosphere model experiments. *J. Climate.*, **30**, 6203–6223.

Donohoe, A. and D. S. Battisti, 2012: What determines meridional heat transport in climate models? *J. Climate.*, **25**, 3832–3850.

Donohoe, A., J. Marshall, D. Ferreira, and D. Mcgee, 2013: The relationship between ITCZ location and cross-equatorial atmospheric heat transport: From the seasonal cycle to the last glacial maximum. *Amer. Meteor. Soc.*, 3597–3618.

Dufresne, J.-L., M.-A. Foujols, S. Denvil, A. Caubel, O. Marti, O. Aumont, Y. Balkanski, S. Bekki, H. Bellenger, R. Benshila, et al., 2013: Climate change projections using the IPSL-CM5 earth system model: from CMIP3 to CMIP5. *Clim. Dyn.*, **40**, 2123–2165.

Dunning, C. M., E. Black, and R. P. Allan, 2018: Later wet seasons with more intense rainfall over africa under future climate change. *J. Climate.*, **31**, 9719–9738.

Eady, E., 1950: The cause of the general circulation of the atmosphere. *Centen. Proc. Roy. Meteor. Soc*, **76**, 156–172.

Emanuel, K. A., 1995: On thermally direct circulations in moist atmospheres. *J. Atmos. Sci.*, **52**, 1529–1534.

FAO, 2018: World food and agriculture - statistical pocketbook. Technical report, Rome.

Fasullo, J. T. and K. E. Trenberth, 2008: The annual cycle of the energy budget. Part II: Meridional structures and poleward transports. *J. Climate.*, **21**, 2313–2325.

Fermepin, S. and S. Bony, 2014: Influence of low-cloud radiative effects on tropical circulation and precipitation. *J. Adv. Model. Earth Sy.*, **6**, 513–526.

Ferrel, W., 1856: An essay on the winds and the currents of the ocean. *Nashville Journal of Medicine and Surgery.*, **11**.

Fläschner, D., T. Mauritsen, B. Stevens, and S. Bony, 2018: The signature of shallow circulations, not cloud radiative effects, in the spatial distribution of tropical precipitation. *J. Climate.*, **31**, 9489–9505.

Frierson, D. and Y. Hwang, 2012: Extratropical influence on ITCZ shifts in slab ocean simulations of global warming. *J. Climate.*, 720–733.

Frierson, D. M. W., 2007: The dynamics of idealized convection schemes and their effect on the zonally averaged tropical circulation. *J. Atmos. Sci.*, **64**, 1959–1976.

Fritsch, J. M. and C. F. Chappell, 1980: Numerical prediction of convectively driven mesoscale pressure systems. Part I: Convective parameterization. *J. Atmos. Sci.*, **37**, 1722–1733.

Garcia-Carreras, L., J. Marsham, D. Parker, C. Bain, S. Milton, A. Saci, M. Salah-Ferroudj, B. Ouchene, and R. Washington, 2013: The impact of convective cold pool outflows on model biases in the sahara. *Geophys. Res. Lett.*, **40**, 1647–1652.

Geen, R., F. H. Lambert, and G. K. Vallis, 2018: Regime change behavior during Asian monsoon onset. *J. Climate.*, **31**, 3327–3348.

Grant, A., 2001: Cloud-base fluxes in the cumulus-capped boundary layer. *Q. J. Roy. Meteor. Soc.*, **127**, 407–421.

Grant, A. and A. Brown, 1999: A similarity hypothesis for shallow-cumulus transports. *Q. J. Roy. Meteor. Soc.*, **125**, 1913–1936.

Green, B. and J. Marshall, 2017: Coupling of trade winds with ocean circulation damps ITCZ shifts. *J. Climate.*, **30**, 4395–4411.

Gregory, D., R. Kershaw, and P. Inness, 1997: Parametrization of momentum transport by convection. II: Tests in single-column and general circulation models. *Q. J. Roy. Meteor. Soc.*, **123**, 1153–1183.

Gregory, D. and P. Rowntree, 1990: A mass flux convection scheme with representation of cloud ensemble characteristics and stability-dependent closure. *Mon. Weat. Rev.*, **118**, 1483–1506.

Hadley, G., 1735: Concerning the cause of the general trade-winds. *Philosophical Transactions of the Royal Society of London*, **39**, 58–62.

Halpern, D. and C.-W. Hung, 2001: Satellite observations of the southeast Pacific Intertropical Con-

vergence Zone during 1993-1998. *J. Geophys. Res-Atmos.*, **106**, 28107–28112.

Hannah, W. M. and E. D. Maloney, 2011: The role of moisture-convection feedbacks in simulating the Madden-Julian Oscillation. *J. Climate.*, **24**, 2754–2770.

Harrop, B. and D. Hartmann, 2016: The role of cloud radiative heating in determining the location of the ITCZ in aquaplanet simulations. *Amer. Meteor. Soc.*, 2714–2763.

Haug, G. H., K. A. Hughen, D. M. Sigman, L. C. Peterson, and U. Röhl, 2001: Southward migration of the Intertropical Convergence Zone through the Holocene. *Science*, **293**, 1304–1308.

Hawcroft, M., J. M. Haywood, M. Collins, A. Jones, A. C. Jones, and G. Stephens, 2017: Southern Ocean albedo, inter-hemispheric energy transports and the double ITCZ: Global impacts of biases in a coupled model. *Clim. Dyn.*, **48**, 2279–2295.

Hayashi, Y.-Y. and A. Sumi, 1986: The 30-40 day oscillations simulated in an "aqua planet" model. *J. Meteorol. Soc. Jap.*, **64**, 451–467.

Haynes, J. M., C. Jakob, W. B. Rossow, G. Tselioudis, and J. Brown, 2011: Major characteristics of southern ocean cloud regimes and their effects on the energy budget. *J. Climate.*, **24**, 5061–5080.

Held, I. M., 2001: The partitioning of the poleward energy transport between the tropical ocean and atmosphere. *J. Atmos. Sci.*, **58**, 943–948.

— 2018: 100 Years of Progress in Understanding the General Circulation of the Atmosphere. *Meteorological Monographs*.

Held, I. M. and A. Y. Hou, 1980: Nonlinear axially symmetric circulations in a nearly inviscid atmosphere. *J. Atmos. Sci.*, **37**, 515–533.

Hess, P. G., D. S. Battisti, and P. J. Rasch, 1993: Maintenance of the Intertropical Convergence Zones and the large-scale tropical circulation on a water-covered earth. *J. Atmos. Sci.*, **50**, 691–713.

Heus, T., G. Van Dijk, H. J. Jonker, and H. E. Van den Akker, 2008: Mixing in shallow cumulus clouds studied by Lagrangian particle tracking. *J. Atmos. Sci.*, **65**, 2581–2597.

Hirons, L., P. Inness, F. Vitart, and P. Bechtold, 2013: Understanding advances in the simulation of intraseasonal variability in the ECMWF model. Part II: The application of process-based diagnostics. *Q. J. Roy. Meteor. Soc.*, **139**, 1427–1444.

Hirons, L., N. Klingaman, and S. Woolnough, 2015: MetUM-GOML: a near-globally coupled atmosphere-ocean-mixed-layer model. *Geosci. Model. Dev.*, **8**, 363–379.

Hohenegger, C. and B. Stevens, 2013: Controls on and impacts of the diurnal cycle of deep convective precipitation. *J. Adv. Model. Earth Sy.*, **5**, 801–815.

Holloway, C. E. and S. J. Woolnough, 2016: The sensitivity of convective aggregation to diabatic processes in idealized radiative-convective equilibrium simulations. *J. Adv. Model Earth Sy.*, **8**, 166–195.

Holton, J. R., J. M. Wallace, and J. Young, 1971: On boundary layer dynamics and the ITCZ. *J. Atmos. Sci.*, **28**, 275–280.

Hoskins, B., R. Neale, M. Rodwell, and G.-Y. Yang, 1999: Aspects of the large-scale tropical atmospheric circulation. *Tellus B*, **51**, 33–44.

Huang, P., S.-P. Xie, K. Hu, G. Huang, and R. Huang, 2013: Patterns of the seasonal response of tropical rainfall to global warming. *Nat. Geosci.*, **6**, 357.

Hwang, Y.-T. and D. M. W. Frierson, 2010: Increasing atmospheric poleward energy transport with global warming. *Geophys. Res. Lett.*, **37**, l24807.

— 2013: Link between the double-Intertropical Convergence Zone problem and cloud biases over the Southern Ocean. *P. Natl. Acad. Sci. USA*, **110**, 4935–4940.

Iovino, D., S. Masina, A. Storto, A. Cipollone, and V. N. Stepanov, 2016: A 1/16 eddying simulation of the global NEMO sea-ice-ocean system. *Geosci. Model. Dev.*, **9**, 2665–2684.

James, I. N., 1995: *Introduction to circulating atmospheres*. Cambridge University Press.

Kain, J. S. and J. M. Fritsch, 1990: A one-dimensional entraining/detraining plume model and its application in convective parameterization. *J. Atmos. Sci.*, **47**, 2784–2802.

Kalnay, E., M. Kanamitsu, R. Kistler, W. Collins, D. Deaven, L. Gandin, M. Iredell, S. Saha, G. White, J. Woollen, et al., 1996: The NCEP/NCAR 40-year reanalysis project. *Bulletin of the American Meteorological Society*, **77**, 437–472.

Kang, S., D. Frierson, and I. Held, 2009: The tropical response to extratropical thermal forcing in an idealized GCM: The importance of radiative feedbacks and convective parameterization. *Amer. Meteor. Soc.*, **66**, 2812–2827.

Kang, S., I. Held, D. Frierson, and Z. Ming, 2008: The response of the ITCZ to extratropical thermal forcing: Idealized slab-ocean experiments with a GCM. *Amer. Meteor. Soc.*, **21**, 3521–3532.

Kang, S. M., Y. Shin, and S.-P. Xie, 2018: Extratropical forcing and tropical rainfall distribution: energetics framework and ocean Ekman advection. *Nature Partner Journals Climate and Atmospheric Science*, **1**, 2–12.

Kay, J. E., C. Wall, V. Yettella, B. Medeiros, C. Hannay, P. Caldwell, and C. Bitz, 2016: Global climate impacts of fixing the southern ocean shortwave radiation bias in the community earth system model (CESM). *J. Climate*, **29**, 4617–4636.

Kirtman, B. P. and E. K. Schneider, 2000: A spontaneously generated tropical atmospheric general circulation. *J. Atmos. Sci.*, **57**, 2080–2093.

Klingaman, N. and S. Woolnough, 2014a: The role of air–sea coupling in the simulation of the Madden-Julian oscillation in the Hadley Centre model. *Q. J. Roy. Meteor. Soc.*, **140**, 2272–2286.

— 2014b: Using a case-study approach to improve the Madden-Julian oscillation in the Hadley Centre model. *Q. J. Roy. Meteor. Soc.*, **140**, 2491–2505.

Kniffka, A., P. Knippertz, and A. H. Fink, 2019: The role of low-level clouds in the West African monsoon system. *Atmos. Chem. Phys.*, **19**, 1623–1647.

Knutti, R. and J. Sedláček, 2013: Robustness and uncertainties in the new CMIP5 climate model

projections. *Nat. Clim. Change.*, **3**, 369–373.

Koutavas, A. and J. Lynch-Stieglitz, 2003: Glacial-interglacial dynamics of the eastern equatorial Pacific cold tongue-Intertropical Convergence Zone system reconstructed from oxygen isotope records. *Paleoceanography*, **18**, 1089.

Kucharski, F., A. Pirani, A. Tompkins, M. Biasutti, A. Voigt, M. Byrne, and R. Farneti, 2018: WCRP grand challenge on clouds, circulation and climate sensitivity: 2nd meeting on monsoons and tropical rain belts. International Centre for Theorectical Physics.

Kuo, H. L., 1974: Further studies of the parameterization of the influence of cumulus convection on large-scale flow. *J. Atmos. Sci.*, **31**, 1232–1240.

Lambert, F. H., A. J. Ferraro, and R. Chadwick, 2017: Land-ocean shifts in tropical precipitation linked to surface temperature and humidity change. *J. Climate*, **30**, 4527–4545.

Landu, K., L. R. Leung, S. Hagos, V. Vinoj, S. A. Rauscher, T. Ringler, and M. Taylor, 2014: The dependence of ITCZ structure on model resolution and dynamical core in aquaplanet simulations. *J. Climate.*, **27**, 2375–2385.

Lau, W. K. and K.-M. Kim, 2015: Robust Hadley circulation changes and increasing global dryness due to CO2 warming from CMIP5 model projections. *P. Natl. Acad. Sci. USA*, **112**, 3630–3635.

Levitus, S., 1987: Meridional ekman heat fluxes for the world ocean and individual ocean basins. *J. of Phys. Ocean.*, **17**, 1484–1492.

Li, Y., D. W. J. Thompson, and S. Bony, 2015: The influence of atmospheric cloud radiative effects on the large-scale atmospheric circulation. *J. Climate.*, **28**, 7263–7278.

Lin, J., 2007: The double-ITCZ problem in IPCC AR4 coupled GCMs: Ocean-atmosphere feedback analysis. *Amer. Meteor. Soc.*, **20**, 4497–4525.

Lindzen, R. S. and A. V. Hou, 1988: Hadley circulations for zonally averaged heating centered off the equator. *J. Atmos. Sci.*, **45**, 2416–2427.

Lindzen, R. S. and S. Nigam, 1987: On the role of sea surface temperature gradients in forcing low-level winds and convergence in the tropics. *J. Atmos. Sci.*, **44**, 2418–2436.

Liu, Y., L. Guo, G. Wu, and Z. Wang, 2010: Sensitivity of ITCZ configuration to cumulus convective parameterizations on an aqua planet. *Clim. Dyn.*, **34**, 223–240.

Madec, G., R. Bourdall-Badie, P.-A. Bouttier, C. Bricaud, D. Bruciaferri, D. Calvert, J. Chanut, E. Clementi, A. Coward, D. Delrosso, C. Eth, S. Flavoni, T. Graham, J. Harle, D. Iovino, D. Lea, C. Lvy, T. Lovato, N. Martin, S. Masson, S. Mocavero, J. Paul, C. Rousset, D. Storkey, A. Storto, and M. Vancoppenolle, 2017: NEMO ocean engine. Revision 8625 from SVN repository.

Manabe, S., J. Smagorinsky, and R. F. Strickler, 1965: Simulated climatology of a general circulation model with a hydrologic cycle. *Mon. Weat. Rev.*, **93**, 769–798.

Manners, J., J.-C. Thelen, J. Petch, P. Hill, and J. Edwards, 2009: Two fast radiative transfer methods to improve the temporal sampling of clouds in numerical weather prediction and climate models.

Q. J. Roy. Meteor. Soc., **135**, 457–468.

Marshall, J., A. Adcroft, C. Hill, L. Perelman, and C. Heisey, 1997: A finite-volume, incompressible navier stokes model for studies of the ocean on parallel computers. *J. Geophys. Res-Ocn.*, **102**, 5753–5766.

Martin, G., S. Milton, C. Senior, M. Brooks, S. Ineson, T. Reichler, and J. Kim, 2010: Analysis and reduction of systematic errors through a seamless approach to modeling weather and climate. *J. Climate.*, **23**, 5933–5957.

Mechoso, C. R., A. W. Robertson, N. Barth, M. Davey, P. Delecluse, P. Gent, S. Ineson, B. Kirtman, M. Latif, H. L. Treut, et al., 1995: The seasonal cycle over the tropical Pacific in coupled ocean–atmosphere general circulation models. *Mon. Weat. Rev.*, **123**, 2825–2838.

Merlis, T. M., T. Schneider, S. Bordoni, and I. Eisenman, 2013: Hadley circulation response to orbital precession. Part I: Aquaplanets. *J. Climate.*, **26**, 740–753.

Mobis, B. and B. Stevens, 2012: Factors controlling the position of the Intertropical Convergence Zone on an aquaplanet. *J. Adv. Model. Earth Sy.*, **4**, m00A04.

Nakajima, K., Y. Yamada, Y. O. Takahashi, M. Ishiwatari, W. Ohfuchi, and Y.-Y. Hayashi, 2013: The variety of forced atmospheric structure in response to tropical SST anomaly in the aqua-planet experiments. *J. Meteorol. Soc. Jap.*, **91**, 143–193.

NCAR, 2014: The climate data guide. SST data sets: Overview and comparison table. *Retrieved from https://climatedataguide.ucar.edu/climate-data/sst-data-sets-overview-comparison-table*.

Neale, R. and B. Hoskins, 2001: A standard test for AGCMs including their physical parametrizations: I: The proposal. *Atmos. Sci. Lett.*, **1**, 101–107.

Neale, R. B. and B. J. Hoskins, 2001: A standard test for AGCMs including their physical parametrizations. II: results for the Met Office model. *Atmos. Sci. Lett.*, **1**, 108–114.

Neelin, J., C. Chou, and H. Su, 2003: Tropical drought regions in global warming and El Niño teleconnections. *Geophys. Res. Lett.*, **30**, 2275.

Neelin, J. D. and I. M. Held, 1987: Modeling tropical convergence based on the moist static energy budget. *Mon. Weat. Rev.*, **115**, 3–12.

Nolan, D., S. Tulich, and J. Blanco, 2016: ITCZ structure as determined by parameterized versus explicit convection in aquachannel and aquapatch simulations. *J. Adv. Model. Earth Sy.*, **8**, 1–28.

Nordeng, T. E., 1994: *Extended versions of the convective parametrization scheme at ECMWF and their impact on the mean and transient activity of the model in the tropics*. European Centre for Medium-Range Weather Forecasts.

Numaguti, A., 1993: Dynamics and energy balance of the Hadley circulation and the tropical precipitation zones: Significance of the distribution of evaporation. *J. Atmos. Sci.*, **50**, 1874–1887.

— 1995: Dynamics and energy balance of the Hadley circulation and the tropical precipitation zones. Part II: Sensitivity to meridional SST distribution. *J. Atmos. Sci.*, **52**, 1128–1141.

Numaguti, A. and Y.-Y. Hayashi, 1991: Behavior of cumulus activity and the structures of circulations in an “Aqua Planet” model. *J. Meteorol. Soc. Jap.*, **69**, 541–561.

Oort, A. and E. Rasmussen, 1970: Global atmospheric circulation statistics, 1958-1973. *U.S. Dept. of Commerce, National Oceanic and Atmospheric Administration*, **5**.

Oueslati, B. and G. Bellon, 2013: Convective entrainment and large-scale organization of tropical precipitation: Sensitivity of the CNRM-CM5 hierarchy of models. *J. Climate.*, **26**, 2931–2946.

— 2015: The double ITCZ bias in CMIP5 models: interaction between SST, large-scale circulation and precipitation. *Clim. Dyn.*, **44**, 585–607.

Oueslati, B., S. Bony, C. Risi, and J.-L. Dufresne, 2016: Interpreting the inter-model spread in regional precipitation projections in the tropics: role of surface evaporation and cloud radiative effects. *Clim. Dyn.*, **47**, 2801–2815.

Peatman, S. C., J. Methven, and S. J. Woolnough, 2018: Isolating the effects of moisture entrainment on convectively coupled equatorial waves in an aquaplanet GCM. *J. Atmos. Sci.*, **75**, 3139–3157.

Peterson, L. C., G. H. Haug, K. A. Hughen, and U. Röhl, 2000: Rapid changes in the hydrologic cycle of the tropical Atlantic during the last glacial. *Science*, **290**, 1947–1951.

Pike, A. C., 1971: Intertropical Convergence Zone studied with an interacting atmosphere and ocean model. *Mon. Weat. Rev.*, **99**, 469–477.

Plumb, R. A. and A. Y. Hou, 1992: The response of a zonally symmetric atmosphere to subtropical thermal forcing: Threshold behavior. *J. Atmos. Sci.*, **49**, 1790–1799.

Popp, M. and L. G. Silvers, 2017: Double and single ITCZs with and without clouds. *J. Climate.*, **30**, 9147–9166.

Rädel, G., T. Mauritsen, B. Stevens, D. Dommenget, D. Matei, K. Bellomo, and A. Clement, 2016: Amplification of El Niño by cloud longwave coupling to atmospheric circulation. *Nat. Geosci.*, **9**, 106.

Randall, D. A., Harshvardhan, D. A. Dazlich, and T. G. Corsetti, 1989: Interactions among radiation, convection, and large-scale dynamics in a general circulation model. *J. Atmos. Sci.*, **46**, 1943–1970.

Retsch, M. H., T. Mauritsen, and C. Hohenegger, 2019: Climate change feedbacks in aquaplanet experiments with explicit and parametrized convection for horizontal resolutions of 2,525 up to 5 km. *J. Adv. Model. Earth Sy.*, **11**, 2070–2088.

Rincón-Martínez, D., F. Lamy, S. Contreras, G. Leduc, E. Bard, C. Saukel, T. Blanz, A. Mackensen, and R. Tiedemann, 2010: More humid interglacials in Ecuador during the past 500 kyr linked to latitudinal shifts of the equatorial front and the Intertropical Convergence Zone in the eastern tropical Pacific. *Paleoceanography and Paleoclimatology*, **25**, PA2210.

Santer, B. D., P. Thorne, L. Haimberger, K. E. Taylor, T. Wigley, J. Lanzante, S. Solomon, M. Free, P. J. Gleckler, P. Jones, et al., 2008: Consistency of modelled and observed temperature trends in the tropical troposphere. *Int. J. Climatology*, **28**, 1703–1722.

Schneider, T., 2018: Feedback of atmosphere-ocean coupling on shifts of the Intertropical Convergence Zone. *Geophys. Res. Lett.*, **44**, 11,644–11,653.

Schneider, T., T. Bischoff, and G. Haug, 2014: Migrations and dynamics of the Intertropical Convergence Zone. *Nature*, **513**, 45–53.

Schott, F. A., J. P. McCreary Jr, and G. C. Johnson, 2004: Shallow overturning circulations of the tropical-subtropical oceans. *Earth's Climate*, **147**, 261–304.

Sherwood, S. C., S. Bony, and J.-L. Dufresne, 2014: Spread in model climate sensitivity traced to atmospheric convective mixing. *Nature*, **505**, 37.

Sherwood, S. C., V. Ramanathan, T. P. Barnett, M. K. Tyree, and E. Roeckner, 1994: Response of an atmospheric general circulation model to radiative forcing of tropical clouds. *J. Geophys. Res-Atmos.*, **99**, 20829–20845.

Slingo, A. and J. M. Slingo, 1988: The response of a general circulation model to cloud longwave radiative forcing. I: Introduction and initial experiments. *Q. J. Roy. Meteor. Soc.*, **114**, 1027–1062.

Sobel, A. H., 2007: Simple models of ensemble-averaged precipitation and surface wind, given the sea surface temperature. *The Global Circulation of the Atmosphere, edited by T. Schneider and AH Sobel*, 219–251.

Sobel, A. H. and C. S. Bretherton, 2000: Modeling tropical precipitation in a single column. *Journal of climate*, **13**, 4378–4392.

Sobel, A. H. and J. D. Neelin, 2006: The boundary layer contribution to Intertropical Convergence Zones in the quasi-equilibrium tropical circulation model framework. *Theoretical and Computational Fluid Dynamics*, **20**, 323–350.

Sobel, A. H., J. Nilsson, and L. M. Polvani, 2001: The weak temperature gradient approximation and balanced tropical moisture waves. *J. Atmos. Sci.*, **58**, 3650–3665.

Song, X. and G. J. Zhang, 2018: The roles of convection parameterization in the formation of double ITCZ syndrome in the NCAR CESM: I. Atmospheric processes. *J. Adv. Model. Earth Sy.*, **10**, 842–866.

Sperber, K. R., H. Annamalai, I.-S. Kang, A. Kitoh, A. Moise, A. Turner, B. Wang, and T. Zhou, 2013: The Asian summer monsoon: an intercomparison of CMIP5 vs. CMIP3 simulations of the late 20th century. *Clim. Dyn.*, **41**, 2711–2744.

Stevens, B., M. Giorgetta, M. Esch, T. Mauritsen, T. Crueger, S. Rast, M. Salzmann, H. Schmidt, J. Bader, K. Block, et al., 2013: Atmospheric component of the MPI-M Earth system model: ECHAM6. *J. Adv. Model. Earth Sy.*, **5**, 146–172.

Sumi, A., 1992: Pattern formation of convective activity over the aqua-planet with globally uniform sea surface temperature (SST). *J. Meteorol. Soc. Jap.*, **70**, 855–876.

Sušelj, K., J. Teixeira, and D. Chung, 2013: A unified model for moist convective boundary layers based on a stochastic eddy-diffusivity/mass-flux parameterization. *J. Atmos. Sci.*, **70**, 1929–1953.

Talib, J., S. J. Woolnough, N. P. Klingaman, and C. E. Holloway, 2018: The role of the cloud radiative effect in the sensitivity of the Intertropical Convergence Zone to convective mixing. *J. Climate.*, **31**, 6821–6838.

Terray, L., 1998: Sensitivity of climate drift to atmospheric physical parameterizations in a coupled ocean-atmosphere general circulation model. *J. Climate.*, **11**, 1633–1658.

Thil, J., 1998: Unified Model documentation paper C6: OASIS coupling. Technical overview. Technical report, Met Office.

Tian, B. and V. Ramanathan, 2002: Role of tropical clouds in surface and atmospheric energy budget. *J. Climate.*, **15**, 296–305.

Tiedtke, M., 1989: A comprehensive mass flux scheme for cumulus parameterization in large-scale models. *Mon. Weat. Rev.*, **117**, 1779–1800.

Todd, A., M. Collins, F. H. Lambert, and R. Chadwick, 2018: Diagnosing enso and global warming tropical precipitation shifts using surface relative humidity and temperature. *J. Climate*, **31**, 1413–1433.

Tomas, R. A., C. Deser, and L. Sun, 2016: The role of ocean heat transport in the global climate response to projected Arctic sea ice loss. *J. Climate.*, **29**, 6841–6859.

Trenberth, K. E. and J. T. Fasullo, 2010: Simulation of present-day and twenty-first-century energy budgets of the southern oceans. *J. Climate.*, **23**, 440–454.

Valcke, S., T. Craig, and L. Coquart, 2013: OASIS3 user guide. Technical Report TR/CMGC/13/17, CERFACS (Centre Europen de Recherche et de Formation Avance en Calcul Scientifique).

Vallis, G. K., 2017: *Atmospheric and ocean fluid dynamics. Fundamentals and large-scale circulation.*, Cambridge University Press, chapter 14. 511–538.

Vishal, D., G. Olivier, and S. S. C., 2018: Control of ITCZ width by low-level radiative heating from upper-level clouds in aquaplanet simulations. *Geophys. Res. Lett.*, **45**, 5788–5797.

Voigt, A., M. Biasutti, J. Scheff, J. Bader, S. Bordoni, F. Codron, R. D. Dixon, J. Jonas, S. M. Kang, N. P. Klingaman, R. Leung, J. Lu, B. Mapes, E. A. Maroon, S. McDermid, J.-y. Park, R. Roehrig, B. E. J. Rose, G. L. Russell, J. Seo, T. Toniazzo, H.-H. Wei, M. Yoshimori, and L. R. Vargas Zeppetello, 2016: The tropical rain belts with an annual cycle and a continent model intercomparison project: TRACMIP. *J. Adv. Model. Earth Sy.*, **8**, 1868–1891.

Voigt, A., S. Bony, J.-L. Dufresne, and B. Stevens, 2014: The radiative impact of clouds on the shift of the Intertropical Convergence Zone. *Geophys. Res. Lett.*, **41**, 4308–4315.

Voigt, A. and T. A. Shaw, 2015: Circulation response to warming shaped by radiative changes of clouds and water vapour. *Nat. Geosci.*, **8**, 102–106.

Waliser, D. E. and C. Gautier, 1993: A satellite-derived climatology of the ITCZ. *J. Climate.*, **6**, 2162–2174.

Waliser, D. E. and N. E. Graham, 1993: Convective cloud systems and warm-pool sea surface tem-

peratures: Coupled interactions and self-regulation. *J. Geophys. Res-Atmos.*, **98**, 12881–12893.

Waliser, D. E. and R. C. Somerville, 1994: Preferred latitudes of the intertropical convergence zone. *J. Atmos. Sci.*, **51**, 1619–1639.

Walker, C. C. and T. Schneider, 2006: Eddy influences on hadley circulations: Simulations with an idealized gcm. *J. Atmos. Sci.*, **63**, 3333–3350.

Walters, D., M. Brooks, I. Boutle, T. Melvin, R. Stratton, S. Vosper, H. Wells, K. Williams, N. Wood, T. Allen, A. Bushell, D. Copsey, P. Earnshaw, J. Edwards, M. Gross, S. Hardiman, C. Harris, J. Heming, N. Klingaman, R. Levine, J. Manners, G. Martin, S. Milton, M. Mittermaier, C. Morcrette, T. Riddick, M. Roberts, C. Sanchez, P. Selwood, A. Stirling, C. Smith, D. Suri, W. Tennant, P. L. Vidale, J. Wilkinson, M. Willett, S. Woolnough, and P. Xavier, 2017: The Met Office Unified Model Global Atmosphere 6.0/6.1 and JULES Global Land 6.0/6.1 configurations. *Geosci. Model Dev.*, **2016**, 1–52.

Wang, C.-c. and G. Magnusdottir, 2006: The ITCZ in the central and eastern Pacific on synoptic time scales. *Mon. Weat. Rev.*, **134**, 1405–1421.

Wang, X., A. S. Auler, R. L. Edwards, H. Cheng, P. S. Cristalli, P. L. Smart, D. A. Richards, and C.-C. Shen, 2004: Wet periods in northeastern Brazil over the past 210 kyr linked to distant climate anomalies. *Nature*, **432**, 740–743.

Wang, Y., S.-P. Xie, B. Wang, and H. Xu, 2005: Large-scale atmospheric forcing by southeast Pacific boundary layer clouds: A regional model study. *J. Climate.*, **18**, 934–951.

Wang, Y., L. Zhou, and K. Hamilton, 2007: Effect of convective entrainment/detrainment on the simulation of the tropical precipitation diurnal cycle. *Mon. Weat. Rev.*, **135**, 567–585.

Wei, H.-H. and S. Bordoni, 2018: Energetic constraints on the ITCZ position in idealized simulations with a seasonal cycle. *J. Adv. Model. Earth Sy.*, **10**, 1708–1725.

Williams, K., D. Copsey, E. Blockley, A. Bodas-Salcedo, D. Calvert, R. Comer, P. Davis, T. Graham, H. Hewitt, R. Hill, et al., 2018: The Met Office global coupled model 3.0 and 3.1 (GC3. 0 and GC3. 1) configurations. *J. Adv. Model. Earth Sy.*, **10**, 357–380.

Williamson, D. L., 2008: Convergence of aqua-planet simulations with increasing resolution in the community atmospheric model, version 3. *Tellus A: Dynamic Meteorology and Oceanography*, **60**, 848–862.

Williamson, D. L., M. Blackburn, K. N. W. Ohfuchi, Y. O. Takahashi, Y.-Y. Hayashi, H. Nakamura, M. Ishiwatari, J. L. McGregor, H. Borth, V. Wirth, H. Frank, P. Bechtold, N. P. Wedi, H. Tomita, M. Satoh, M. Zhao, I. M. Held, M. J. Suarez, M.-I. Lee, M. Watanabe, M. Kimoto, Y. Liu, Z. Wang, A. Molod, K. Rajendran, A. Kitoh, and R. Stratton, 2013: The aqua-planet experiment (APE): Response to changed meridional SST profile. *J. Meteorol. Soc. Jap.*, **91A**, 57–89.

Williamson, D. L., J. T. Kiehl, V. Ramanathan, R. E. Dickinson, and J. J. Hack, 1987: *Description of NCAR community climate model (CCM1)*. National Center for Atmospheric Research Boulder

Colorado.

Wood, N., A. Staniforth, A. White, T. Allen, M. Diamantakis, M. Gross, T. Melvin, C. Smith, S. Vosper, M. Zerroukat, and J. Thuburn, 2013: An inherently mass-conserving semi-implicit semi-lagrangian discretization of the deep-atmosphere global non-hydrostatic equations. *Q. J. Roy. Meteor. Soc.*, **140**, 1505–1520.

Xiang, B., M. Zhao, I. M. Held, and J.-C. Golaz, 2017: Predicting the severity of spurious "double ITCZ" problem in CMIP5 coupled models from AMIP simulations. *Geophys. Res. Lett.*, **44**, 1520–1527.

Yoshimori, M. and A. J. Broccoli, 2008: Equilibrium response of an atmosphere–mixed layer ocean model to different radiative forcing agents: Global and zonal mean response. *J. Climate.*, **21**, 4399–4423.

— 2009: On the link between Hadley circulation changes and radiative feedback processes. *Geophys. Res. Lett.*, **36**, L20703 (1–5).

Zhang, C., M. Dong, S. Gualdi, H. H. Hendon, E. D. Maloney, A. Marshall, K. R. Sperber, and W. Wang, 2006: Simulations of the Madden–Julian oscillation in four pairs of coupled and uncoupled global models. *Clim. Dyn.*, **27**, 573–592.

Zhang, G. J. and H. Wang, 2006: Toward mitigating the double ITCZ problem in NCAR CCSM3. *Geophys. Res. Lett.*, **33**, L06709 (1–4).

Zhang, R. and T. L. Delworth, 2005: Simulated tropical response to a substantial weakening of the Atlantic thermohaline circulation. *J. Climate.*, **18**, 1853–1860.